



<https://theses.gla.ac.uk/>

Theses Digitisation:

<https://www.gla.ac.uk/myglasgow/research/enlighten/theses/digitisation/>

This is a digitised version of the original print thesis.

Copyright and moral rights for this work are retained by the author

A copy can be downloaded for personal non-commercial research or study,
without prior permission or charge

This work cannot be reproduced or quoted extensively from without first
obtaining permission in writing from the author

The content must not be changed in any way or sold commercially in any
format or medium without the formal permission of the author

When referring to this work, full bibliographic details including the author,
title, awarding institution and date of the thesis must be given

Enlighten: Theses

<https://theses.gla.ac.uk/>
research-enlighten@glasgow.ac.uk

THE GROWTH OF UNINTENTIONAL- AND SULPHUR-DOPED
INDIUM PHOSPHIDE BY MOLECULAR BEAM EPITAXY.

A THESIS

SUBMITTED TO THE FACULTY OF ENGINEERING OF THE UNIVERSITY OF
GLASGOW FOR THE DEGREE OF

DOCTOR OF PHILOSOPHY

BY

TREVOR MARTIN B.Sc.

ProQuest Number: 10998019

All rights reserved

INFORMATION TO ALL USERS

The quality of this reproduction is dependent upon the quality of the copy submitted.

In the unlikely event that the author did not send a complete manuscript and there are missing pages, these will be noted. Also, if material had to be removed, a note will indicate the deletion.



ProQuest 10998019

Published by ProQuest LLC (2018). Copyright of the Dissertation is held by the Author.

All rights reserved.

This work is protected against unauthorized copying under Title 17, United States Code
Microform Edition © ProQuest LLC.

ProQuest LLC.
789 East Eisenhower Parkway
P.O. Box 1346
Ann Arbor, MI 48106 – 1346

CONTENTS

| | |
|--|-----|
| ACKNOWLEDGEMENTS | III |
| SUMMARY | IV |
| LIST OF PUBLISHED WORK | VI |
| 1 DEVICE APPLICATIONS AND EPITAXIAL GROWTH OF INDIUM PHOSPHIDE | 1 |
| 1.1 Introduction | 2 |
| 1.2 The Device Applications of Indium Phosphide | 2 |
| 1.3 The Epitaxial Growth of Indium Phosphide | 5 |
| 1.4 Molecular Beam Epitaxy of Indium Phosphide | 8 |
| 1.5 Summary | 13 |
| 2 PROPERTIES OF UNINTENTIONALLY DOPED INDIUM PHOSPHIDE GROWN IN MBE CHAMBER 1 | 14 |
| 2.1 Introduction | 15 |
| 2.2 Impurity Assessment of Early Indium Phosphide Layers Grown | 15 |
| 2.3 The Properties of Epitaxial Indium Phosphide Grown Following Modifications to the Indium Cell. | 18 |
| 2.4 Morphological Studies of the Early Indium Phosphide Layers Grown | 22 |
| 2.5 Summary of the Design Weaknesses of MBE Chamber 1 | 24 |
| 2.6 Summary | 25 |
| 3 CHARACTERISATION OF UNINTENTIONALLY DOPED INDIUM PHOSPHIDE GROWN IN CHAMBER 2 | 26 |
| 3.1 Introduction | 27 |
| 3.2 Design and Performance of Chamber 2 | 27 |
| 3.3 Properties of Unintentionally Doped Indium Phosphide Grown in Chamber 2 | 32 |
| 3.4 Sims Analysis | 35 |
| 3.5 Origin of the Impurities | 37 |
| 3.6 Photoluminescence from MBE Grown Indium Phosphide | 43 |
| 3.7 Summary | 45 |

| | | |
|-----|--|-----|
| 4 | SULPHUR DOPING OF INDIUM PHOSPHIDE | 46 |
| 4.1 | Introduction | 47 |
| 4.2 | Electrochemical Sulphur Cell | 49 |
| 4.3 | Properties of Sulphur Doped Indium Phosphide | 49 |
| 4.4 | Sulphur Incorporation as a Function of Growth Conditions | 54 |
| 4.5 | Summary | 59 |
| 5 | ROUTES TO THE REDUCTION OF THE SULPHUR CONCENTRATION IN UNINTENTIONALLY DOPED InP | 60 |
| 5.1 | Introduction | 61 |
| 5.2 | Growth Optimisation | 61 |
| 5.3 | Comparison of Red Phosphorus Source Material | 66 |
| 5.4 | Alternative Sources of Phosphorus | 68 |
| 5.5 | Summary | 70 |
| 6 | CONCLUSION AND SUGGESTIONS FOR FURTHER WORK | 71 |
| 6.1 | Conclusion | 72 |
| 6.2 | Further Work | 75 |
| | APPENDICES - ANALYSIS TECHNIQUES | 77 |
| A.1 | Introduction | 78 |
| A.2 | Secondary Ion Mass Spectroscopy | 78 |
| A.3 | Electrochemical Capacitance-Voltage Profiling | 82 |
| A.4 | Van-Der-Pauw Hall Measurement | 84 |
| A.5 | Photoluminescence | 88 |
| | REFERENCES | 91 |
| | LIST OF FIGURES | 107 |
| | LIST OF TABLES | 109 |

ACKNOWLEDGEMENTS

I wish to acknowledge the contribution, however small, of all those who have been involved with this work. In particular I would like to express my sincere thanks to Professor J. Lamb for the provision of the research facilities in the Department of Electronic and Electrical Engineering and to my supervisor Dr C.R. Stanley for his advice and enthusiastic support throughout.

It is also a pleasure to be able to thank Dr C.R. Whitehouse (RSRE Malvern) for his positive interest and input while I was at Glasgow University and his ceaseless support over the past years.

I am indebted to Dr D.E. Sykes for the many long but crucial hours of SIMS analysis and to C. Kippen for his invaluable contribution to the successful fabrication of Chamber 2.

To the many colleagues at Glasgow University for their technical and spirited contributions and without whom life would not have been the same I extend a deep thanks, particularly, R. Hutchins, R. Devine, J. Cochrane, P. Tasker, J. Young, J. Frost and A. Iliadis.

Thanks must also go to those who educated me in life north of the border: Jill, Dave and Liam, to my colleagues in the MBE group at RSRE Malvern for their continued support since leaving Glasgow, to Peggy whom I was fortunate to have to type this thesis, and to Tricia for proof reading and the understanding she has shown.

Finally and by no means least I would like to thank my mother for her patience, and support throughout.

The following work was supported by the Science and Engineering Research Council.

SUMMARY

This thesis describes a detailed and systematic investigation of those factors which influence the properties of InP grown by Molecular Beam Epitaxy. The growth of any semiconductor material for device applications requires that the growth process is reproducible, and its capabilities characterised. Both the published literature and the analysis of epitaxial InP grown at the start of this programme indicated that neither of these criteria were satisfied for the MBE growth of InP.

A detailed assessment of InP grown using an existing MBE chamber and involving Photoluminescence (PL), Secondary Ion Mass Spectroscopy (SIMS) and residual carrier concentration profiles is presented. This assessment and particularly the results of the SIMS analysis was able to identify a significant concentration of impurities in the epitaxial layers and, more importantly, enabled the source of these impurities to be determined. Further experiments which involved deliberate changes in the growth conditions (growth temperature, growth rate, and V:III flux ratio) during the growth of single epitaxial layers are reported. The results from the SIMS and residual carrier concentration profiles of these layers are shown to identify limitations imposed by the construction of the existing growth chamber. Such limitations were overcome by the design and commissioning of a second growth chamber.

The significant improvement in both the purity and the growth control achieved using this second chamber enabled a detailed and systematic analysis of the influence of growth conditions on the properties of epitaxial InP to be undertaken. The results of PL, SIMS, Hall and residual carrier profiles of an extensive series of layers are presented. From these results the purity and properties of unintentionally doped InP grown from solid sources are shown to be dominated by a single extrinsic impurity. The origin of this impurity is unequivocally identified as the red phosphorus source material and it is believed that this impurity is responsible for the universal n-type behaviour of InP grown by solid source MBE to date. The role of Calcium shown by SIMS to be present in the epitaxial InP is also discussed.

The intentional doping of InP using Sulphur from an electrochemical source has been characterised. No evidence of Sulphur diffusion has been observed but a previously unsuspected temperature sensitivity of the electrochemical cell has been identified. The use of Sulphur as an n-type dopant in the MBE growth of InP is shown to be an attractive alternative to Si, especially when the improved morphology at high doping concentrations and the reduced dependence of incorporation rate on the group V flux are considered.

In the light of the limitation on the purity of InP grown by MBE from solid sources which is identified in this study, a detailed assessment of the routes available for reducing this impurity concentration is presented. Results from a comparison of different batches of nominally high purity red phosphorus source material reveal a variation in impurity concentration of over 2 orders of magnitude, while optimisation of the growth conditions is shown only to be viable at reduced growth temperatures. However, it is clear that using the appropriate phosphorus source high purity ($N_D+N_A < 5 \times 10^{14} \text{cm}^{-3}$) InP with reproducible properties can be obtained using molecular beam growth techniques.

LIST OF PUBLISHED WORK

A Model for Uncured Rubber Behaviour

R A Dove, D M Turner and T Martin

Presented at the Rubber Conference, Brighton, 1977

Identification of the Major Residual Donor and its Source in Unintentionally Doped MBE InP

T Martin, C R Stanley, A Iliadis, C R Whitehouse, D E Sykes

Presented at the Third European Molecular Beam Epitaxy Workshop, Aussois, France; March 1985

Identification of the Major Residual Donor in Unintentionally Doped InP grown by Molecular Beam Epitaxy

T Martin, C R Stanley, A Iliadis, C R Whitehouse, D E Sykes

1985, Appl Phys Lett 46, 994

The Influence of Growth Conditions on Undoped and Sulphur Doped InP Grown by MBE

A Iliadis, K A Prior, C R Stanley, T Martin, G J Davies

1986, J Appl Phys 60, 213

Substrate Temperature Calibration during III-V MBE Growth using RHEED Reconstructions

C R Whitehouse, M T Emeny, L Davies, G M Williams and T Martin

Presented at the Fourth International Conference on MBE, University of York; September 1986

UV-Ozone Preparation of III-V Compounds for MBE Growth Applications - a Detailed Appraisal

C R Whitehouse, L Davies, M T Emeny, T Martin, G M Williams, I Sutherland and D E Sykes

Presented at the Fourth International Conference on MBE, University of York; September 1986

The MBE Growth of InSb and InSb-based Heterostructures for Novel Device Applications

G M Williams, C R Whitehouse, T Martin, N G Chew, A G Cullis, T Ashley, D E Sykes and K Mackey

Presented at the Fourth International Conference on MBE, University of York; September 1986

Molecular-Beam Epitaxy of (100) InSb for CdTe/InSb Device Applications

G M Williams, C R Whitehouse, T Martin, N G Chew, A G Cullis, T Ashley, D E Sykes, K Mackey and R H Williams

1988, J Appl Phys 63, 1526

Modulated-Beam Mass Spectrometer Studies (MBMS) of III-V Growth Processes in Metalorganic MBE

T Martin, C R Whitehouse, A E Terry, R M Bush, P J Wright

To be presented at the First International Workshop on MOMBE, Sapporo, Japan; September 1988

CHAPTER 1

THE DEVICE APPLICATIONS AND EPITAXIAL GROWTH OF INDIUM PHOSPHIDE

- 1.1 INTRODUCTION
- 1.2 THE DEVICE APPLICATIONS OF
INDIUM PHOSPHIDE
- 1.3 THE EPITAXIAL GROWTH OF INDIUM PHOSPHIDE
- 1.4 MOLECULAR BEAM EPITAXY OF
INDIUM PHOSPHIDE
- 1.5 SUMMARY

1.1 INTRODUCTION

The development of Indium Phosphide (InP) has been central to major advances in both microwave and optical communications over the last two decades. InP microwave devices operating in excess of 90GHz have been successfully demonstrated [1.01] [1.02], and optical communication systems in the 1.3 to 1.55 micron range are a commercial reality [1.03] [1.04].

Devices are frequently fabricated from complex multilayer epitaxial structures whose properties have been carefully tailored for optimum performance. A range of different epitaxial growth techniques has been developed, therefore, to satisfy the ever-more demanding specifications on epilayer purity, composition and thickness. The leading techniques include Liquid Phase Epitaxy (LPE), Vapour Phase Epitaxy (VPE), Metal-Organic Vapour Phase Epitaxy (MOVPE) and Molecular Beam Epitaxy (MBE). Experience gained in the growth of GaAs using these techniques would indicate that MBE should provide the highest level of growth control for InP.

The primary objective of the current programme of work was therefore to develop a full understanding of those factors influencing the growth and doping of high purity InP grown by MBE. Before describing the MBE growth technique in detail (section 1.4), the advantages to be gained from the use of InP for both electronic and optoelectronic device applications, and the capabilities of each growth technique are reviewed.

1.2 THE DEVICE APPLICATIONS OF INDIUM PHOSPHIDE

1.2.1 TRANSFERRED ELECTRON DEVICES

The band structure of InP is compared with that of GaAs and Si in figure 1.1, from which a number of significant differences are immediately evident. Whilst Si is an indirect semiconductor, the III-V compounds are direct-gap and also exhibit two subsidiary energy minima in the conduction band at the X and L points respectively. Under sufficiently high electric fields ($>10.5\text{kVcm}^{-1}$ in InP and $>3.2\text{kVcm}^{-1}$ in GaAs), electrons transfer from energy states associated with the principal minimum (Γ point) to the L point minimum. Since the effective mass of electrons (m^*) in this subsidiary minimum is significantly higher than that for electrons at the Γ point ($m_{L^*} = 0.4$ and $m_{\Gamma^*} = 0.08$ respectively for InP), a negative differential resistance (NDR) characteristic is observed with the transfer (Fig 1.2). This effect has been

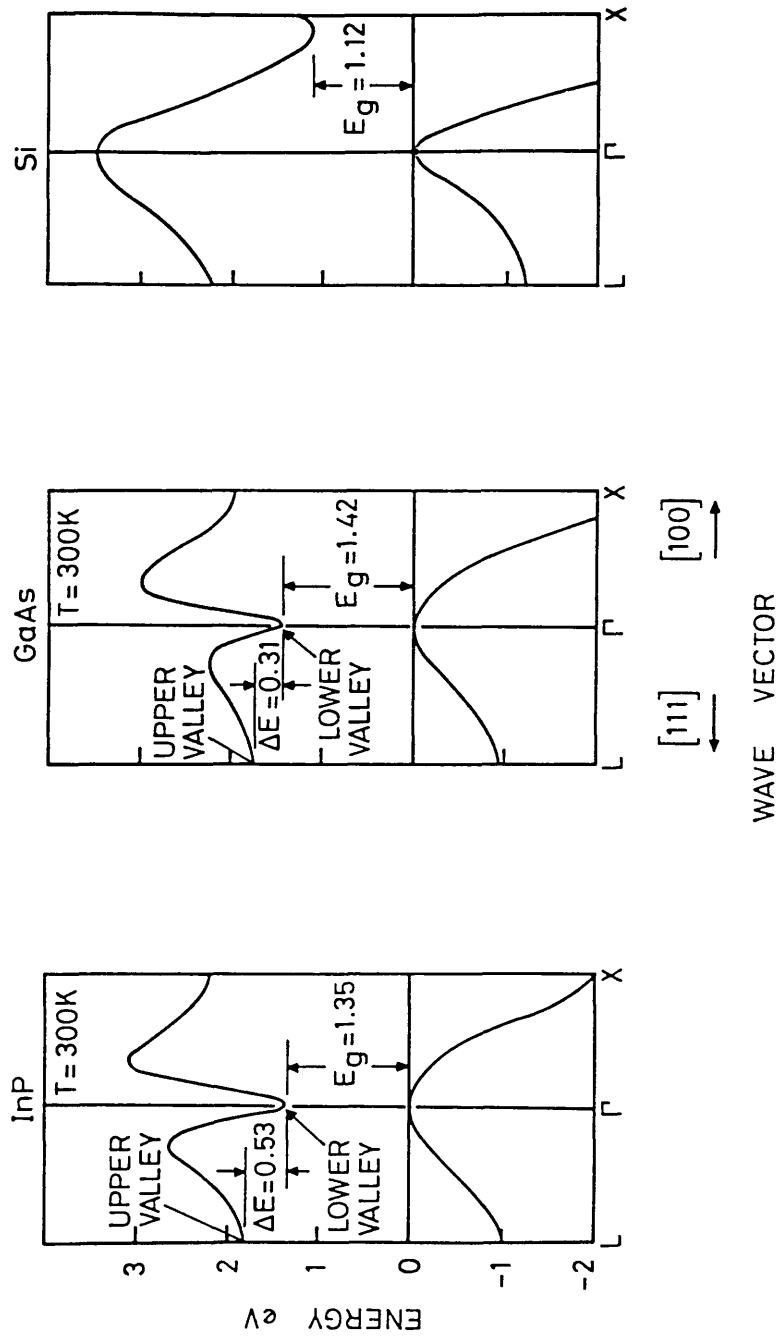


FIGURE .1-1 THE BAND STRUCTURE OF InP, GaAs AND Si

exploited to produce a range of important high frequency (mm wave) amplifiers and oscillators known as transferred electron devices (TEDs) [1.05]

A TED is based on a $n^+ - n^- - n^+$ structure and can exhibit a range of operating modes depending primarily on the product of the carrier concentration (n^-) and the length (l) of the active region. For $n^- l$ products $> 10^{12} \text{cm}^{-2}$ large space charge instabilities can be obtained whereas for smaller values of $n^- l$ the field distribution within the active region is stable [1.06]. In InP devices operating at, say, 90GHz and for modes where the frequency is controlled by the transit time, the length l is typically $\sim 1 \mu\text{m}$ and therefore the required residual carrier concentrations are $\sim 10^{16} \text{cm}^{-3}$ [1.02]. Lower frequency devices (increased l) require lower residual carrier concentrations and, in certain applications, carrier concentrations as low as 10^{14}cm^{-3} are the optimum [1.07] [1.01].

TEDs are relatively broad band devices and do not therefore demand precise control of the thickness of the active region. However, later designs of TED structures have included complex doping profiles in the cathode region involving the use of dopant spikes 20–30nm wide [1.07]. The fabrication of state-of-the-art TEDs, therefore, places stringent demands on the purity and thickness control of the growth technique in use.

InP TEDs exhibit higher efficiency compared to GaAs due to both the larger peak-to-valley ratio (4.8 and 3.2 respectively) and the higher threshold field (10.5kVcm^{-1} versus 3.2kVcm^{-1}) required to initiate electron transfer (Fig 1.2) [1.06] [1.08]. In addition, the maximum operating frequency achievable using InP is superior, the upper limit being related to the rate at which carriers can be successively heated and cooled within the central valley [1.09]. Furthermore, an InP transferred electron amplifier can achieve a noise figure 3 to 6dB lower than a comparable GaAs device [1.07] [1.10].

1.2.2 FIELD EFFECT TRANSISTORS

InP also offers performance benefits when used in field effect transistors (FETs), as illustrated by the velocity-field characteristics presented in figure 1.2. The peak electron drift velocity in InP is $\sim 2.5 \times 10^7 \text{cm s}^{-1}$ and is higher than that of Si and GaAs by factors of 2.5 and 1.14 respectively. Therefore, for devices of comparable geometry, proportionate increases in maximum operating frequency should be expected. Furthermore, because this peak velocity arises at significantly higher fields (10kVcm^{-1} compared to 3.2kVcm^{-1}) and InP has a higher thermal conductivity

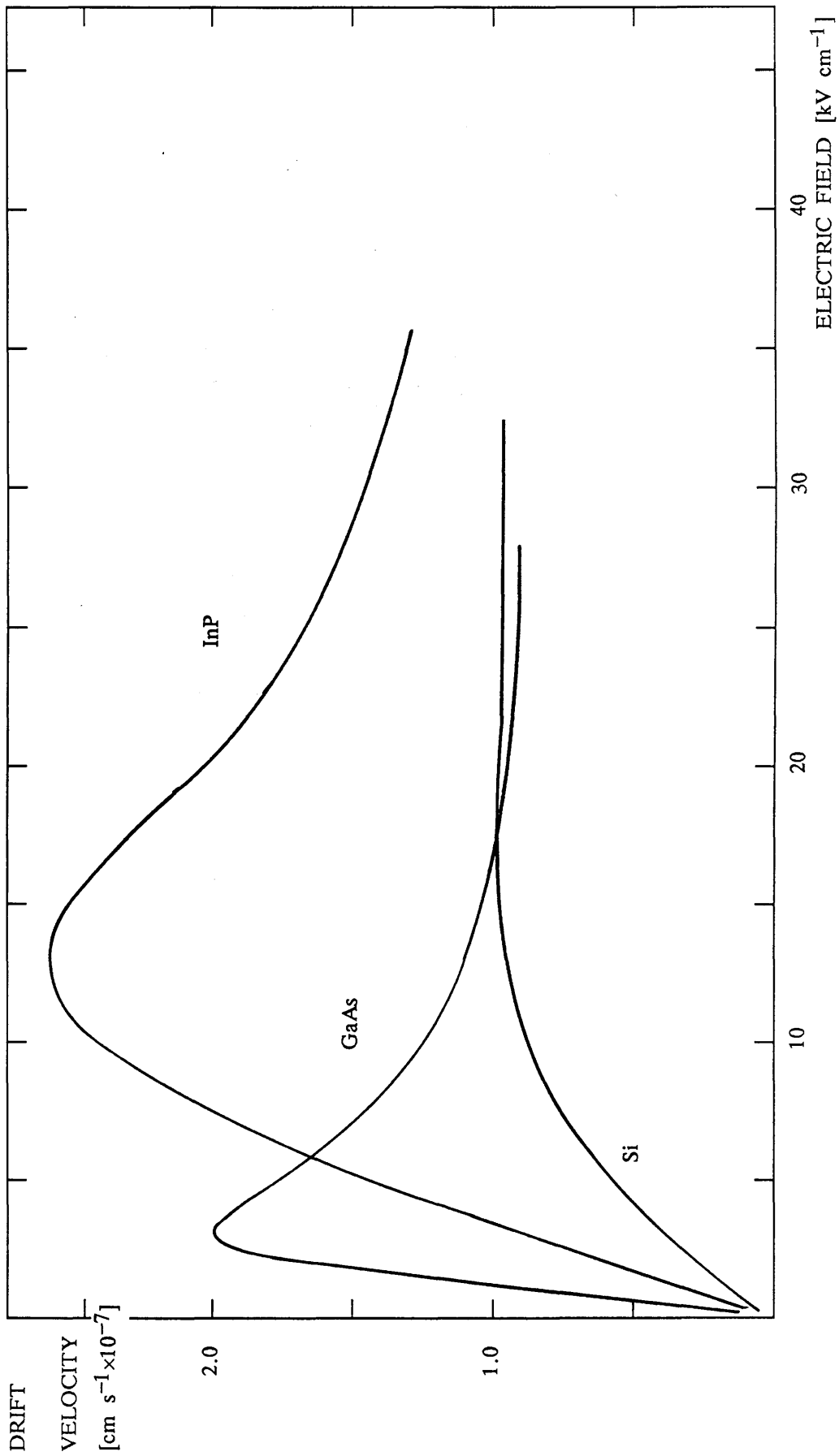


FIGURE 1.2 VELOCITY-FIELD CHARACTERISTICS

($0.68\text{Wcm}^{-1}\text{C}^{-1}$ versus 0.44) than GaAs, InP based circuits are used for higher power applications than GaAs [1.11] [1.12].

An additional important advantage of InP over GaAs for FET applications relates to differences in their surface band structure [1.13]. In the case of InP the surface Fermi level is pinned close to the conduction band edge by a comparatively low density of surface states, while in GaAs the surface Fermi level is pinned mid-gap by a density of surface states approximately $\times 10$ higher [1.14]. The available excursion in surface potential is therefore larger for InP and in MISFET applications can exceed 1 volt. In addition, p-type InP can be readily inverted [1.15]. Normally-off MISFET structures, of interest because of their low power consumption, can therefore be fabricated in InP but not in GaAs.

Typical FET channel layers are of the order of 100nm thick and require doping in the low 10^{17}cm^{-3} range. Whilst these specifications are not in themselves over-demanding, cross-wafer layer thickness and doping uniformity is vital to avoid unacceptable variations in pinch-off voltage.

1.2.3 HETEROJUNCTION DEVICES

InP has rapidly become a major material for use in optoelectronic device structures. The significance of InP can be seen from a plot of energy gap versus lattice constant for the III-V semiconductors, figure 1.3. The lattice constant of InP (0.58686nm) allows for the epitaxial growth of $\text{Ga}_{0.47}\text{In}_{0.53}\text{As}$, $\text{In}_{0.523}\text{Al}_{0.477}\text{As}$, and quaternary InGaAsP and AlGaInAs compounds. These latter materials, with band gaps spanning the $0.93\text{--}1.65\mu\text{m}$ and $0.85\text{--}1.65\mu\text{m}$ range respectively are of vital importance in view of their wavelength match to fibre optic transmission windows [1.03] [1.16] [1.17] [1.18]. It must also be emphasised that InP epitaxial layers themselves provide essential low refractive index (3.1–3.6) optical confinement barriers in these structures [1.19].

1.2.4 SUMMARY OF THE MATERIAL REQUIREMENTS

The preceding review indicates that device demands place very exacting requirements on the semiconductor growth technique in use. In many cases, unintentionally doped InP layers must have a total ionized impurity concentration less than $5 \times 10^{14}\text{cm}^{-3}$ (corresponding to a 77K n-type mobility ($\mu_{77\text{K}}$) of greater than $90,000\text{cm}^2\text{V}^{-1}\text{s}^{-1}$ [1.20]) and dopant/thickness profiles often need to be controlled at the sub 10nm level. Both n and p doping capability is required over the range from $\sim 1 \times 10^{15}\text{cm}^{-3}$

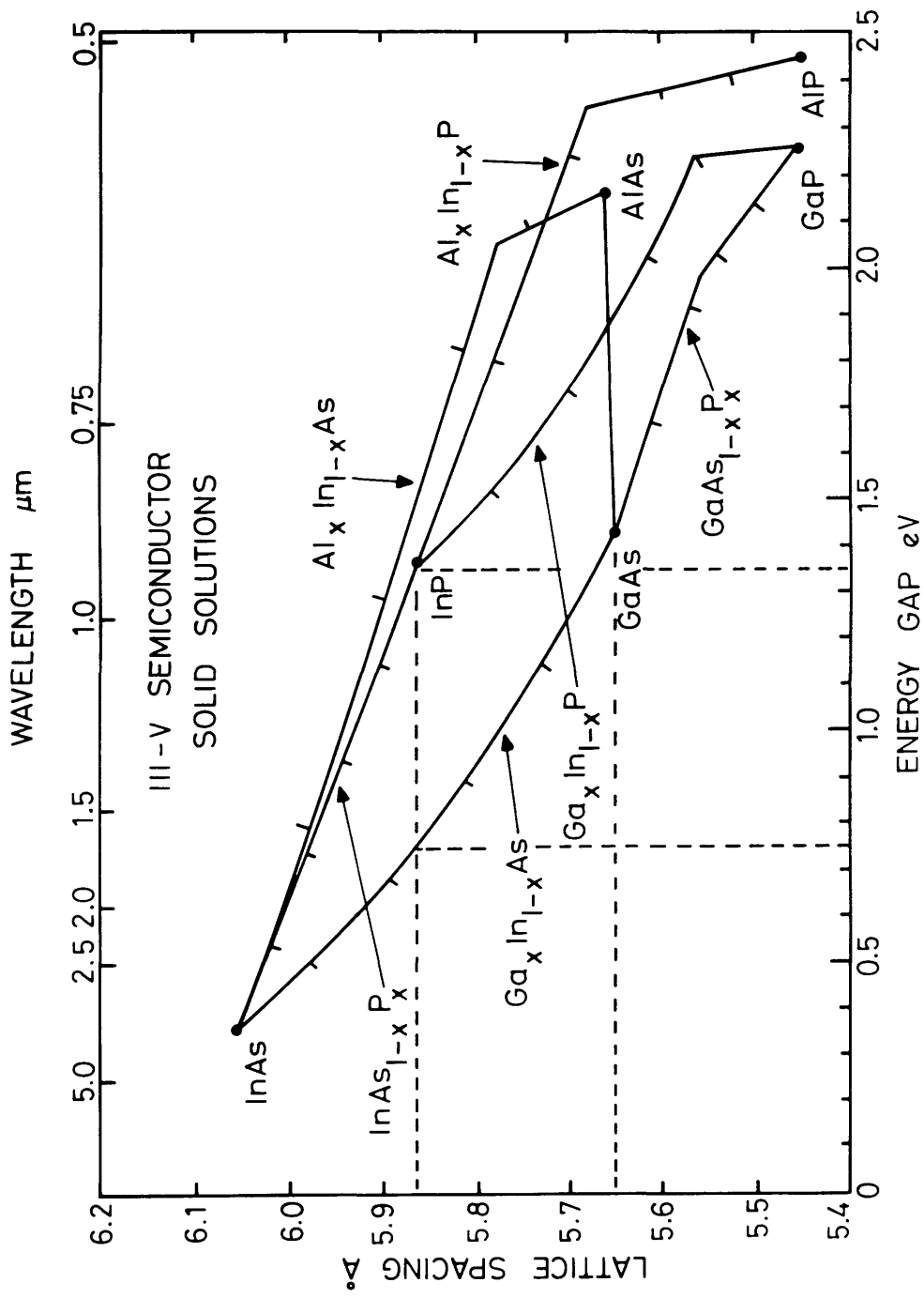


FIGURE 1.3 ENERGY GAP VERSUS LATTICE CONSTANT FOR III-V SEMICONDUCTORS

to $>1 \times 10^{18} \text{cm}^{-3}$ and lateral thickness/doping uniformity is crucial for many applications.

The following section compares the ability of the major epitaxial growth techniques to meet these criteria.

1.3 THE EPITAXIAL GROWTH OF INDIUM PHOSPHIDE

Four principal epitaxial techniques have been used for the growth of InP device structures: Liquid Phase Epitaxy (LPE), Chloride/Hydride Vapour Phase Epitaxy (VPE), Metal–Organic Vapour Phase Epitaxy (MOVPE) and Molecular Beam Epitaxy (MBE)[†]. Each technique is briefly reviewed below.

1.3.1 LIQUID PHASE EPITAXY

In the LPE process, InP is deposited onto a single crystal substrate by cooling a supersaturated solution of InP in molten indium at a rate of between 20°C and 40°C hr^{-1} [1.21]. It is a relatively low cost production-scale growth technique and has been used widely for the growth of heterostructure optoelectronic devices [1.16]. The growth of high purity InP ($\mu_{77\text{K}} \sim 94,000 \text{cm}^2 \text{V}^{-1} \text{s}^{-1}$) has been demonstrated [1.22], Si and S being identified as the dominant residual impurities [1.23]. Whilst individual layers as thin as 10nm have been successfully grown using LPE [1.24], typical growth rates lie in the range from $2\text{--}20 \text{nm s}^{-1}$ and restrict routine thickness control to no better than 100nm [1.24]. A major disadvantage of the LPE technique, however, relates to the surface morphology of the grown epitaxial layers, which can typically exhibit terracing on a $20\mu\text{m}$ scale and create problems at the device fabrication stage.

1.3.2 CHLORIDE/HYDRIDE VAPOUR PHASE EPITAXY

Chloride VPE

The chloride process was the first of the vapour phase techniques to be developed

[†]Footnote:

Since the completion of the present work, an important new epitaxial growth technique, Metal–Organic MBE (MOMBE) has been successfully applied to the growth of high purity InP (table 1.1). The potential of this new technique is further discussed in chapter 5.

[1.25] and has established a strong reputation for its ability to produce extremely high purity semiconductor material. The growth reactor consists of a higher temperature ($\sim 750^\circ\text{C}$) source zone and a lower temperature ($\sim 650^\circ\text{C}$) reaction region. In the case of InP growth, PCl_3 is passed over high purity indium in the source zone, where it reacts to produce InCl and volatile phosphorus species [1.26] [1.27]. These products are then transported to the cooler zone where a reverse reaction occurs and epitaxial deposition of InP takes place. The potential of the technique to grow high purity InP has been demonstrated by the results of both Fairhurst ($\mu_{77\text{K}} \sim 121,000\text{cm}^2\text{V}^{-1}\text{s}^{-1}$) [1.27] and Taylor ($\mu_{77\text{K}} \sim 130,000\text{cm}^2\text{V}^{-1}\text{s}^{-1}$) [1.28]. Whilst silicon was reported to be the dominant residual impurity in early layers grown [1.29], improved experimental procedures have significantly reduced this concentration and Si levels are now comparable to those of S and Zn [1.30] [1.31]. Despite the success of this technique in the development of microwave devices [1.01], control over layer thickness to better than $\pm 25\text{nm}$ is extremely difficult to achieve [1.32]. In addition, the need to saturate the source prior to growth has limited the technique to homoepitaxial growth applications.

Hydride VPE

In more recent years, the hydride VPE technique has attracted increasing interest [1.33] since it allows mixed group V materials to be grown. Gaseous hydrides (PH_3 or AsH_3) are used to provide the group V species whilst the volatile group III component is generated by the passage of HCl over the elemental source. The need for source saturation is therefore eliminated. Nevertheless, epitaxial layer purity achieved by the hydride process ($\mu_{77\text{K}} \sim 71,000\text{cm}^2\text{V}^{-1}\text{s}^{-1}$) [1.34] has not yet matched that demonstrated by the chloride technique and layer thickness control is also limited by the high growth rates typically used [1.33].

1.3.3 METAL-ORGANIC VAPOUR PHASE EPITAXY

MOVPE is a further extension of the vapour deposition process, in which the group III and V sources are metal alkyls, (e.g. trimethyl indium) and hydrides (e.g. phosphine) respectively. Since both the group III and V sources are now in gaseous form, the use of high flow-rates and carefully designed switching manifolds allows thickness control to much better than 5nm [1.35] [1.36]. Furthermore, this change of source materials eliminates the need for any chemical reactions prior to growth, and therefore ensures that the growth is controlled by reactions at the hot substrate surface. InP growth temperatures typically lie in the range from $550\text{--}750^\circ\text{C}$. Growth at lower temperatures gives rise to metal rich conditions due to insufficient hydride

decomposition, whilst the upper temperature value is limited by excessive group V desorption [1.37].

Prior to the commencement of the present study, the highest mobility reported for MOCVD grown InP was $\mu_{77K} \sim 30,000 \text{cm}^2 \text{V}^{-1} \text{s}^{-1}$ [1.38]. However, subsequent improvements in source purification [1.39] [1.40] have since led to significantly higher purity material, with 77K mobilities as large as $264,000 \text{cm}^2 \text{V}^{-1} \text{s}^{-1}$ being reported [1.41]. Difficulties still exist with this technique, particularly in relation to the toxicity of the hydrides used and also the layer uniformity routinely achieved [1.37].

1.3.4 MOLECULAR BEAM EPITAXY

MBE differs from both the liquid and vapour phase techniques described earlier in that it is an ultra-high vacuum (UHV) process. III-V growth is generally performed using elemental sources evaporated from temperature controlled cells, and growth now occurs in a regime dominated by kinetics [1.42]. For any given material, MBE growth temperatures are typically 200°C lower than those of other epitaxial growth techniques, a very important factor in minimising interface/dopant diffusion effects.

Under typical MBE growth conditions (10^{-6}mbar), the mean free path between collisions in the thermal beams is significantly greater than the separation between the source and substrate (10cm). The combination of low growth rates (typically $0.1 \mu\text{m} - 10 \mu\text{m} \text{hr}^{-1}$) and the use of fast-acting cell shutters therefore provides unique thickness control at the monolayer level [1.43]. Additional advantages relate to the use of substrate rotation to produce high thickness uniformity, ($\pm 0.5\%$ across a 2 inch diameter wafer) [1.44] and also the unparalleled availability of a wide range of UHV surface analytical and monitoring equipment such as: flux monitoring ion gauge, Residual Gas Analyser (RGA), Reflection High Energy Electron Diffraction (RHEED), Auger Electron Spectroscopy (AES), Secondary Ion Mass Spectroscopy (SIMS) etc.

However, the purity of unintentionally-doped InP grown by MBE to date is significantly inferior to that of layers grown using the other epitaxial techniques. Indeed the highest 77K mobility reported prior to the present study was $34,000 \text{cm}^2 \text{V}^{-1} \text{s}^{-1}$ [1.45] and even at the time of writing, the highest reported mobility is only $55,000 \text{cm}^2 \text{V}^{-1} \text{s}^{-1}$ [1.46].

1.3.5 SUMMARY

A summary of the current status of the major epitaxial growth techniques, as applied to the growth of InP, is presented in table 1.1. This data, as well as the preceding

| TECHNIQUE | GROWTH CONDITIONS | | DOPANTS | | UNINTENTIONALLY DOPED | | | QUALITY | REFERENCE |
|----------------------------|----------------------|---------------|-----------------------------------|------------|-----------------------|--|---|--------------------|-----------|
| | PRESSURE (atm) | TEMP. (°C) | RATE ($\mu\text{m hr}^{-1}$) | P-TYPE | N-TYPE | N_D-N_A (77K) (cm^{-3}) | MOBILITY (77K) ($\text{cm}^{-2}\text{V}^{-1}\text{s}^{-1}$) | | |
| LPE | 1 | 600-700 | ~10 | Cd, Zn, Mg | Sn, Te | 4×10^{14} | 94,000 | 5×10^{14} | 1.22 |
| VPE chloride hydride | 1 | 600-700 | 1-10 | Zn | S, Si, Sn | 6×10^{13} | 130,000 | 2×10^{14} | 1.28 |
| | | | | | | 7×10^{14} | 71,000 | 1×10^{14} | 1.34 |
| MOVPE | 0.1-1 | 550-750 | 1-8 | Zn, Cd, Mg | Sn, Se | 5×10^{15} | 30,000 | 6×10^{15} | 1.38 |
| | | | | | | 7×10^{13} | 147,000 | 2×10^{14} | 1.47 |
| | | | | | | 3×10^{13} | 264,000 | 3×10^{13} | 1.41 |
| MBE | $< 1 \times 10^{-8}$ | 350-650 | 0.1-10 | Be, Mg | Si, Sn, S | 6×10^{14} | 34,000 | 3×10^{15} | 1.45 |
| | | | | | | 2×10^{15} | 55,000 | 2×10^{15} | 1.46 |
| MOMBE | $\sim 10^{-7}$ | 350-650 | 0.1-10 | Be, Mg | Si, S | 5×10^{14} | 105,000 | 5×10^{14} | 1.48 |

* - Calculated using the data of Walukiewicz et al. [1.20]

TABLE 1.1 SUMMARY OF THE MAJOR EPITAXIAL GROWTH TECHNIQUES USED FOR InP

review of growth techniques serves to stress that MBE provides the ultimate level of growth control for the fabrication of state-of-the-art microwave and optoelectronic devices. In addition, the unique *in situ* monitoring facilities available with MBE allows a detailed understanding of the growth process to be obtained. A detailed review of the published literature relating to the MBE growth of InP is presented in the next section.

1.4 MOLECULAR BEAM EPITAXY OF INDIUM PHOSPHIDE

Many reviews of the MBE technique have been published [1.49] [1.50] [1.51] [1.52] [1.53] [1.54] which concentrate mainly on the growth of GaAs and GaAlAs. The MBE technique evolved directly from the "three temperature" technique of Gunther [1.55] [1.56] and subsequent UHV-based surface kinetic studies reported by Arthur [1.57]. This latter study established the sticking coefficients for both Ga and As₂ on (100) GaAs and also demonstrated that the growth of stoichiometric GaAs could proceed provided an excess of arsenic was available. Subsequently, Foxon et al. [1.58] extended these studies using modulated beam mass spectroscopy techniques (MBMS), and established the congruent temperature of GaAs under free evaporation as 657°C. Later work by the same authors [1.59] demonstrated that the As₂ and As₄ species are incorporated via first and second order processes respectively and that, in the latter case, the sticking coefficient never exceeds 0.5. The simpler incorporation mechanism associated with the use of the dimer has been shown more recently, as predicted, to give rise to a significant reduction in deep level concentration for GaAs MBE layers, particularly when using lower growth temperatures [1.60] [1.61].

Major experimental challenges exist in the growth of InP by MBE, due primarily to difficulties associated with the safe handling of phosphorus [1.62], the requirements for specialized vacuum pumping, and the thermal instability of InP (congruent temperature ~365°C) under typical MBE growth conditions. In fact, only one review article relating to the MBE growth of InP has been published [1.63], despite its important electronic and optoelectronic applications. The first reported investigation relevant to the MBE growth of InP was the MBMS study of Langmuir and Knudsen evaporation undertaken by Farrow [1.64]. The work demonstrated that, under free evaporation conditions, the congruent temperature of InP is 365°C, while only P₂ and In species were detected in the desorbing beam. This data therefore suggests that the growth kinetics for InP are similar to those of GaAs for which there is a large body of information. Specific aspects of the MBE growth of InP are summarised in the following sections:

Substrate Preparation

Farrow identified InP substrate preparation as being critical for successful epitaxial growth, even in his earliest publication [1.65]. Initial attempts to clean the substrate by simply heating to 300°C for 30 mins *in vacuo* led to the subsequent deposition of polycrystalline layers, an effect attributed to the presence of residual carbon contamination [1.66]. A further paper [1.67] described attempts made to heat clean at temperatures up to 500°C but despite patenting this heat cleaning process for III-V semiconductors [1.68], Farrow in fact used a combined ion bombardment/annealing process to clean substrates in all of his subsequent InP growth experiments. This ion cleaning process involved 2 cycles of 500eV Ar ions at $2\mu\text{Acm}^{-2}$, each followed by a 1hr anneal at 200–250°C [1.69].

Similar ion cleaning techniques were adopted by all other laboratories involved in InP MBE growth [1.70] [1.71] [1.72]. However, by the late 1970's, serious problems had been identified with regard to this ion cleaning process, in particular the generation of an n-type interface layer typically 100nm thick on semi-insulating Fe-doped substrates [1.73], with carrier concentrations as high as $1\times 10^{18}\text{cm}^{-3}$ [1.74]. Furthermore, both Dowsett [1.75] and Cullis [1.76] reported that ion cleaning led to the formation of significant concentrations ($>10^6\text{cm}^{-2}$) of indium microdroplets, each typically 15–50nm across [1.77]. Ion cleaning was hence no longer regarded as an acceptable technique for InP MBE growth applications.

Interest in the heat cleaning process was therefore revived. Davies et al [1.78] developed a modified process whereby the substrates were first etched *ex vacuo* in $\text{H}_2\text{SO}_4:\text{H}_2\text{O}_2:\text{H}_2\text{O}$ (7:1:1) and then subsequently heated to $\sim 500^\circ\text{C}$ *in vacuo* in order to induce oxide desorption. This procedure was found to reduce interface carbon contamination to below the Auger detection limit ($<0.1\%$). Davies' initial experiments in fact used As_4 to stabilise the InP surface during the heat cleaning process, but subsequent work by Roberts et al [1.79] showed that the same level of cleanliness could be achieved using a P_2 beam. This latter process has now become the standard InP cleaning procedure for MBE growth applications [1.80] [1.81].

Phosphorus Sources

A number of different source materials have been used to generate a phosphorus beam for the MBE growth of InP. In the earliest experiments, Farrow [1.65] used polycrystalline InP as a source of P_2 . However, whilst the use of InP overcomes safety difficulties associated with the use of an elemental source, serious growth

control problems arise due to unpredictable fluctuations in the group V flux [1.63]. More recent studies have therefore tended to concentrate on the use of elemental phosphorus. For example, McFee et al. [1.82] used red phosphorus to provide a tetramer source. However, the tetramers redeposit in the form of white phosphorus [1.83] and present a considerable safety hazard whenever the MBE machine is vented to atmosphere [1.62].

Most laboratories have therefore adopted the use of phosphorus dimers for InP growth. This species offers the advantage that it condenses as a form of red phosphorus which possesses a significantly lower ($\times 10^3$) vapour pressure than white phosphorus so that the safety risks involved when venting the MBE machine are much reduced. An additional benefit to be derived from the use of the dimer relates to the expected reduction in the concentration of deep levels and the more efficient incorporation referred to earlier in section 1.3.

The most common dimer source, which utilizes a thermal "cracking cell" [1.84], was demonstrated by Neave et al. [1.85] for the generation of As_2 from As_4 and subsequently used by Roberts et al [1.79] for the growth of InP from In and P_2 . Tetramers generated from elemental phosphorus contained in the lower temperature ($\sim 350^\circ C$) zone of this cell are subsequently dimerised on passage through a second high temperature ($\sim 900^\circ C$) region. A "cracker cell" was used throughout the present study†.

Growth Temperature

Previously reported studies of the MBE growth of InP have tended to concentrate on the use of (100) substrates, since growth on both (111)A and (111)B surfaces gives rise to significant faceting [1.82]. Single-crystal (100) InP layers have been successfully grown over a substrate temperature range from 110 to $650^\circ C$, and a surprisingly wide range of optimum growth temperatures (spanning the range from 350 – $580^\circ C$) have been reported [1.90] [1.80]. In many cases, the phosphorus source directly affects the data obtained; for example, the minimum growth temperatures at which single crystal InP can be grown using either a tetramer or a dimer source (for

†Footnote:

A number of laboratories [1.86] [1.87] [1.88] have reported the use of phosphine as an alternative group V source. The use of a gaseous source offers a number of important advantages relating, particularly to flux stability and source replenishment, and has also been shown [1.89] to produce high mobility material ($\mu_{77K} \sim 105,000 \text{cm}^2 \text{V}^{-1} \text{s}^{-1}$). This technique is further discussed in chapter 5.

a nominally identical growth rate) are 350°C [1.73] and 110°C [1.90] respectively. This difference can be understood, in part, on the basis that insufficient thermal energy is provided to dissociate the tetramer when using low substrate temperatures.

Unintentionally Doped Purity

Table 1.2 summarises the published electrical data for InP MBE layers, including data reported since the conclusion of the current project. The data has been processed using the analysis of Walukiewicz [1.20] to derive values for the total ionised impurity concentration (N_D+N_A).

It is evident from the results that all MBE layers grown prior to the present investigation (i.e. before 1982) were n-type with residual impurity concentrations lying in the range from 10^{16} to 10^{17}cm^{-3} . The highest mobility MBE layer grown prior to 1982 was that reported by Sullivan et al. [1.45] which exhibited a 77K value of $34,000\text{cm}^2\text{V}^{-1}\text{s}^{-1}$. However, the data obtained from this layer is particularly noteworthy in view of the very significant reduction in carrier concentration "freezeout" ($\times 20$) observed on cooling the Hall sample to 77K (Table 1.2). Sullivan [1.45] accounted for this effect on the basis of the presence of a high concentration of oxygen impurity-induced deep donor levels in the layer. However, no supportive data was presented and, furthermore, the result could not be reproduced [1.97]. One explanation which was not considered by Sullivan was the presence of a varying carrier concentration as a function of thickness through the layer. Such a variation can also produce significant carrier freezeout on cooling to 77K, as shown in Appendix A4. Unfortunately, no electrical profile data was recorded by Sullivan [1.97] and hence it is impossible to accurately model his particular result. However, since the layers were grown on ion cleaned substrates, it is likely that a thin, highly-doped n-type layer ($\sim 1 \times 10^{18}\text{cm}^{-3}$ [1.98]) would have been present at the substrate/epitaxial layer interface in his samples. Assuming such a presence, the parallel layer conduction model (Appendix A4) would predict the observed experimental behaviour.

In more recent work, Tsang [1.80] reported the growth of InP layers with much lower residual carrier concentrations ($(N_D-N_A) \sim 5 \times 10^{14} - 5 \times 10^{15}\text{cm}^{-3}$). However no mobility data was presented and hence the degree of carrier compensation is unknown. Furthermore, even at the time of writing, only two further reports [1.46] [1.95] exist of the MBE growth of InP possessing residual donor concentrations less than 10^{16}cm^{-3} . The success achieved in both of these later studies has, however, arisen as a direct consequence of the work described in the present thesis and references [1.94] [1.99].

| AUTHOR [AFFILIATION] | HALL (300K) (conc) {3} (mobility){4} | HALL (77K) (conc) {3} (mobility){4} | N_D+N_A (77K) {5} (conc) {3} | C-V DATA (conc) {3} | GROWTH TEMP. | PHOSPHORUS SOURCE | IN VACUO PREP. | REFERENCE |
|-------------------------|---|--|--------------------------------------|---------------------------|-----------------|--|-------------------|-----------|
| MILLER [BELL] | $1-5 \times 10^{16}$ 2,000-3,500 | | | | 410°C | RED P 6N's [Tetramers] | Ar ion | 1.70 |
| FARROW [R.S.R.E.] | 1×10^{17} 1,500-2,000 | | | | 390°C | InP [Dimers] | Ar ion {1} | 1.69 |
| MILLER [BELL] | | 5×10^{15} 20,000 | 1×10^{16} | | 510°C | | Ar ion {2} | 1.91 |
| KAWAMURA [N.T.T.] | 2×10^{16} 3,000 | 1×10^{16} 7,000 | 5×10^{16} | | 450°C | RED P. 6N's [Tetramers] | Ar ion | 1.71 |
| NORRIS [GLASGOW] | $\sim 10^{16}$ 3,000 | $\sim 10^{16}$ 9,250 | 3×10^{16} | | 100 - 405°C | POLY InP $n \approx 3 \times 10^{15}$ [Dimers] | Ar ion | 1.90 |
| ROBERTS [P.R.L.] | 3×10^{16} 3,500 | 3×10^{16} 11,200 | 4×10^{16} | | 430 - 500°C | RED P. [Dimers] | Heat 500°C | 1.79 |
| SULLIVAN [GLASGOW] | $1-5 \times 10^{16}$ 3,000 | 7×10^{14} 34,000 | 3×10^{15} | | 310 - 360°C | POLY InP $n \approx 8 \times 10^{15}$ [Dimers] | Ar ion | 1.45 |

TABLE 1.2a SUMMARY OF THE PUBLISHED DATA ON THE MBE GROWTH OF UNINTENTIONALLY DOPED InP

| AUTHOR [AFFILIATION] | HALL (300K) (conc) {3} (mobility){4} | HALL (77K) (conc) {3} (mobility){4} | $N_D + N_A$ {5} (77K) (conc) {3} | C-V DATA (conc) {3} | GROWTH TEMP. | PHOSPHORUS SOURCE | IN VACUO PREP. | REFERENCE |
|-------------------------|---|--|--|--|-----------------|-------------------------------|------------------------|-----------|
| ASAHI [N.T.T.] | 1×10^{16} 3,000 | 2×10^{16} 8,000 | 5×10^{16} | 10^{16} | 450°C | RED P. 6N's [Tetramers] | Ar ion | 1.92 |
| TSANG [BELL] | | | | 5×10^{14} - 5×10^{15} | 450 - 650°C | RED P. 6N's [Dimers] | Heat | 1.80 |
| CHOW [VARIAN] | 7×10^{15} 2,000 | 1×10^{16} 12,250 | | | 240 - 450°C | PHOSPHINE 5N's [Dimers] | Heat 500°C 2 min | 1.87 |
| KAWAMURA [N.T.T.] | $1 - 2 \times 10^{16}$ 3,000 | | | | 450°C | RED P. 6N's [Tetramers] | Heat 480°C 1 min | 1.81 |
| PANISH [BELL] | 1.6×10^{16} 2,600 | | | | 450 - 600°C | PHOSPHINE [Dimers] | Heat 600°C | 1.93 |
| MARTIN [GLASGOW] | 2.5×10^{16} 3,300 | 1.5×10^{16} 13,300 | 2×10^{16} | $1 - 2 \times 10^{16}$ | 450 - 550°C | RED P. 6N's [Dimers] | Heat 500°C | 1.94 |
| KAWAGUCHI [N.T.T.] | | 9×10^{13} 105,000 | 3×10^{14} | | 500°C | PHOSPHINE | | 1.89 |

TABLE 1.2b SUMMARY OF THE PUBLISHED DATA ON THE MBE GROWTH OF UNINTENTIONALLY DOPED InP

| AUTHOR [AFFILIATION] | HALL (300K) (conc) {3} (mobility){4} | HALL (77K) (conc) {3} (mobility){4} | N_D+N_A (77K) (conc){3} | C-V DATA (conc) {3} | GROWTH TEMP. | PHOSPHORUS SOURCE | IN VACUO PREP. | REFERENCE |
|-------------------------|---|--|---------------------------------|---------------------------|--------------------|----------------------|---|-----------|
| ROBERTS [SHEFFIELD] | | 2×10^{15} 55,000 | 2×10^{15} | | 630°C indicated | RED P. [Dimers] | Heat 670°C indicated | 1.46 |
| AIRAKSINEN [GLASGOW] | $2-4 \times 10^{15}$ 3,500 | 30,000 | 5×10^{15} | | | RED P. [Dimers] | Heat 530°C | 1.95 |
| MARUNO [MITSUBISHI] | 2×10^{16} 3,260 | 1.3×10^{16} 21,200 | 1.5×10^{16} | | 250 - 490°C | P ⁺ IONS | P ⁺ ions 100eV,110uA 10min@200°C | 1.96 |

NOTES:

- {1} 2X: 500eV $2 \mu\text{Acm}^{-2}$ + 1hr 200-250°C
- {2} 5 min at 365°C, 5kV $5 \mu\text{Acm}^{-2}$ + 1hr at 365°C
- {3} Carrier Concentrations: cm^{-3}
- {4} Mobilities: $\text{cm}^{-2}\text{V}^{-1}\text{s}^{-1}$
- {5} Calculated using the data of Walukiewicz et al [1.20]

TABLE 1.2c SUMMARY OF THE PUBLISHED DATA ON THE MBE GROWTH OF UNINTENTIONALLY DOPED InP

Dopants

A wide range of both n and p type dopant species have been used in InP MBE growth studies, as summarised in table 1.3. In all cases, the lower limit of intentional doping, typically $5 \times 10^{16} \text{cm}^{-3}$, has been limited by the background purity level.

In the case of n-type doping, Sn and Si have been the most commonly studied species [1.79] [1.97] [1.100] and have been found to produce well behaved doping over the carrier concentration range 10^{17}cm^{-3} to 10^{19}cm^{-3} .

In contrast, the behaviour of p-type dopants has been found to be much less predictable. The successful use of Be to produce hole concentrations in the range 10^{17}cm^{-3} to 10^{19}cm^{-3} has been reported by Kawamura [1.81], but both Park [1.101] and Kerr [1.102] have subsequently reported problems associated with this dopant species. Park [1.101] reported the incorporation of Be to levels as high as $2 \times 10^{19} \text{cm}^{-3}$ but nevertheless found that all such layers exhibited n-type behaviour. In contrast, Kerr [1.102] reported the successful growth of p-type layers but found that the measured hole concentrations were unrelated to the Be source temperature.

The use of both magnesium [1.73] and manganese [1.73] [1.103] have also been studied. Whilst Mg was found to dope successfully to levels higher than 10^{18}cm^{-3} , serious problems with reproducibility and layer morphology were encountered. In contrast, Mn has been found to be active only at less than 1 part per 100 due to the formation of deep levels [1.73]. In addition, Asahi et al. [1.103] reported the Mn incorporation to be a complex function of growth conditions, resulting in the formation of both a shallow level 40meV above the valence band and a deeper level 280meV above the valence band. The occupation of these two levels was observed to be dependent on the III:V flux ratio and, under certain growth conditions, the net hole concentration was actually found to be inversely related to the Mn cell temperature. No detailed explanation of this behaviour was presented by Asahi [1.103], although it is interesting to note that the Mn source material used in his work was only 99.995% pure and contained 50p.p.m.a. Mg. For any given cell temperature, Mg will have a vapour pressure at least six orders of magnitude greater than that of Mn. Therefore, since more recent work [1.104] has shown conclusively that Mg forms an acceptor level positioned 37meV below the conduction band of InP, it is possible that the shallow level observed in Asahi's study [1.103] was related to Mg.

| ELEMENT | CONC. RANGE (cm^{-3}) | REFERENCE | COMMENTS |
|---------------|---|-------------------|---|
| <u>n-type</u> | | | |
| Sn | 10^{17} - 2×10^{19} | [1.97] | Twinning at concentrations above $5 \times 10^{18} \text{cm}^{-3}$ |
| | 10^{17} - 10^{18} | [1.79] | $N_A/N_D < 0.2$ |
| Si | 10^{17} - 10^{19} | [1.100] | Well behaved but $N_A/N_D \sim 0.5$ |
| Ge | 10^{18} - 10^{19} | [1.105] | No evidence for p-type behaviour [1.63]. |
| — O — | | | |
| <u>p-type</u> | | | |
| Be | 10^{17} - 10^{19} | [1.73] [1.105] | "Limited success" |
| | 5×10^{17} - 2×10^{19} | [1.101] | All layers n-type |
| | 10^{17} - 10^{19} | [1.81] | Well behaved |
| | 10^{17} - 10^{19} | [1.102] | Hole concentration $\sim 10^{17} \text{cm}^{-3}$ and unrelated to Be source temperature |
| Mg | 10^{16} - 10^{18} | [1.73] | Unpredictable hole concentration and poor morphology at $> 10^{18} \text{cm}^{-3}$ |
| Mn | | [1.73] | Deep level, hole conc. $< 1\%$ of Mn |
| | 2×10^{16} - 2×10^{18} | [1.103] | Hole concentration complex function of growth conditions |

TABLE 1.3
DOPANT SPECIES USED IN THE MBE GROWTH OF InP

1.5 SUMMARY

The device applications of InP and the major epitaxial techniques available for InP growth have been reviewed. Whilst high purity material ($\mu_{77K} > 90,000 \text{ cm}^2\text{V}^{-1}\text{s}^{-1}$) has been grown using LPE, Chloride VPE and MOVPE, solid source MBE is believed to offer the highest level of growth control in terms of layer thickness interface sharpness and *in situ* characterisation etc. for the growth of state-of-the-art device structures. However, prior to the commencement of the present investigation, the highest purity unintentionally doped MBE grown InP possessed a relatively high carrier concentration at 300K of $\sim 10^{16} \text{ cm}^{-3}$ and correspondingly low 77K mobility, $\sim 34,000 \text{ cm}^2\text{V}^{-1}\text{s}^{-1}$. The objective the work described in subsequent chapters was, therefore, to perform a detailed investigation of those factors which influence the purity of MBE grown InP.

The early attempts to grow undoped InP using an existing MBE growth facility are described in chapter 2, and several experimental factors contributing to the serious lack of reproducibility observed at that time are highlighted. Chapter 3 presents full details of a new MBE reactor, purpose-built following the outcome of the preliminary experiments, and discusses the subsequent growth of state-of-the-art InP MBE layers.

Chapter 4 contains a detailed study of sulphur doping of InP MBE layers, and is then followed in chapter 5 by an appraisal of those factors generating background sulphur levels in unintentionally doped layers.

Conclusions and suggestions for further work are given in chapter 6.

CHAPTER 2

PROPERTIES OF UNINTENTIONALLY DOPED InP GROWN IN MBE CHAMBER 1

2.1 INTRODUCTION

2.2 IMPURITY ASSESSMENT OF EARLY InP LAYERS GROWN

2.3 THE PROPERTIES OF EPITAXIAL InP GROWN FOLLOWING MODIFICATIONS TO THE INDIUM CELL

2.4 MORPHOLOGICAL STUDIES OF THE EARLY InP LAYERS GROWN

2.5 SUMMARY OF THE DESIGN WEAKNESSES OF MBE CHAMBER 1

2.6 SUMMARY

2.1 INTRODUCTION

At the start of the present investigation, layers grown using the existing MBE growth facility, under nominally identical conditions, exhibited very significant differences in residual impurity concentration, photoluminescence signature, layer thickness and morphology. It was therefore impossible to achieve any real understanding of the factors limiting epitaxial layer purity, without first identifying the source of this unacceptable variability.

The initial phase of the project consequently involved a detailed and systematic assessment of the existing MBE facility (referred to as Chamber 1 throughout this thesis), and the identification of important design weaknesses which were responsible for the wide range of layer properties observed.

2.2 IMPURITY ASSESSMENT OF EARLY InP LAYERS GROWN

Layer growth rates observed at the outset of this project were very low and unpredictably variable ($0.05\text{--}0.2\mu\text{m hr}^{-1}$) and the maximum epitaxial thickness which could be grown in a typical growth run was less than $1\mu\text{m}$. Electrical measurements attempted on these thin layers were unsuccessful due to problems of high resistance ($>1\text{M}\Omega$) and non-ohmic contacts. On the assumption that surface and interface depletion effects were responsible for the poor contacts [2.01], it was deduced that the residual carrier concentration was less than $\sim 10^{16}\text{cm}^{-3}$.

The only assessment technique readily applicable to these initial layers was therefore 15K photoluminescence (PL). The luminescence spectra obtained from four such layers (TM 39, 49, 50 and 55), grown under nominally identical conditions, are illustrated in figures 2.1 and 2.2 and major differences are immediately evident. In three cases (TM 39, 50 and 55), weak band edge luminescence at $\sim 1.42\text{eV}$ is detected, but all four spectra are dominated by either shallow acceptor transitions ($1.35\text{--}1.4\text{eV}$, f.w.h.m. $30\text{--}100\text{meV}$) or broad (f.w.h.m. $100\text{--}200\text{meV}$) deep level recombinations in the region of $1.1\text{--}1.2\text{eV}$. The specific shallow acceptor(s) present cannot be positively identified because of the broad width of the observed transition(s), although acceptor impurities known to produce transitions in this region are Be, C, Cd, Mg and Zn (Appendix A.5). The recorded deep level recombinations are, however, characteristic of two transition elements, Mn and Fe[2.02].

This data illustrates the inability of PL to identify specific acceptors when impurity

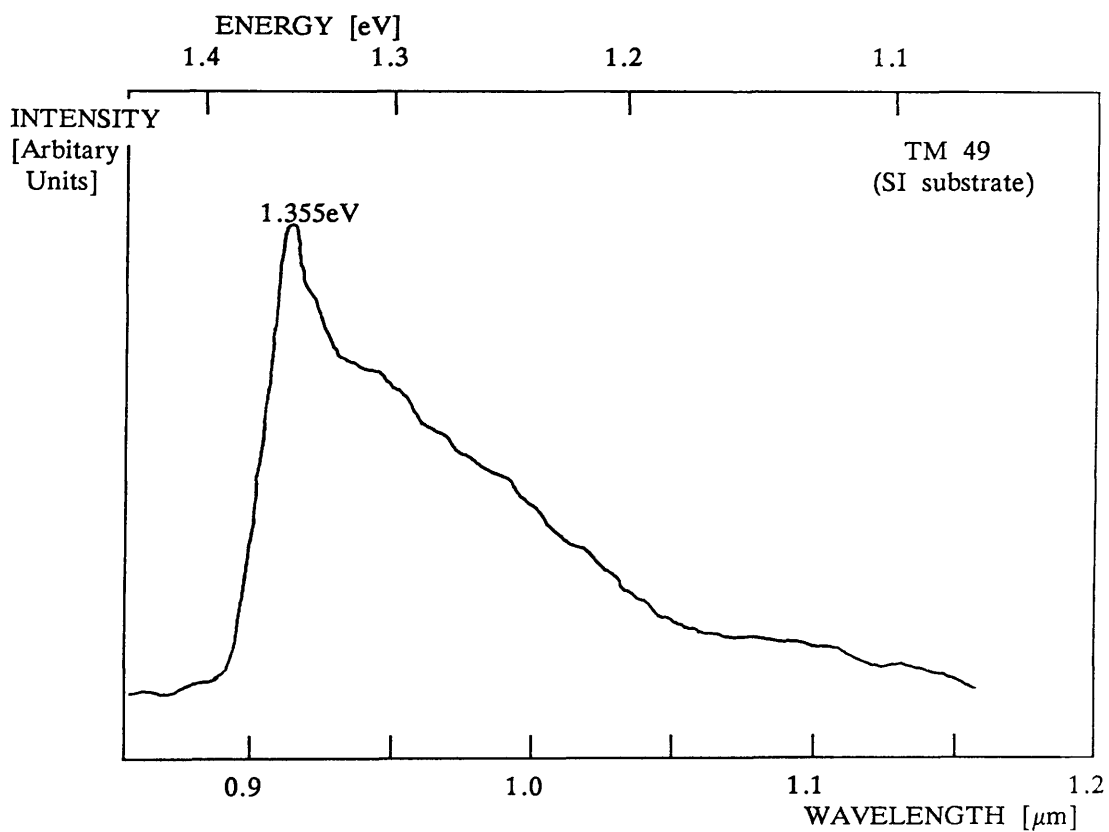
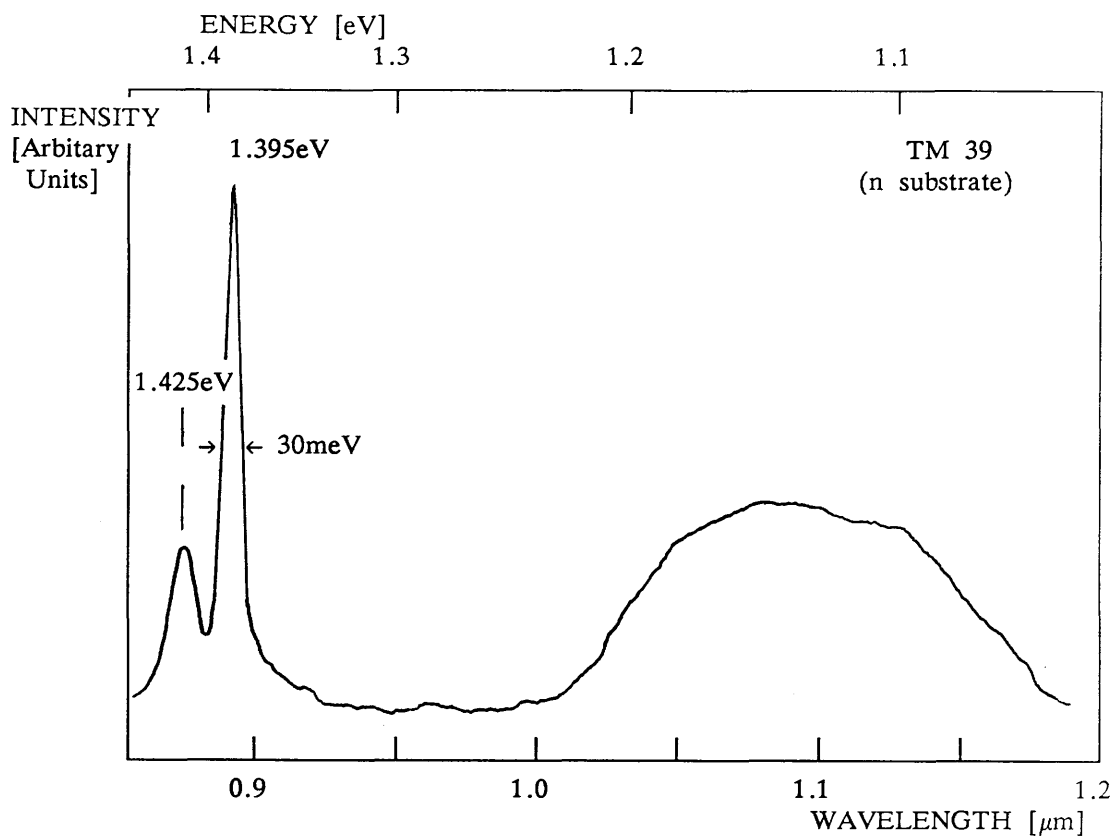


FIGURE 2.1

PHOTOLUMINESCENCE SPECTRA OF LAYERS TM 39 and TM 49

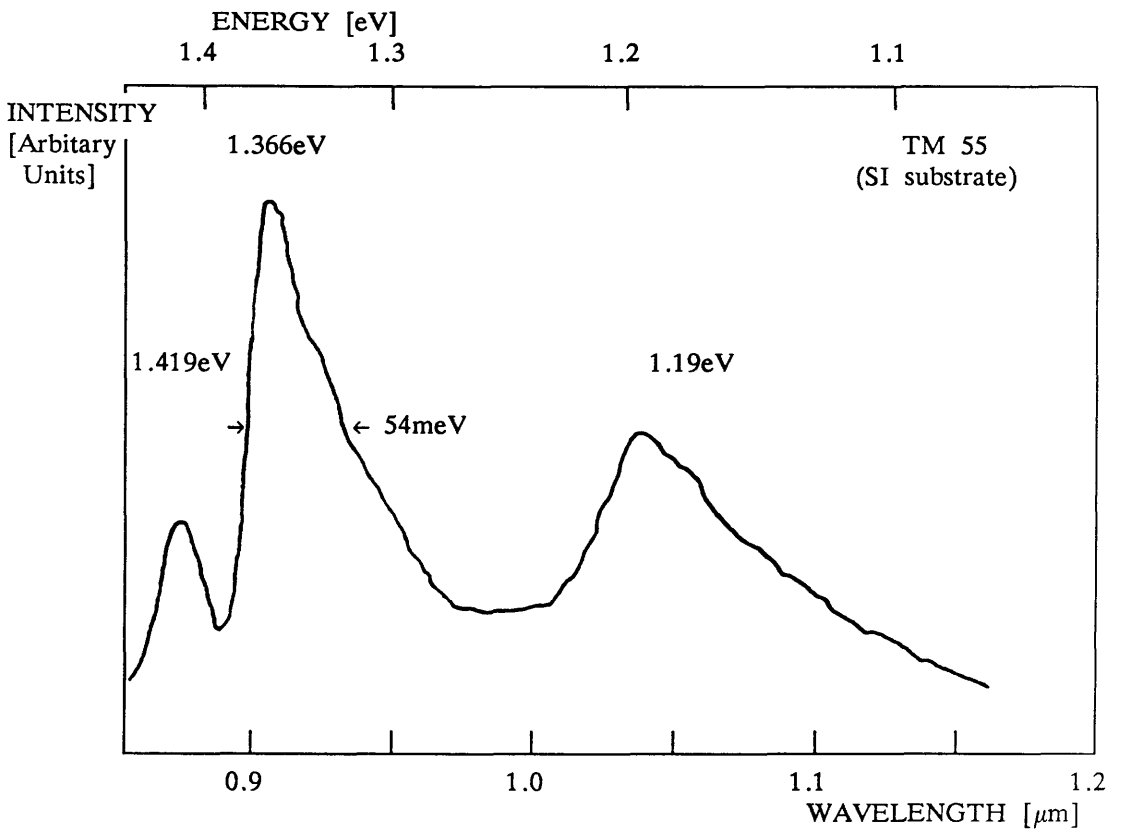
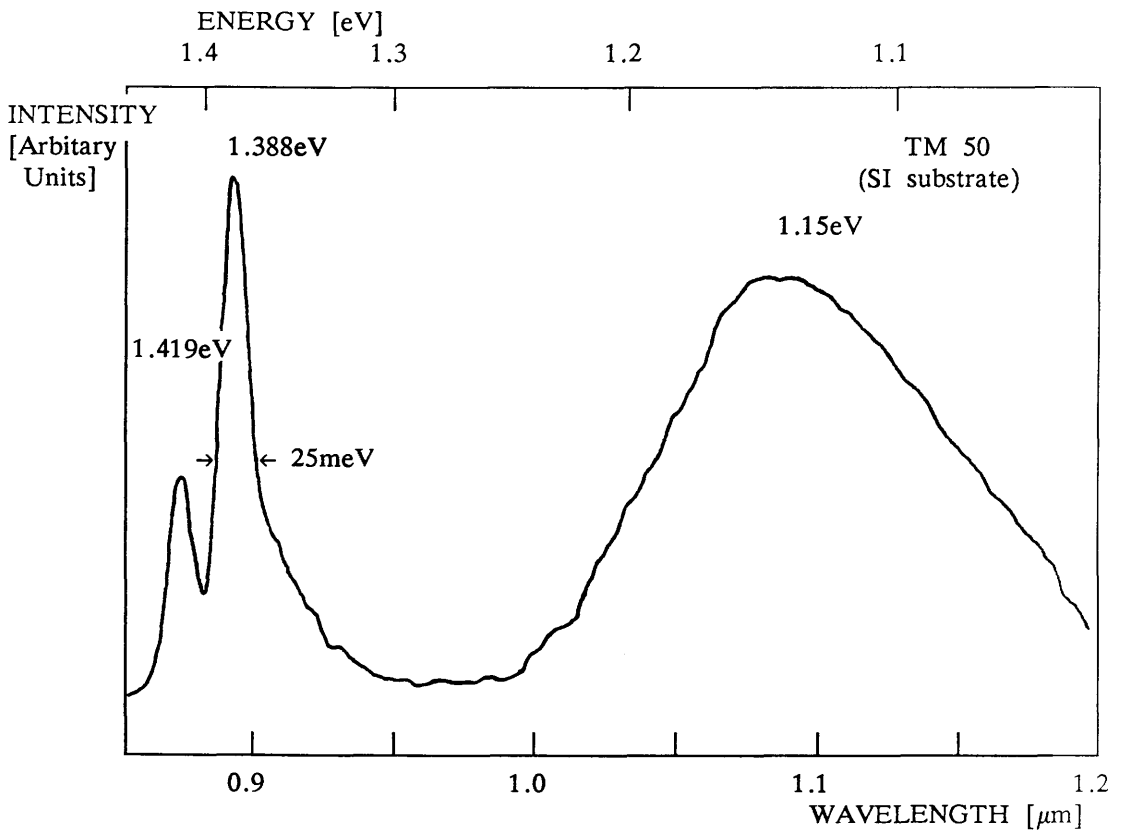


FIGURE 2.2

PHOTOLUMINESCENCE SPECTRA OF LAYERS TM 50 and TM 55

concentrations are high ($>5 \times 10^{15} - 10^{16}$) [2.03] and an alternative assessment technique had to be considered. The most powerful technique capable of providing the required data is Secondary Ion Mass Spectroscopy (SIMS) which can be used to provide quantitative information regarding both the concentration and depth distribution of specific impurities present (Appendix A.2). Arrangements were therefore made, via RSRE Malvern, for SIMS analyses of layers to be performed using facilities at Loughborough Consultants [2.04].

2.2.1 SIMS ANALYSIS

The elements scanned in the initial SIMS study were Mn, Fe, Cr, Al, and Si. Mn and Fe were selected on the basis of the earlier PL data (section 2.2). The presence of Mn and Fe impurities in MBE grown layers, when detected on non Fe-doped substrates (TM 39), can often be attributed to hot ($T > 400^\circ\text{C}$) stainless steel within the UHV growth environment [2.05]. From vapour pressure considerations [2.06] a significant Cr flux would also be expected to be generated by hot steel and Cr was therefore also included in the preliminary SIMS scans. (If incorporated, Cr would not have been observed in the luminescence spectra since the associated recombination is known to occur at 0.85eV [2.07] i.e. beyond the detection limit of the S1 photocathode detector used [2.08]). SIMS scans for Al were performed because of the use of Al_2O_3 components in the evaporation cells. Alumina tubing [2.09] was used to provide electrical isolation between each element of the heater assembly and typically reached temperatures in excess 1000°C during growth. This tubing was therefore a major potential source of impurities. Si SIMS profiles were also included since not only is this element one of the most common residual impurities in InP grown by other techniques [2.10] [2.11] but it is also a constituent of alumina (concentration $\sim 0.5\%$) [2.09].

A summary of the SIMS data recorded for four representative layers (TM 16, 28, 31 and 44) is presented in table 2.1, and indicates that all five of the scanned elements were detected in different layers. Calibrated implant standards (Appendix A.2) were therefore specially prepared for three of the detected elements Fe, Si and Mn, and revealed that Fe and Si concentrations varied within the range $10^{17} - 2 \times 10^{17} \text{cm}^{-3}$ and $10^{17} - 5 \times 10^{18} \text{cm}^{-3}$ respectively. Three of the layers (TM 28, 31 and 44) were also shown to contain Mn at the 10^{17}cm^{-3} level. Calibration standards were not available for Al and Cr, although their presence was verified by a step reduction in counts at the layer/substrate interface. A careful analysis of this data immediately indicated that the differences in impurity concentrations observed for layers TM 16 and 28 reflected a major alteration to the design of the indium cell. Furthermore,

| Element Layer | cm ⁻³ | | | count rate relative to phosphorus | |
|------------------|--------------------|--------------------|--------------------|---|--------------------|
| | Si (28 AMU) | Mn (55 AMU) | Fe (56 AMU) | Cr (52 AMU) | Al (27 AMU) |
| TM 16 | 2×10 ¹⁷ | 3×10 ¹⁵ | 10 ¹⁷ | < 10 ⁻⁵ | 3×10 ⁻⁴ |
| TM 28 | 5×10 ¹⁸ | 10 ¹⁷ | 2×10 ¹⁷ | 2×10 ⁻⁴ | 5×10 ⁻¹ |
| TM 31 | 2×10 ¹⁷ | 10 ¹⁷ | 2×10 ¹⁷ | 10 ⁻³ | 2×10 ⁻³ |
| TM 44 | 4×10 ¹⁷ | 2×10 ¹⁷ | 2×10 ¹⁷ | 10 ⁻⁴ | 8×10 ⁻³ |

All impurity profiles except those of Fe and that of Cr in TM 16 exhibit a lower count rate in the substrate than the epitaxial layer.

TABLE 2.1 SIMS IMPURITY ANALYSIS OF
UNINTENTIONALLY DOPED InP EPITAXIAL LAYERS
GROWN AT THE START OF THE PROGRAMME

since the same batch of indium source material was used in each case, two potential sources of the Mn, Fe and Cr impurities were addressed:

(a) Radiant heating of the stainless steel cryopanel fin adjacent to the mouth of the indium evaporation cell.

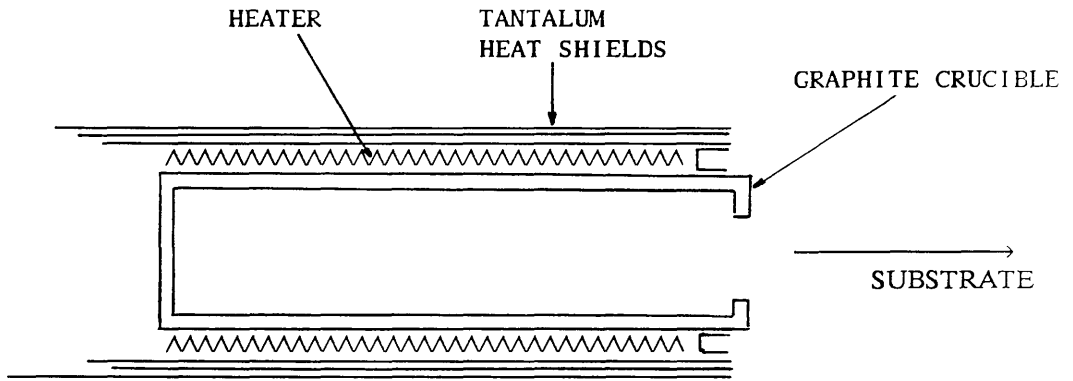
In the growth chamber used (Chamber 1), the area of stainless steel adjacent to the mouth of the group III evaporation cell was cooled by conduction from a liquid nitrogen reservoir, sited some 20mm away. The residual Mn, Fe and Cr impurities detected in the analysed samples could therefore have originated from this stainless steel due to inadequate cooling. Careful measurements of the temperature of this stainless steel fin were consequently performed using a thermocouple clamped in the region where maximum radiant heating was expected. With the indium cell maintained at a temperature well in excess of its normal operating value (1100°C compared to 900°C), the maximum temperature recorded was 150°C, even when no liquid nitrogen cooling was present. Vapour pressure data [2.06] shows that for temperatures of this order, the vapour pressures of Mn, Cr and Fe are less than 10^{-11} mbar and cannot therefore be expected to give rise to the detected levels of these impurities[†].

b) Outgassing of impurities from the components of the indium cell structure.

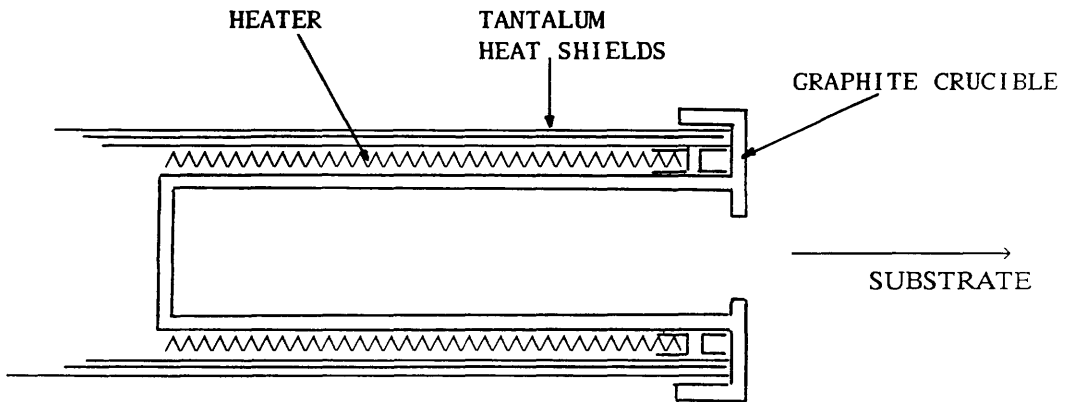
In view of the inability to explain the incorporation of Mn, Fe and Cr due to the presence of regions of hot stainless steel, attention was directed to the indium cell. The cell used at this preliminary stage of the work is shown schematically in figure 2.3a. The front of the cell is seen to be enclosed only by a thin tantalum baffle which is a loose push-fit into the outer radiation shields. Consequently any gap around its outer diameter presents a line-of-sight path for impurities from the heater to the substrate. The cell was therefore modified, as illustrated in figure 2.3b, by combining the use of a new twin baffle assembly and a redesigned crucible. This crucible incorporated a lip which fitted over the outside of the entire cell assembly,

[†]Footnote:

Of the elements Mn, Cr and Fe, Mn is the most volatile with an equilibrium vapour pressure of 10^{-11} mbar at 435°C [2.06]. If the entire Mn flux obtained from a square cm of pure Mn at 435°C was incident on the substrate it would have produced a Mn concentration of $\sim 1 \times 10^{17} \text{cm}^{-3}$. Therefore, when the Mn concentration in stainless steel ($\sim 2\%$ Mn), the separation of the substrate from the fin (~ 10 cm) and the maximum temperature of the fin (150°C) are included, the fin cannot have been the source of the Mn impurity.



(a) Early design with poor shielding of the heater



(b) Modified design incorporating extensive shielding of the heater assembly at the front of the cell

FIGURE 2.3

SCHEMATIC ILLUSTRATING THE IMPROVEMENTS MADE TO THE
INDIUM CELL FITTED IN CHAMBER 1

and therefore eliminated any possibility of direct line-of-sight between the heater and the substrate.

2.3 THE PROPERTIES OF EPITAXIAL InP GROWN FOLLOWING MODIFICATIONS TO THE INDIUM CELL.

Following the cell modifications, both the PL and SIMS analyses immediately indicated a marked and consistent improvement in the purity of the epitaxial layers grown. For example, the photoluminescence signature of the first layer (TM 63) grown with the modified cell (Fig 2.3b) is now dominated by band edge exciton luminescence (Fig 2.4). In addition, the previously observed broad band centred at $\sim 1.1\text{eV}$ is also reduced in intensity (compare figures 2.1, 2.2 and 2.4). Subsequent SIMS experiments (Table 2.2) also confirmed that the concentrations of incorporated Mn, Cr and Fe had been significantly reduced (by approximately an order of magnitude in each case).

This marked improvement in material properties now allowed more systematic growth studies to commence.

2.3.1 ELECTRICAL PROPERTIES

Electrochemical carrier profiles (Appendix A.3) recorded from layers grown following the indium cell modification also revealed a marked change in electrical properties. Unintentionally doped layers were no longer depleted and exhibited clear n-type conduction, with carrier concentrations varying between 10^{16}cm^{-3} and 10^{18}cm^{-3} .

Nevertheless, examples of C-V profiles recorded for layers TM 65, 66, 80 and 81 are illustrated in figures 2.5 and 2.6, and indicate significant variations in residual carrier concentration for layers grown under nominally identical conditions. These variations occurred not only between successive layers (e.g. TM 65-66 and 80-81) but also within single layers (TM 66 and 81) and highlighted the fact that the growth was still not adequately controlled.

The variation in carrier concentration within single layers was considered to be the most significant and can be divided into two distinct categories:

- (a) Large interface spikes with peak concentrations typically two orders of magnitude greater than those present in the epitaxial layer (e.g. layer TM 65, 66 and 80; Figs 2.5 and 2.6). These interface spikes are potentially a

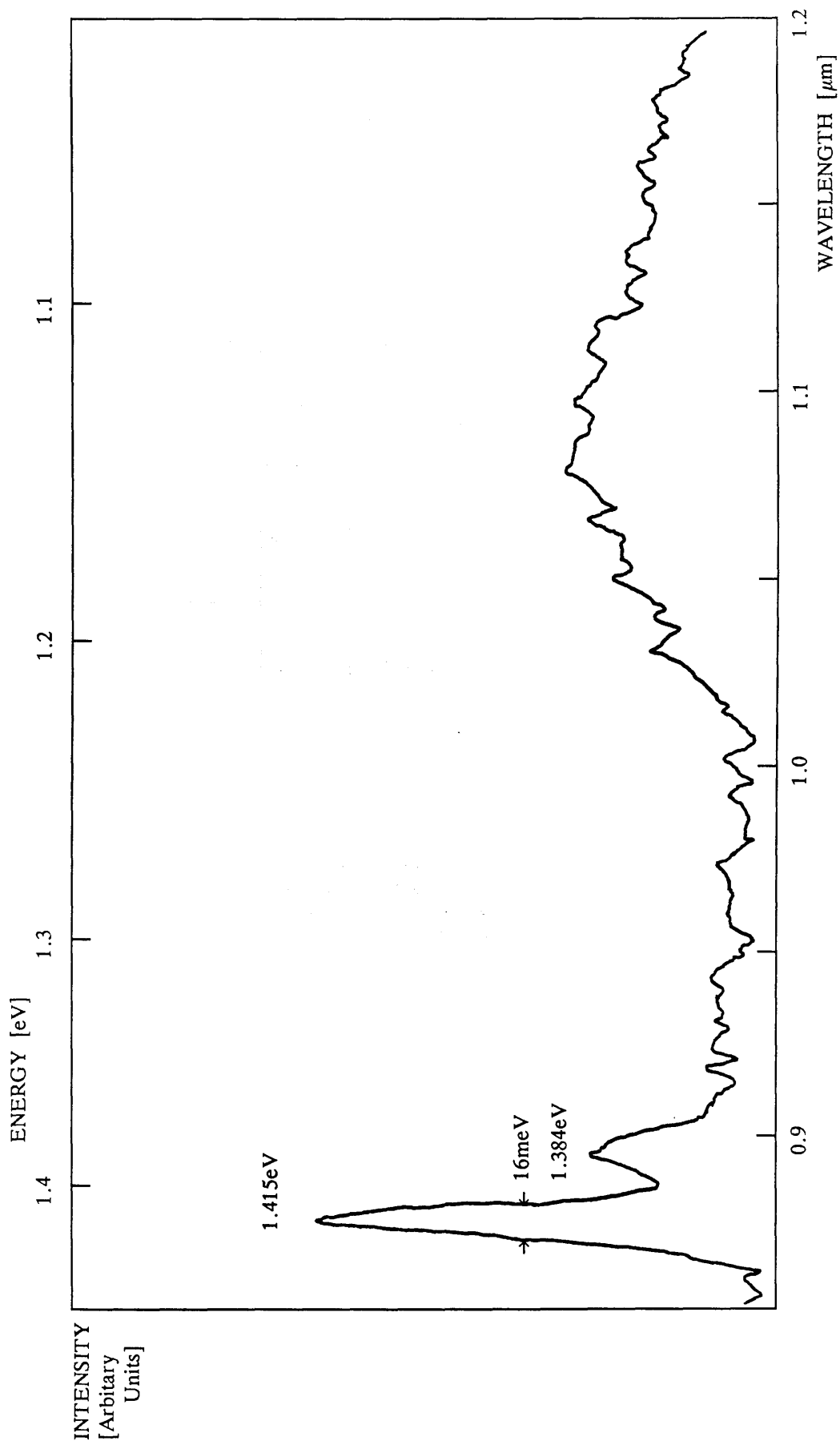


FIGURE 2.4 PHOTOLUMINESCENCE SPECTRUM OF TM 63

| Element Layer | cm ⁻³ | | | count rate relative to phosphorus | |
|------------------|----------------------|--------------------|----------------------|---|---------------------|
| | Si (28 AMU) | Mn (55 AMU) | Fe (56 AMU) | Cr (52 AMU) | Al (27 AMU) |
| TM 62 | < 2×10 ¹⁷ | 2×10 ¹⁶ | < 2×10 ¹⁶ | <7×10 ⁻⁵ | <3×10 ⁻³ |
| TM 63 | < 2×10 ¹⁷ | 2×10 ¹⁶ | < 2×10 ¹⁶ | <6×10 ⁻⁵ | <3×10 ⁻³ |
| TM 64 | < 2×10 ¹⁷ | 2×10 ¹⁶ | < 2×10 ¹⁶ | <5×10 ⁻⁵ | <3×10 ⁻³ |

In the initial SIMS scans the detection limit for Si was limited at $\sim 2 \times 10^{17} \text{ cm}^{-3}$ due to the instrument having previously been used for a study of Si wafers. Profiles for Si performed on these layers subsequently and after the apertures in the SIMS analyser adjacent to the sample had been changed, indicated that the Si levels were actually $< 10^{16} \text{ cm}^{-3}$.

TABLE 2.2

SIMS IMPURITY ANALYSIS OF UNINTENTIONALLY DOPED InP EPITAXIAL LAYERS GROWN USING THE MODIFIED In CELL.

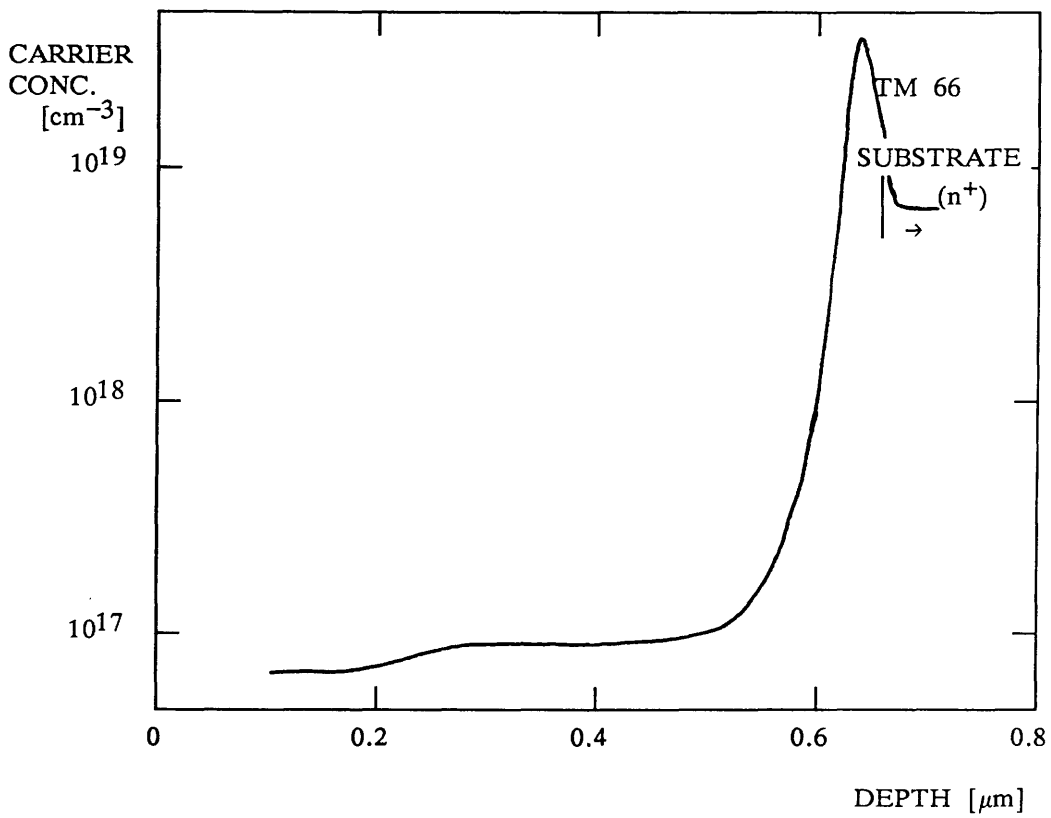
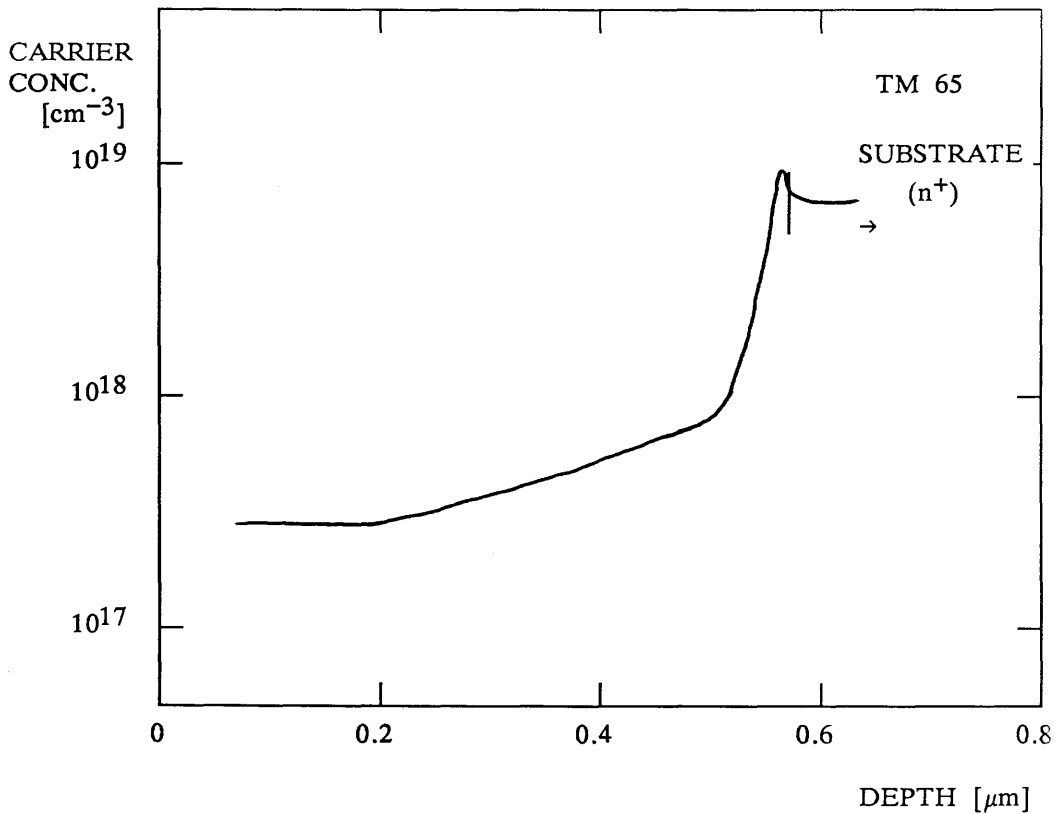


FIGURE 2.5 C-V PROFILES OF TM 65 AND 66

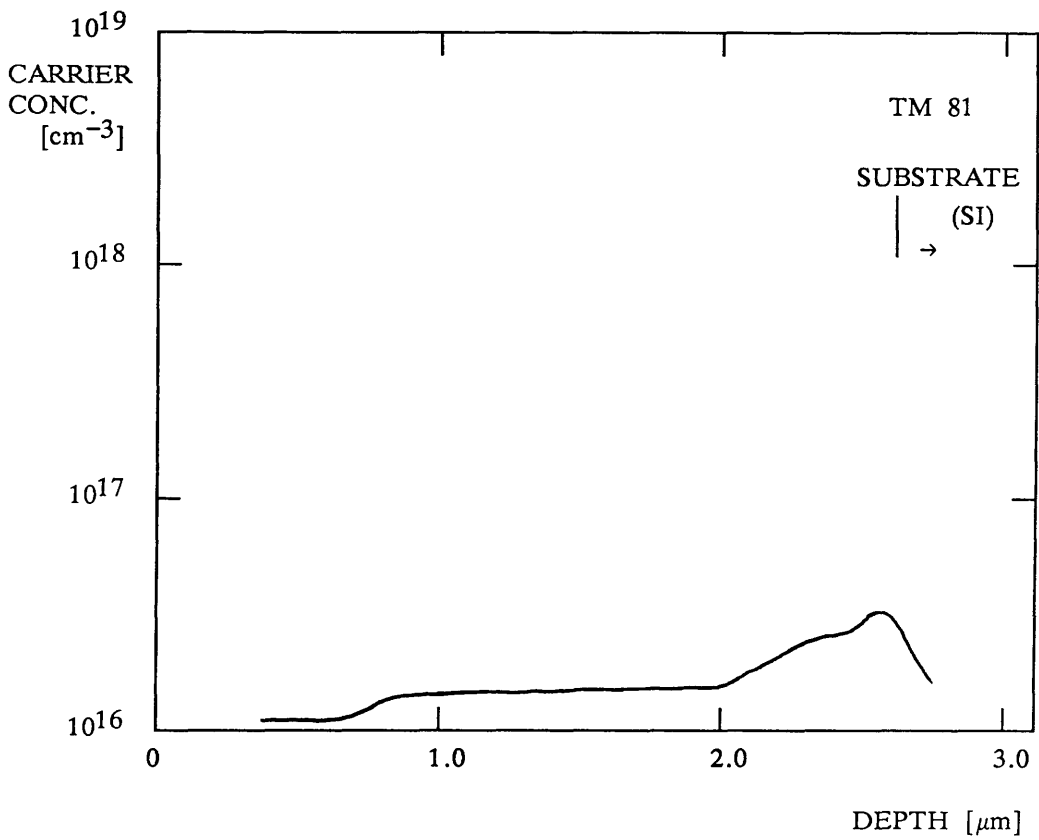
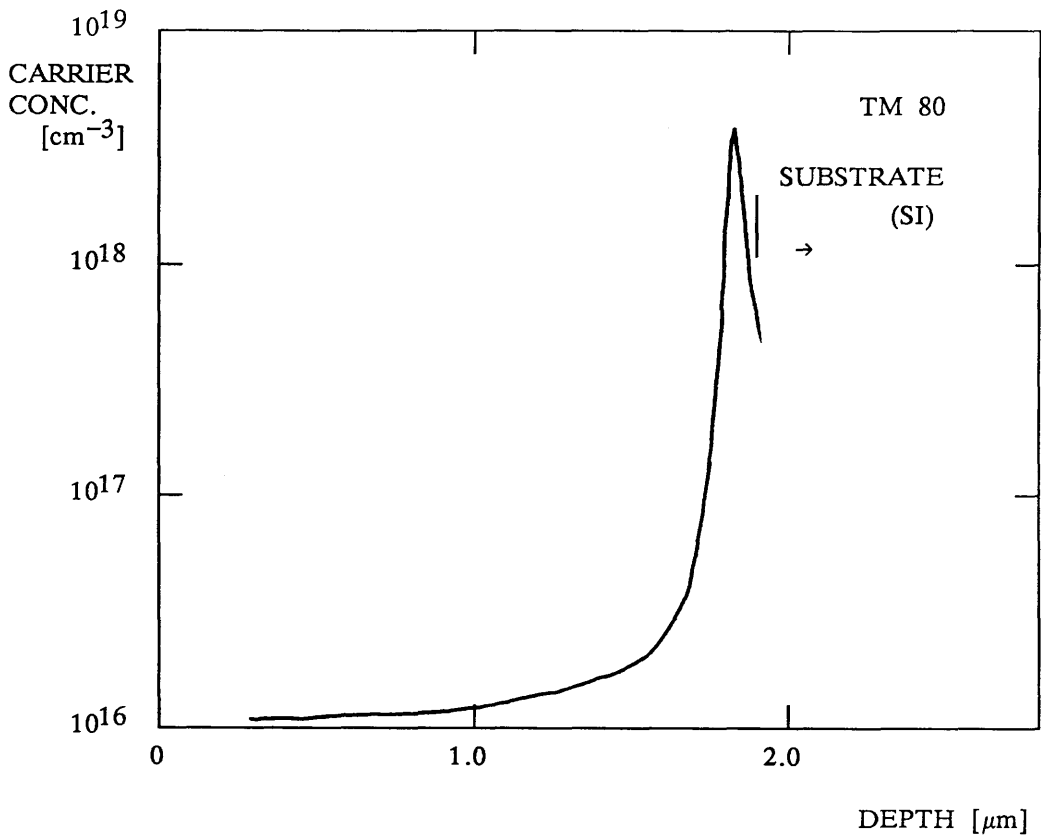


FIGURE 2.6 C-V PROFILES OF TM 80 AND 81

combination of two problems: one associated with the substrate cleaning and the other relating to the growth process. This aspect is discussed later in section 2.4.

(b) Smaller (~30%) steps in the carrier concentration, occurring at apparently random depths through the epitaxial InP layer (e.g. layers TM 66 and 81; Figs 2.5 and 2.6). These changes are related to variations in the concentration of impurities incorporated during growth, as confirmed by the SIMS analysis described in the following section.

2.3.2 SIMS ANALYSIS

The only donor impurity studied in the SIMS experiments discussed in section 2.2 was silicon. However, the Si concentration in layers grown following the modifications to the indium cell had been calibrated (again using the specially prepared implant standard) and found to be $\sim 5 \times 10^{15} \text{cm}^{-3}$. Since this concentration is significantly less than the total donor concentration indicated by the electrical data ($10^{16} - 10^{18} \text{cm}^{-3}$), further SIMS experiments were needed to identify both the additional donor impurity(ies) present and also explain the observed step variations in carrier concentration.

Initial SIMS scans were recorded for two epitaxial layers (TM 75 and 82) in which pronounced step changes in residual carrier concentration had been observed. SIMS profiles were recorded for both the major group IV (Si, Sn) and group VI (S, Se, Te) potential n-type dopant species, and also the transition elements Mn, Cr and Fe, as before. The SIMS data are compared with the corresponding electrical data in figures 2.7 and 2.8.

The SIMS experiments showed that Te, Se, and Sn could not be detected in any of the epitaxial layers (detection limits were $\sim 5 \times 10^{14}$, $\sim 10^{14}$ and $\sim 4 \times 10^{15} \text{cm}^{-3}$ respectively), and thus eliminated them as the dominant donor impurities in the epitaxial layers. However, a clear correlation is observed to exist between the step reductions in carrier concentration (Figs 2.7a and 2.8a) and the recorded SIMS profiles for S and Mn (Figs 2.7b and 2.8b). Subsequent SIMS calibration experiments indicated that S and Mn were present at concentrations of $\sim 2 - 8 \times 10^{16} \text{cm}^{-3}$ and $\sim 1 - 3 \times 10^{16} \text{cm}^{-3}$ respectively. It is therefore concluded that the observed variations in residual carrier concentration can be attributed principally to changes in the sulphur incorporation, with the corresponding variations in Mn acceptor concentration actually acting to reduce the magnitude of the detected carrier change, by compensation.

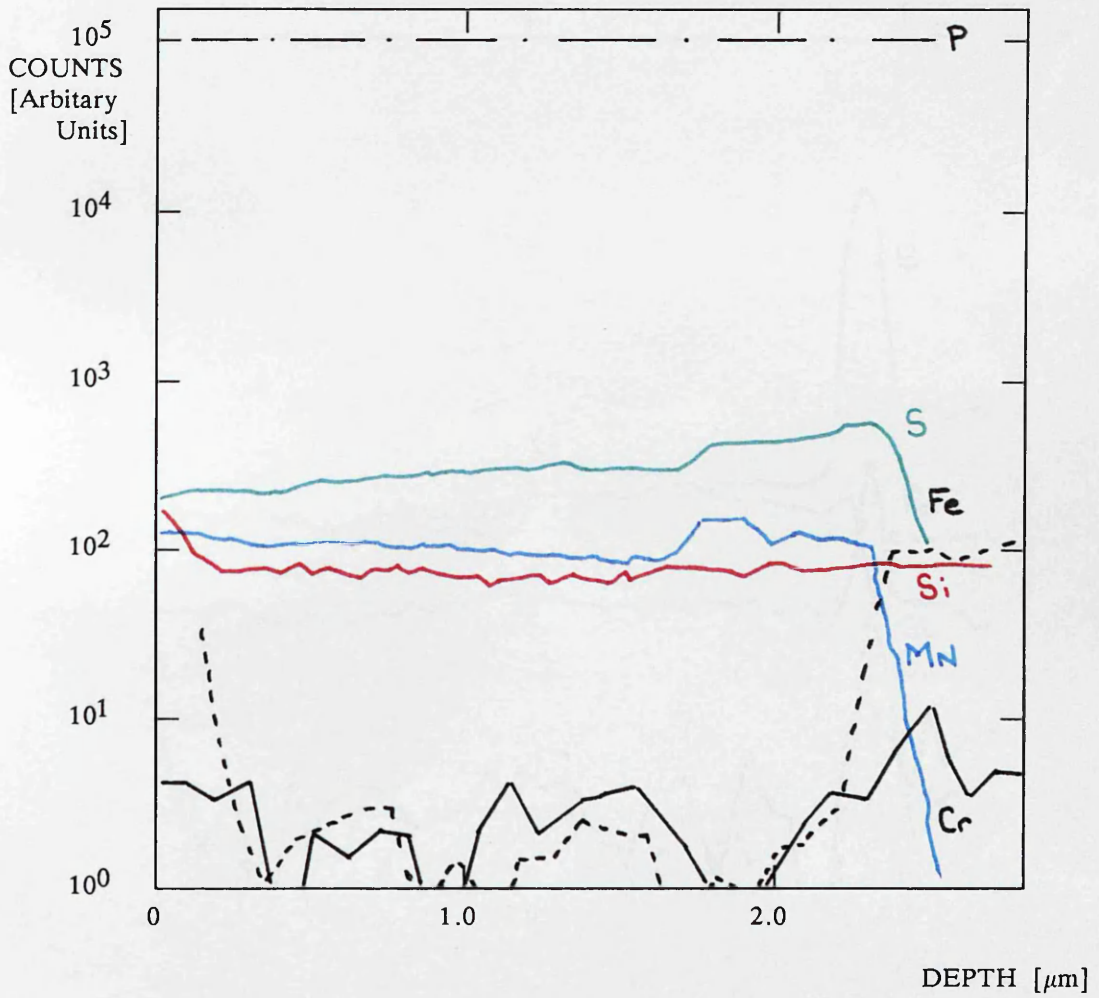
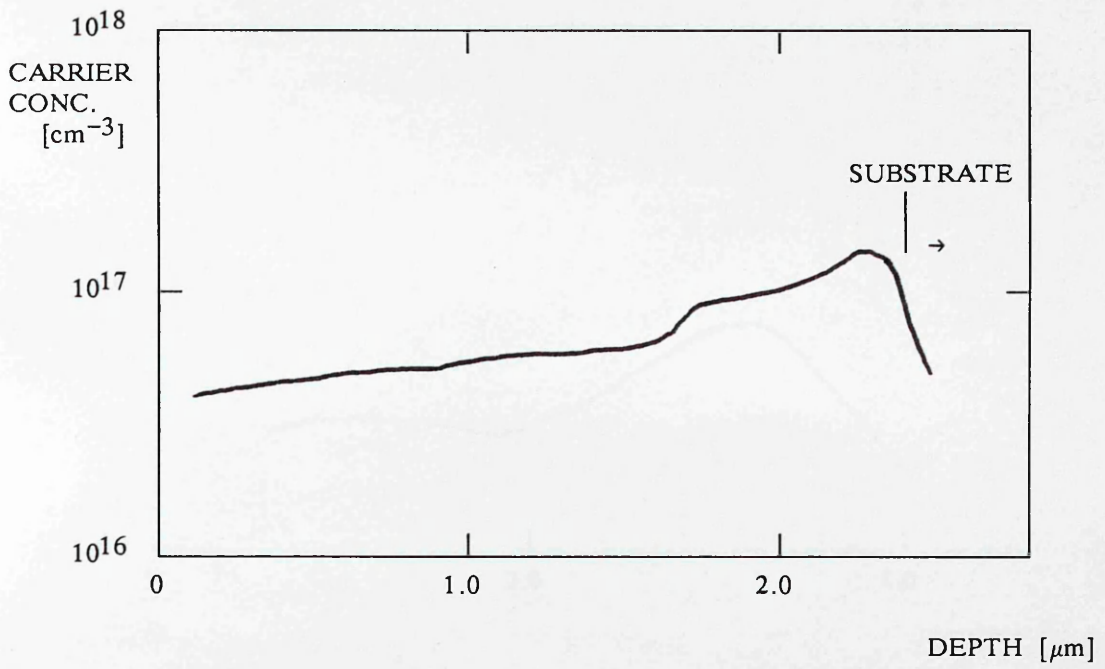


FIGURE 2.7 C-V and SIMS PROFILES OF TM 75

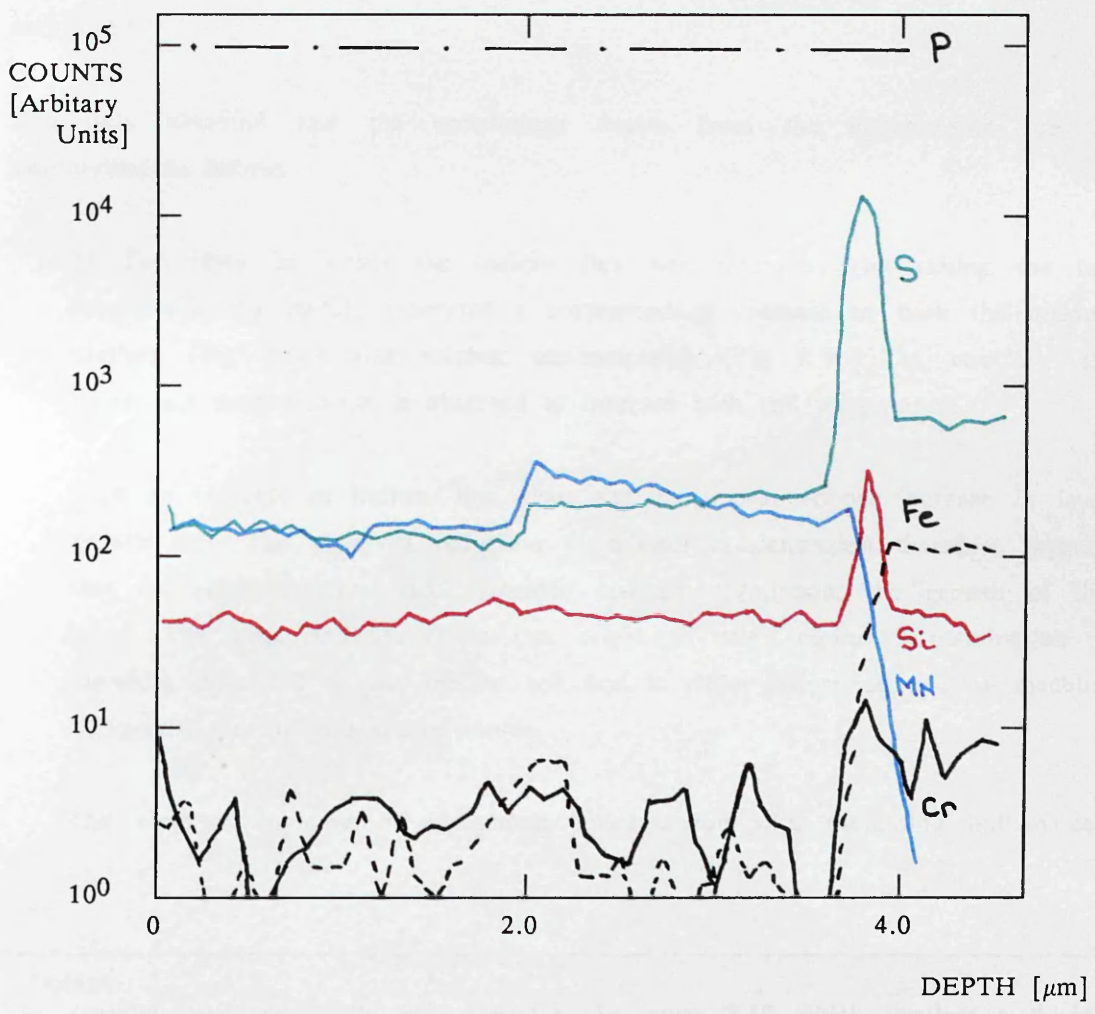
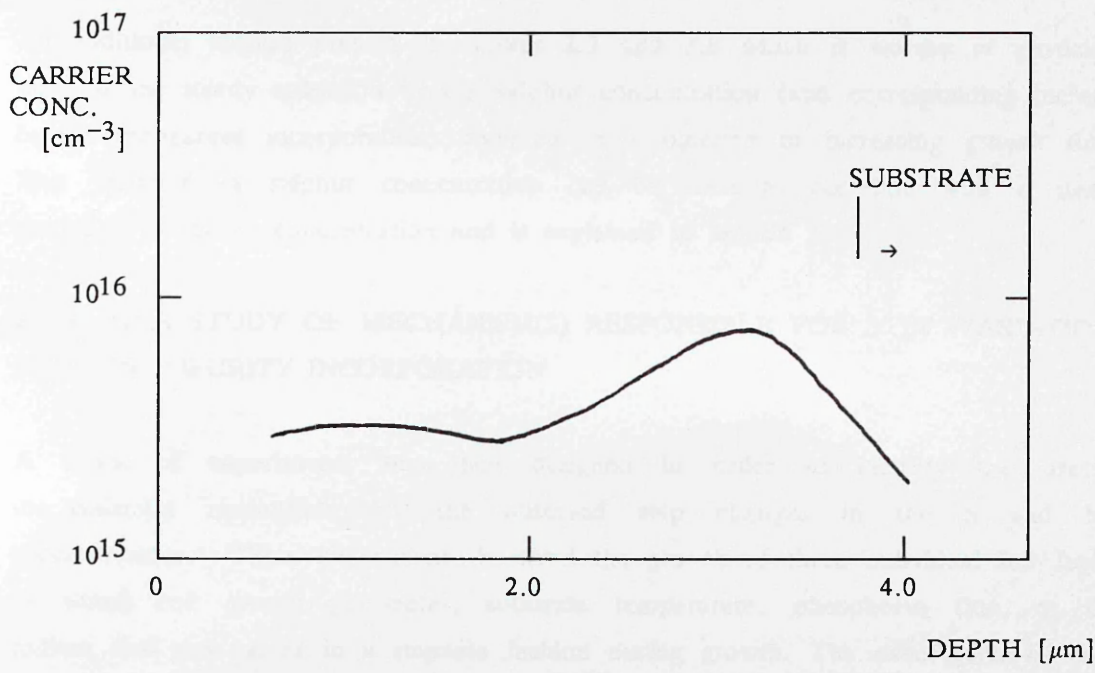


FIGURE 2.8 C-V and SIMS PROFILES OF TM 82

An additional feature present in figures 2.7 and 2.8 which is worthy of particular note, is the steady reduction in the sulphur concentration (and corresponding increase in the manganese incorporation) observed as a function of increasing growth time. This variation in sulphur concentration can be seen to correlate with a steady reduction in carrier concentration and is explained in section 3.5.1.

2.3.3 SIMS STUDY OF MECHANISM(S) RESPONSIBLE FOR STEP VARIATIONS IN IMPURITY INCORPORATION

A series of experiments was then designed in order to identify the precise mechanism(s) responsible for the observed step changes in the S and Mn concentrations. These experiments involved the growth of three individual InP layers in which one growth parameter, substrate temperature, phosphorus flux, or the indium flux was varied in a stepwise fashion during growth. The exact form of each intentional change is illustrated schematically in the lower sections of figures 2.9, 2.10 and 2.11[†].

The data obtained and the conclusions drawn from the experiments can be summarised as follows:

- a) The layer in which the indium flux was increased (by raising the cell temperature by 20°C), generated a corresponding decrease in both the residual carriers (Fig 2.9a) and sulphur concentration (Fig 2.9b). In contrast, the manganese concentration is observed to increase with cell temperature.

Such an increase in indium flux gives rise to a proportional increase in layer growth rate. The observed reduction in sulphur concentration therefore suggests that the sulphur arrival rate remained constant throughout the growth of this layer. The data indicates that the origin of the sulphur contamination is therefore unrelated to the indium cell and is either associated with a machine background or the phosphorus source.

The observed increase in manganese concentration with increasing indium cell

[†]Footnote:

This method, and specifically that illustrated in figure 2.10 which involves a double step and enables the effect of a deliberately introduced change to be readily isolated from both random growth variations and analysis noise, has since been adopted in several other studies directed at identifying specific sources of impurities in MBE grown layers [2.12] [2.13] .

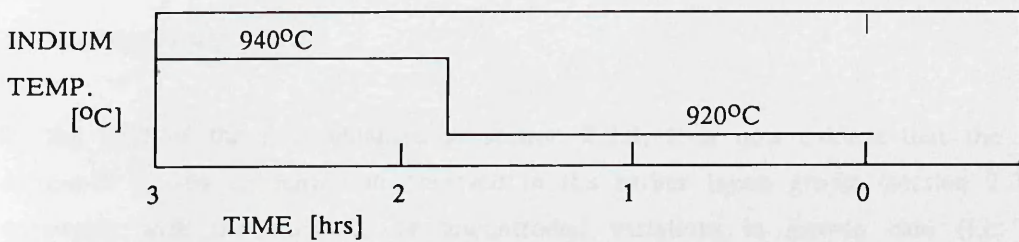
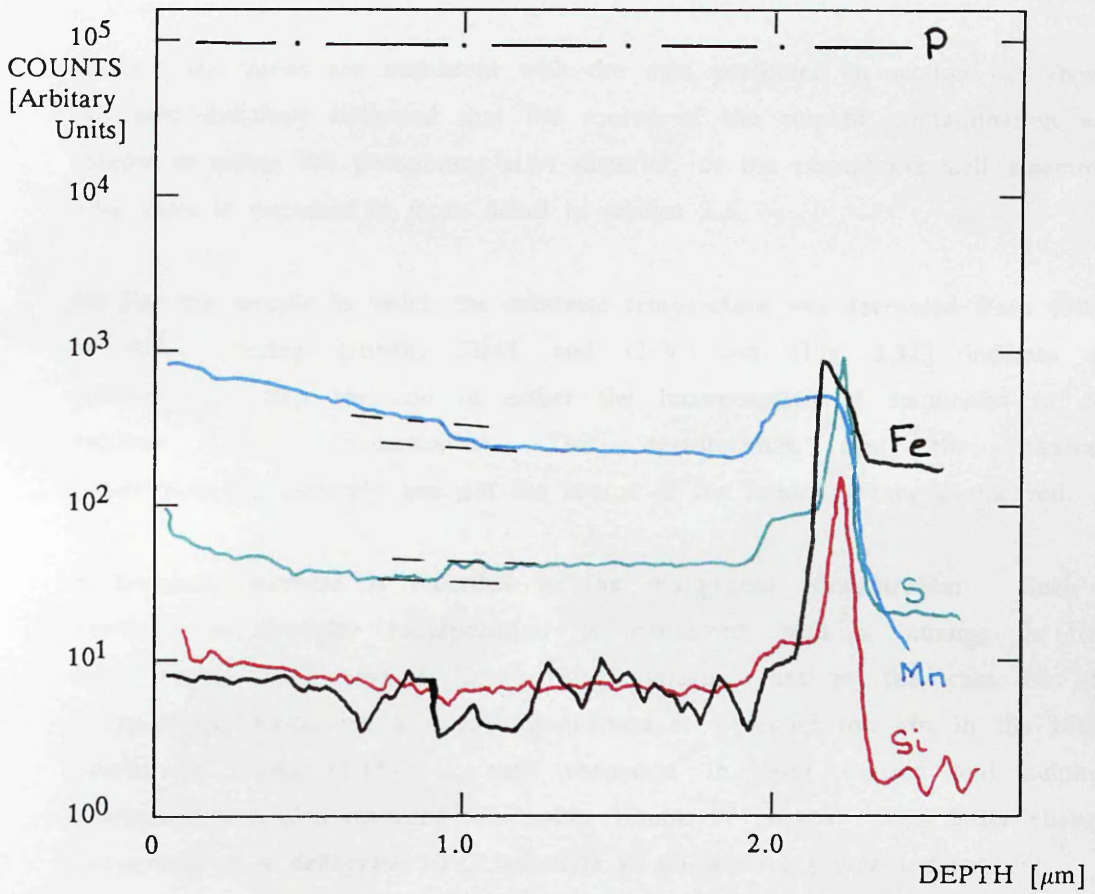
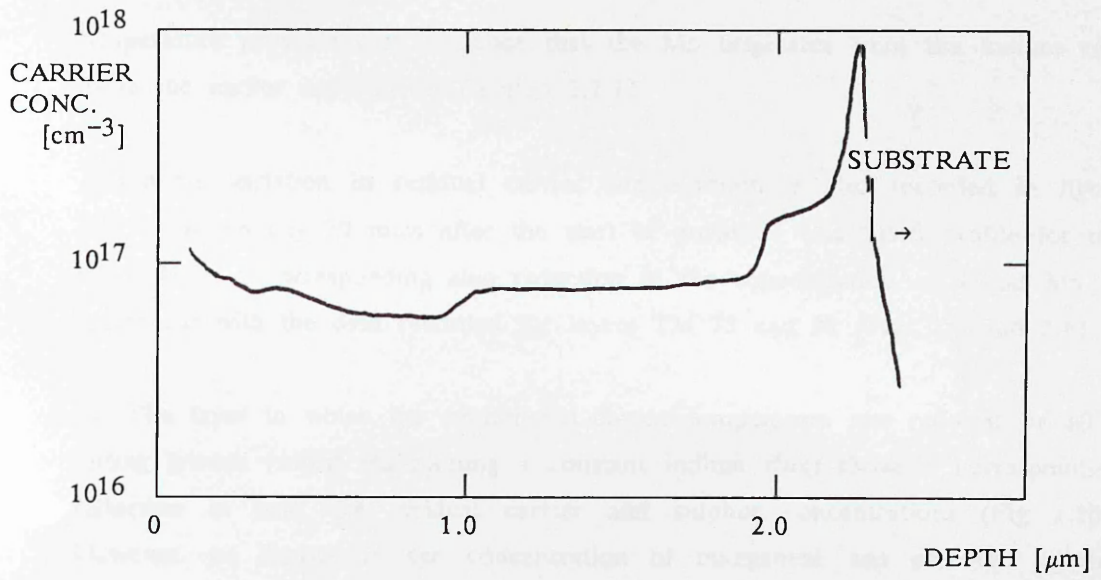


FIGURE 2.9 C-V and SIMS PROFILES OF TM 86

temperature provides firm evidence that the Mn originates from the indium cell, as in the earlier experiments (section 2.2.1).

A random variation in residual carrier concentration is also recorded in figure 2.9, approximately 20 mins after the start of growth. The SIMS profile for the layer shows a corresponding step reduction in the concentration of S and Mn in agreement with the data recorded for layers TM 75 and 82 (Figs 2.7 and 2.8).

(b) The layer in which the phosphorus source temperature was reduced by 10°C during growth (whilst maintaining a constant indium flux) shows a corresponding reduction in both the residual carrier and sulphur concentrations (Fig 2.10). However, no change in the concentration of manganese was observed in this case.

These observations are consistent with the data presented in section (a) above, but now definitely indicated that the source of the sulphur contamination was related to either the phosphorus start material, or the phosphorus cell assembly. This topic is discussed in more detail in section 3.5.

(c) For the sample in which the substrate temperature was decreased from 490°C to 450°C during growth, SIMS and C-V data (Fig 2.11) indicate no corresponding step variation in either the incorporation of impurities or the residual carrier concentration. This demonstrates that the substrate heater/mounting assembly was not the source of the random changes observed.

A transient decrease is recorded in the manganese concentration. Such a transient in impurity incorporation is consistent with a change in the incorporation rate constant [2.14], and indicates that in the case of Mn incorporation occurs via a surface population as observed for Mn in the MBE growth of GaAs [2.15]. A step reduction in both carrier and sulphur concentration is also recorded after $\sim 2\text{hr } 10\text{mins}$ of growth. This latter change corresponds to a deliberate 10°C reduction in phosphorus source temperature.

2.3.4 SUMMARY

In the light of the data obtained in section 2.3.3, it is now evident that the random variations in Mn concentration observed in the earlier layers grown (section 2.3.1) are consistent with the existence of uncontrolled variations in growth rate (i.e. indium flux). The observed corresponding changes in sulphur and residual carrier

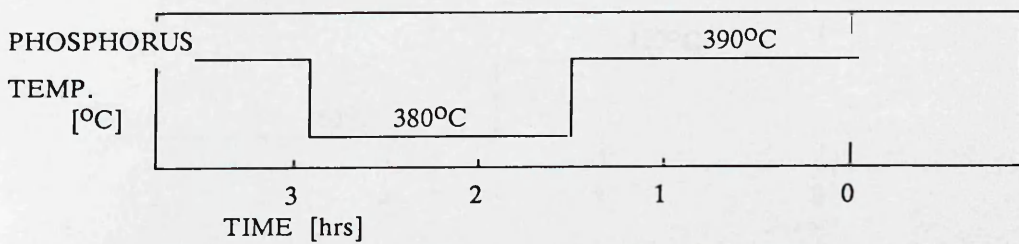
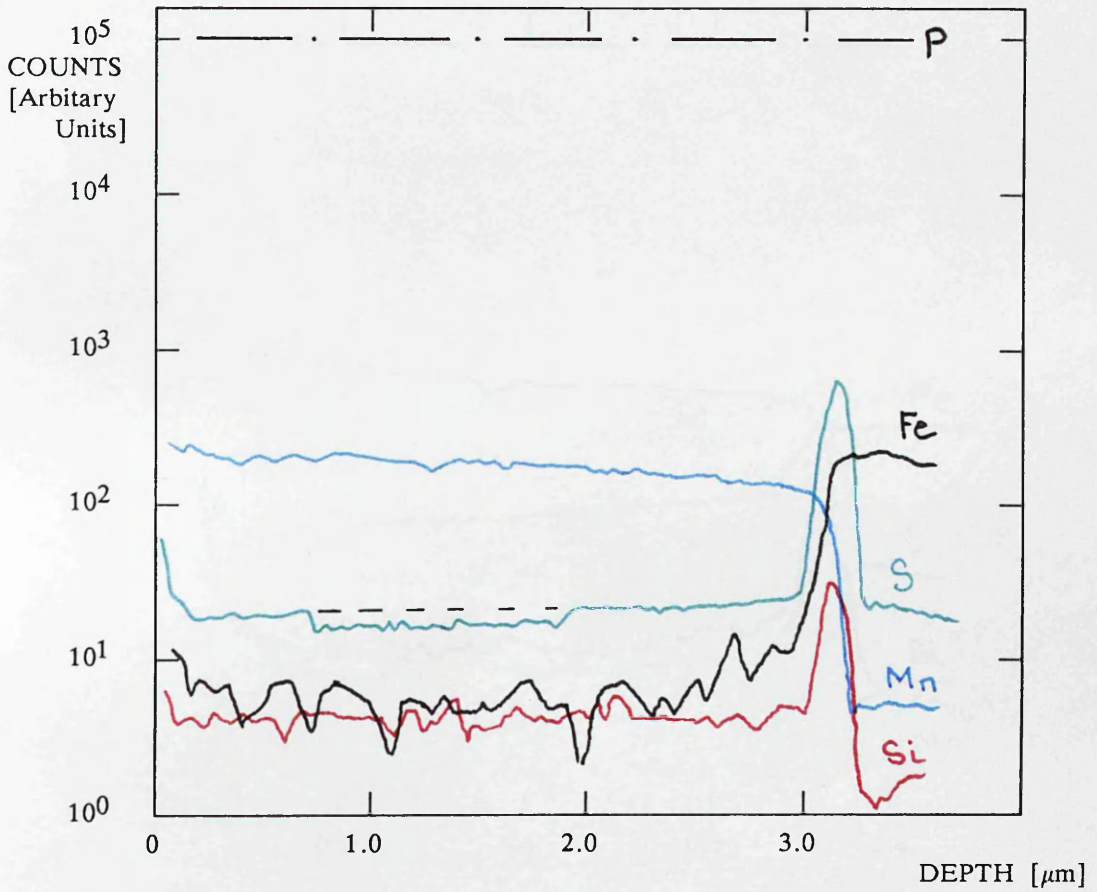
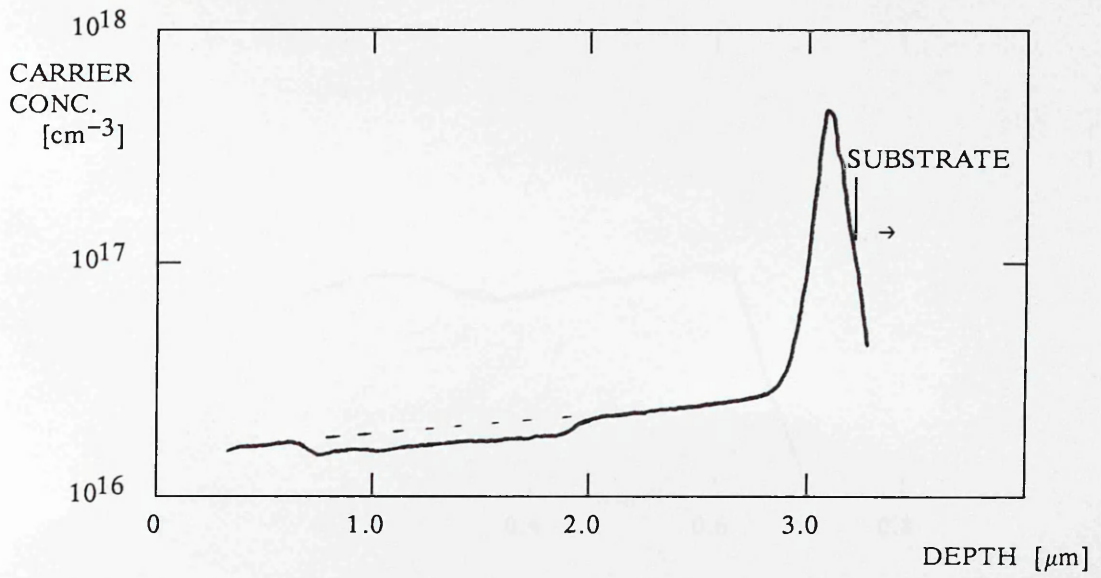


FIGURE 2.10

C-V and SIMS PROFILES OF TM 84

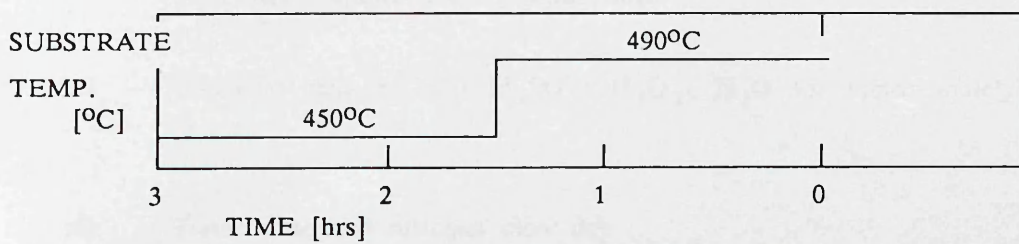
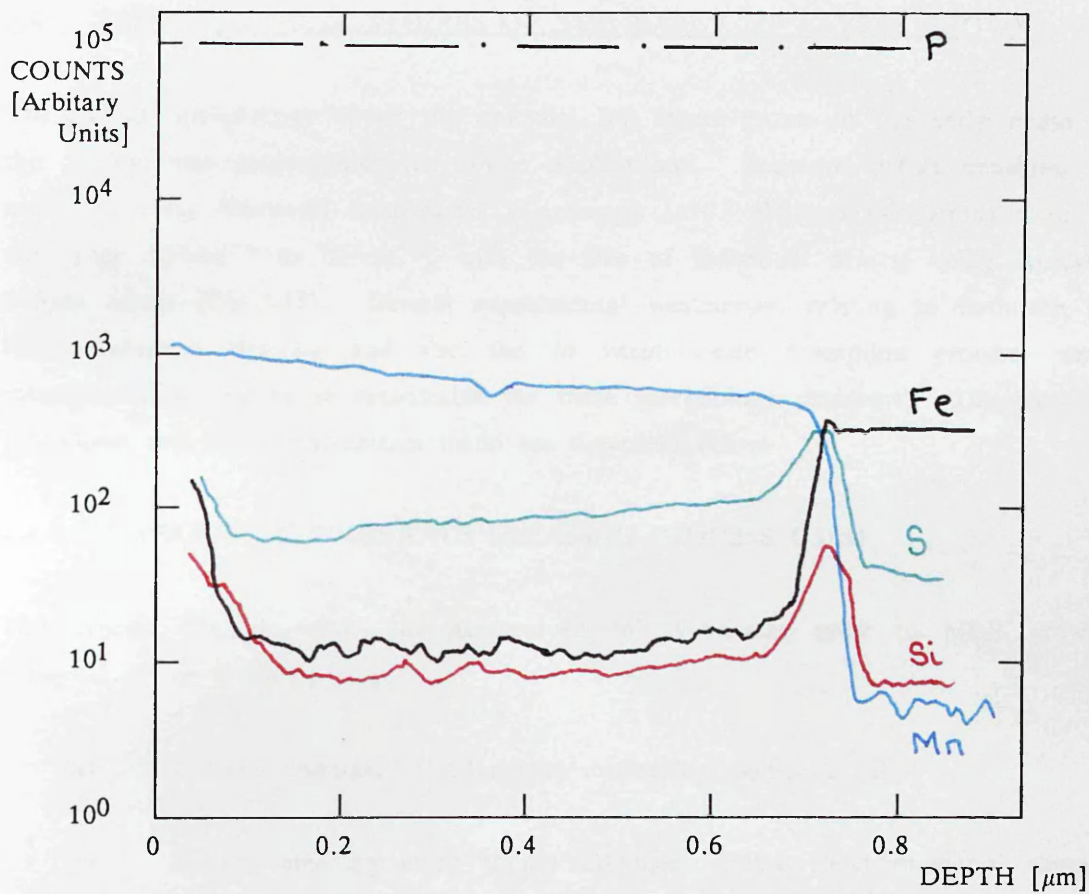
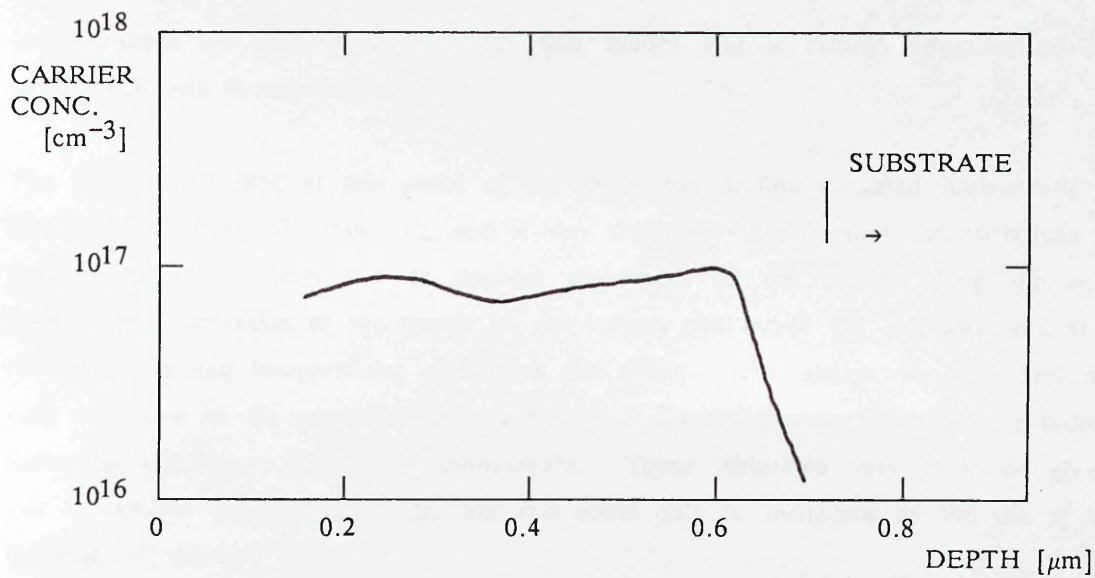


FIGURE 2.11

C-V and SIMS PROFILES OF TM 90

concentration are also consistent with this model and a critical appraisal of the indium cell was therefore performed.

The indium cell used at this phase of the work was in fact mounted horizontally in the MBE chamber (Chamber 1), and it was therefore possible that the variations in growth rate could arise due to random movement of the charge along the cell. Subsequent observation of the mouth of the indium cell, while the cell was held at a constant indicated temperature, confirmed this effect. The charge was observed not only to move in an unpredictable manner, but also to change noticeably in colour indicating significant changes of temperature. These variations were obviously giving rise to random changes in growth rate and could only be overcome by the use of an inclined cell (section 3.2).

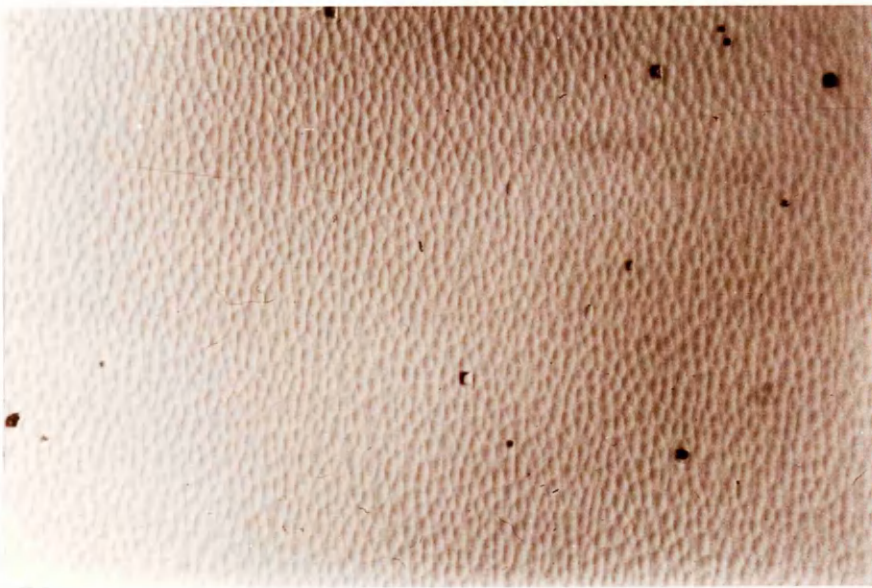
2.4 MORPHOLOGICAL STUDIES OF THE EARLY InP LAYERS GROWN

The surface morphology of all the epitaxial InP layers grown in the early phase of this project was unacceptable for device applications. Recorded defect densities, as measured using Nomarski interference microscopy ($\times 10^2$ – $\times 10^3$ magnification) were in the range 10^6cm^{-2} to 10^8cm^{-2} , with the size of individual defects being typically 2–5 μm across (Fig 2.12). Several experimental weaknesses, relating to both the *ex vacuo* substrate cleaning and also the *in vacuo* oxide desorption process, were subsequently proved to be responsible for these morphology problems. The cleaning procedures and the improvements made are described below.

2.4.1 SUMMARY OF SUBSTRATE CLEANING PROCESS USED

The process used to clean the as-received InP substrates prior to MBE growth consisted of the following steps:

- (a) Bromine methanol (1%) chemo-mechanical polish [2.16]
- (b) Solvent cleaning using trichloroethylene, acetone and methanol vapour reflux stills, followed by a water rinse
- (c) Chemical etch in 7:1:1 H_2SO_4 , H_2O_2 , H_2O for approximately 30secs [2.17]
- (d) Water rinse and nitrogen blow dry



10 μ m

(a) Morphology Considered Characteristic of Large Interfacial Carbon Contamination [2.20]



10 μ m

(b) Morphology Characteristic of Group III Rich Growth [2.21]

FIGURE 2.12 EXAMPLES OF GROSS MORPHOLOGICAL PROBLEMS ENCOUNTERED AT AN EARLY STAGE IN THE PROJECT

(e) *In vacuo* oxide desorption under a stabilising phosphorus flux [2.18]

Significant improvements were made to all stages of the process, as follows:

2.4.2 *EX VACUO* SUBSTRATE PREPARATION

Nomarski interference microscopy studies of layers TM 10–TM 50 indicated that the majority of the morphological defects were characteristic of the presence of high carbon concentrations at the substrate/epitaxial layer interface [2.19] (Fig 2.12a) or group III rich growth [2.20] (Fig 2.12b). In addition, other morphological features were also observed which were typical of both tweezer marks and drying stains (Fig 2.13). A number of steps were therefore taken to improve all aspects of the *ex vacuo* cleaning process. These improvements included the installation of class 100 clean air hoods and a new millipore "Milli Q" water system with "Organix Q cartridge" [2.21], and also the use of superior (v.l.s.i. grade) chemicals and wafer handling procedures.

These process changes produced a consistent improvement in layer morphology with defect densities of the order of 10^4cm^{-3} being eventually achieved (TM 81, Fig 2.14).

2.4.3 *IN VACUO* SUBSTRATE PREPARATION

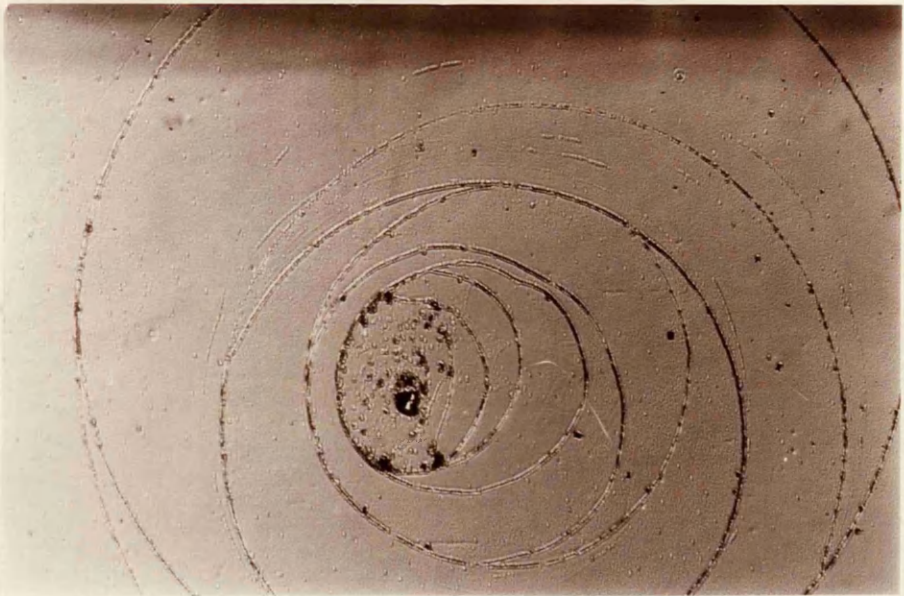
The *in vacuo* oxide desorption procedure involved increasing the substrate temperature (under an incident P_2 beam) up to a preset value of $\sim 500^\circ\text{C}$. However, flux monitoring facilities were not available in chamber, and hence the intensity of this P_2 beam could only be crudely estimated using a background ion gauge. Two major problems were apparent with this procedure:

(a) Substrate Temperature Stability

For a set of typical heat-cleaning conditions (i.e. a substrate temperature of 500°C , and an incident phosphorus flux corresponding to, say, twice that of the desorbing beam), vapour pressure data (section 5.2) would indicate that a substrate temperature increase of only 11°C will result in net group V loss. This value, therefore, defines the maximum substrate temperature excursion which can be tolerated under these conditions. (The parallel calculation for a phosphorus flux $10\times$ that desorbing indicates that a temperature excursion of $\sim 35^\circ\text{C}$ could be tolerated.)

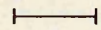
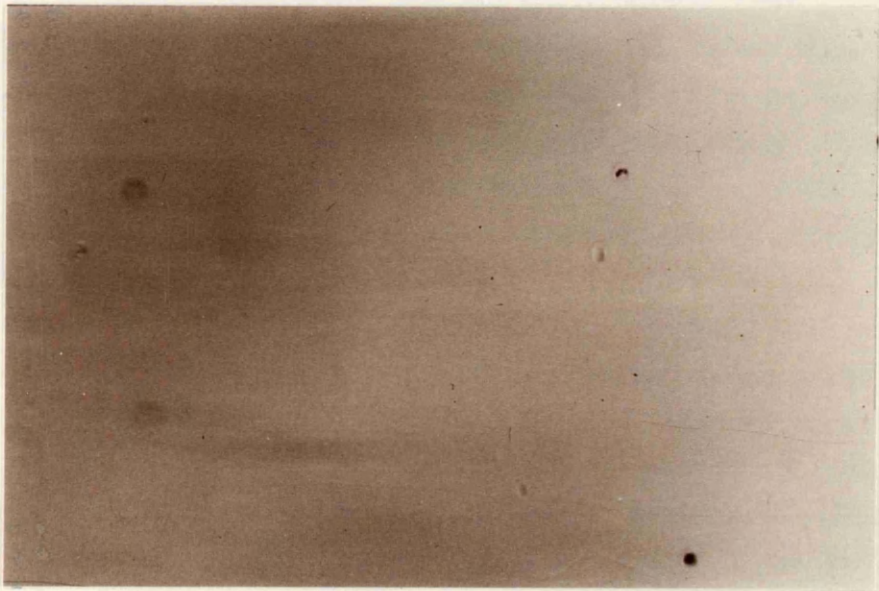


(a) Tweezer Marks - The Flat Ended Pattern Corresponds to the Flat Round Ended Tweezers Used to Handle the Substrates.



(b) Drying Stains - Circularly Symmetric Pattern Due to Residues Left on the Substrate as the Wafer was Force Dried using N_2 Gas

FIGURE 2.13 POOR EPITAXIAL MORPHOLOGY ATTRIBUTED TO EX-VACUO SUBSTRATE PREPARATION PROCEDURES



10 μ m

FIGURE 2.14 NOMARSKI MICROGRAPH OF EPITAXIAL InP
 $\sim 3\mu$ m THICK WITH DEFECT DENSITY $\sim 2 \times 10^4 \text{ cm}^{-2}$ [LAYER TM 81]

The substrate thermocouple assembly used in the initial stage of this project (Fig. 2.15a) consisted of two spring-loaded T1/T2 thermocouple contacts, with the molybdenum substrate holder forming the common junction. This assembly was found to generate unacceptable temperature variations (the spring loading mechanism was very unreliable), and a large proportion of substrates was lost due to thermal decomposition. A new assembly was therefore designed (Fig 2.15b) incorporating a fixed thermocouple junction, positioned in a small recess machined in the rear of the substrate block. This modification produced a significant improvement in temperature stability.

(b) Impurities originating from the Phosphorus Cracker Cell

A phosphorus cracker-cell [2.22] was used throughout the present investigation in view of the advantages to be gained from the use of a dimer source (section 1.4). However, the initial layers grown (with the cracker section temperature at 1100°C) exhibited a markedly inferior morphology compared with earlier layers grown using tetramers [2.23]. Modulated Beam Mass Spectroscopy (MBMS) was therefore used to characterise the cell [2.24] and revealed (Fig. 2.16) that efficient cracking (>95%) occurred for an indicated cracking section temperature as low as 900°C. Epitaxial layers subsequently grown using this reduced cracking zone temperature showed an immediate improvement in morphology.

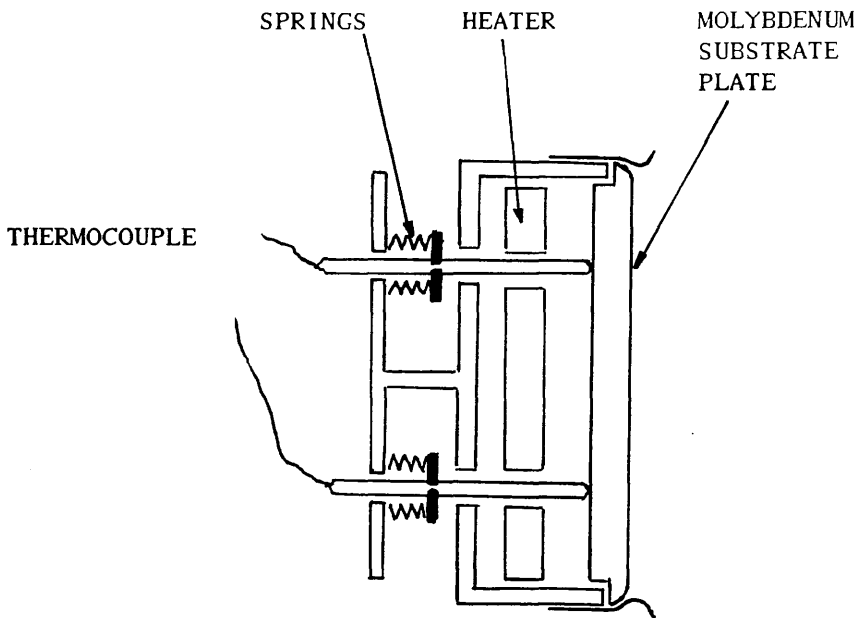
In fact the design of the cracker section was very similar to that of the indium cell used in the earlier experiments (section 2.2) which produced epitaxial impurity concentrations of 10^{17}cm^{-3} for an operating temperature of 900°C. The concentration of impurities generated by the cracker operating at 1100°C would be expected to be at least three orders of magnitude higher, on the basis of vapour pressure considerations [2.06]. Concentrations comparable to the solid solubility limit [2.25] could therefore have been generated, resulting in a marked deterioration in morphology [2.26].

2.5 SUMMARY OF THE DESIGN WEAKNESSES OF MBE CHAMBER 1

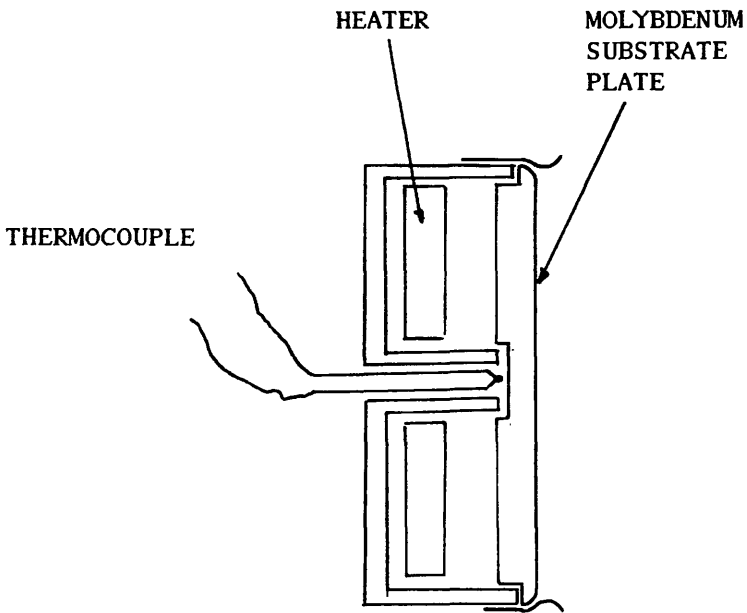
The experimental data described in this chapter highlights several serious weaknesses in the design of Chamber 1, summarised as follows:

(a) Evaporation Cells

A significant reduction in the impurities originating from the structure of the original



(a) Separate spring loaded thermocouple elements with the molybdenum substrate block the common



(b) Fixed common junction

FIGURE 2.15
 SCHEMATIC OF THE SUBSTRATE THERMOCOUPLE
 CONFIGURATIONS USED IN CHAMBER 1

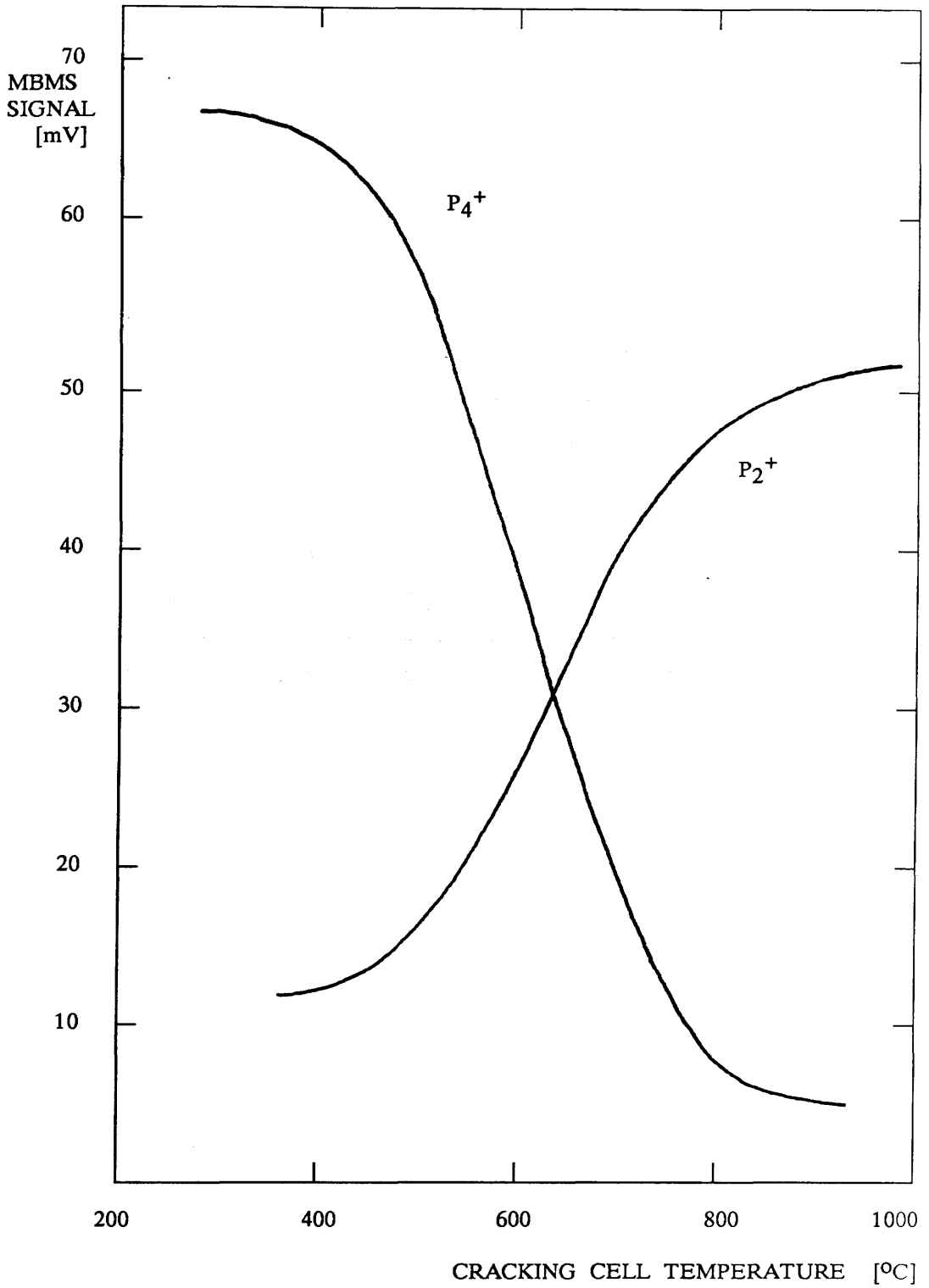


FIGURE 2.16

CHARACTERISTIC OF THE PHOSPHORUS CRACKING SOURCE

In cell was achieved by improved baffling of the heater. However, the epitaxial concentration of transition elements was still unacceptably high for device applications. New cells, constructed from higher purity materials, were therefore required and chamber modifications needed to allow the group III cells to be operated in an inclined position. In addition, larger capacity group V sources were essential in order to achieve longer run times.

(b) *In situ* Monitoring Facilities

The lack of a flux monitoring ion gauge and RHEED facilities was a severe limitation. A flux monitoring gauge would allow both short- and long-term monitoring of flux stability and also enable variable III:V flux ratio growth experiments to be performed.

A RHEED monitoring facility would allow the *in vacuo* oxide desorption process to be carefully monitored, a prerequisite for successful MBE growth [2.20]. The RHEED system could also be used to provide crystallographic information from the growing layers [2.27] and accurate temperature calibration [2.28].

2.6 SUMMARY

Major problems encountered at the outset of the project centred on the total lack of run-to-run repeatability of InP layer properties. An extensive series of layers has been assessed by photoluminescence, SIMS and C-V measurements and major weaknesses relating to the cell design, substrate temperature control and *ex vacuo* substrate cleaning procedure highlighted. However, serious shortcomings in the overall design of the growth chamber became apparent, particularly relating to the use of horizontal cells and the absence of flux monitoring and RHEED facilities. These deficiencies were rectified by designing an entirely new growth chamber (Chamber 2) which allowed InP layers of significantly higher purity to be grown, as described in the next chapter.

CHAPTER 3

CHARACTERISATION OF UNINTENTIONALLY DOPED InP GROWN IN CHAMBER 2

3.1 INTRODUCTION

3.2 DESIGN AND PERFORMANCE OF CHAMBER 2

3.3 PROPERTIES OF UNINTENTIONALLY DOPED InP
GROWN IN CHAMBER 2

3.4 SIMS ANALYSIS

3.5 ORIGIN OF THE IMPURITIES

3.6 PHOTOLUMINESCENCE FROM MBE GROWN InP

3.7 SUMMARY

3.1 INTRODUCTION

Chapter 3 conveniently divides into three main parts: (i) a description of the design and performance of the new MBE growth chamber, Chamber 2; (ii) a discussion of the growth of unintentionally doped InP in Chamber 2 and (iii) an analysis of a series of experiments to identify the causes of the principal residual impurities in MBE grown InP, which became feasible with the dramatic improvement in system performance and reliability.

The first series of epitaxial layers grown in Chamber 2, TM 96-TM 126, were not intentionally doped and to avoid both unnecessary contamination and to minimise complications during the growth of these layers, the number of sources was limited to two - one indium and one phosphorus.

The quality of the InP as a function of growth conditions was monitored using electrochemical carrier (C-V) profiles, Hall measurements (Van der Pauw technique), SIMS and 15K Photoluminescence. By correlating SIMS and C-V profiles with deliberately introduced changes in the growth conditions, the origins of the residual impurities have been investigated.

3.2 DESIGN AND PERFORMANCE OF CHAMBER 2

3.2.1 INTRODUCTION

The broad objectives placed on the design of the new growth chamber were as follows:

- (1) The chamber had to be compatible with the existing UHV rig.
- (2) The problems previously encountered with growth rate, cell design, flux monitoring and the ultimate vacuum had to be eliminated.
- (3) The design of the chamber had to be sufficiently flexible to allow for the growth at a later date of both ternary and quaternary semiconductors based on Ga, In, As and P.

3.2.2 CHAMBER

The main features of the chamber are highlighted schematically in figure 3.1 and pictorially in figure 3.2.

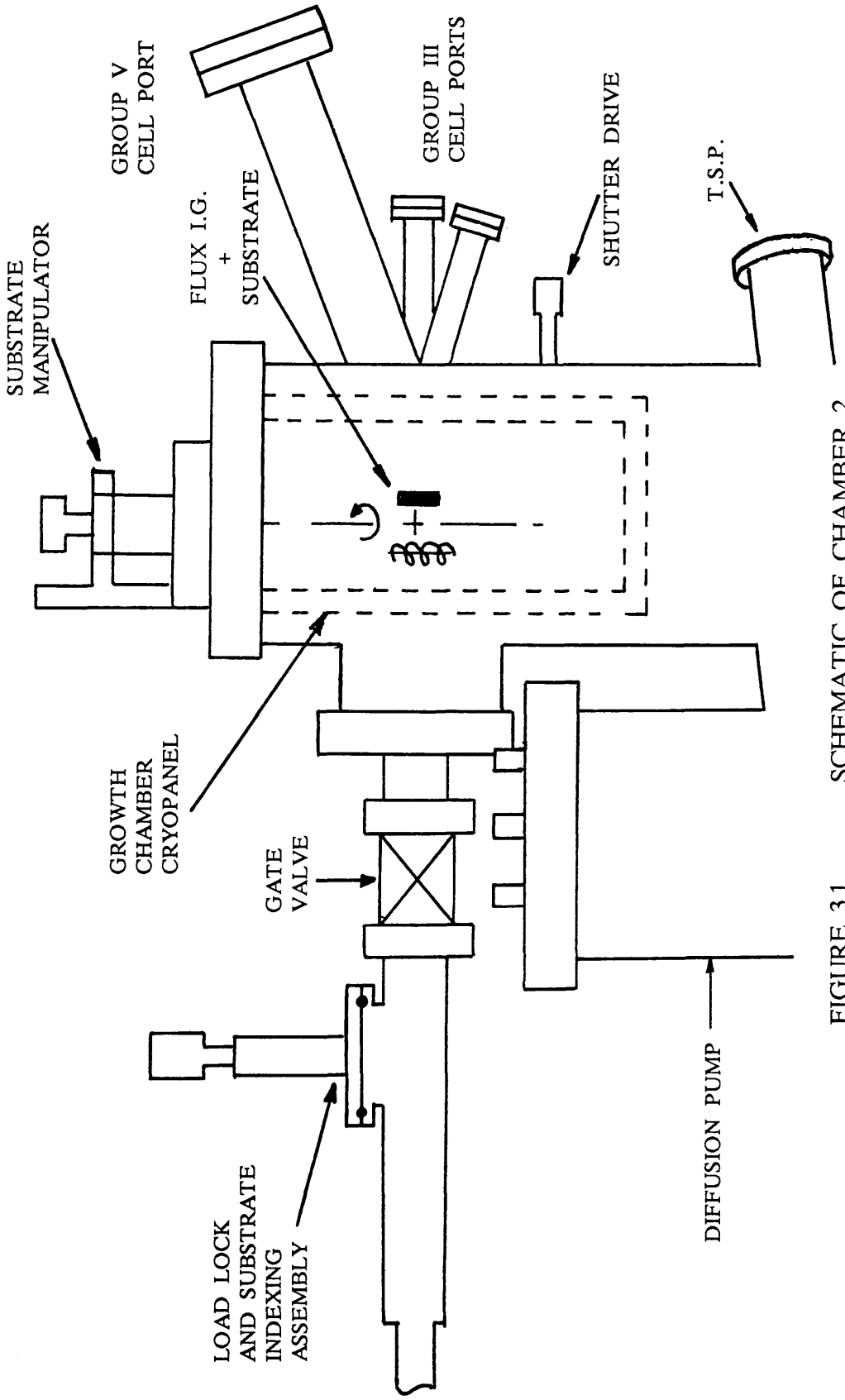
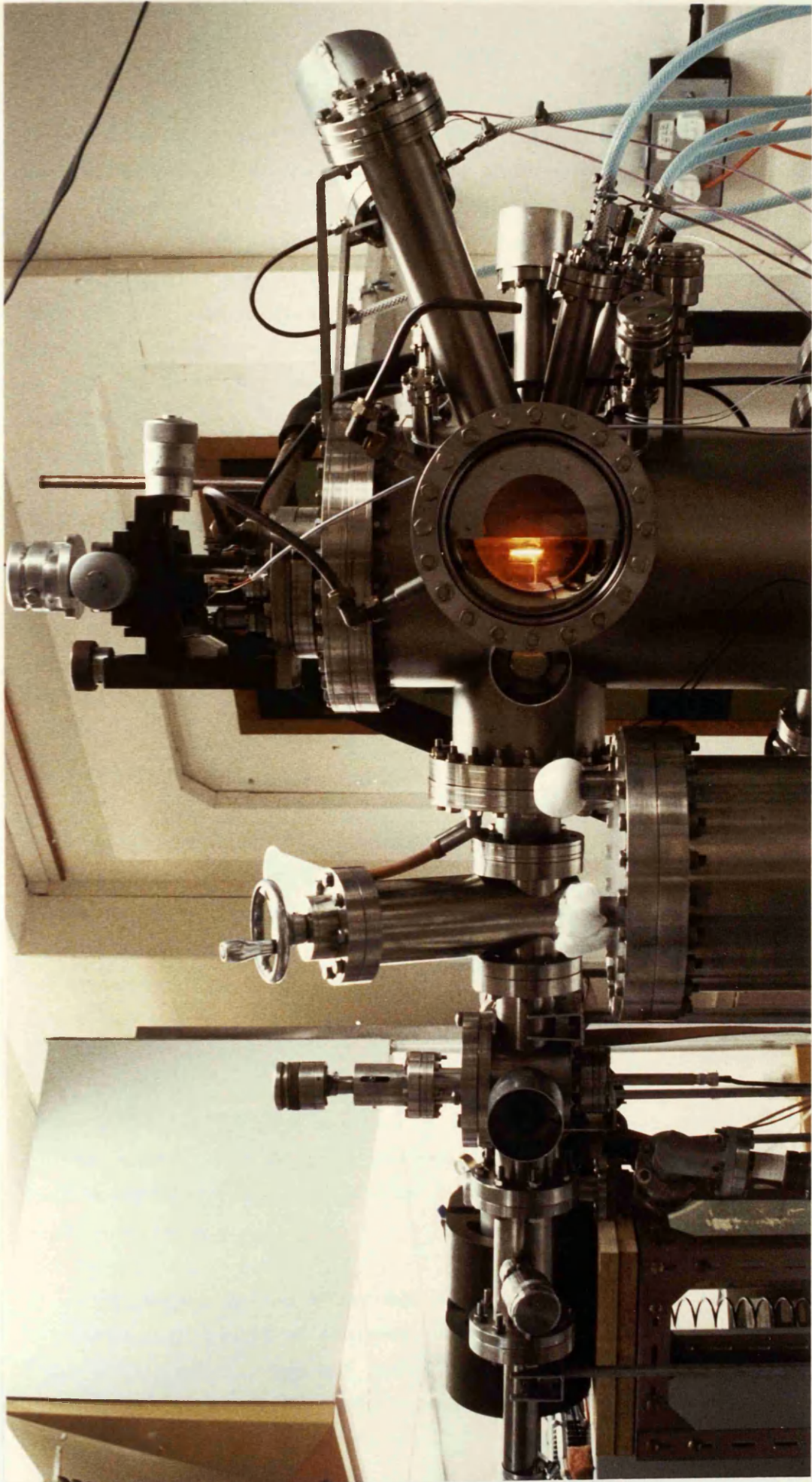


FIGURE 3.1 SCHEMATIC OF CHAMBER 2



CHAMBER 2

FIGURE 3.2

(a) Cell Layout

The new design allowed for up to six effusion cells to be installed, each with its own shutter and a cell to substrate distance of 10cm. The installation of shutters was a substantial improvement over the earlier chamber in which the group V cells had no shutters at all, making flux monitoring impossible.

Two cell ports were made to be compatible with large capacity, 50cm³, group V cells. The chamber could therefore be configured with either two phosphorus cells or one phosphorus and one arsenic cell. The ports were inclined downwards, subtending an angle of ~15° with the substrate normal. No loss of source material occurred as the group V cells had integral cracking sections.

The remaining four ports were intended for smaller capacity (3cm³) group III and dopant cells, providing a capability for the growth of quaternary semiconductors with two dopants. Three of the ports were inclined below the horizontal, to accommodate liquid sources, while the fourth was horizontal with its axis normal to the growth surface. This fourth port could also be used as a viewport. The inclined cells subtended an angle of ~12° with the substrate normal.

(b) Substrate Assembly

The modified version of the 4cm diameter substrate mount and heater assembly used in the Chamber 1 (section 2.4.3) was transferred to the new chamber. However, greater control over the positioning of the assembly was achieved by mounting it on a three axis (X, Y, Z) manipulator, thus simplifying alignment for RHEED studies and substrate transfer.

(c) Flux Monitoring

A flux monitoring ion gauge was mounted on the same universal manipulator as the substrate assembly, with the gauge positioned so that, on rotation about the z-axis, it could be moved into the growth position. Additional factors considered in the design of this assembly were:

- (i) The relative position of the flux gauge with respect to the substrate heater. This was arranged so that most of the flux passing through the gauge was incident on the cryopanel rather than the rear of the substrate assembly, thereby minimising any bounce contribution to the flux measurement.

- (ii) The extensive shielding of all leads to prevent electrical shorts
- (iii) The use of silver instead of copper conductors to minimise corrosion by phosphorus [3.01].

(d) Analysis

A RHEED facility and a quadrupole mass spectrometer were fitted to the chamber with the following precautions taken over the positioning of the mass spectrometer:

- (i) The ionising section was not enclosed in stainless steel. Experience with Chamber 1 had shown that a number of peaks in the residual gas spectrum, e.g. 18, 28a.m.u., were falsely exaggerated with the ioniser mounted in a close-fitting stainless steel tube.
- (ii) The spectrometer was positioned out of line of sight of the cells. This limited the build up of source material in both the ioniser and analyser, and thereby increased the 'up time'.

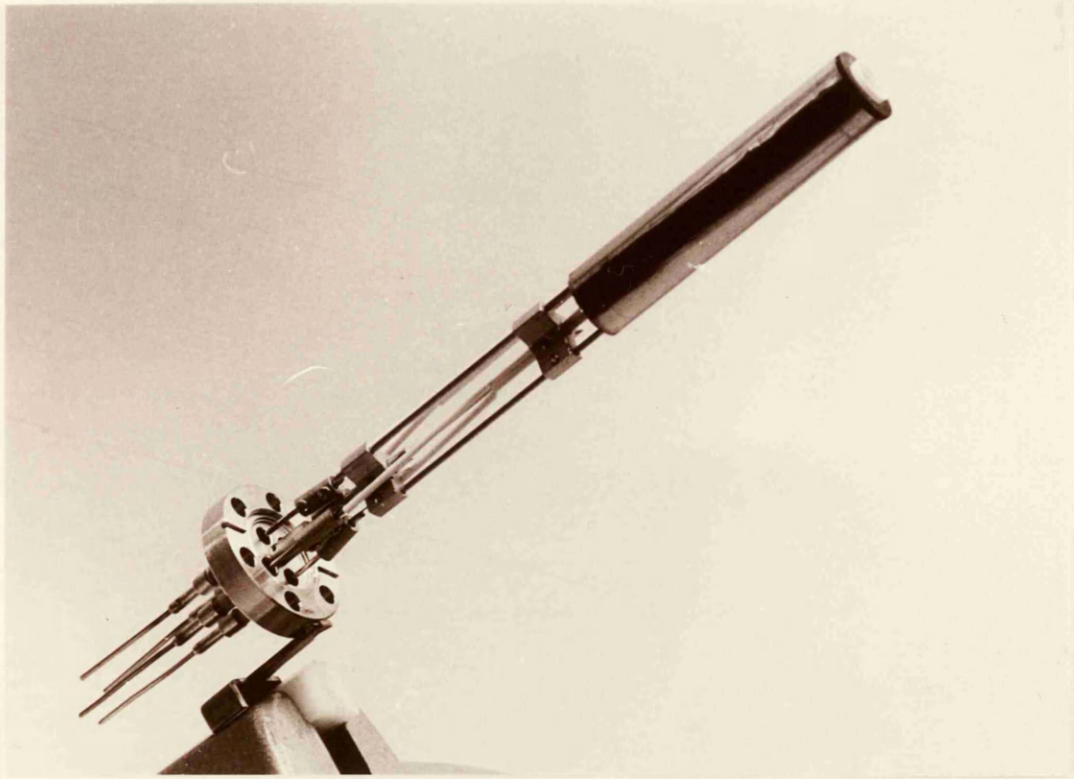
(e) Cryopanelling

The substrate assembly was surrounded by a liquid nitrogen cooled cylindrical skirt. Holes in the skirt corresponding to the ports in the chamber were provided for the cells, viewports, substrate transfer and RHEED. Additional cryopanelled were fitted to the three 150mm diameter ports, which supported the load lock, RHEED screen and electron gun.

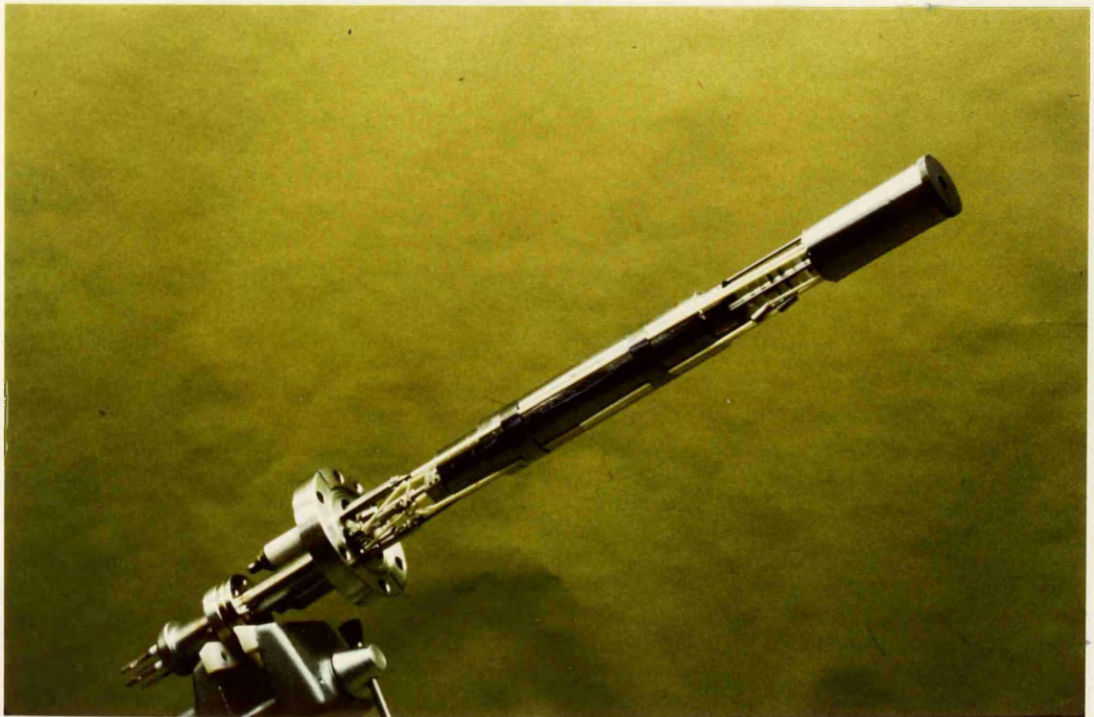
3.2.3 CELL DESIGN

(a) Group III Cells

Two separate group III cells were used in Chamber 2 with the second cell being introduced after growth TM 105. These cells were identical, except that in the first alumina, as opposed to p-BN, was used to electrically isolate the heater wires. Both cells had a p-BN crucible and each had a cap made of graphite fitted around the crucible at the front of the cell. This cap acted as a baffle to impurities from the hot heater filaments and prevented indium passing back into the cell structure (Fig. 3.3a).



(a) GROUP III CELL



(b) GROUP V CELL

FIGURE 3.3 ILLUSTRATION OF THE GROUP III AND GROUP V CELLS DESIGNED AND CONSTRUCTED FOR USE IN CHAMBER 2

Previous experience had shown the importance of simple structures which were easy to service in order to achieve reliability. The cells were therefore designed to be modular and either the thermocouple or the heater could be changed without the one disturbing the other. The technical specification of the cells was as follows:

CAPACITY: 3cm^{-3} (9mm dia. \times 50mm long)

HEATER: Impedance at 30°C - 5ohm
Impedance at 900°C - 15ohm
Power at 900°C - 48 Watts

(b) Group V Cells

The group V cracking cells were similarly of modular construction, a principle which is even more important where two separate heaters and thermocouples are involved. Details of the design, which follows the principles established by Neave et al [3.02], [3.03] are shown in Figure 3.3b. Both the crucible and the cracking section were constructed in graphite, with the two sections joined by a p-BN tube (2mm i.d.) and thermally isolated by tantalum baffles. As in the group III/dopant cell, close fitting graphite caps covered the high temperature heater assemblies. The cell was recharged by unscrewing and withdrawing the complete cracker assembly, including the p-BN link tube. The power requirements and capacity of the cracker cell are summarised below:

CAPACITY: 49cm^{-3} (25mm dia. \times 100mm long)

K CELL HEATER: Impedance at 250°C - 8ohm
Power at 250°C - 8 Watts

CRACKER HEATER: Impedance at 900°C - 20ohm
Power at 900°C - 125 Watts

3.2.4 VACUUM PERFORMANCE

The diffusion and rotary pump configuration used for Chamber 1 was transferred directly to Chamber 2 with the following changes made to improve both the reliability and the ultimate vacuum.

- (1) To reduce the significant oil contamination which had resulted from failure of either electricity, water cooling or backing-line vacuum on Chamber 1, the rotary pump was isolated from the diffusion pump using a solenoid valve. The operation of the valve was controlled by Pirani pressure gauges located on either side of it, and a 3-litre ballast tank was fitted between the valve and the diffusion pump to reduce the frequency with which the valve opened.
- (2) The failsafe interlock circuits were completely redesigned. Electricity, water supply and backing vacuum were all monitored and in the event of a failure, a controlled shutdown of the diffusion pump and all hot filaments was initiated. The system could only be restarted manually after such a shutdown.

With these modifications, a significant improvement in reliability was obtained and in the event of any service failure growth could recommence within twenty-four hours. This contrasted with a corresponding period of typically a week before the modifications were made.

Day-to-day operating procedures for the diffusion pump were also revised to ensure the clean operation of the pump and an improved ultimate vacuum. The redesigned interlock circuits eliminated the possibility of major oil contamination, and the combination of ballast tank and backing valve reduced the backstreaming of rotary pump oil [3.04]. A further reduction in the backstreaming and an improvement in the pump performance was achieved by continuously cooling the liquid nitrogen trap fitted to the diffusion pump [3.05]. Finally, to accelerate the pump-down cycle and increase the ultimate vacuum, the whole trap assembly was baked at $\sim 190^{\circ}\text{C}$ [3.06]. In Chamber 1, the maximum bake out temperature had been $\sim 120^{\circ}\text{C}$. As a direct consequence of all these changes, the ultimate pressure of the diffusion pump improved from $\sim 10^{-9}\text{mbar}$ to $< 5 \times 10^{-11}\text{mbar}$, despite the presence of residual phosphorus.

Outgassing routines associated with the chamber were similarly altered to minimise impurities. The cells and charges were outgassed prior to use for $\sim 6\text{hrs}$ at $\sim 20^{\circ}\text{C}$ above their growth temperature and specific procedures were introduced to address the problem of handling phosphorus. The main problems in handling phosphorus, especially when compared with arsenic, are that phosphorus is chemically more reactive and has a large number of allotropic forms, each with a different vapour pressure [3.07]. The two principal classes of allotropes are white phosphorus with a vapour pressure at 300K of $\sim 5 \times 10^{-2}\text{mbar}$ [3.08] and which spontaneously ignites on exposure to air, and red phosphorus with a vapour pressure at 300K of $\sim 10^{-9}\text{mbar}$

[3.08] ($10^4\times$ greater than arsenic). White phosphorus is formed by the condensation of phosphorus tetramers while the condensation of dimers produces predominantly red phosphorus [3.07]. The two allotropes deposit on the cryopanel during growth and when exposed to atmosphere can, on occasions, spontaneously ignite.

To remove a significant amount of the reactive phosphorus, a procedure was adopted which involved baking the reactor at $\sim 190^\circ\text{C}$ for ~ 12 hrs prior to venting (vapour pressure of red phosphorus at 190°C $\sim 1\times 10^{-2}$ mbar). The residual background pressure after such a bake was typically 5×10^{-9} mbar compared to pressures of 10^{-6} – 5×10^{-7} mbar prior to the bake. After making repairs to the chamber or recharging the cells, UHV conditions were re-established by baking the chamber for a further 48hrs at $\sim 190^\circ\text{C}$.

Following this procedure, a residual gas analysis, taken with the liquid nitrogen panels cold and all-but the phosphorus cell and substrate at their growth temperature, showed that all partial pressures, with the exception of P_4 , P_3 , P_2 and P , were $< 5\times 10^{-11}$ mbar and comparable to those found in commercial systems.

3.3. PROPERTIES OF UNINTENTIONALLY DOPED InP GROWN IN CHAMBER 2

The first thirty unintentionally doped InP layers (TM 96–TM 125) deposited in Chamber 2 were grown from the same start materials. The growth rate was varied between 0.5 and $3.0\mu\text{m hr}^{-1}$, the growth temperature from 50°C below the oxide desorption temperature to the oxide desorption temperature ($\text{Temp}_{\text{oxide desorption}} \sim 500^\circ\text{C}$ [3.09] [3.10]) and the V:III nude ion gauge current ratio between 10:1 and 80:1. All layers in this growth series were characterised by 15K photoluminescence and C–V profiles, while selected layers were analysed by Hall effect measurements and SIMS. With the exception of a dependence of carrier concentration on V:III flux ratio, no systematic variation in material properties with growth conditions was apparent.

The growth conditions and properties of five representative layers (TM 97, 117, 119, 120 and 122) are summarised in table 3.1 and 3.2 and figure 3.4. Layer TM 97 typifies the improvement in the quality of material produced in Chamber 2 where the linewidth of the band edge (BE) in the photoluminescence spectrum is only 5.9meV (Fig 3.5) compared to a typical value of 16meV recorded for layers grown in Chamber 1 (TM 63, Fig 2.4). In addition, emission at $\sim 1.1\text{eV}$, associated with the transition metals Mn and Fe, is reduced from $\sim 40\%$ of the band edge recombination

| LAYER | GROWTH CONDITIONS | | C-V DATA | | COMMENTS |
|--------|---------------------------------------|---|-----------------|------------------------------------|--|
| | GROWTH RATE ($\mu\text{m hr}^{-1}$) | GROWTH TEMP. ($^{\circ}\text{C}$) {1} | V:III RATIO {2} | SURFACE CONC. (cm^{-3}) | |
| TM 97 | 2.5 | 490 | $\sim 10:1$ | $\sim 10^{16}$ | $\times 10$ Second layer grown in Chamber 2 PL spectrum figure 3.5 |
| TM 117 | 1.5 | 460 | $\sim 20:1$ | $\sim 1.5 \times 10^{16}$ | 30% PL spectrum figure 3.7a |
| TM 119 | 1.6 | 460 | $\sim 20:1$ | $\sim 2 \times 10^{16}$ | 25% PL spectrum figure 3.7b |
| TM 120 | 1.2 | 500 | $\sim 20:1$ | $\sim 2 \times 10^{16}$ | 20% PL spectrum figure 3.16 |
| TM 122 | 1.5 | 460 | $\sim 20:1$ | $\sim 2 \times 10^{16}$ | 30% PL spectrum figure 3.7c |

{1} - Quoted growth temperature is referenced to the oxide desorption temperature which was taken as 500°C [3.09] [3.10]
 {2} - Nude ion gauge current ratio

TABLE 3.1 SUMMARY OF THE GROWTH CONDITIONS AND C-V DATA FOR LAYERS TM 97, 117, 119, 120 AND 122

InP HALL DATA

| LAYER | Nd-Na 300K (cm ⁻³) | MOBILITY 300K (cm ² V ⁻¹ s ⁻¹) | Nd-Na 77K (cm ⁻³) | MOBILITY 77K (cm ² V ⁻¹ s ⁻¹) | COMPENSATION RATIO (77K DATA) | CARRIER FREEZEOUT | Nd (cm ⁻³) | Na (cm ⁻³) |
|-------|--------------------------------------|--|-------------------------------------|---|-------------------------------------|----------------------|---------------------------|---------------------------|
| 97 | 5.5 × 10 ¹⁶ | 2,900 | 2.6 × 10 ¹⁶ | 9,500 | 0.25 | 0.47 | 3.5 × 10 ¹⁶ | 8.6 × 10 ¹⁵ |
| 117 | 1.8 × 10 ¹⁶ | 3,615 | 1.2 × 10 ¹⁶ | 11,219 | 0.35 | 0.67 | 1.8 × 10 ¹⁶ | 6.5 × 10 ¹⁵ |
| 119 | 2.5 × 10 ¹⁶ | 3,675 | 1.5 × 10 ¹⁶ | 9,314 | 0.4 | 0.60 | 2.5 × 10 ¹⁶ | 1.0 × 10 ¹⁶ |
| 120 | 2.5 × 10 ¹⁶ | 3,350 | 1.5 × 10 ¹⁶ | 13,300 | 0.2 | 0.60 | 1.9 × 10 ¹⁶ | 3.8 × 10 ¹⁵ |
| 122 | 2.9 × 10 ¹⁶ | 3,840 | 2.1 × 10 ¹⁶ | 9,200 | 0.3 | 0.72 | 3 × 10 ¹⁶ | 9 × 10 ¹⁵ |

TABLE 3.2 SUMMARY OF THE HALL DATA RECORDED FOR LAYERS TM 97, 117, 119, 120 AND 122

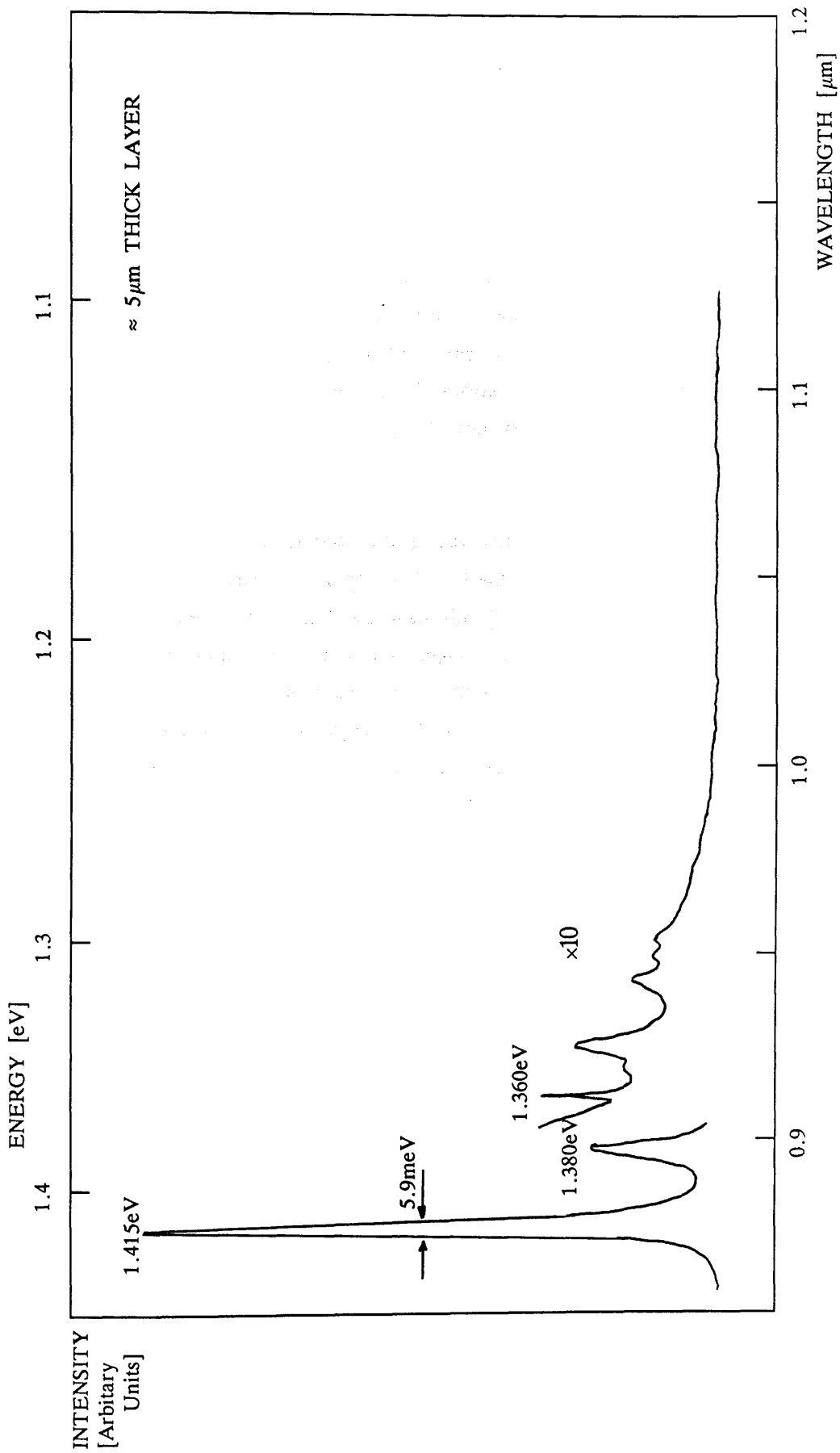


FIGURE 3.5 PHOTOLUMINESCENCE SPECTRUM OF TM 97

(TM 63, Fig 2.4) to less than 0.5% (TM 97). This implied reduction in the concentration of deep acceptors was quantified by SIMS (Table 3.3) with the Mn concentration reduced from $2 \times 10^{16} \text{cm}^{-3}$ for material grown in Chamber 1 to $< 10^{14} \text{cm}^{-3}$ in Chamber 2 and the Fe concentration reduced from $< 2 \times 10^{16} \text{cm}^{-3}$ to below the SIMS detection limit of $\sim 10^{15} \text{cm}^{-3}$ for this element.

The carrier profile for the same sample is shown in figure 3.6, revealing a reduction in carrier concentration through the layer from $\sim 10^{17} \text{cm}^{-3}$ at the start of growth to $\sim 10^{16} \text{cm}^{-3}$ after $5 \mu\text{m}$. The Hall measurement of the room temperature carrier concentration (Table 3.2) is seen to agree with the average of the free electron concentration measured by the C-V profile and the anomalously large carrier freezeout on cooling to 77K (Table 3.2) can be related to this non-uniform profile (Appendix A4).

The phosphorus flux, measured before and after the growth of TM 97, showed a reduction by more than a factor of 2. Evidence had already been obtained from results in Chamber 1 of a link between the phosphorus flux and the residual carrier concentration (section 2.3.3), and the change in carrier concentration in TM 97 may be partly explained by the reduction in phosphorus. In subsequent growth runs, a much smaller reduction in phosphorus flux of $\sim 20\%$ was recorded. This is reflected in a correspondingly smaller decrease in free electron concentration through the associated epitaxial layers. For layers TM 117, 119 and 122, which were all grown under nominally the same conditions, the measured carrier concentrations lie within the range $1-3 \times 10^{16} \text{cm}^{-3}$ and the 77K Hall mobilities within 10% of $10,000 \text{cm}^2 \text{V}^{-1} \text{s}^{-1}$.

The photoluminescence spectra recorded from the same three layers (TM 117, 119 and 122, figure 3.7a, b and c respectively), are also comparable, except for the large band to acceptor (e-A) recombination in TM 117 which is believed to have been caused by a pump failure prior to the growth of this sample. The e-A intensity in the layer grown prior to the pump failure was 1.5% of the band edge emission; in layer TM 117 this ratio was 36% and following a bake of the system, the intensity ratio in all layers grown subsequent to TM 117 was restored to $< 3\%$.

It should be re-emphasised that the first 9 layers grown in Chamber 2 (TM 97-TM 105) involved the use of an In cell in which the heater wires were electrically isolated with alumina tubing (section 3.2.3). Layers TM 106 onwards were grown with an In cell in which this alumina was totally replaced by p-BN. Hall and C-V data recorded from layers grown before and after this change show no

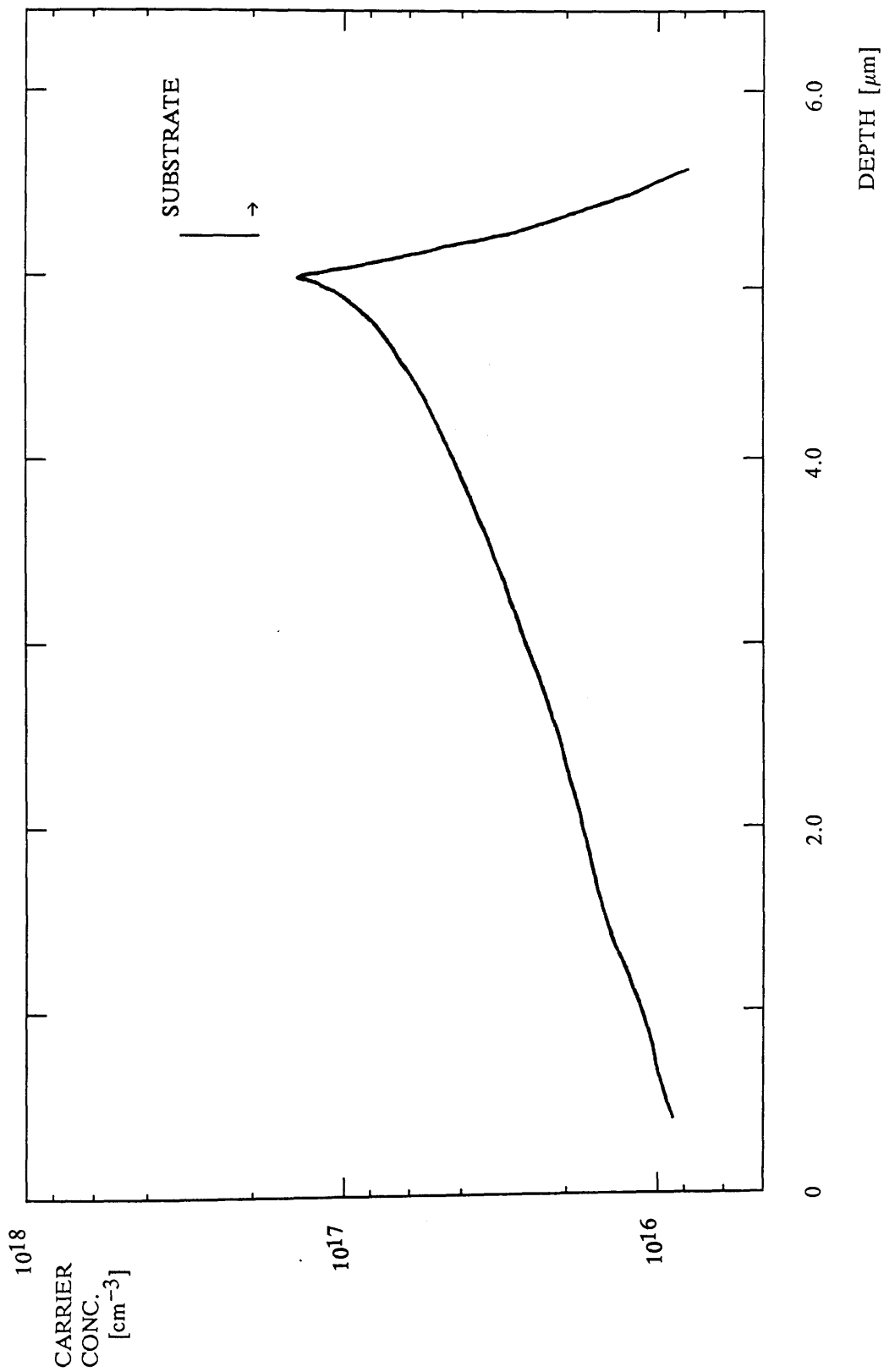


FIGURE 3.6 C-V PROFILE OF TM 97

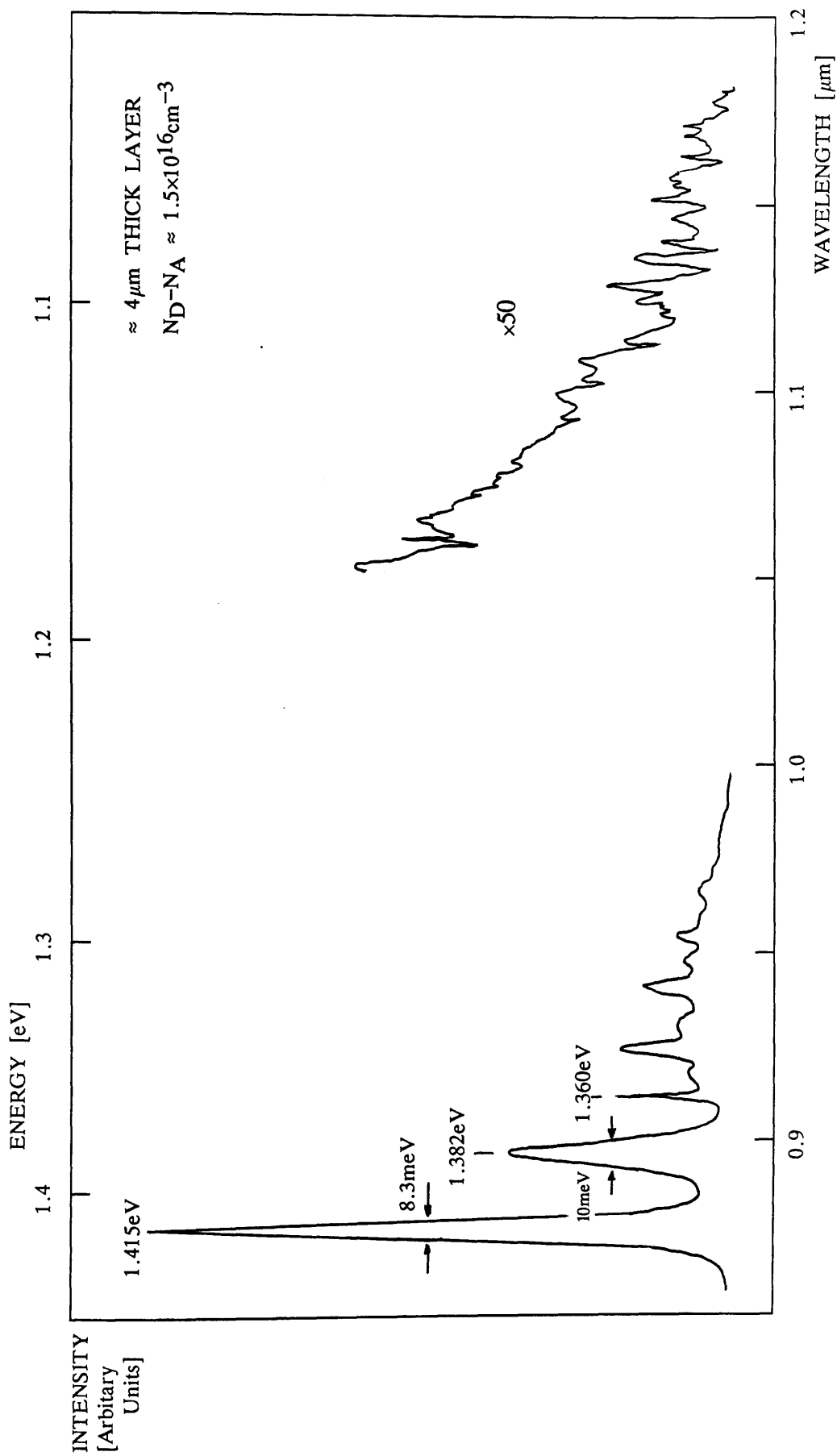


FIGURE 3.7a PHOTOLUMINESCENCE SPECTRUM OF TM 117

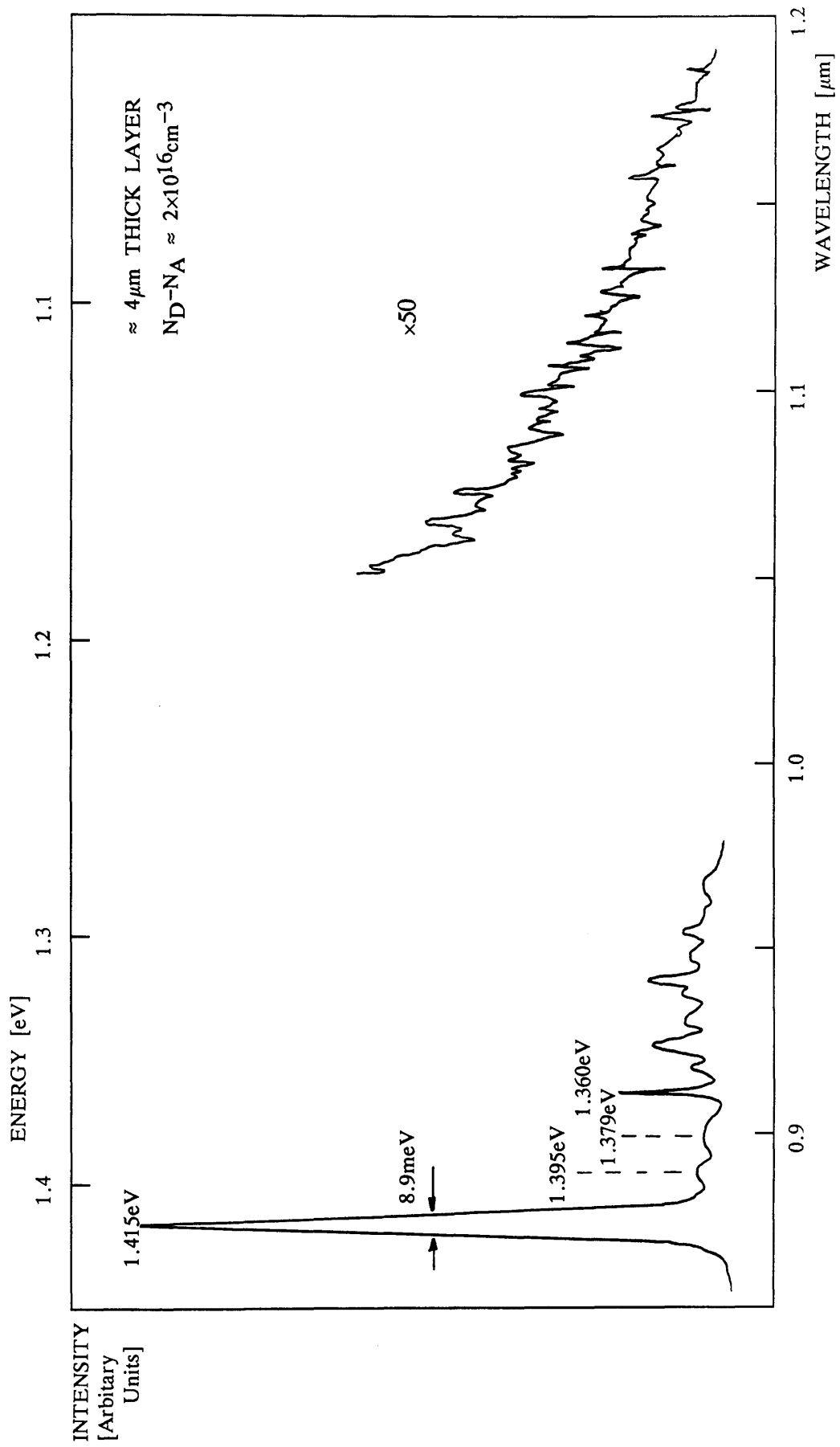


FIGURE 3.7b PHOTOLUMINESCENCE SPECTRUM OF TM 119

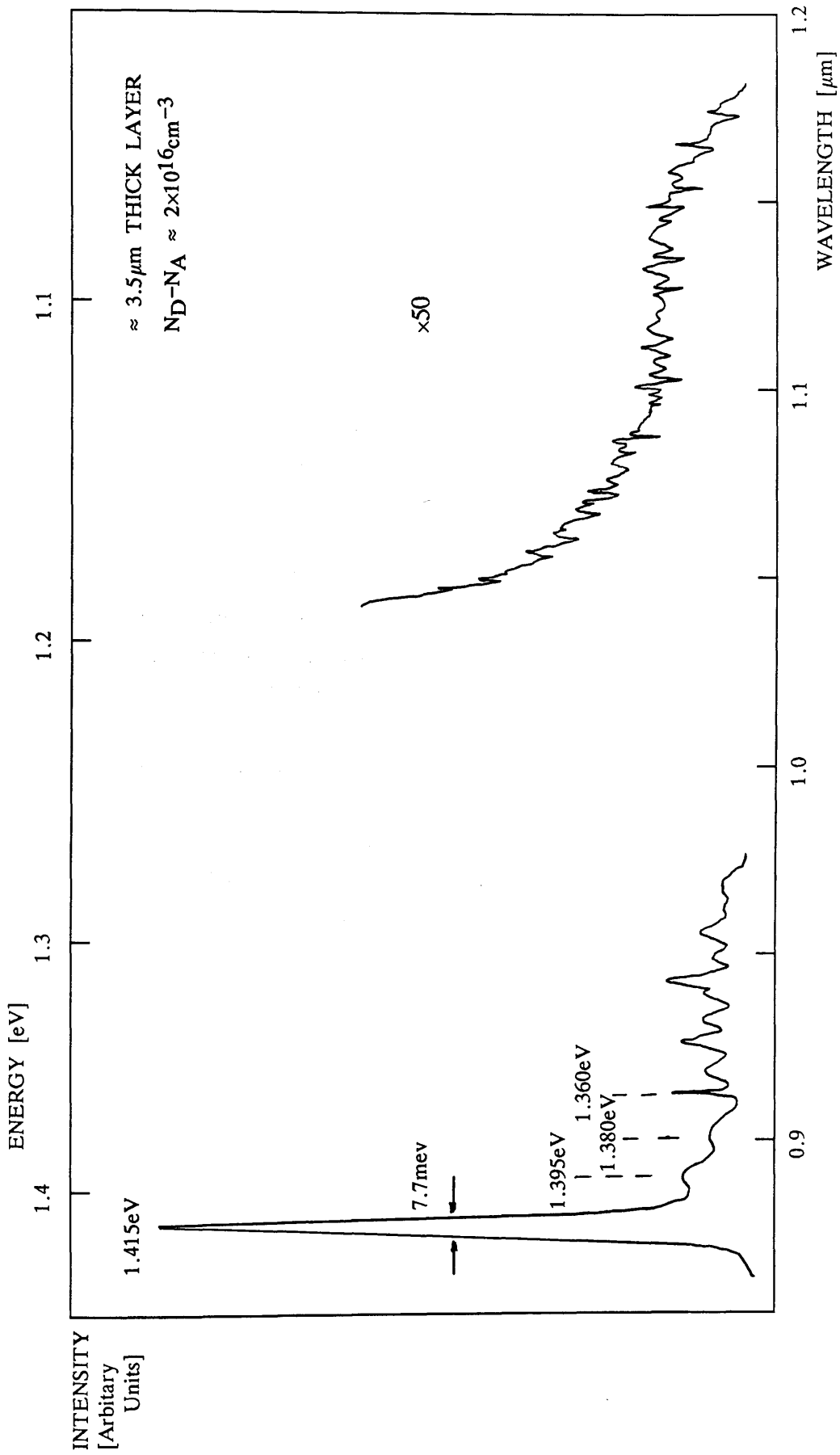


FIGURE 3.7c PHOTOLUMINESCENCE SPECTRUM OF TM 122

significant differences (Tables 3.1, 3.2), whereas SIMS and photoluminescence data provide evidence for a substantial reduction in the Mg concentration. Specifically, a reduction of $\times 7$ in the Mg concentration to $\sim 10^{14} \text{cm}^{-3}$ is identified from the SIMS profiles of TM 99 (Fig 3.9) (alumina insulation) and TM 123 (Fig 3.10) (p-BN insulation). The photoluminescence spectra of layers grown either side of the change (TM 105 and 111, Fig 3.8) show a factor of 10 reduction in the intensity of the e-A recombination at 1.382eV. This recombination may be associated with Mg acceptor impurities [3.11]. That the change in e-A intensity coincided with the change in indium cell was confirmed by analysing the intensity ratio of the BE and e-A peaks for all thirty layers grown (excluding TM 117, see above). Under the same photoluminescence excitation conditions, this ratio showed a sustained decrease of $\sim \times 10$ following the cell change, while the maximum variation in the band edge intensity through all layers was less than 4.

The assignment of Mg to the e-A recombination observed in InP grown in Chamber 2 has been confirmed by subsequent studies [3.12] in which the change from donor to acceptor D-A to e-A recombination as a function of temperature and pump intensity has been correlated with the data of Skromme [3.11] for low concentration ($\sim 10^{15} \text{cm}^{-3}$) Mg implants in InP.

A number of points arise from this change in cell construction:

- (i) Magnesium, an impurity present in the alumina (0.1% MgO) used in the heater assembly was incorporated into the epitaxial layer despite the attention paid to the shielding (sections 2.2.1 and 3.2.3).
- (ii) A significant decrease in both the Mg concentration and the dominant acceptor recombination produced no related increase in the free electron concentration or mobility.
- (iii) The compensation deduced from the Hall data indicates a total concentration of ionised acceptors of $\sim 7 \times 10^{15} \text{cm}^{-3}$ whereas the principal shallow optically active acceptor (Mg) identified in the photoluminescence spectra has a concentration of $\sim 10^{14} \text{cm}^{-3}$.

The origin of the Mg present in the epitaxial InP grown after the change to p-BN isolation could not be identified from subsequent SIMS data. However, at a concentration of $\sim 10^{14} \text{cm}^{-3}$ it is not significant in this InP.

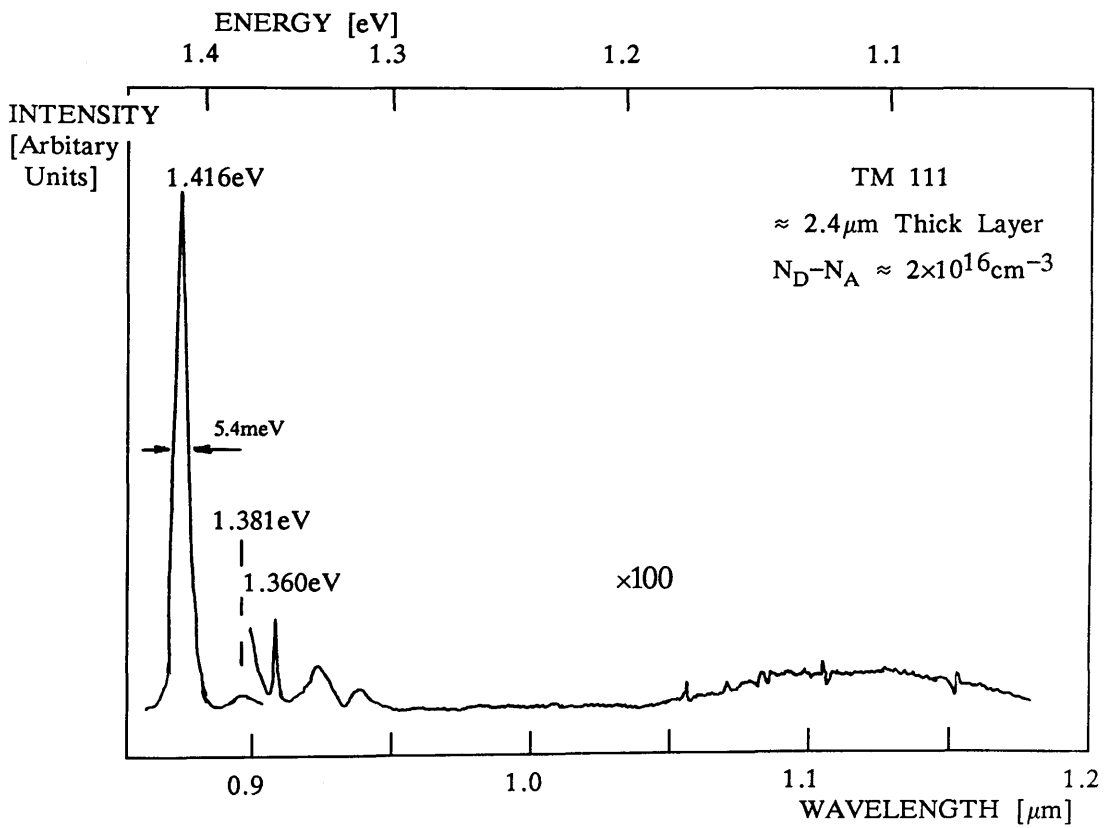
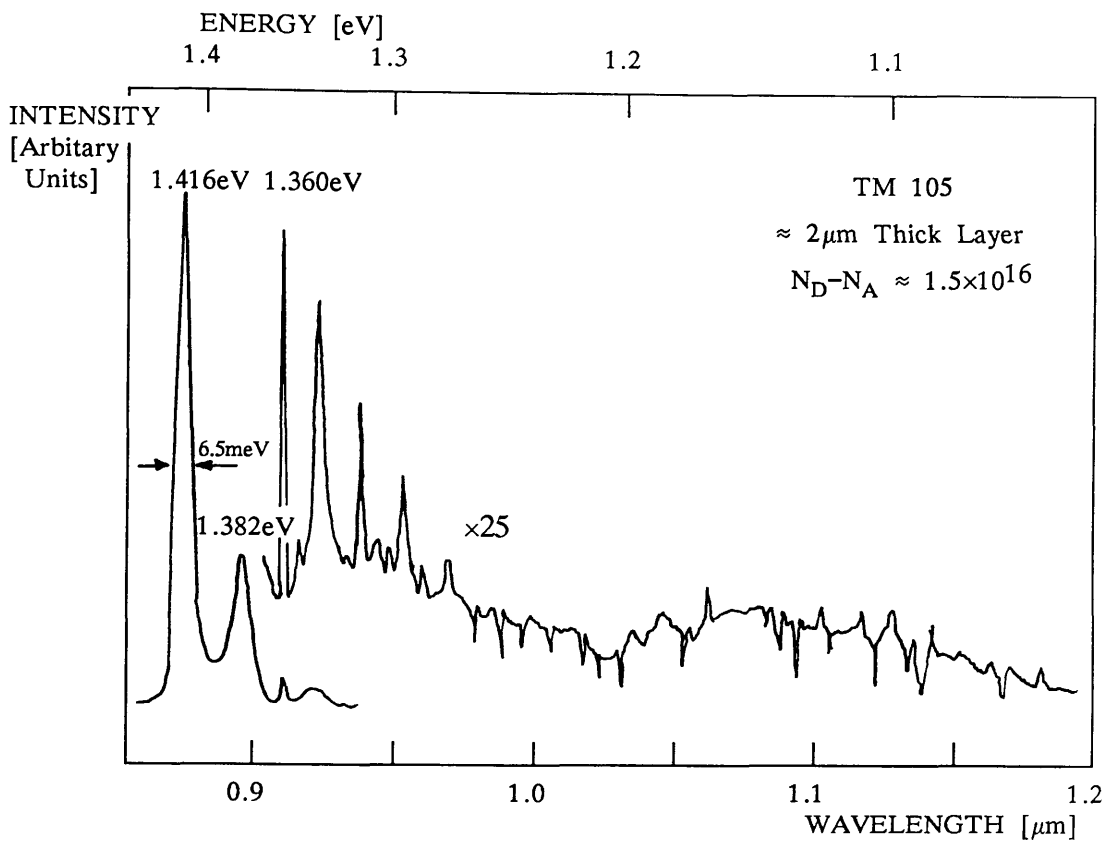


FIGURE 3.8

PHOTOLUMINESCENCE SPECTRA OF LAYERS TM 105 and TM 111

The most striking feature of the results discussed above is that ALL unintentionally doped InP layers are n-type, a universal property of MBE grown InP (section 1.4). In addition, most contemporary data indicated that residual carrier concentrations are in the range $1-3 \times 10^{16} \text{cm}^{-3}$ (table 1.2) with 77K mobilities 10,000 to $12,250 \text{cm}^2 \text{V}^{-1} \text{s}^{-1}$ in close agreement with the data for material grown in Chamber 2. Recent papers discuss material with improved electron mobilities: $55,000 \text{cm}^2 \text{V}^{-1} \text{s}^{-1}$ [3.13] and $30,000 \text{cm}^2 \text{V}^{-1} \text{s}^{-1}$ [3.14] (due primarily to reductions in the dominant donor impurity identified in this work) but no evidence has been published of a switch in residual carrier type from n- to p-type as observed in undoped GaAs [3.15].

3.4 SIMS ANALYSIS

The power of SIMS to provide quantitative information on the concentrations of both electrically active and inactive residual impurities has been amply demonstrated on layers grown in Chamber 1. The technique was again applied to layers produced in Chamber 2 and the data for the elements Al, Ca, C, Cr, Cu, Ge, Fe, Mg, Mn, Ni, Se, Si, Ag, Na, S, Te, Sn and Zn is summarised in table 3.3.

The most prominent result of the SIMS analyses is that sulphur is the dominant impurity with a concentration, as determined from specially commissioned implant standards, in the range $1-3 \times 10^{16} \text{cm}^{-3}$. The only other donor impurity positively identified is Si with a concentration of $1-2 \times 10^{15} \text{cm}^{-3}$, again quantified by comparison with calibrated implant standards. All other potential donor impurities (Se, Sn, Te and Ge) are at concentrations $< 4 \times 10^{15} \text{cm}^{-3}$.

Of the remaining elements, only Ca is at a concentration greater than 10^{15}cm^{-3} . Calcium implant standards were unavailable during the present investigation and hence the calcium concentration was established using two techniques: by comparison with the known concentration in the LEC substrates and by using the ion yield of Ca with respect to Mg for which accurate implant standards had been obtained (Appendix A.2). Both techniques placed the Ca concentration in the epitaxial layers in the range $2 \times 10^{15} \text{cm}^{-3}$ to $2 \times 10^{16} \text{cm}^{-3}$.

The presence of C in the layers could not be established by SIMS which had a detection limit of $\sim 10^{17} \text{cm}^{-3}$ for this element [3.16]. However, evidence from the photoluminescence spectra indicates that C is not the dominant acceptor since the e-A recombination is centred at 1.382eV and not 1.379eV, the transition associated with e-A_C [3.11]. The apparent absence of carbon from the epitaxial InP is also

| ELEMENT | CONCENTRATION [cm ⁻³] | CALIBRATION | COMMENTS |
|---------|--|------------------------------|---------------------------------------|
| Ag | | | Below detection limit |
| Al | | | Below detection limit |
| C | | | Below detection limit |
| Ca | 2×10 ¹⁵ –2×10 ¹⁶ | Ion yield Sub. comparison | Section 3.5.2 |
| Cr | < 1×10 ¹⁴ | Implant | Below detection limit |
| Cu | | | No signal detected |
| Ge | < 4×10 ¹⁵ | Implant | No signal detected |
| Fe | < 1×10 ¹⁵ | Implant | Below detection limit |
| Mg | < 1×10 ¹⁴ | Implant | Section 3.3 |
| Mn | < 1×10 ¹⁴ | Implant | No signal detected |
| Na | < 3×10 ¹⁴ –1×10 ¹⁵ | Sub. comparison | Below detection limit |
| Ni | | | Below detection limit |
| S | ~2×10 ¹⁶ | Implant | Section 3.5.1 |
| Se | < 10 ¹⁴ | Implant | No signal detected |
| Si | 1.5×10 ¹⁵ | Implant | |
| Sn | < 4×10 ¹⁵ | Implant | Below detection limit Appendix A.2 |
| Te | < 5×10 ¹⁴ | Ion yield | Below detection limit |
| Zn | < 4×10 ¹⁴ | Implant | No signal detected |

"Below detection limit" -

Signal recorded was shown either by the use of step changes in the sputter rate or isotope ratios not to be related to the epitaxial layer.

TABLE 3.3 SUMMARY OF THE IMPURITIES IN
UNINTENTIONALLY DOPED InP GROWN IN CHAMBER 2
- AS IDENTIFIED BY SIMS

consistent with thermodynamic calculations [3.17] which show that the equilibrium pressure of CO for C incorporation into InP is ~ 0.1 mbar (i.e. more than 8 orders of magnitude larger than that actually present).

A number of specific layers were grown to establish the dependence of the impurity concentrations on substrate temperature, phosphorus flux and indium flux. The three step deposition technique originally devised for use with layers grown in Chamber 1 (section 2.3.3) and illustrated in figure 3.9 (TM 99) and 3.10 (TM 123) was again employed.

(a) Substrate Temperature Dependence

For growth at constant In and P flux, no change in the SIMS or residual carrier concentration could be associated with step changes in substrate temperature within the range ~ 450 – 500°C .

(b) Phosphorus Flux Dependence

A reduction in phosphorus flux of $\sim 33\%$, at a fixed growth temperature and indium flux produced a comparable decrease in both the sulphur and residual carrier concentrations. Reductions of 25% in sulphur and 34% in free electron concentration were recorded for TM 123 (Fig 3.10) while in TM 99 (Fig 3.9) the reduction in free electron concentration was 34%. SIMS profiles of the sulphur concentration in TM 99 were not recorded.

A reduction in Ca by 30% was also recorded in TM 99 (Fig 3.9); however, in TM 123, which has a 50% lower Ca concentration, the statistical variation in the Ca count prevents 30% variations from being discerned. No change in the concentration of other known impurities was detected as a function of phosphorus flux.

(c) Indium Flux Dependence

The In flux was also reduced by $\sim 33\%$ with the growth temperature and phosphorus flux constant; SIMS profiles reveal related changes in the S and Ca impurities only. The S concentration increases by 32% in response to the reduced In flux (growth rate) (TM 123 Fig 3.10) while the Ca concentration increases by 37% (TM 99 Fig 3.9). The low count for Ca in TM 123 (Fig 3.10) prevented detection of any changes in Ca concentration with In flux.

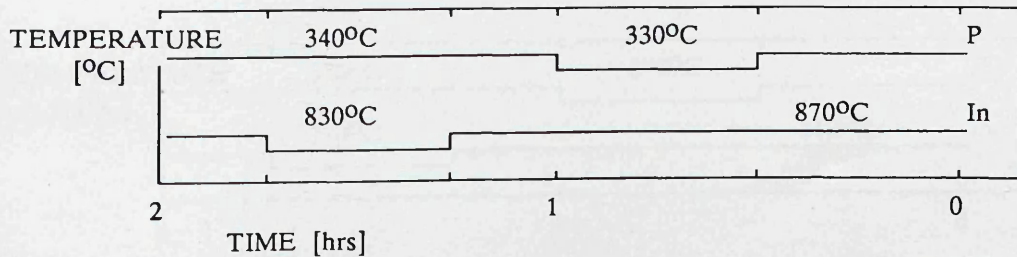
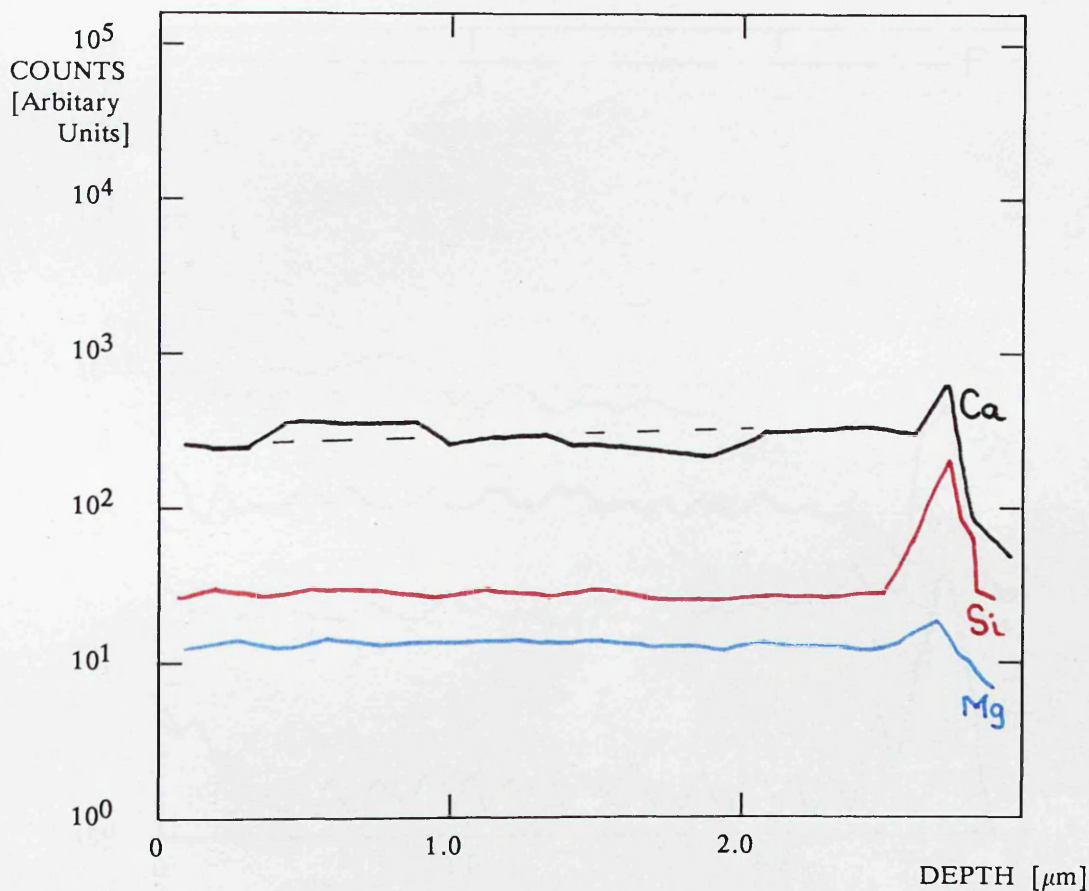
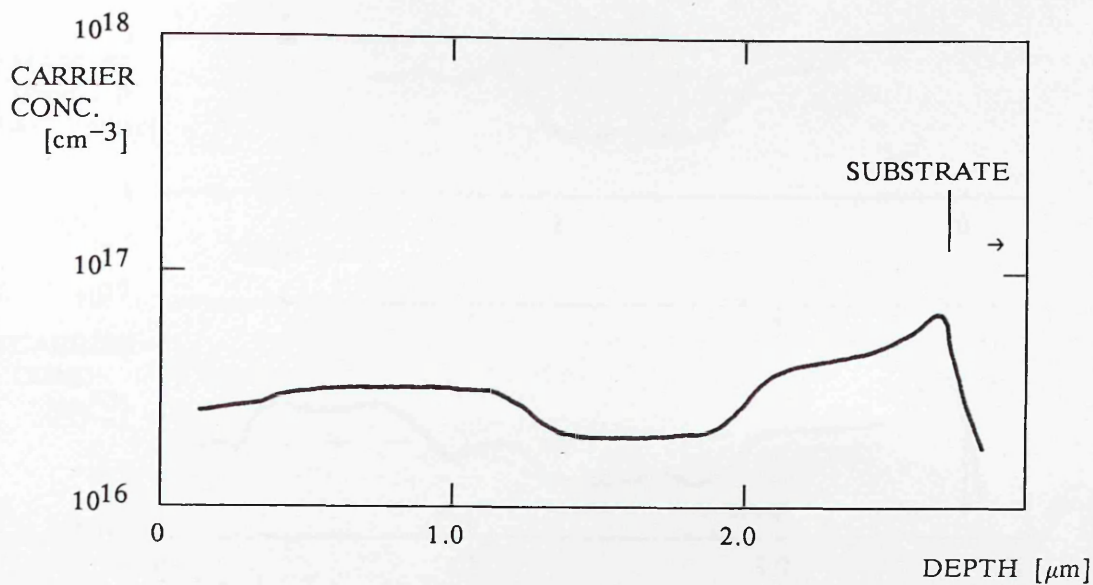


FIGURE 3.9 C-V and SIMS PROFILES OF TM 99

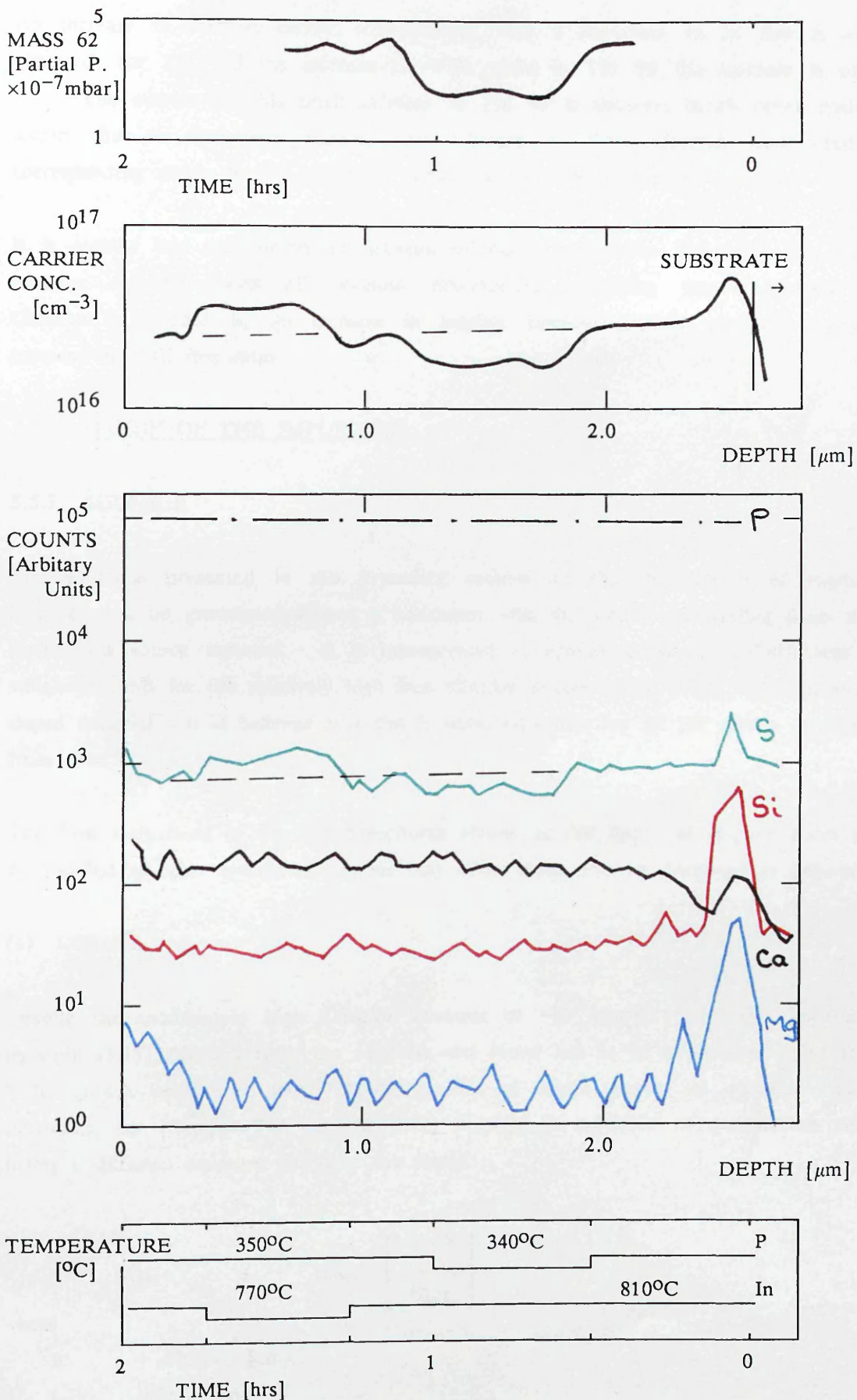


FIGURE 3.10 C-V and SIMS PROFILES OF TM 123

An increase in residual carrier concentration with a reduction in In flux is also observed; for TM 123 the increase is ~40% while in TM 99 the increase is only 3%. The reason for this small increase in TM 99 is unclear; in all other studies where the In flux was reduced, an increase in free electron concentration corresponding simply to the change in growth rate has been detected.

It is notable that the correlation between sulphur concentration and V:III flux ratio remains consistent with all previous observations, including those recorded in Chamber 1. That is, an increase in sulphur concentration is produced by an increase in V:III flux ratio.

3.5 ORIGIN OF THE IMPURITIES

3.5.1 SULPHUR

The evidence presented in the preceding section on the dependence of sulphur incorporation on growth conditions is consistent with the sulphur originating from the phosphorus source material. It is incorporated at concentrations of $1-3 \times 10^{16} \text{cm}^{-3}$ which accounts for the relatively high free electron concentration in all unintentionally doped material. It is believed that this is universally true for all InP grown by MBE from solid sources.

The firm assignment of the red phosphorus charge as the origin of sulphur needs to be justified as other sources of sulphur may exist; these may be dismissed as follows:

(a) Diffusion

Despite the anomalously high diffusion constant of $\sim 10^{-8} \text{cm}^2 \text{s}^{-1}$ at 550°C reported by Chin [3.18] diffusion from the substrate was found not to be a problem under the MBE growth conditions used. SIMS profiles of layers grown on sulphur doped substrates, for example TM 66 (Fig 3.11) provide no evidence of outdiffusion and fitting a diffusion equation [3.19] of the form:

$$C(x, t) \propto \exp \left[\frac{-x^2}{4D_s t} \right]$$

where

- x - distance (cm)
- t - time (sec)
- D_s - Diffusion coefficient ($\text{cm}^2 \text{s}^{-1}$)

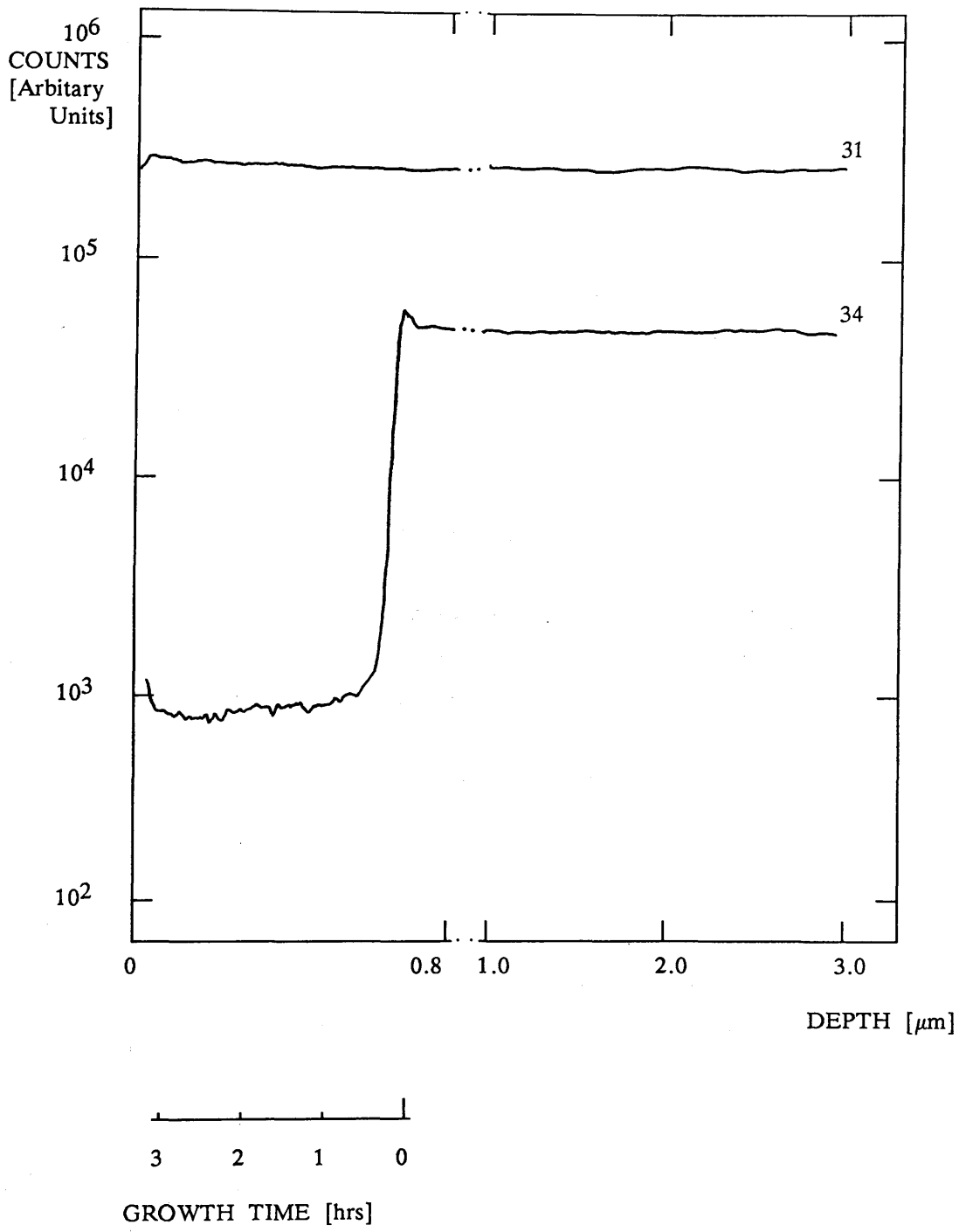


FIGURE 3.11 SIMS SULPHUR PROFILE OF LAYER GROWN ON SULPHUR DOPED SUBSTRATE (TM 66)

to the SIMS sulphur profile for TM 66 indicates $D_S < 2 \times 10^{-16} \text{cm}^2 \text{s}^{-1}$.

The diffusion constant D_S both here and in the experiments of Chin will be a function of impurity concentration since $N_D \gg N_i$ ($N_i \sim 10^{15} \text{cm}^{-3}$) [3.19]. However in both studies $N_D \sim 5 \times 10^{18} \text{cm}^{-3}$ and if the diffusion constant were of the magnitude reported by Chin the sulphur concentration throughout the $0.65 \mu\text{m}$ thick epitaxial layer of TM 66 would have been within $\sim 1\%$ of that in the substrate. Clearly a strong temperature dependence of D_S could account for the discrepancy, as TM 66 was grown at $\sim 450^\circ\text{C}$ in contrast to $\sim 550^\circ\text{C}$ used by Chin. However, the activation energy for diffusion required to bring both results into agreement is 4eV , significantly larger than normally reported [3.19].

(b) Indium Cell and Charge

The indium cell can be eliminated for the following reasons:

(i) If the vapour pressures of sulphur and indium in the temperature range of interest are considered [3.08], then the reduction in sulphur flux produced by a fall in temperature of $\sim 40^\circ\text{C}$ is comparable with, or greater than, the associated reduction in indium flux. The decrease in any sulphur flux from the indium cell at the substrate will therefore be equal to or greater than the associated reduction in the indium flux, resulting in either no net change in sulphur concentration or a slight decrease. This is in contrast to the observed increase (Fig 3.10).

(ii) A change in indium flux varies the effective V:III ratio at the growth surface. An increase in V:III ratio may either: (i) enhance the incorporation of sulphur by reducing the desorption of indium sulphides as observed for S in GaAs [3.20] or (ii) suppress the inclusion of sulphur by reducing the number of phosphorus vacancies, in a manner analogous to the incorporation of Si in GaAs [3.21]. It is difficult, from available experimental data, to discriminate between these two effects but the evidence from intentional sulphur doping studies (section 4.4) indicates that an increase in the V:III ratio at constant growth rate results in a slight decrease in sulphur incorporation.

(iii) Layer TM 83 (Fig 3.12) provides conclusive evidence that the sulphur is not associated with the indium cell. On two occasions during the deposition of this layer growth was interrupted by shuttering the indium cell. Both SIMS and C-V profiles show that the sulphur concentration increased when the indium cell was shuttered but the phosphorus flux continued to be incident on the surface.

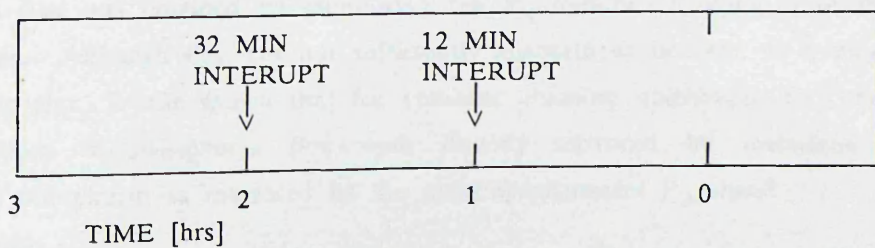
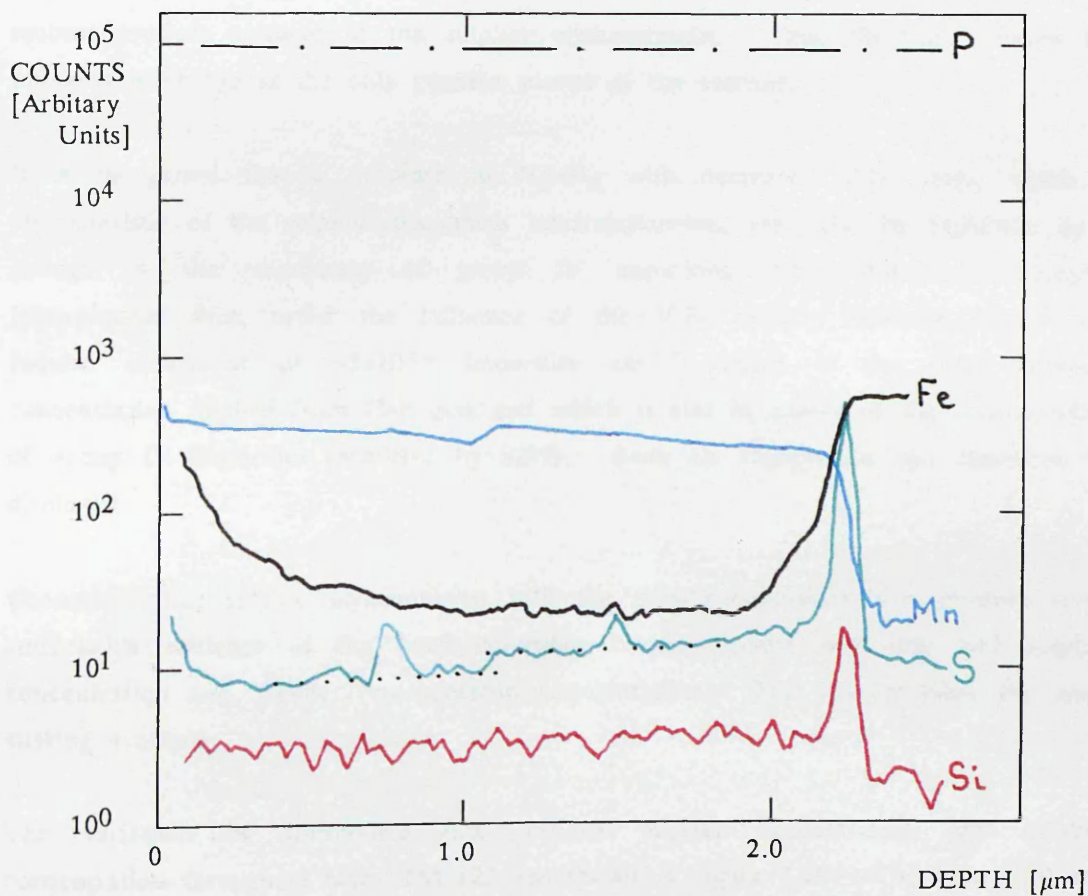
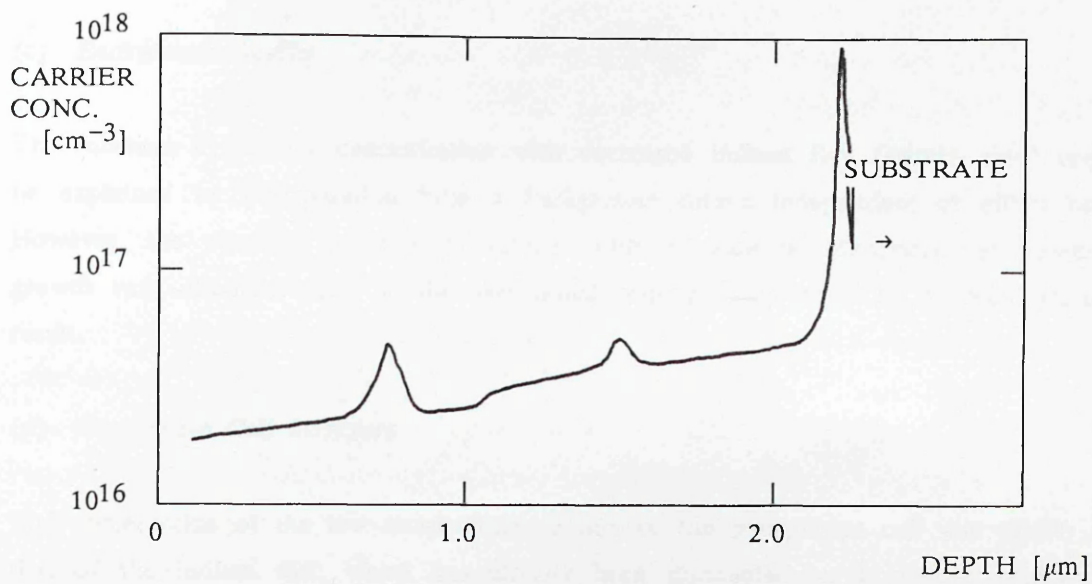


FIGURE 3.12 C-V and SIMS PROFILES OF TM 83

(c) Background Source

The increase in sulphur concentration with decreased indium flux (growth rate) could be explained by incorporation from a background source independent of either cell. However, the observed decrease in sulphur with decrease in phosphorus at constant growth rate discounts this, as the intentional doping data shows an increase should result.

(d) Phosphorus Cell Structure

The construction of the low temperature section of the phosphorus cell was similar to that of the indium cell, which has already been discounted as a possible source of sulphur. In addition, only changes to the source section as opposed to the cracking section produce changes in the sulphur concentration. This, therefore, leaves the phosphorus charge as the only possible source of the sulphur.

It is recognised that a decrease in $N_D - N_A$ with decreased V:III ratio, which is characteristic of the sulphur/phosphorus interrelationship, may also be explained by a change in site occupancy of group IV impurities, from donor to acceptor (phosphorus) sites, under the influence of the V:III ratio. However, this would require movement of $\sim 5 \times 10^{15}$ impurities cm^{-3} , which is the total acceptor concentration implied from Hall data and which is also in excess of the concentration of group IV impurities identified by SIMS. Such an explanation can therefore be dismissed.

Changes in the sulphur concentration with the growth conditions also produce some remarkable evidence of the interrelationship between phosphorus flux and sulphur concentration and, hence, free electron concentration. TM 123 provides the most striking example:

The variations in phosphorus flux, residual carrier concentration and sulphur concentration throughout layer TM 123 are shown in figure 3.10. The record of the phosphorus flux was obtained by monitoring the P_2 (62a.m.u.) signal from the mass spectrometer. Although this was not sufficiently accurate to be used as a monitor of the absolute flux, it was shown that for constant chamber conditions, i.e. cryopanel full, variations in phosphorus flux were directly mirrored by variations in the background phosphorus as measured by the mass spectrometer P_2 signal.

Monitoring the phosphorus flux during growth revealed that when step changes were

introduced in the set temperature of the phosphorus cell, damped oscillations in the phosphorus flux resulted. These oscillations reflect the attempts of this particular controller to stabilise the cell temperature in response to the step change. Examination of the SIMS and C-V profiles shows that these oscillations in phosphorus are exactly replicated in the sulphur and residual carrier concentrations (Fig 3.10).

The results for sample TM 83, during which growth was interrupted and sulphur was observed to accumulate, could have serious implications for thermal cleaning of InP in a phosphorus flux. The first pause was for a period of ~12 mins and the second for ~32 mins. Integration of the SIMS concentration profile at each interrupt shows that the accumulated sulphur is equivalent to $\sim 2 \times 10^{-4}$ of a monolayer (bulk concentration $\sim 4 \times 10^{18} \text{cm}^{-3}$). The sulphur flux estimated from the concentration of sulphur incorporated in the epitaxial layer is $\sim 6 \times 10^8 \text{atoms cm}^{-2} \text{s}^{-1}$ which would result in accumulation of 1×10^{-3} of a monolayer in 20 minutes, in good agreement with the measured value. The evidence suggests that sulphur is replacing phosphorus from the group V surface lattice sites and, taken to the limit, the surface would become indium sulphide. Fortunately, the accumulation of a monolayer of sulphur would take >250hr while heat cleaning is usually complete within ~30 minutes. It is interesting to note that indium sulphides, InS_2 and In_2S_3 formed by the reaction of sulphur or H_2S with InP in vacuum are actively being studied as dielectrics for InP MISFETS [3.22].

3.5.2 CALCIUM

The origin of the Ca in the layers is more obscure and cannot be unequivocally identified from variations in concentration with growth conditions. This is principally because Ca incorporation and, more importantly, its dependence on phosphorus overpressure, has not been characterised either in this study or in the literature [3.24]. However, it is reasonable to assume that under the growth regimes discussed here, Ca will incorporate with unity sticking coefficient and will not be affected by the changes in the phosphorus overpressure at constant growth rate. Evidence to support this assumption is provided by the detailed studies of the incorporation of the group IIa impurities Be and Mg into GaAs. Be incorporation is found [3.25] to be independent of both growth temperature and III:V flux ratio, while Mg, which has a vapour pressure 100× higher than Ca, is reported [3.26] to have a unity incorporation coefficient for growth temperatures <490°C. The only other element whose incorporation onto the group III site in MBE growth has been characterised in detail, is Mn [3.27]. For Mn desorption is again reported to be negligible at temperatures below 500°C, although incorporation is complicated by

surface segregation.

There are five high temperature components within the chamber which are potential sources of Ca: indium, phosphorus, tantalum, graphite and p-BN. These sources may be examined by techniques similar to those used to isolate the origin of the residual sulphur:

(a) Background

If the incorporation of Ca from a background source as opposed to either the indium or phosphorus cell is not dependent on the group V overpressure, then the concentration will increase with a decrease in indium flux (growth rate) and will be unchanged by a change in phosphorus flux. The SIMS profile for TM 99 (Fig 3.9) shows an increase in Ca concentration with reduction in indium flux (growth rate) and a decrease when the phosphorus flux is reduced; it is unlikely, therefore, that Ca is incorporated from a background source.

(b) In charge and cell structure

A comparison of the vapour pressure of indium and calcium shows that similar reductions in flux are produced by a 40°C reduction in cell temperature [3.08]. Therefore, if the Ca was an impurity in either the In cell or charge, a reduction in In flux would produce, at most, a small change in the concentration of Ca. In contrast, an increase in Ca inverse to the change in growth rate is observed (Fig 3.9) indicating that neither the indium cell nor the indium charge is the source of Ca.

(c) P cell structure

The structures of both the phosphorus cell and the indium cell were similar. This factor, combined with the evidence that the indium cell was not the origin of the Ca, indicates that the structure of the phosphorus cell is unlikely to be the source of Ca.

(d) Red phosphorus

It would appear from the available evidence that Ca originates from the phosphorus source and arrives at the substrate in coincidence with the P₂ flux. Such a mechanism is not inconsistent with the purity specification of red phosphorus as the

detection limit for Ca is ~ 1 p.p.m.a. [3.28] and the phosphorus flux used for growth was $\sim 9 \times 10^{15}$ atoms $\text{cm}^{-2}\text{s}^{-1}$ (section 5.2). Hence the Ca flux co-evaporating with the phosphorus and incident on the substrate could be as large as 9×10^9 atoms $\text{cm}^{-2}\text{s}^{-1}$, which for a growth rate of $1.5 \mu\text{m hr}^{-1}$ would produce a Ca concentration of $3 \times 10^{17} \text{cm}^{-3}$.

Since Ca is a group IIa element it should exhibit behaviour similar to that of Be and Mg in III-V semiconductors. In practice, the data from various analyses are not self-consistent and further discussion of the role of Ca as the dominant "acceptor like" impurity identified by SIMS is required.

In the first place, the concentration of Ca established by SIMS is comparable to the ionised acceptor concentration (N_A) deduced from the 77K Hall data [3.29] (Table 3.2 and 3.3), which would seem to offer a direct correlation between N_{Ca} and N_A .

However, if $N_{\text{Ca}} \approx N_A \approx 5 \times 10^{15} \text{cm}^{-3}$ then one would expect a strong photoluminescence signal due to $e-A_{\text{Ca}}$ recombinations. The only published data on Ca in InP is the work of Kubota et al [3.30] relating to bulk material, who report a $e-A_{\text{Ca}}$ recombination centred at 1.382eV for residual acceptor concentrations in the range 10^{16} to 10^{18}cm^{-3} . This is close in energy to transitions produced by Be, C, Mg and Zn. However, the accuracy of Kubota et al's result is questionable given both the high residual acceptor concentrations used and the large variation in acceptor concentrations for nominally the same Ca concentration.

Since the recombination at $\sim 1.382\text{eV}$ in layers TM 93-TM 123 has already been firmly assigned to Mg, both by correlation with a calibrated change in Mg concentration (section 3.3) and by a detailed comparison [3.12] with the low temperature and low pump intensity results of Skromme [3.11], Ca does not appear to be incorporated as a shallow ionised acceptor in the present material. If it is incorporated as a neutral species then another defect(s) must be invoked to account for the apparent concentration of ionised acceptors (N_A). This is discussed further in section 4.3.

Alternatively, it is possible that Ca is incorporated as a deep ionised acceptor similar to Ca in MBE grown GaAs [3.31], where the large Ca atom disrupts the GaAs lattice. In this case it must either be a non-radiative recombination centre or cause luminescence outside the spectral range of the Ge photodetector employed, $< 0.7\text{eV}$ (Appendix A.5). A comparison of the covalent radii of Ga, As, In, P, Ca and Mg

is presented in table 3.4:

TABLE. 3.4

COVALENT RADII (Angstroms)

| | | | | | |
|----|------|----|------|----|------|
| Mg | 1.36 | Ga | 1.26 | P | 1.06 |
| Ca | 1.74 | In | 1.44 | As | 1.2 |

From this comparison it can be seen that the strain introduced by Ca in InP (~20%) will be less than in GaAs (~40%) because of the large In atom, and the formation of a deep level less probable. Further studies, including deep level transient spectroscopy (DLTS) would be required to fully characterise the behaviour of Ca in InP.

3.6. PHOTOLUMINESCENCE FROM MBE GROWN InP

Photoluminescence was used routinely to provide a rapid assessment of the quality of the epitaxial InP grown. 15K photoluminescence spectra were recorded for layers TM 96–TM 126 under an excitation intensity of 10Wcm^{-2} at 633nm. The spectra were found to be essentially independent of growth conditions and the observed features can be divided into four, associated with band edge (BE), band to acceptor (e–A), 1.36eV exciton and deep level recombination mechanisms.

The principal transition, at $1.415\text{eV}\pm 1\text{meV}$, is produced by band edge recombination and is assigned to an exciton bound to a neutral acceptor (A^0X) [3.32]. Measured linewidths typically 7meV (f.w.h.m.) and at best 4.5meV (TM 114, Fig 3.13) are also a function of excitation intensity. This dependence on excitation intensity can be attributed to local heating [3.33] and is illustrated for TM 121 in figure 3.14 where a reduction in intensity to 0.5Wcm^{-2} reduces the linewidth from 7 to ~4.5meV; the study of further reductions was limited by signal to noise considerations.

Such linewidths demonstrate that the optical properties of the InP grown in Chamber 2 were equivalent to what was then state of the art data for MBE InP. For example, the data recorded from layer TM 114 was comparable with the narrowest bound exciton linewidth, of 4meV, obtained under similar excitation conditions by Tsang [3.34].

e–A recombination at $\sim 1.382\text{eV}$ (f.w.h.m. 10–20meV) was detected in all layers and

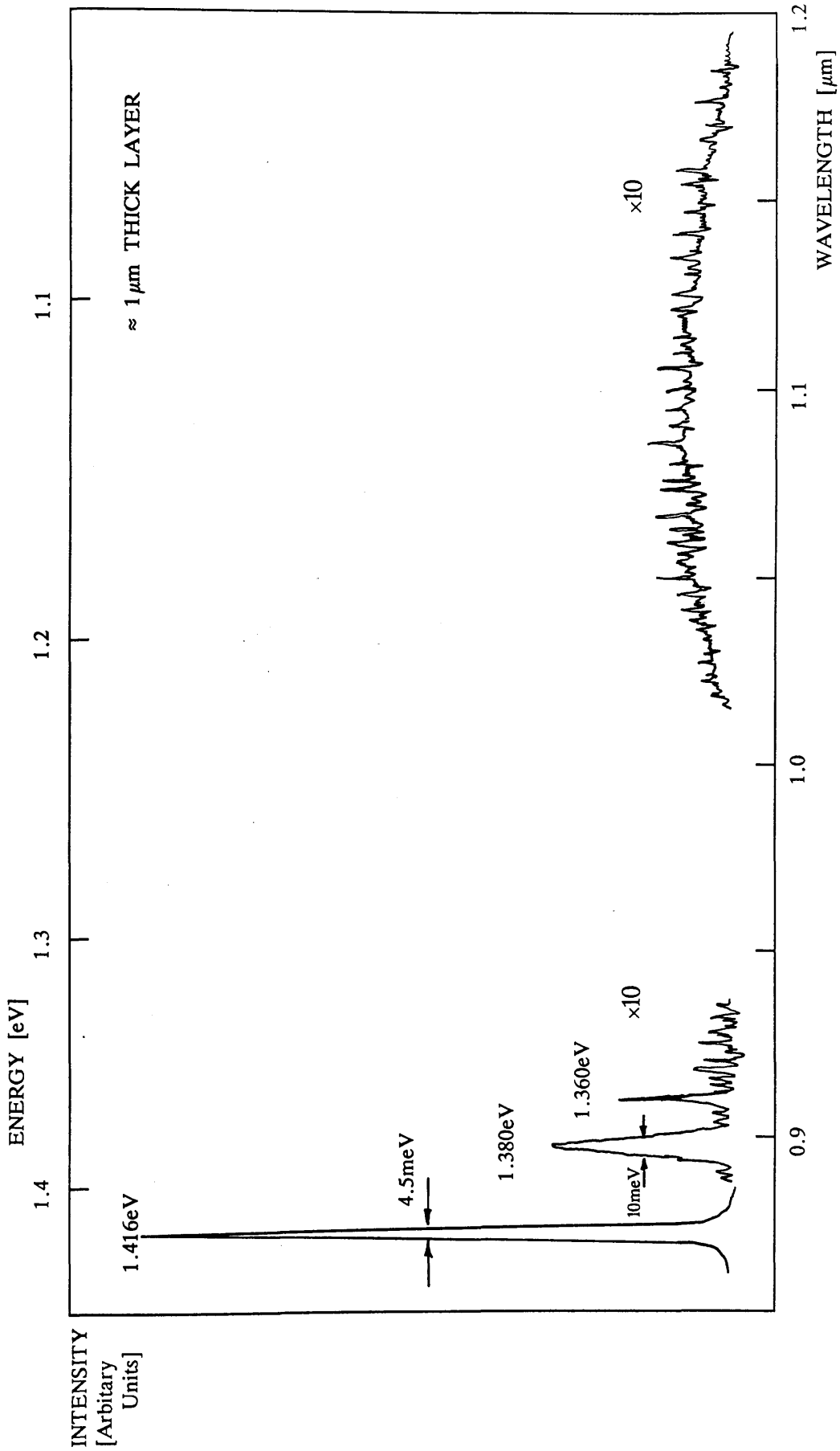
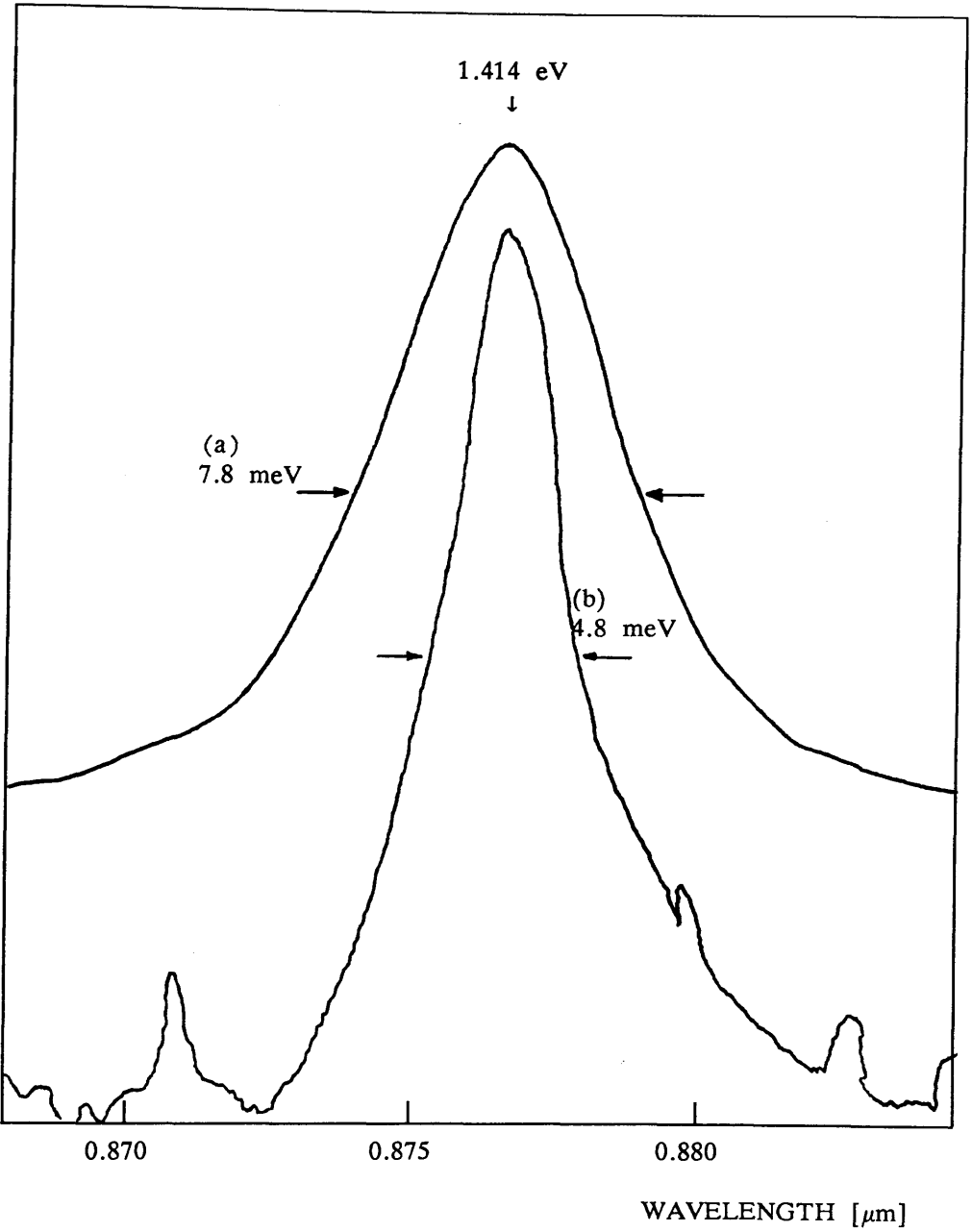


FIGURE 3.13 PHOTOLUMINESCENCE SPECTRUM OF TM 114



(a) excitation intensity 10Wcm^{-2}

(b) excitation intensity 0.5Wcm^{-2}

FIGURE 3.14 THE F.W.H.M. OF THE BAND EDGE RECOMBINATION VERSUS EXCITATION INTENSITY.

(LAYER TM 121)

discussed in detail in section 3.3. Three layers also exhibited two additional e-A like recombinations, one at 1.394eV (TM 119 and 122, Fig 3.7) and one at 1.40eV (TM 123, Fig 3.15). However, the lineshape and energy of these transitions is masked by the dominant BE and e-A recombinations on either side (1.414eV and 1.38eV), and their origin remains the subject of debate. Numerous reports of PL transitions with energies at these values have been published and are summarised by Kim et al [3.35]. Although the origins proposed for many of these transitions are tentative a recent study [3.36] of recombination attributed to surface states appears to be most consistent with the luminescence at 1.394 and 1.40eV observed in this work.

Excitation recombination at 1.36eV was observed in all layers and has been assigned by Duncan et al [3.37] to an exciton bound to a deep donor. The linewidth of the exciton, ~ 1.5 meV, was comparable with Duncan's published data but the number of associated phonon lines was larger, extending to 100meV below the zero phonon line (TM 120, Fig 3.16). Such extended phonon replicas are indicative of high crystal quality. However, the number of replicas cannot be compared directly with replica of the band edge recombination as the two centres have different lattice coupling factors [3.38].

Although the ratio between the intensity of the emission at 1.36eV and the band edge varied by a factor of 40 between all samples examined, no correlation between absolute intensity at 1.36eV and growth conditions could be identified. This observation is in contrast to the results of Wakefield et al [3.39] who found that a 50°C increase in the growth temperature, from 520°C to 570°C, produced "a stronger intensity 1.36eV line". The possibility proposed by Wakefield that the centre was a complex involving a phosphorus vacancy is not, therefore, substantiated, despite the growth temperature being varied by 50°C and the V:III ratio by 8×. A more detailed investigation of the 1.36eV recombination, including the possibility that it is a function of phosphorus overpressure and at least one other variable, is clearly required.

Subsequent analysis of this transition [3.40] has revealed a thermal activation energy for the photoluminescence intensity of ~ 10 meV and shown that the recombination can be suppressed by growth at both low temperatures, $< 400^\circ\text{C}$, and high temperatures, $> 550^\circ\text{C}$.

The deep level recombination band at ~ 1.1 eV, related to the transition metals Fe and Mn was observed in only a limited number of layers and was always dominated by the tail of the 1.36eV replica.

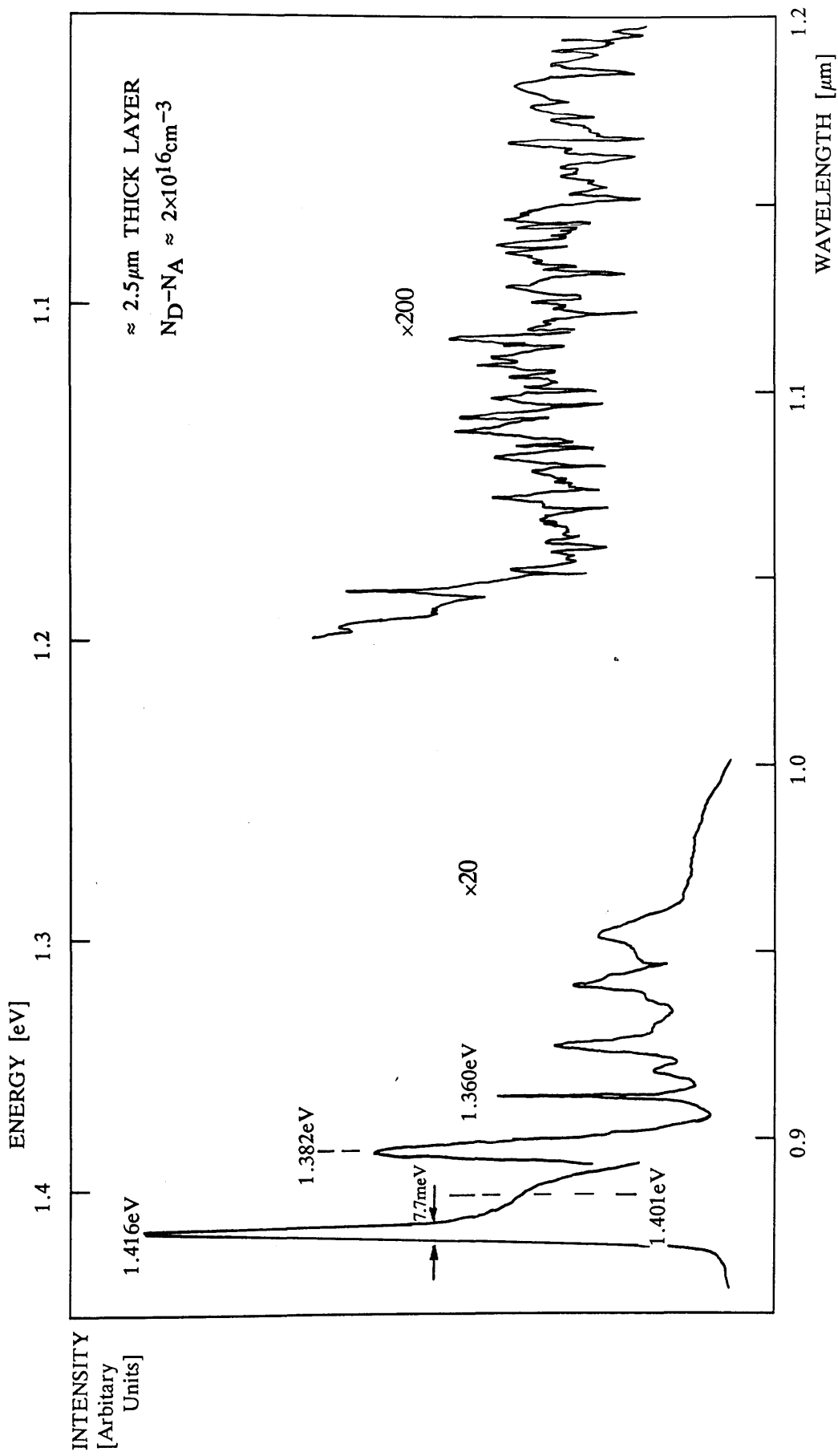


FIGURE 3.15 PHOTOLUMINESCENCE SPECTRUM OF TM 123

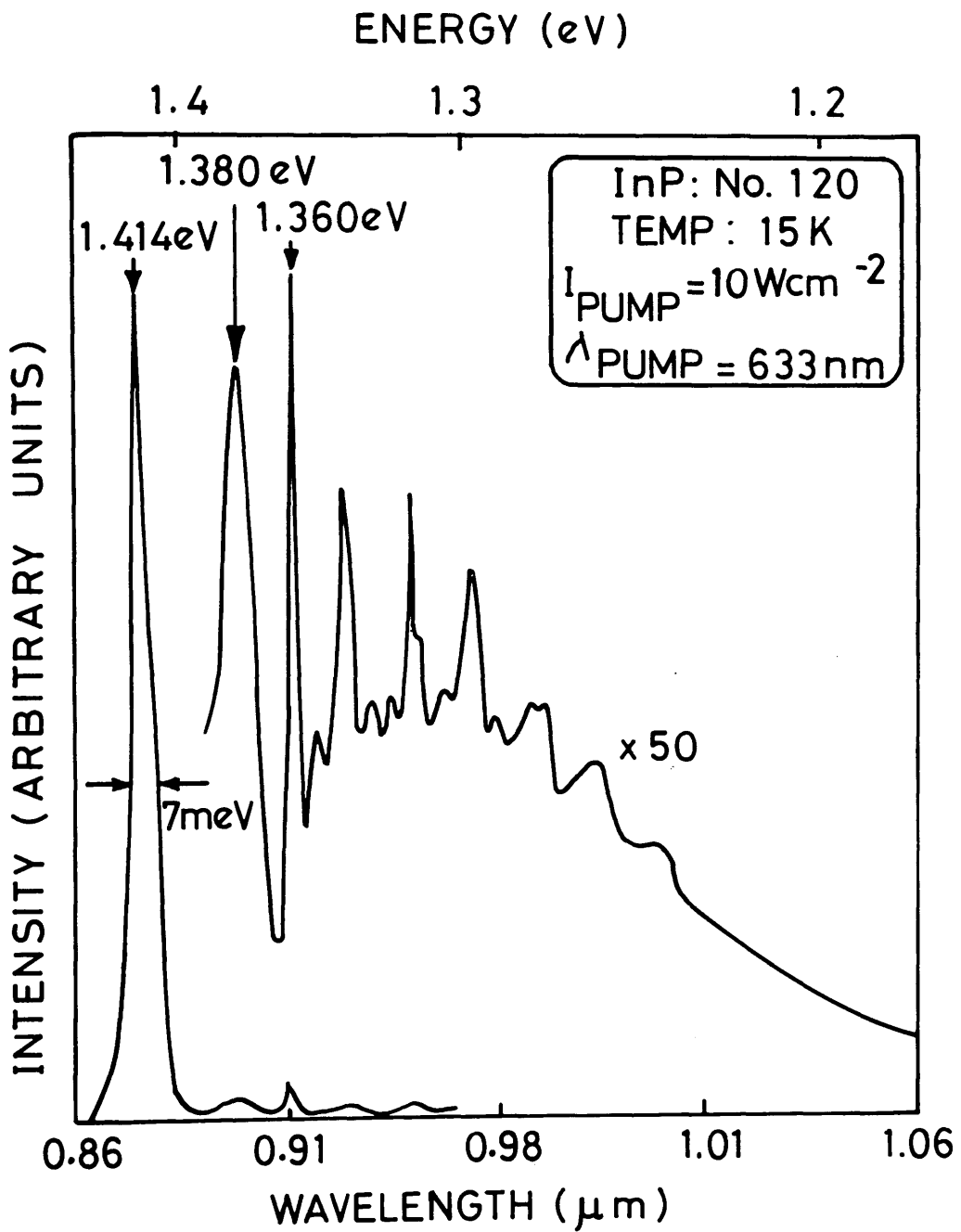


FIGURE 3.16 PHOTOLUMINESCENCE SPECTRUM OF TM 120

3.7 SUMMARY

The principal impurity present in unintentionally doped InP is sulphur which, at a concentration of $\sim 10^{16}\text{cm}^{-3}$, dominates the electrical properties. The origin of this sulphur has been shown to be the phosphorus source material. The universal n-type behaviour of InP grown from solid sources is believed to be a direct consequence of sulphur contamination in red phosphorus.

Silicon at a concentration $1-2 \times 10^{15}\text{cm}^{-3}$ is the only other donor impurity known to be present. The origin of Si has been associated by Roberts [3.13] with graphite used in the group V cracker zone, although it can also be present in AlA grade indium (T.M.I. $< 0.5\text{p.p.m.a.}$) at concentrations of $\sim 0.2\text{p.p.m.a.}$ [3.41].

Calcium is present in the epitaxial layers at an estimated concentration of $\sim 5 \times 10^{15}\text{cm}^{-3}$. The role of Ca is, however, unclear as the dominant e-A recombination in the photoluminescence spectra has been assigned to Mg, the concentration of which was $\sim 10^{14}\text{cm}^{-3}$. The most likely source of Ca is believed to be the red phosphorus charge, in common with the principal residual donor impurity, sulphur.

CHAPTER 4

SULPHUR DOPING OF InP

- 4.1 INTRODUCTION
- 4.2 ELECTROCHEMICAL SULPHUR CELL
- 4.3 PROPERTIES OF SULPHUR DOPED InP
- 4.4 SULPHUR INCORPORATION AS A FUNCTION OF GROWTH CONDITIONS
- 4.5 SUMMARY

4.1 INTRODUCTION

The choice of suitable n-type dopants for use in the MBE growth of III–V semiconductors is limited to either group IVb or VIb elements of the periodic table. The group IVb elements are potentially amphoteric but are generally incorporated as donors under the group V rich growth conditions used for MBE growth [4.01] [4.02]. The exception is carbon, which is an acceptor [4.03]. In contrast, the group VIb elements only incorporate as donors but are more volatile than the group IVb elements [4.04].

Silicon doping of InP was studied over the concentration range 2×10^{17} – $1 \times 10^{19} \text{cm}^{-3}$ by Kawamura et al [4.05]. Incorporation was independent of growth temperature and no evidence for surface segregation was reported. However, Si has been criticised because it is a low vapour pressure element requiring the use of high cell temperatures [4.06] which are a potential source of unintentional impurities. Evidence for this was presented by Kawamura, who reports a compensation ratio of 0.5. Recent developments in cell design and outgassing procedures have minimised this problem [4.07].

Sn, in contrast, has a vapour pressure 4–5 orders of magnitude greater than that of Si enabling significantly lower source temperatures to be used. Indeed, Roberts et al [4.08] have described intentional Sn doping of InP over the limited range 9×10^{16} – 9×10^{17} with compensation ratios of 0.2, while Sullivan [4.09] has obtained Sn concentrations as high as $2 \times 10^{19} \text{cm}^{-3}$ although reporting twinning at these high concentrations. Sn doping profiles are less abrupt than those obtained with Si [4.05] although the surface segregation observed in GaAs has not been reported in InP.

Prior to the present investigation, sulphur had not been employed as an intentional n-type dopant in the MBE growth of InP. However, it was and still is used in the growth of InP by other epitaxial techniques [4.10] [4.11] [4.12] and in the MBE growth of GaAs [4.13] [4.14] [4.15]. In addition to providing an alternative n-type dopant to Si and Sn, intentional sulphur doping enables the incorporation of sulphur to be characterised as a function of growth conditions. This information is essential if the concentration in inadvertently doped material is to be reduced by optimising the growth parameters. The data cannot be obtained directly from the growth of unintentionally doped InP since the sulphur in the phosphorus flux is not independently variable. A separate sulphur source which can be controlled to provide a flux at least an order of magnitude larger than the unintentional concentration is essential.

The principal problem with the use of sulphur and the other chalcogens, Se and Te, is their high vapour pressure, an equilibrium value of 10^{-6} mbar (1 monolayer s^{-1}) being obtained at 20°C for S, 105°C for Se and 225°C for Te [4.16]. Doping from an elemental source, therefore, requires control of the source at and below ambient temperatures, while UHV baking procedures result in the loss of the charge. To overcome this, two types of "captive" sources have been developed for the chalcogens:

- (a) Sn and Pb chalcogenides, e.g. SnTe and PbSe, which operate typically at temperatures in the range 350°C to 600°C [4.06] [4.13] but whose use is complicated by the co-evaporation of Sn or Pb. In the case of the Sn compounds, the dopant flux is the dimer, e.g. SnTe, and surface segregation of both the Sn and Te as well as a temperature dependent incorporation has been reported [4.06]. Pb in contrast is not incorporated [4.17] but segregates on the surface modifying the surface reconstruction [4.13].
- (b) Electrochemical sources which operate at temperatures in the range 200–350°C and produce a pure group VIb flux controlled by an applied EMF (section 4.2). The advantages of this source over conventional thermal sources are (i) the cell operates at low temperatures where impurities evaporating from the cell structure are not generally a problem and (ii) the flux is controlled by an applied EMF and not the thermal response of the cell. Flux variations with a time constant of less than 1 sec [4.14] can be readily achieved.

In the experiments described in this chapter, the sulphur was generated by an electrochemical cell based on a design previously developed at British Telecom Research Labs (BTRL) and used for studying S and Se doping of GaAs [4.15] [4.18].

The chapter is divided into three further sections. In section 4.2, details of the electrochemical source are presented while section 4.3 describes the electrical and morphological properties of the sulphur doped InP epitaxial layers. The dependence of sulphur incorporation on growth conditions is considered in section 4.4. The incorporation mechanism(s) is of interest because of the potential similarity with GaAs where S desorption has been identified [4.15].

4.2 ELECTROCHEMICAL SULPHUR CELL

The Electrochemical Knudsen cell was developed by Ratchford et al [4.19] and used to provide detailed quantitative data on the thermodynamics of the evaporation of sulphur [4.20]. Subsequently, Davies et al [4.14] recognised the potential of the cell as a dopant source for MBE. A complete experimental and theoretical characterisation of the cell has been given by Rickert [4.21].

A schematic of the cell is shown in figure 4.1. It consists of a disc of silver sulphide, one face of which is the source of sulphur and has a line of sight with the substrate; the other face is in intimate contact with a charge of silver iodide which, in turn, is in contact with a disc of silver. The complete $\text{Ag}_2\text{S}:\text{AgI}:\text{Ag}$ sandwich is mounted inside a temperature controlled oven, similar to a conventional Knudsen cell, and an external voltage is applied across the sandwich. The applied EMF depletes or enhances the concentration of silver in the silver sulphide via ionic transport to the adjacent silver electrode. A sulphur flux is then obtained whose magnitude is dependent on the activity of sulphur over the stoichiometry of silver sulphide through the following equation:

$$P_{\text{S}_x} = P^0_{\text{S}_x} \exp \left[\frac{2x[E-E^*]F}{RT} \right] \quad 4.1$$

- P_{S_x} - Equilibrium partial pressure of sulphur molecules S_x over Ag_2S
 $P^0_{\text{S}_x}$ - Equilibrium partial pressure of sulphur molecules S_x over liquid sulphur
 E - Applied EMF
 E^* - EMF of cell in equilibrium with liquid sulphur
 R - Gas constant
 T - Absolute temperature
 F - Faraday's constant

At constant temperature, a change in the applied EMF produces a corresponding change in the sulphur flux, while the current flowing through the cell provides a direct measure of the flux generated.

4.3 PROPERTIES OF SULPHUR DOPED InP

Initial studies were undertaken to characterise both the electrochemical source and also the electrical properties of sulphur doped InP epitaxial layers. These

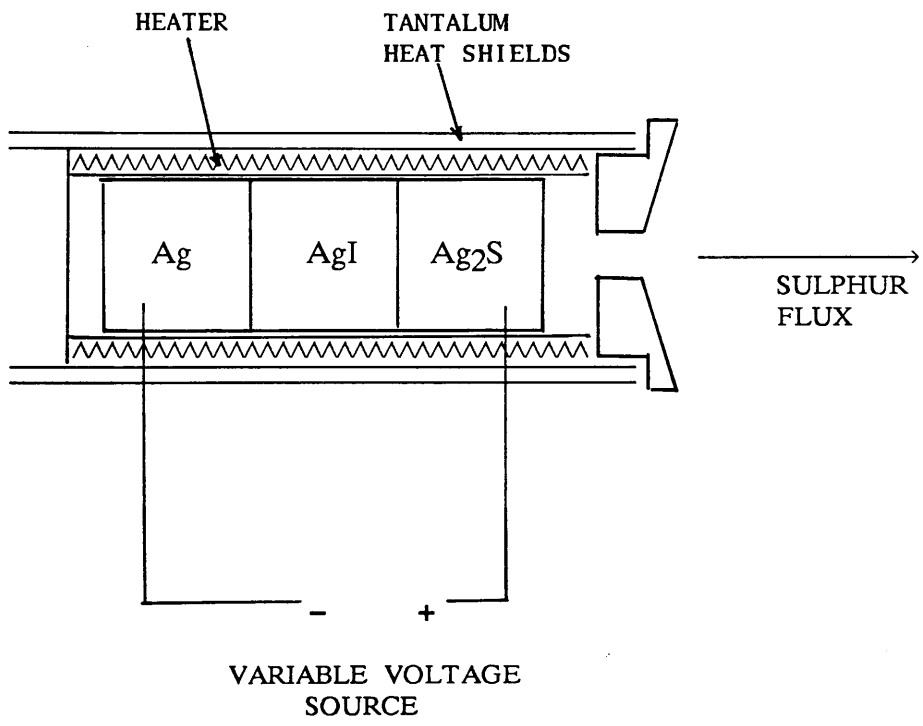


FIGURE 4.1 SCHEMATIC OF THE ELECTROCHEMICAL CELL

experiments were performed using the following growth conditions: the growth temperature was nominally 450°C; the growth rate $\sim 1.5\mu\text{m hr}^{-1}$ and the V:III nude ion gauge current ratio 4:1. The dopant concentration versus cell EMF, its repeatability from run to run and the mobility versus carrier concentration were quantified. The photoluminescence spectra of the intentionally doped epitaxial layers were recorded and the sharpness of the doping profiles assessed.

4.3.1 FREE ELECTRON CONCENTRATION versus CELL EMF

The free electron concentration was measured using C-V profiles. The carrier concentration versus cell EMF obtained from ten epitaxial layers, which included both flat and staircase profiles, is plotted in figure 4.2, covering intentional doping densities in the range $5 \times 10^{16} - 10^{19} \text{cm}^{-3}$.

Although the residual carrier concentration ($N_D - N_A$) is not an absolute measure of the sulphur concentration (C_B), SIMS analyses demonstrate that ($N_D - N_A$) is directly proportional to C_B . Equation 4.1 shows that the gradient of a plot of sulphur concentration versus cell EMF yields a weighted average for the molecular species released from the electrochemical cell. A least squares analysis has been used to obtain a fit to the data and only those points with doping concentrations greater than $1 \times 10^{17} \text{cm}^{-3}$ were included to avoid errors arising from the residual n-type background. The value of x (2.4) obtained from the gradient confirms that S_2 is the dominant species, in agreement with results from sulphur doping of GaAs [4.15].

Some scatter in the sulphur concentration versus EMF is observed and the standard error in the doping is 1.59, indicating that in 95% of all layers grown the dopant concentration would be within a factor of ~ 2 of the required level. When compared with conventional thermal doping sources, e.g. Si, where carrier concentrations within a factor of 1.2 of the required level can readily be achieved, this scatter is significant.

Variations in the growth conditions e.g. growth rate, V:III flux ratio and growth temperature, and errors in the measurement are unable to explain the spread in residual carrier concentration. Similar scatter in the doping concentration is reported in the sulphur doping of GaAs [4.15] and instabilities associated with the electrochemical cell need to be considered. Variations in the applied EMF of 5meV (2%) would be required to produce a factor of 2 variations in the flux, the stability of the supply used was quoted at $< 2\text{meV}$ [4.22] and therefore such variations can be discounted. The effect of changes in the temperature of the cell

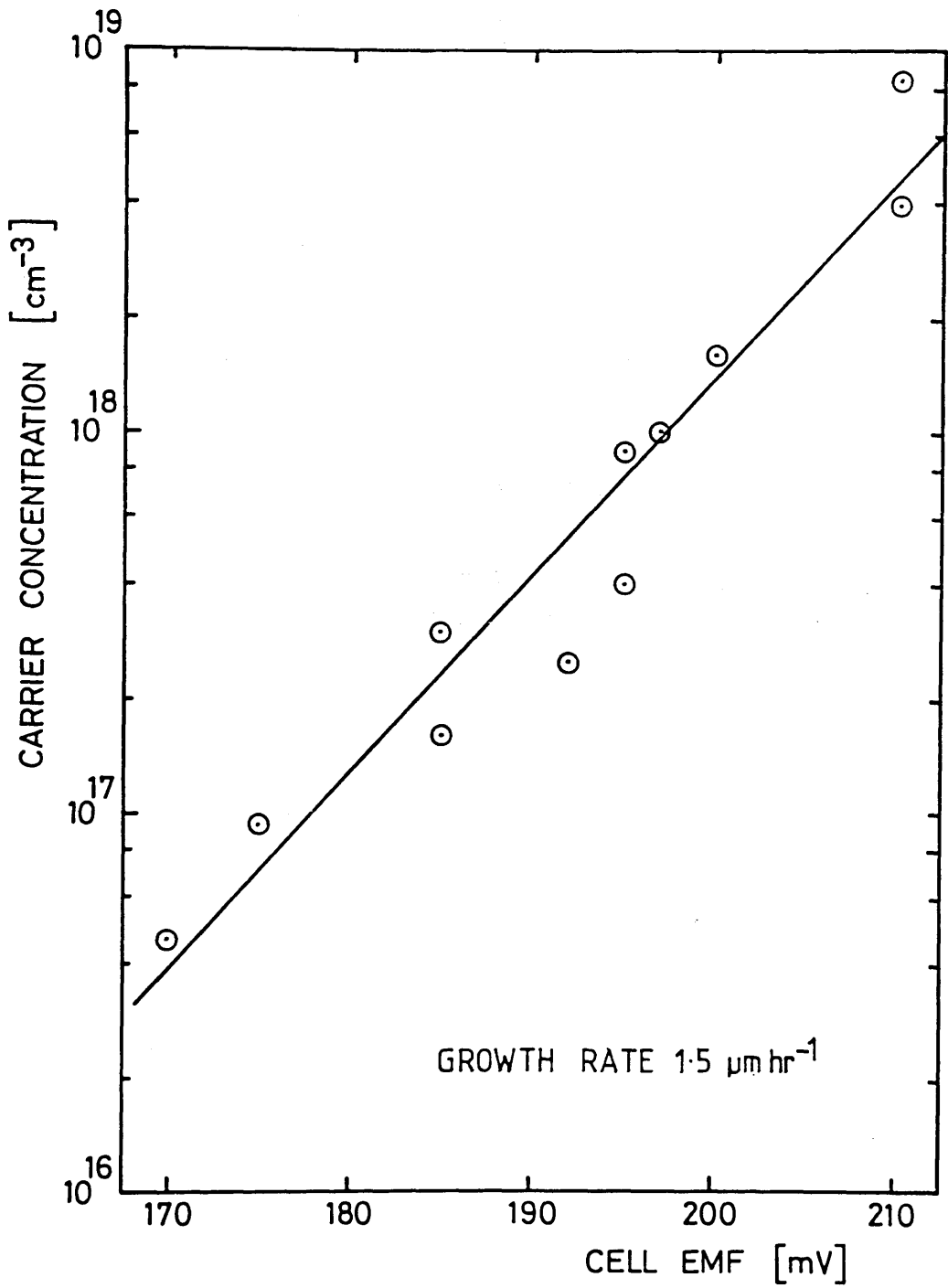


FIGURE 4.2 CARRIER CONCENTRATION VERSUS CELL EMF FOR
SULPHUR DOPED InP

can be assessed using equation 4.1, in which E^* , T and P^0_{Sx} are all temperature dependent. The change in each of these parameters for a 10°C change in temperature has been considered: E^* will increase by $\sim 1.3\text{meV}$ [4.14] and the associated effect will be most significant at high sulphur fluxes, $C_B \approx 4 \times 10^{18}\text{cm}^{-3}$, where $E-E^*$ will increase by $\sim 7\%$. The percentage change in T (nominally 200°C) will be only $\sim 2\%$ and therefore the change in the exponential term of equation 4.1 is $\sim 5\%$, again insignificant. However, the temperature dependence of P^0_{Sx} , determined by Detry et al [4.20] and plotted in figure 4.3, shows that a 10°C change in source temperature produces a factor of 2 change in P^0_{Sx} . Run to run variations in the source temperature of up to 10°C were possible given the low operating temperature of the electrochemical cell, $\sim 200^\circ\text{C}$, and are therefore the most likely cause of the recorded scatter in free electron concentration versus applied EMF.

4.3.2 MOBILITY versus CARRIER CONCENTRATION

Mobility as a function of carrier concentration for six epitaxial layers grown onto semi-insulating (Fe-doped) substrates was characterised over the range $(N_D - N_A) = 5 \times 10^{16}$ to $2 \times 10^{18}\text{cm}^{-3}$. The results from Van-der-Pauw measurements are plotted in figure 4.4 and reveal that at each carrier concentration the measured mobility is $\sim 40\%$ of the maximum predicted from the theoretical calculations of Walukiewicz [4.23]. Cumulative errors in measurements cannot account for the factor of two differences observed and an alternative explanation(s) of the reduced mobility is required.

One possible source of error in Hall measurements is the variation in Hall factor, r_H , as a function of measurement temperature [4.24]. However, although the variation in r_H is most significant for $\mu B < 1$ (B in this study was 0.2Tesla), it is only significant for non-degenerate systems, $n < 10^{16}\text{cm}^{-3}$ [4.24], and does not account for the current results.

The existence of an extrinsic acceptor concentration (N_A) equal to $\sim 0.5N_D$ would also explain the observed results. However, the photoluminescence spectra of two typical layers, TM 165 and TM 168 (Fig. 4.4) with residual carrier concentrations of 2.5×10^{17} and $1.5 \times 10^{18}\text{cm}^{-3}$ respectively, show no evidence for e-A recombination. In addition, no acceptor impurities at concentrations above the levels recorded in the unintentionally doped layers were detected by SIMS. A further possibility is that an acceptor-like defect whose concentration is proportional to the sulphur density is present in the layers. The existence of such a defect has been proposed by Wolfe

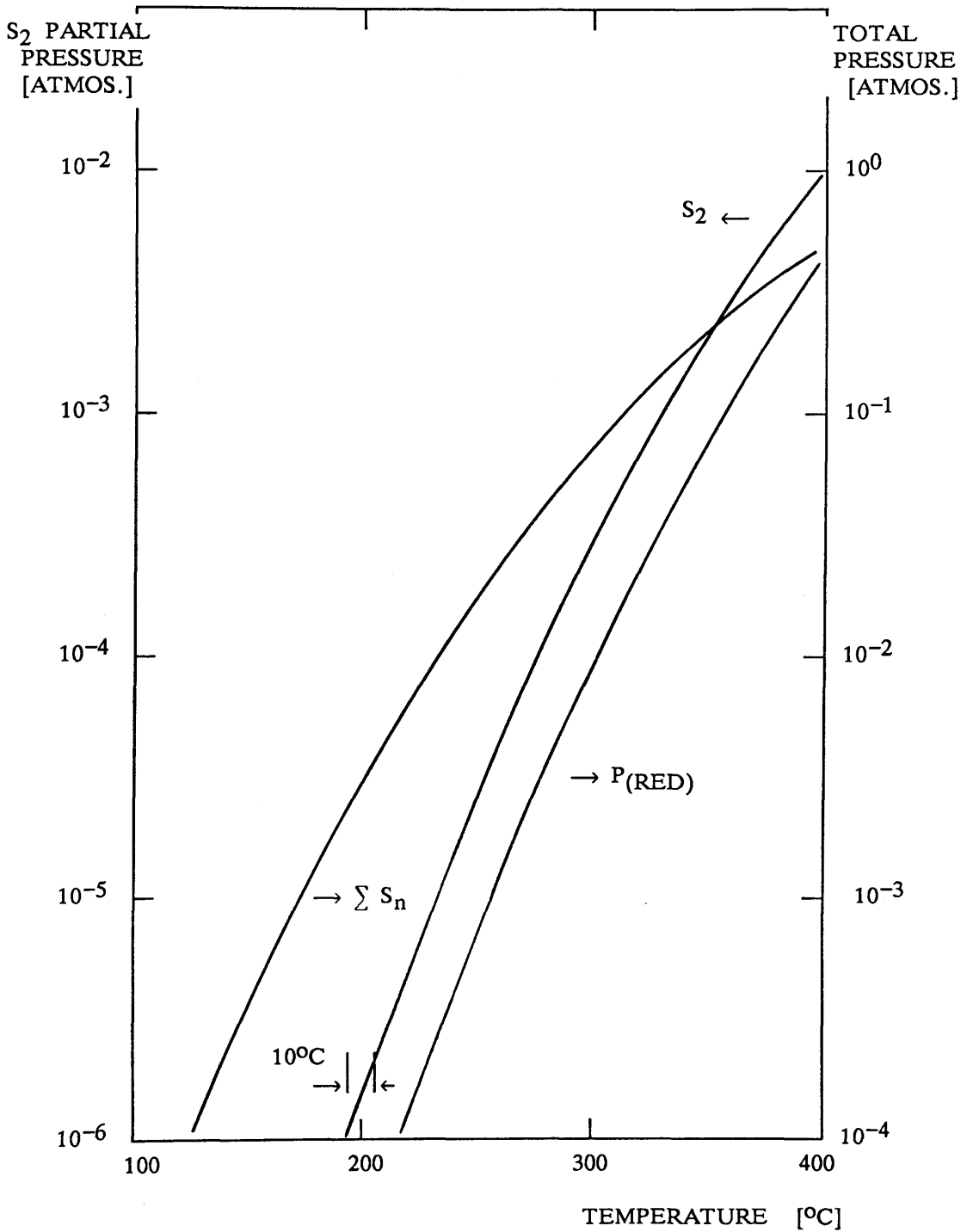


FIGURE 4.3

VAPOUR PRESSURE OF SULPHUR AND RED PHOSPHORUS

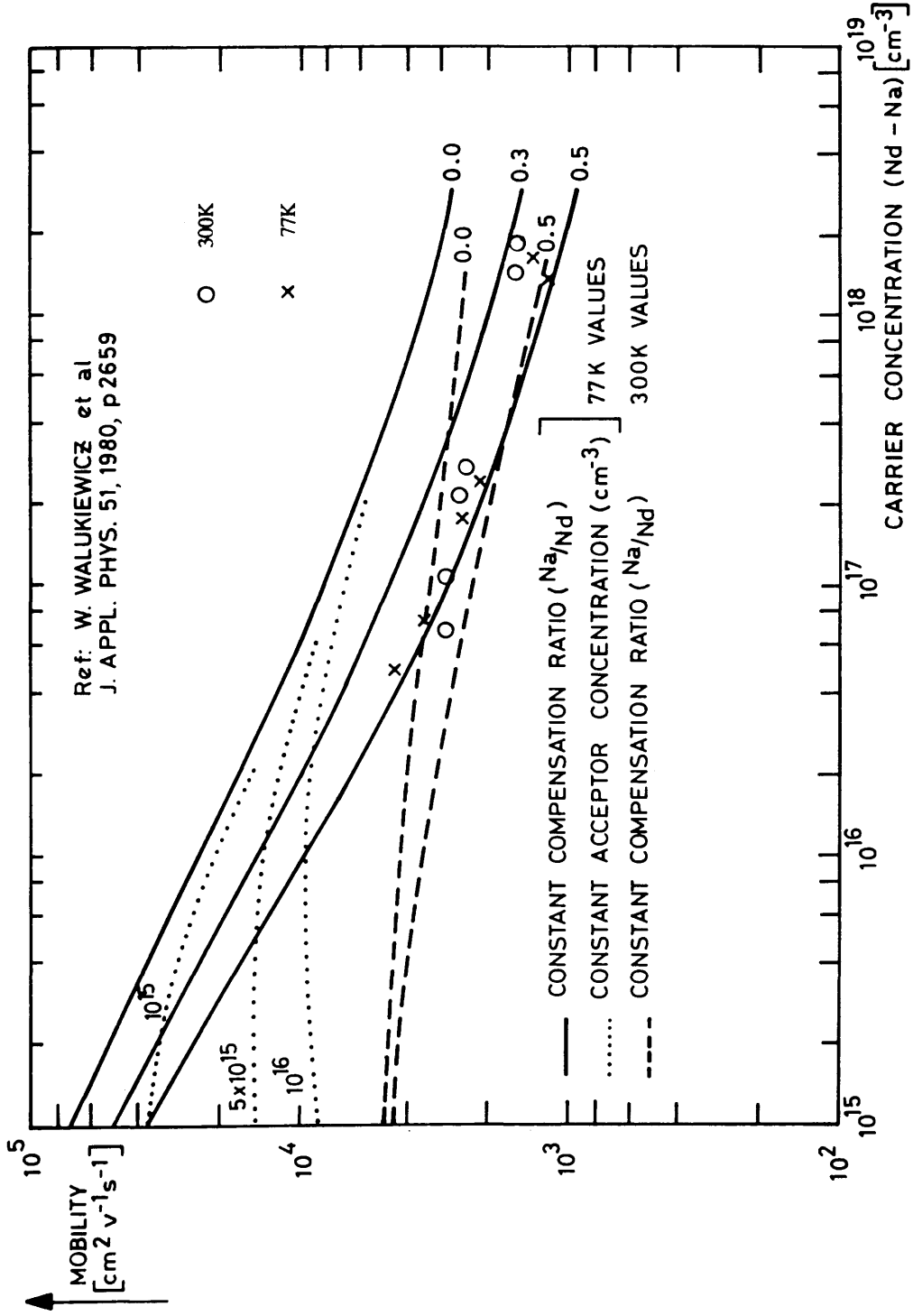


FIGURE 4.4 MOBILITY VERSUS CARRIER CONCENTRATION - SULPHUR DOPED InP

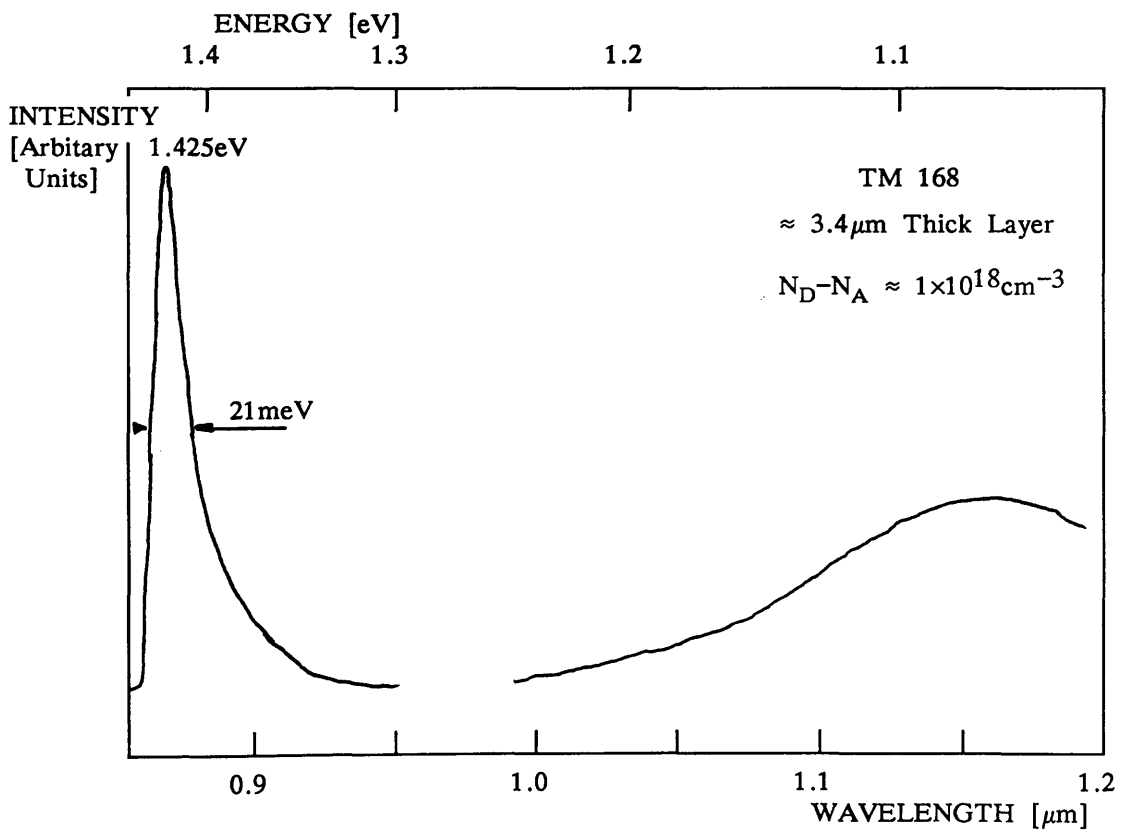
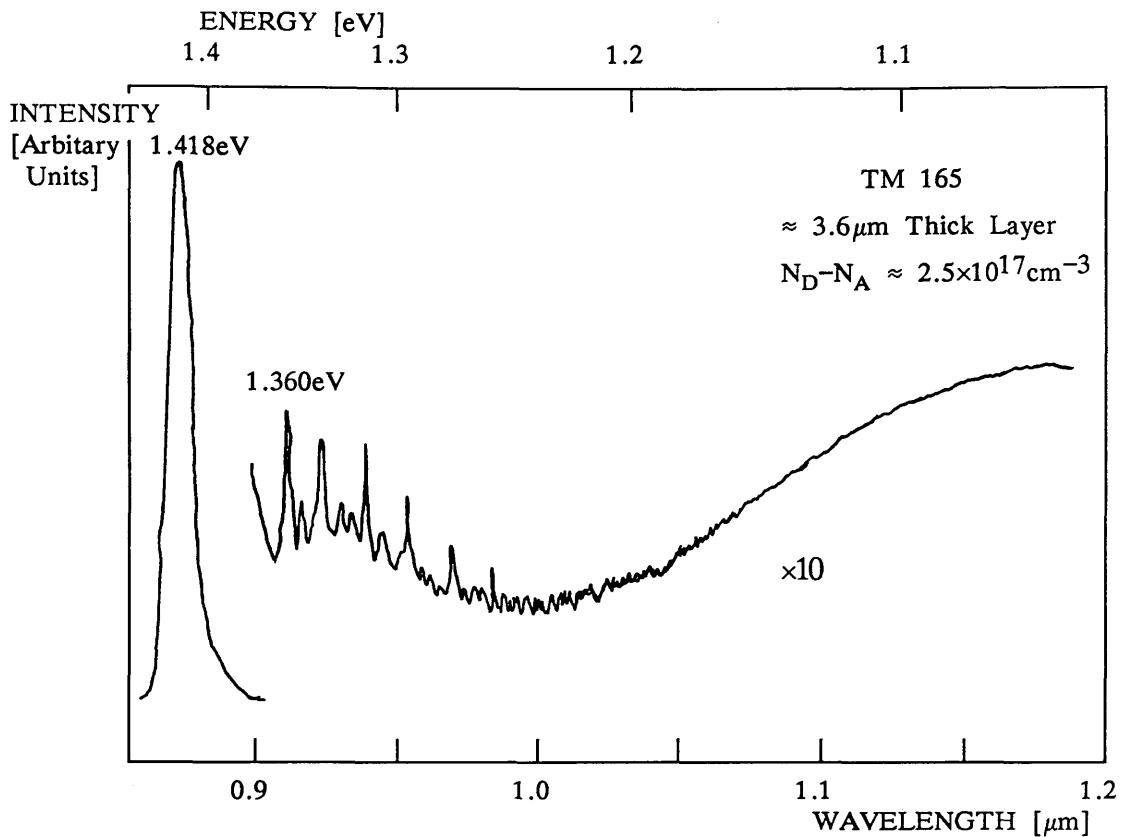


FIGURE 4.5

PHOTOLUMINESCENCE SPECTRA OF LAYERS TM 165 and TM 168

et al [4.25] to explain the self-compensation of donors in high purity GaAs. Wolfe argued that the most likely defect was a complex between a substitutional sulphur atom and an arsenic vacancy ($S_{As}V_{As}^-$), a conjecture supported by recent Extended X-ray-absorption Fine Structure (EXAFS) studies [4.26]. A similar defect centre obtained under non-equilibrium MBE growth conditions might be responsible for the apparently high values of N_A deduced from the comparison of experimental and theoretical mobility versus residual carrier concentration data. However, if such a (S_P-V_P)⁻ complex were present, the total sulphur concentration in the epitaxial layers as measured by SIMS would be expected to be greater than the residual carrier concentration by $\times 2$. A comparison of three intentionally doped levels with SIMS calibrated sulphur concentrations greater than 10^{17}cm^{-3} reveals that the independently calibrated sulphur and free electron concentrations agree to within $\pm 20\%$.

A comparison of the measured Hall data with published results on intentionally doped n-type InP grown by a range of techniques and using a range of dopants (eg S, Si, Sn and Se) indicates that this lower than theoretically predicted mobility is in fact the norm [4.27]. An error in the theoretical analysis of Walukiewicz is, therefore, implied and a detailed consideration by Lancefield of observed and calculated mobility data [4.28], made subsequent to the above results being obtained, has identified the assumption that the impurity distribution is random as the origin of the discrepancy.

4.3.3 DOPING PROFILE SHARPNESS

Factors which can influence the sharpness of abrupt changes in the doping concentration include the response time of the dopant source, the possibility of the dopant accumulating on the surface prior to incorporation and the diffusion of the dopant once incorporated in the epitaxial layer. In addition, the measurement process itself may degrade the profile.

The contribution of these factors to the degradation of an abrupt change in sulphur concentration has been assessed. The SIMS profile of a $0.2 \mu\text{m}$ wide dopant spike initiated by making a step change in the electrochemical cell voltage from 160–190meV and terminated by placing a shutter in front of the cell is shown in figure 4.6 (TM 157).

The falling edge provides no evidence for either surface segregation or diffusion, in agreement with the data in section 3.5.1. Indeed the sharpness of the profile recorded, 1 decade in 27nm, is limited by bombardment induced mixing processes

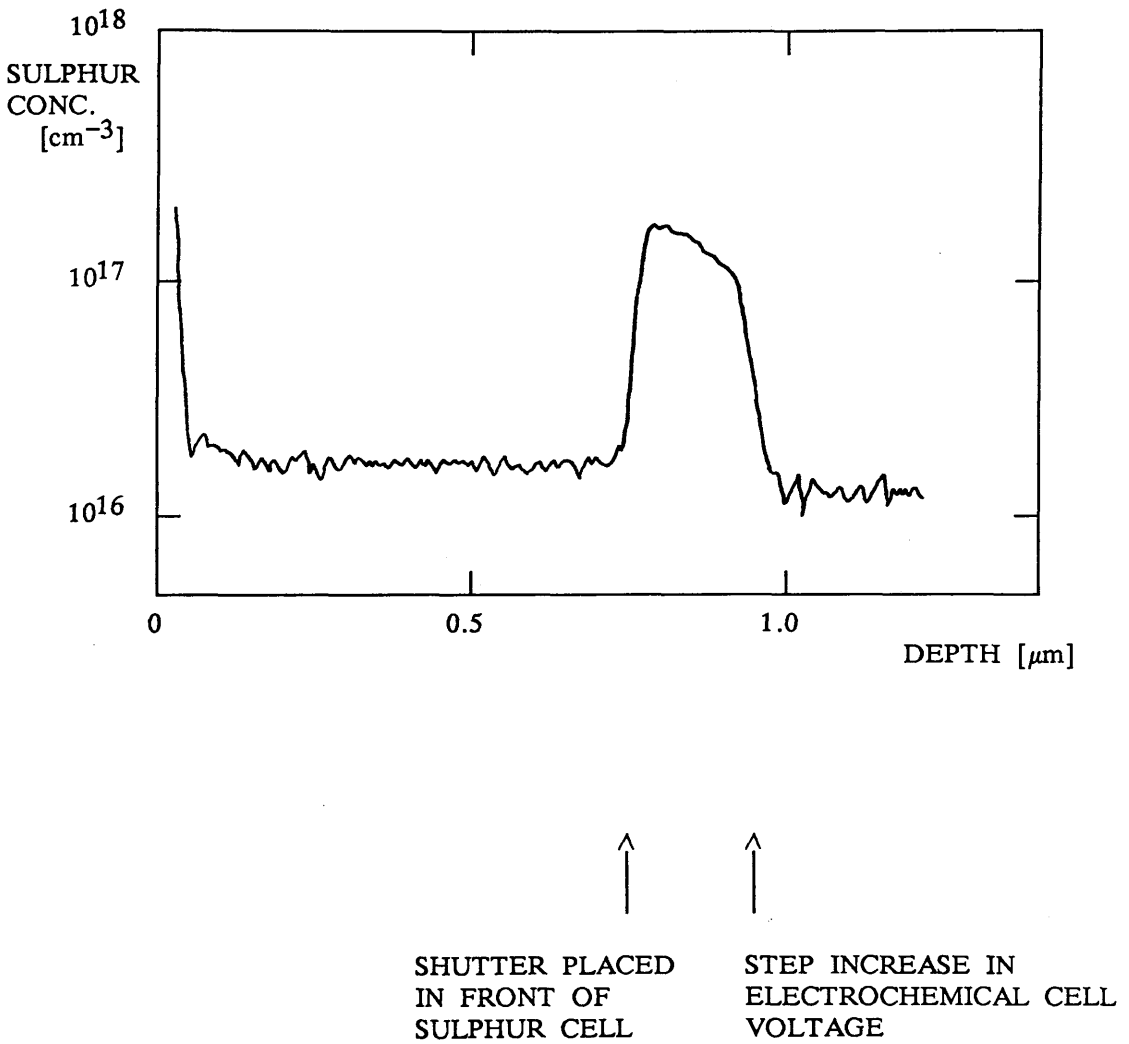


FIGURE 4.6 SIMS DEPTH PROFILE OF A SULPHUR DOPING SPIKE
(LAYER TM 157)

resulting from the use of the heavy Cs^+ ion [4.29]. Attempts to improve this depth resolution by the use of the O_2^+ primary ion, which can resolve changes of 1 decade in less than 3nm [4.30] were unsuccessful due to the low sulphur ion yield obtained with the O_2^+ ion.

The top of the profile provides evidence for a drift in the output of the cell by $\sim \times 2$ over 8 minutes. This drift is comparable to the scatter in free electron concentration versus applied EMF (section 4.3.1) and may again be associated with a temperature drift. Immediately prior to the step change in applied EMF the shutter in front of the cell was opened. This would have resulted in a significant change in the radiant environment of the cell and, in turn, a drift in the temperature of the front of the cell.

4.3.4 MORPHOLOGY

The morphology of sulphur doped InP was found to improve progressively even at concentrations up to $\sim 10^{19}\text{cm}^{-3}$ in contrast to a degradation due to the formation of precipitates which is usually observed for dopants [4.32]. At the maximum concentration studied, $6 \times 10^{19}\text{cm}^{-3}$, this general reduction in the density of all types of defects from 10^4cm^{-2} for unintentionally doped InP to $\sim 500\text{cm}^{-2}$ was maintained. The improvement is believed to result from the small sulphur atom, with a covalent radius $\sim 1.02\text{\AA}$ compared to a value of 1.06\AA for phosphorus, acting to relieve the stress in the lattice [4.33].

The observation of improved morphology is in agreement with the data of Mahajan and Suchow [4.33] [4.34] [4.35], who reported significant reductions in both dislocation and etch pit densities of bulk crystals for sulphur concentrations $\sim 10^{19}\text{cm}^{-3}$. The effect also has significant implications for device applications as growth on a substrate or buffer layer heavily doped with sulphur can produce a significant reduction in the defect density of a subsequent low doped layer [4.34].

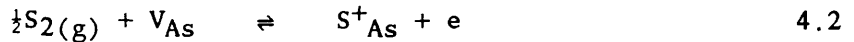
4.3.5 SUMMARY

Sulphur doped InP with free electron concentrations ($N_D - N_A$) in the range $10^{16} - 6 \times 10^{19}\text{cm}^{-3}$ and no evidence for diffusion or surface segregation has been demonstrated. The electrochemical cell was therefore a suitable source of sulphur for the study of incorporation as a function of growth conditions.

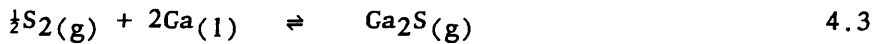
4.4 SULPHUR INCORPORATION AS A FUNCTION OF GROWTH CONDITIONS

Sulphur is readily incorporated during the MBE growth of InP as demonstrated by both the unintentional and intentional doping experiments described in sections 3.4 and 4.2. However, considerable interest and debate centre around the behaviour of high vapour pressure impurities and the mechanisms which influence their incorporation in the MBE growth process.

For example, it can be shown using a thermodynamic approach [4.36] that the incorporation of sulphur into GaAs proceeds according to the reaction :



However, thermodynamic calculations [4.15] also predict that the formation of volatile Ga_2S according to the reaction :



should make sulphur doping impossible.

It is important therefore to quantify the dependence of sulphur incorporation into InP on both the growth temperature and phosphorus flux; this was studied as described below.

(a) Growth temperature

Incorporation of sulphur from the electrochemical source was characterised as a function of growth temperature by depositing a single layer (TM 172) in which the substrate temperature was increased in three stages; 450°C, 490°C and finally 530°C. The growth rate was $1.6\mu\text{m hr}^{-1}$, the V:III flux ratio (as measured by the ion gauge) 10:1 and the nominal carrier concentration $1.9 \times 10^{17} \text{cm}^{-3}$. C-V and SIMS profiles of TM 172 are shown in figure 4.7 and indicate that the sulphur concentration is reduced by only $\times 3$ for a 70°C increase in temperature. When compared with the reduction in concentration with growth temperature observed at higher temperatures ($> 530^\circ\text{C}$), for S and Te in GaAs and S in InP, this 3 \times reduction in carrier concentration for a 70°C increase in temperature is small. For example, Andrews et al. [4.15] reported an activation energy for S and Se desorption in GaAs which would give a 40 \times reduction over the same 70°C range, while the activation energy recently reported by Airaksinen et al. [4.37] for S in InP would be

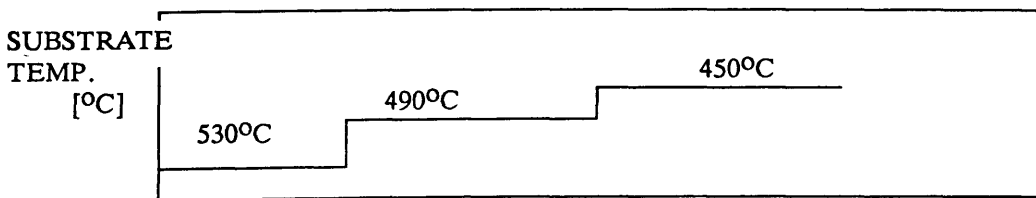
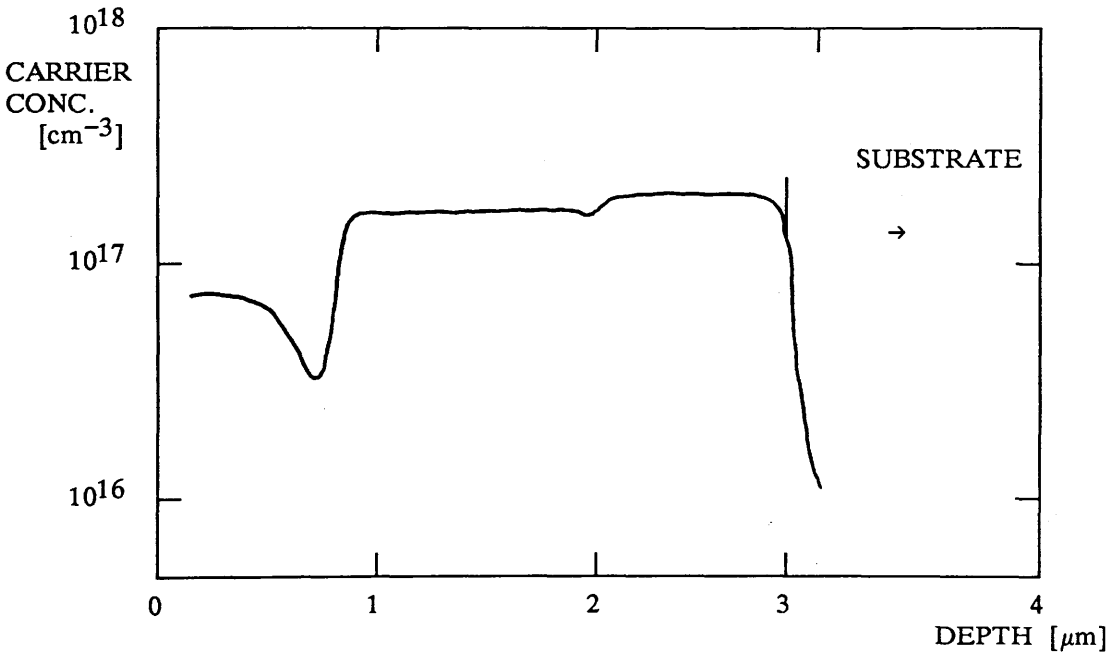
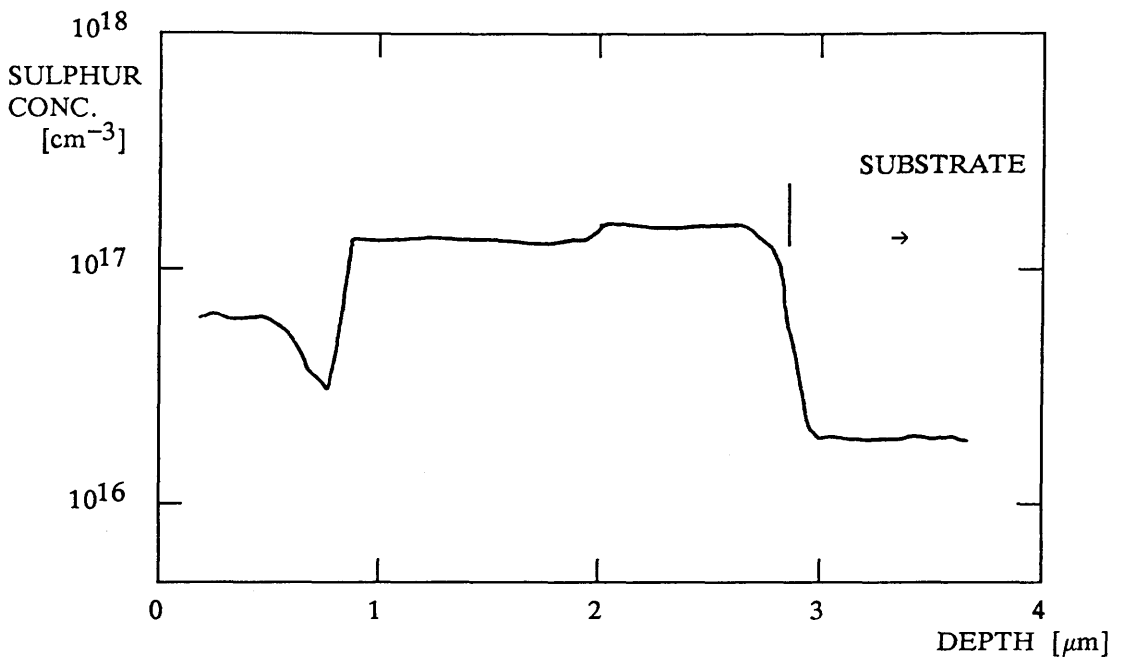


FIGURE 4.7 C-V AND SIMS PROFILES OF SULPHUR CONCENTRATION AS A FUNCTION OF SUBSTRATE TEMPERATURE (LAYER TM 172)

consistent with a 100× reduction over the same 70°C range.

(b) Phosphorus flux

Incorporation as a function of phosphorus flux was studied in layer TM 153 for growth at 450°C, and for two V:III ion gauge current ratios, 4:1 and 8:1. The growth rate was constant throughout, $\sim 1.5 \mu\text{m hr}^{-1}$ and the nominal carrier concentration $(N_D - N_A) \sim 3 \times 10^{17} \text{cm}^{-3}$. A schematic of the growth sequence is shown in figure 4.8; two additional undoped sections were included, one for each of the phosphorus fluxes used. These nominally undoped sections enabled the contribution of the sulphur associated with the phosphorus flux to be quantified. Residual carrier and SIMS profiles of the epitaxial layer (Fig 4.8) indicate that at 450°C incorporation is suppressed by an increase in phosphorus flux. The concentration of incorporated sulphur (C_B) as a function of the P_2 flux ($p(V)$), plotted in figure 4.9, can be characterised according to the relation

$$C_B \propto p(V)^{-0.36} \quad 4.4$$

The reduction in sulphur concentration with increase P_2 flux is consistent with a reduction in the equilibrium concentration of vacant phosphorus sites available for sulphur incorporation. A similar site dependency has been reported [4.31] for the incorporation of Si onto the Ga site in GaAs. However in the case of Si the dependence is much larger, being characterised by:

$$C_B \propto p(V)^z$$

where z is in the range 0.5-1

To summarize these results therefore;

- (a) Sulphur incorporation is reduced by only $\times 3$ for an increase in the growth temperature from 450°C to 530°C.
- (b) At a substrate temperature of 450°C, the sulphur incorporation is reduced by increasing phosphorus flux according to equation 4.4

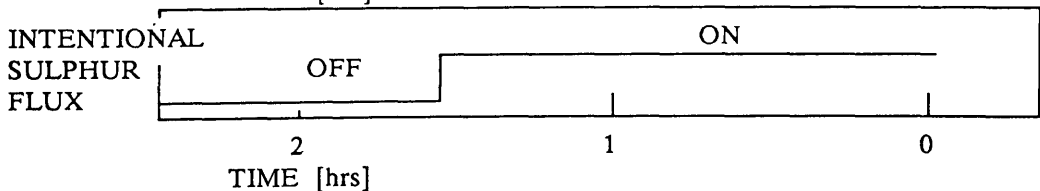
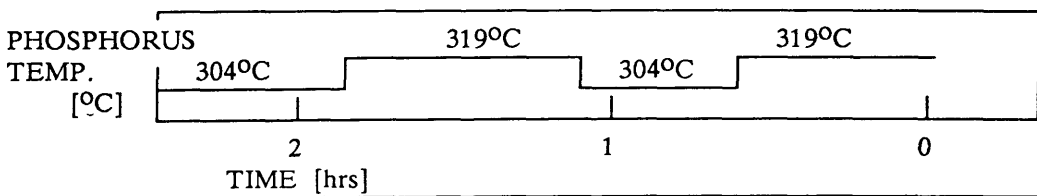
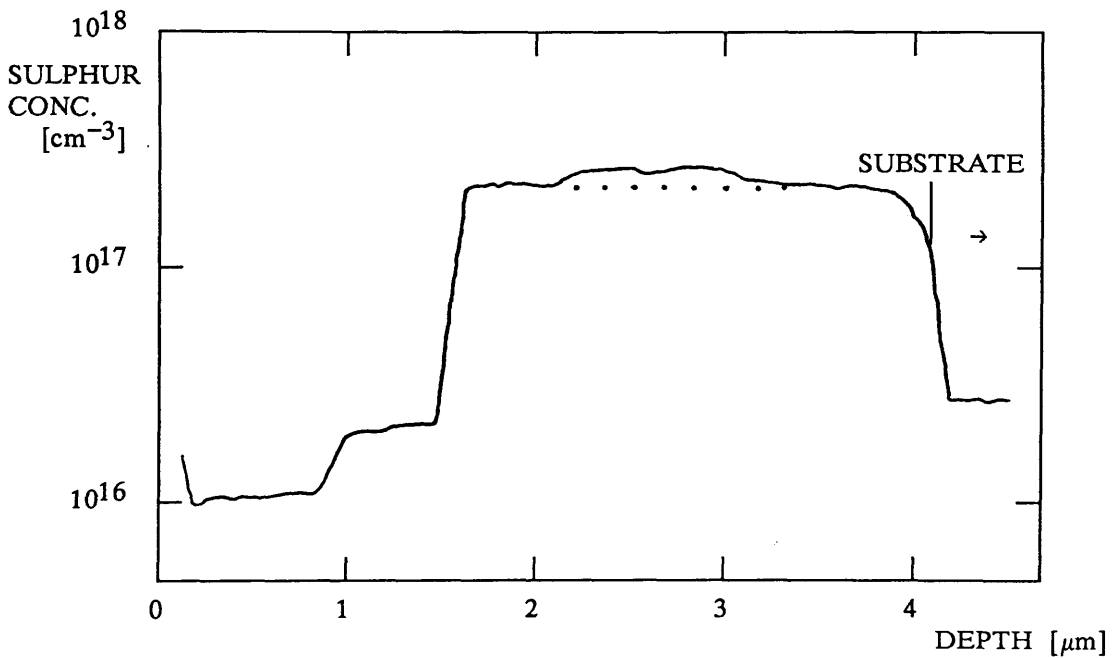
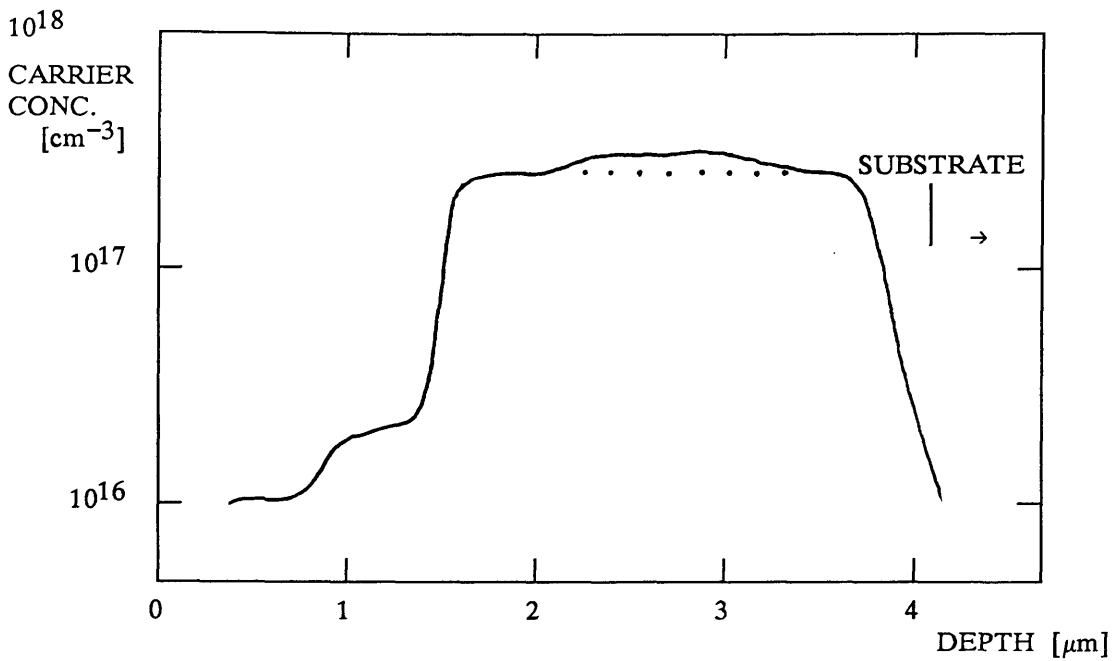


FIGURE 4.8 C-V AND SIMS PROFILES OF SULPHUR CONCENTRATION AS A FUNCTION OF PHOSPHORUS FLUX (LAYER TM 153)

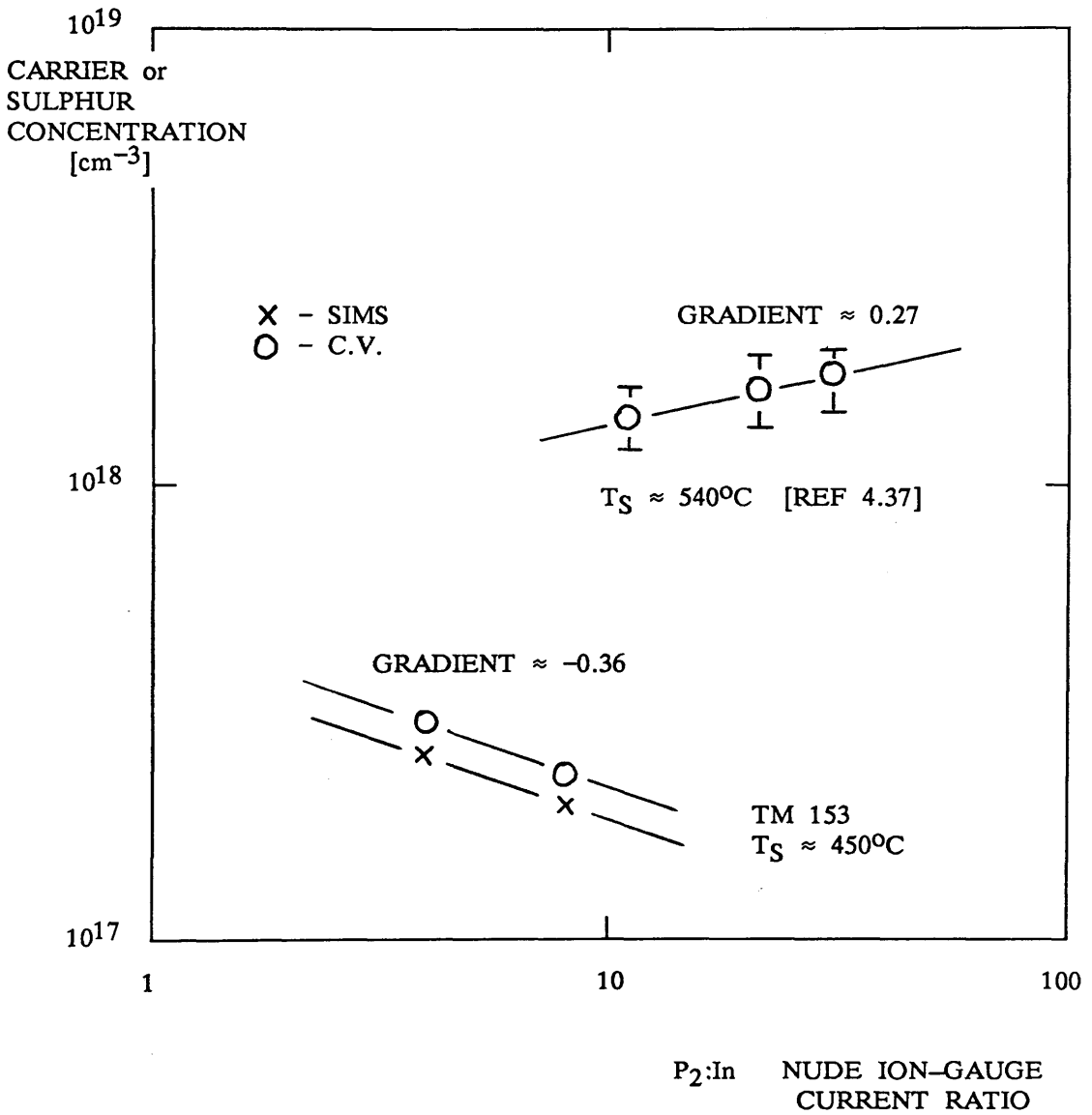


FIGURE 4.9

SULPHUR CONCENTRATION VERSUS V:III FLUX RATIO

A more detailed study of sulphur desorption from InP was undertaken by Airaksinen et al. [4.37] subsequent to the experiments described above. This later work revealed that desorption becomes significant for substrate temperatures greater than 530°C, and is characterised by an activation energy of 4.5eV. In addition, Airaksinen et al. demonstrated [4.38] that sulphur incorporation can be described by the kinetic model developed by Wood et al. [4.39]. According to this model, the general equation for the sulphur concentration is given by:

$$C_B = \frac{F}{G_r \left[1 + \frac{D}{K \times G_r} \right]} \quad 4.5$$

(The notation used is consistent with that of Airaksinen et al.)

- k_B - Boltzmann constant
- $p(V)$ - Group V pressure
- C_B - Concentration of incorporated dopant atoms in the bulk.
- F - Incident dopant flux.
- G_r - Growth rate.
- D - Desorption coefficient. Defined from the net desorption rate (J_{des}) and the surface population of dopant atoms (C_s) by $J_{des} = D \times C_s$ and with units of reciprocal time. The desorption coefficient is assumed to be a function of temperature [T] and group V flux [$p(V)$] with the following dependence.

$$f \left\{ \exp \left[\frac{E_{des}}{k_B \times T} \right] \times p(V)^t \right\}$$

- K' - Incorporation coefficient. Defined from the incorporation rate (J_{inc}) by $J_{inc} = K' \times C_s$ and with units of reciprocal time. The incorporation coefficient is also assumed to be a function of [T] and [$p(V)$] according to

$$f \left\{ \exp \left[\frac{E_{inc}}{k_B \times T} \right] \times p(V)^u \right\}$$

- $K = K'/G_r$ Defined because at high temperatures and low growth rates C_B , which from equation 4.5 is a function of $K'/(D \times G_r)$, is found experimentally [4.37] to be independent of growth rate.

Therefore:

$$\frac{D[T]}{K[T]} \propto \frac{\exp\left[\frac{E_{des}}{k_B \times T}\right]}{\exp\left[\frac{E_{inc}}{k_B \times T}\right]} = \exp\left[\frac{E_a}{k_B \times T}\right]$$

and

$$\frac{D[p(v)]}{K[p(v)]} \propto \frac{p(v)^t}{p(v)^u} = p(v)^{(t-u)} \quad 4.6$$

Equation 4.5 can be simplified to a form which gives the temperature dependence of the carrier concentration at fixed Gr, p(v) and F.

$C_B[T]$ is the concentration at temperature T.

$C_B[0]$ is the concentration at a temperature where desorption is insignificant i.e. where $C_B[T]$ is independent of temperature.

$$\text{Now } C_B[0] = \frac{F}{G_r} \quad 4.7$$

$$\text{and } \frac{D[T]}{K[T]} = \frac{D_1}{K_1} \times \exp\left[\frac{E_a}{k_B \times T}\right] \quad 4.8$$

Substituting 4.7 and 4.8 in 4.5 and solving for the temperature $T_{\frac{1}{2}}$ at which

$$C_B[T_{\frac{1}{2}}] = \frac{C_B[0]}{2} \quad \text{gives:}$$

$$\frac{D_1}{K_1 \times G_r} = \exp\left[\frac{E_a}{k_B \times T_{\frac{1}{2}}}\right]$$

Inspection of the experimental data [4.37] (Figure 4.10) gives $T_{\frac{1}{2}} = 520^\circ\text{C}$ and therefore:

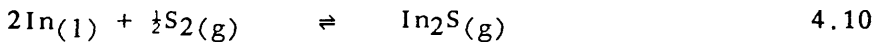
$$\frac{D_1}{K_1 \times G_r} = 4.6072 \times 10^{28}$$

Hence, the temperature dependence of the carrier concentration at fixed G_r , $p(V)$ and F is given by:

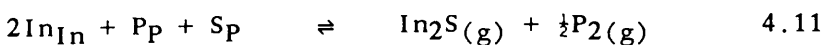
$$C_B[T] = \frac{C_B[0]}{\left\{ 1 + 4.6 \times 10^{28} \times \exp \left[\frac{E_a}{k_B \times T} \right] \right\}} \quad 4.9$$

a convenient form not specifically recognised by Airaksinen et al. Equation 4.9 is compared with the experimental desorption versus temperature results obtained from TM 172, TM 174 (an unintentionally doped layer) and the data of Airaksinen [4.37] in figure 4.9. It can be seen that the equation provides a good fit to all the data underlining the agreement between the separate experiments. The variation in $T_{\frac{1}{2}}$ with growth rate can also be assessed from the above analysis. For a $10\times$ increase in G_r , $T_{\frac{1}{2}}$ will increase to $\sim 550^\circ\text{C}$ while for a $10\times$ decrease $T_{\frac{1}{2}}$ will decrease to $\sim 490^\circ\text{C}$.

The dependence of sulphur incorporation on phosphorus flux in the high temperature regime ($\sim 540^\circ\text{C}$) was also studied by Airaksinen et al. A $3\times$ increase in phosphorus flux produced an increase of $< 20\%$ in residual carrier concentration. It was argued that this small dependence demonstrated that sulphur desorption was essentially independent of the group V pressure. A desorption mechanism involving the reaction of sulphur with liquid indium on the surface of the InP was considered (Equ. 4.10):



However, the kinetic model shows that at high temperature $\{D/(K \times G_r) \gg 1\}$ the dependence of sulphur concentration on phosphorus flux is, using equations 4.5 and 4.6, a function of $P(V)^{u-t}$. The result from TM 153 in which the incorporation of sulphur was characterised as a function of phosphorus flux at a low growth temperature ($\sim 450^\circ\text{C}$) (Fig 4.9) shows that $u = -0.36 \pm 0.2$ (equation 4.4). The power law dependence at high temperature can be estimated from data in figure 5 of reference 4.37 as 0.2 (Fig 4.9); substituting this and the value for u into equation 4.6 gives $t = -0.55$. This value for t is in good agreement with an alternative desorption reaction:



which also has an estimated activation energy of 4.5eV [4.37] in agreement with the

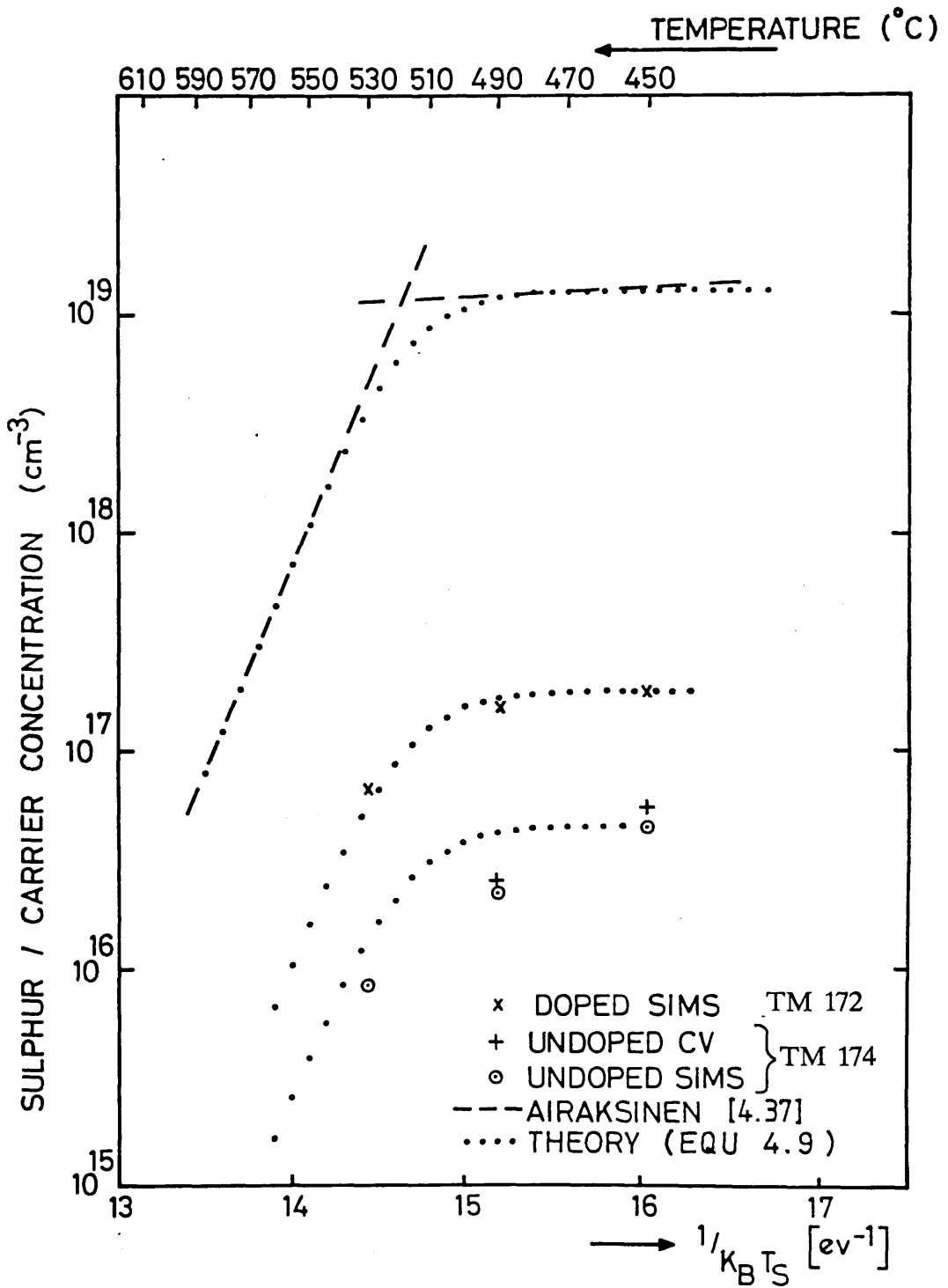


FIGURE 4.10 SULPHUR / CARRIER CONCENTRATION VERSUS RECIPROCAL GROWTH TEMPERATURE FOR SULPHUR DOPED InP

experimental value. Airaksinen et al considered this reaction inconsistent with the experimental data, on account of the $p(V)^{-0.5}$ dependence but given the data presented here, it would seem to offer a convincing explanation of the experimental results.

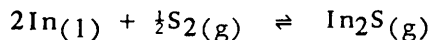
The growth of sulphur doped InP is seen to be a complex function of V:III flux ratio, growth temperature and growth rate. At growth temperatures $<480^{\circ}\text{C}$ the sulphur incorporation mechanism is suppressed by an increase in V:III flux ratio but is nominally independent of both growth temperature and growth rate. In contrast at growth temperatures $>530^{\circ}\text{C}$ incorporation is dominated by a desorption mechanism, activation energy $\sim 4.5\text{eV}$, which itself is suppressed by an increase in the group V flux.

4.5 SUMMARY

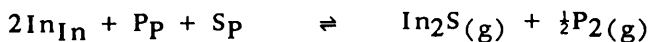
Using an electrochemical source, intentional sulphur doping of MBE grown InP has been demonstrated for the first time. Free electron concentrations in the range 10^{16} to $6 \times 10^{19}\text{cm}^{-3}$ have been achieved with no degradation in morphology at the high concentrations. Indeed, for sulphur concentrations $\sim 10^{19}\text{cm}^{-3}$, the defect densities are significantly reduced from $\sim 10^4\text{cm}^{-2}$, typical of undoped material, to $\sim 500\text{cm}^{-2}$.

No evidence for diffusion or surface segregation has been obtained and at growth temperatures below 480°C the desorption of sulphur from InP is negligible.

The subsequent studies of Airaksinen et al [4.37] have shown that at growth temperatures above 530°C sulphur desorption becomes significant and is characterised by an activation energy of 4.5eV . A desorption mechanism of the form:



was considered, however, taking into account the dependence of sulphur incorporation on phosphorus pressure at low temperatures, the most likely desorption mechanism is:



Sulphur doping using the electrochemical source and growth temperatures $<500^{\circ}\text{C}$ is therefore a very attractive alternative to Si in the MBE growth of InP.

CHAPTER 5

ROUTES TO THE REDUCTION OF THE SULPHUR CONCENTRATION IN UNINTENTIONALLY DOPED InP

5.1 INTRODUCTION

5.2 GROWTH OPTIMISATION

5.3 COMPARISON OF RED PHOSPHORUS SOURCE
MATERIAL

5.4 ALTERNATIVE SOURCES OF PHOSPHORUS

5.5 SUMMARY

5.1 INTRODUCTION

The high concentration of sulphur unintentionally incorporated in InP from the phosphorus source material would prevent the successful demonstration of many devices where total ionised impurity concentrations $\sim 5 \times 10^{14} \text{cm}^{-3}$ are required (section 1.2.4). The options for reducing the sulphur concentration have been assessed.

Firstly, modifications to the growth conditions based on the detailed characterisation of sulphur incorporation presented in section 4.4. have been appraised and are discussed in section 5.2. Secondly, batch to batch variations in the sulphur concentration of the red phosphorus source material have been studied. The sulphur concentration quoted by various vendors is at the detection limit of the chemical analysis technique used [5.01] [5.02] and the most direct method for comparing source purity is therefore the growth of unintentionally doped layers; the results of such a comparison are presented in section 5.3. Finally, alternative sources of phosphorus are appraised (section 5.4).

5.2 GROWTH OPTIMISATION

The growth of InP normally occurs at substrate temperatures (T_s) greater than the congruent temperature ($T_c \sim 365^\circ\text{C}$) (section 1.4). Therefore, to prevent the formation of indium droplets which result from the preferential evaporation of phosphorus, a phosphorus flux is maintained at the surface even when no growth is taking place. As T_s increases, this incident phosphorus flux has to be increased and can eventually exceed the phosphorus flux required for growth. The sulphur present as an impurity in the phosphorus source and incident on the substrate can consequently be divided into two components, that associated with the phosphorus flux required to prevent thermal decomposition (F_{dec}) and that associated with the phosphorus flux required for growth (F_{gro}). The total incident sulphur flux (F_s) is then given by:

$$F_s = F_{\text{dec}} + F_{\text{gro}} \quad 5.1$$

The possibility of reducing the incorporated sulphur concentration by optimising the growth conditions can be considered in two temperature regimes: (i) low temperatures, i.e. below 480°C , where sulphur desorption is negligible but the phosphorus flux used for growth and therefore the associated sulphur flux can be minimised; (ii) high temperatures where the increased phosphorus (and hence sulphur) flux required to prevent thermal decomposition can be offset by the loss of sulphur via desorption.

(i) Low temperature growth

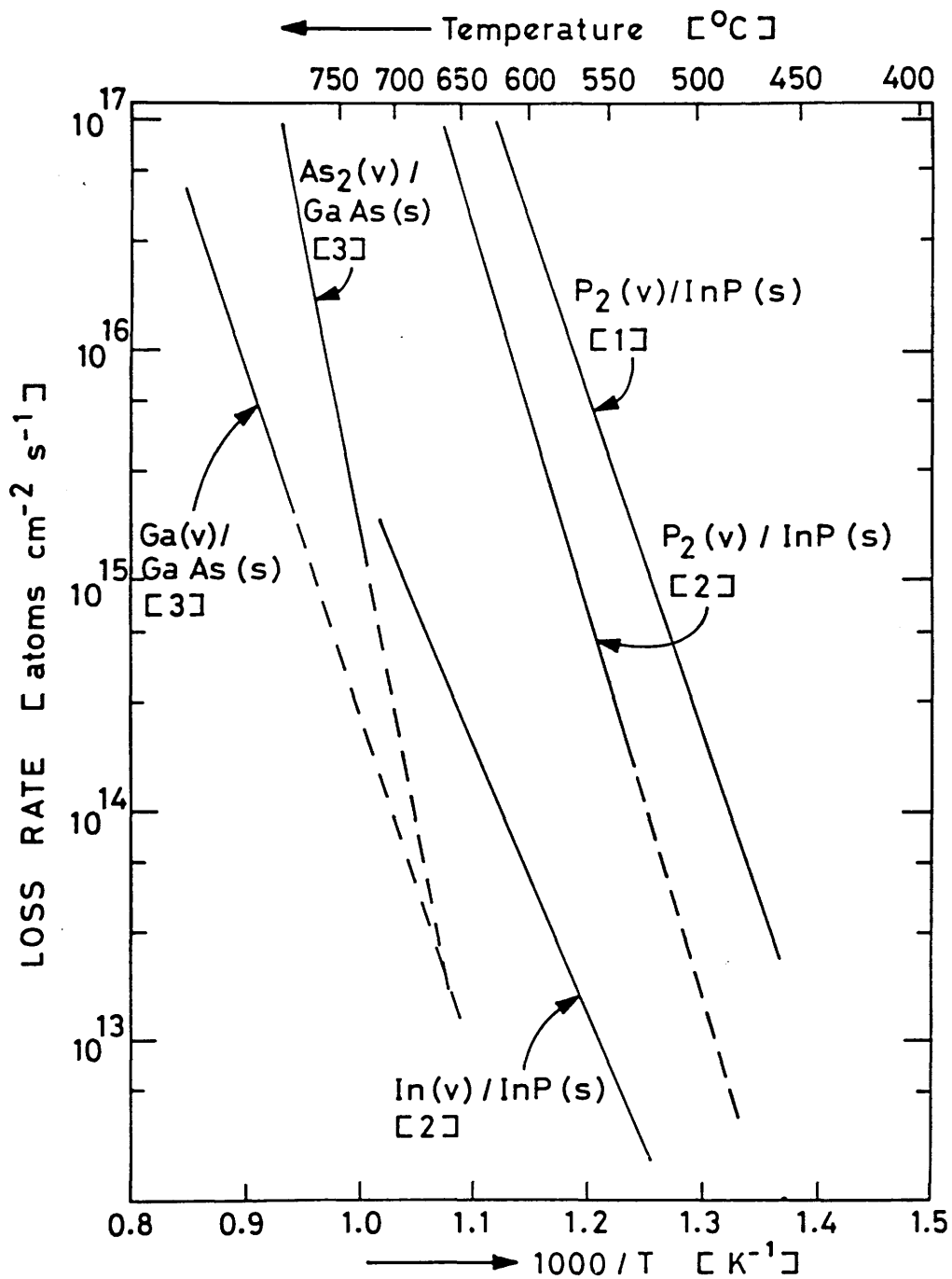
In the low temperature regime the sulphur concentration is a minimum at growth rates where the excess phosphorus flux required to prevent decomposition is small compared to that required for growth, i.e. $F_{dec} < F_{gro}$. The sulphur concentration in the bulk (C_B) is then directly related to the impurity concentration in the phosphorus source material. It is first necessary to quantify F_{dec} before the growth rate as a function of T_s required to achieve the minimum C_B can be established.

Both Panish [5.03] and Farrow [5.04] have measured the equilibrium vapour pressure of phosphorus over InP using mass spectrometry techniques. Panish made measurements over the range 480°C to 670°C, while Farrow, using more sensitive modulated beam techniques, studied the range 545°C to 657°C. A review of both sets of data (Fig 5.1) highlights two problems. Firstly, there are significant differences in the reported equilibrium loss rates; at 500°C the absolute P_2 loss rate deduced from the data of Farrow is 10× lower than the value reported by Panish. Secondly, the equilibrium flux increases significantly for small changes in temperature; an increase of ×10 in flux is obtained for a 35°C increase in T_s , emphasising the need for a detailed characterisation of the phosphorus flux required to prevent thermal decomposition under the experimental conditions used.

In practice, III-V growth by MBE is carried out under group V stable surface conditions with the group V flux adjusted, according to the values of T_s and G_r , to maintain this surface. If either T_s or the indium flux are increased sufficiently the phosphorus flux will no longer be large enough to keep the surface group V stable and a switch to the group III stable surface will take place.

It should be possible to monitor the onset of the group III stable InP surface, analogous to the 3×1 reconstruction observed in GaAs [5.05] [5.06], using RHEED. However, in practice a metal-stable reconstruction is not obtained for InP within the temperature range of interest, namely 400–500°C. Instead a group V stable RHEED reconstruction is retained even when the surface is seen to be covered with indium droplets. This reconstruction is observed because the indium atoms rapidly segregate into indium droplets typically ~0.1µm apart but with the majority of the surface between the indium droplets remaining phosphorus stable [5.07].

The onset of thermal degradation of a "static" surface was monitored experimentally by observing the light scattered from a substrate while the temperature of the substrate was increased slowly, ~5°C min⁻¹. The technique was limited by the size



[1] Panish M.B., J. Cryst. Growth 27, 1974, pp6 - 20

[2] Farrow R.F.C., J. Phys. D., 7, 1974, pp2436 - 48

[3] Foxon C.T., J. Phys. Chem. Solids, 34, 1973, pp1393-1701

FIGURE 5.1 EQUILIBRIUM LOSS RATES FOR InP AND GaAs

and density of the indium droplets required to produce detectable scattering of the incident light and as such provided an under estimate of F_{dec} . However, only a small change in temperature is required to switch from a P-stabilised to an "unstabilised" surface (Fig 5.1), and even with a net phosphorus loss rate as low as 0.01 monolayers s^{-1} the time taken to accumulate sufficient free indium to cover the surface with, for example, droplets 100nm across and density $10^8 cm^{-2}$ is only ~ 3 mins. The process was repeated for different substrates and a range of fixed phosphorus fluxes. The phosphorus flux was quantified using the beam monitoring ion gauge and calibrated using the relative ionisation efficiencies of P_2 and In [5.08] [5.09] and the gauge sensitivity for indium determined directly from growth data. The results are plotted in figure 5.2. The enthalpy for the sublimation [5.10] obtained from a least squares fit to the data is within 1% of the value obtained by Farrow [5.04]. However, the phosphorus flux needed to prevent thermal decomposition at $480^\circ C$ is $\sim 2.3 \times 10^{15}$ atoms $cm^{-2}s^{-1}$, equivalent to ~ 4 monolayers s^{-1} , and is larger than the value estimated from the data of Farrow or Panish by $\times 10$. The discrepancy is not unreasonable given both uncertainties in the calibration of the absolute flux and the difficulty in MBE of assigning an absolute value to substrate temperature [5.11] [5.12].

A further point to consider in establishing the optimum low temperature growth conditions is that an incident phosphorus flux equivalent to 1 monolayer s^{-1} will not necessarily be sufficient for the growth of InP at the same rate, i.e. the accommodation coefficient (a) of the growth component of the phosphorus flux may be less than 1 [5.13]. For $a = 1$ then: at $T_s = 480^\circ C$, growth rates of the order of 4 monolayers s^{-1} ($4 \mu m hr^{-1}$) or greater will be required to minimise the sulphur concentration (fig 5.2) while at $T_s = 450^\circ C$ the corresponding value of growth rate will be $0.5 \mu m hr^{-1}$. Where a is less than 1 these growth rates will be reduced in proportion to the reduction in a .

In practice, a can be estimated when $F_{gro} \gg F_{dec}$ by growing a series of layers with a progressive reduction in phosphorus flux until the minimum phosphorus flux for group V stable growth is reached. Several such layers were grown at $450^\circ C$ and $1.5 \mu m hr^{-1}$, with the $P_2:In$ nude ion-gauge current ratio reduced, progressively, from a value of 10:1 (incident atom flux ratio $\sim 25:1$). Layers TM 147 and TM 154 were successfully grown with V:III ion gauge current ratios of $\sim 3:1$ and indicate that at $450^\circ C$ a is greater than ~ 0.15 . A comparison of Hall measurements on these layers with data reported in section 3.3 (Table 5.1 and Fig 5.3) shows that the residual donor concentrations were reduced by between $\times 2$ and $\times 3$, comparable with the reduction in the V:III ratio.

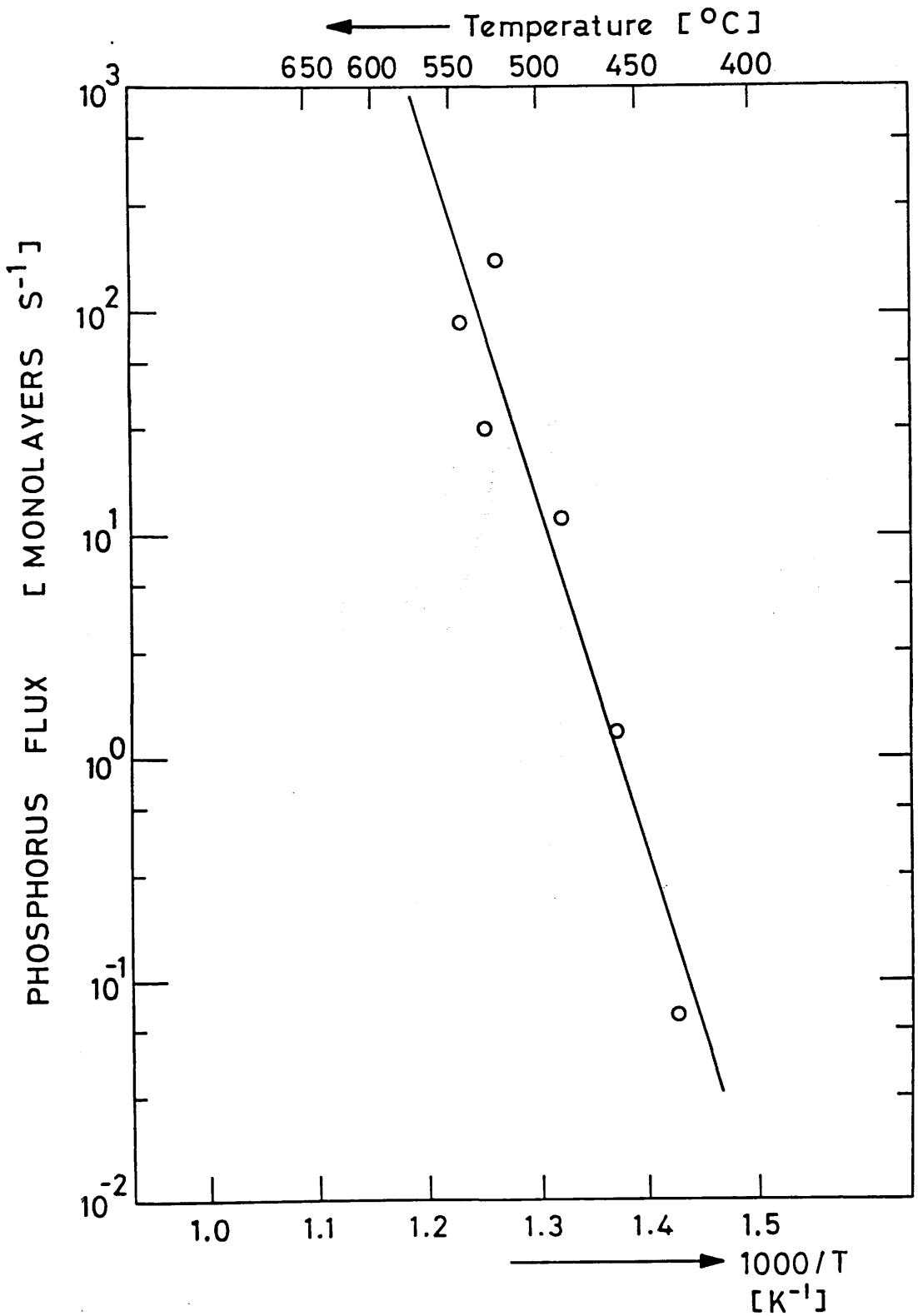


FIGURE 5.2 MINIMUM PHOSPHORUS FLUX REQUIRED TO PREVENT THERMAL DECOMPOSITION OF InP

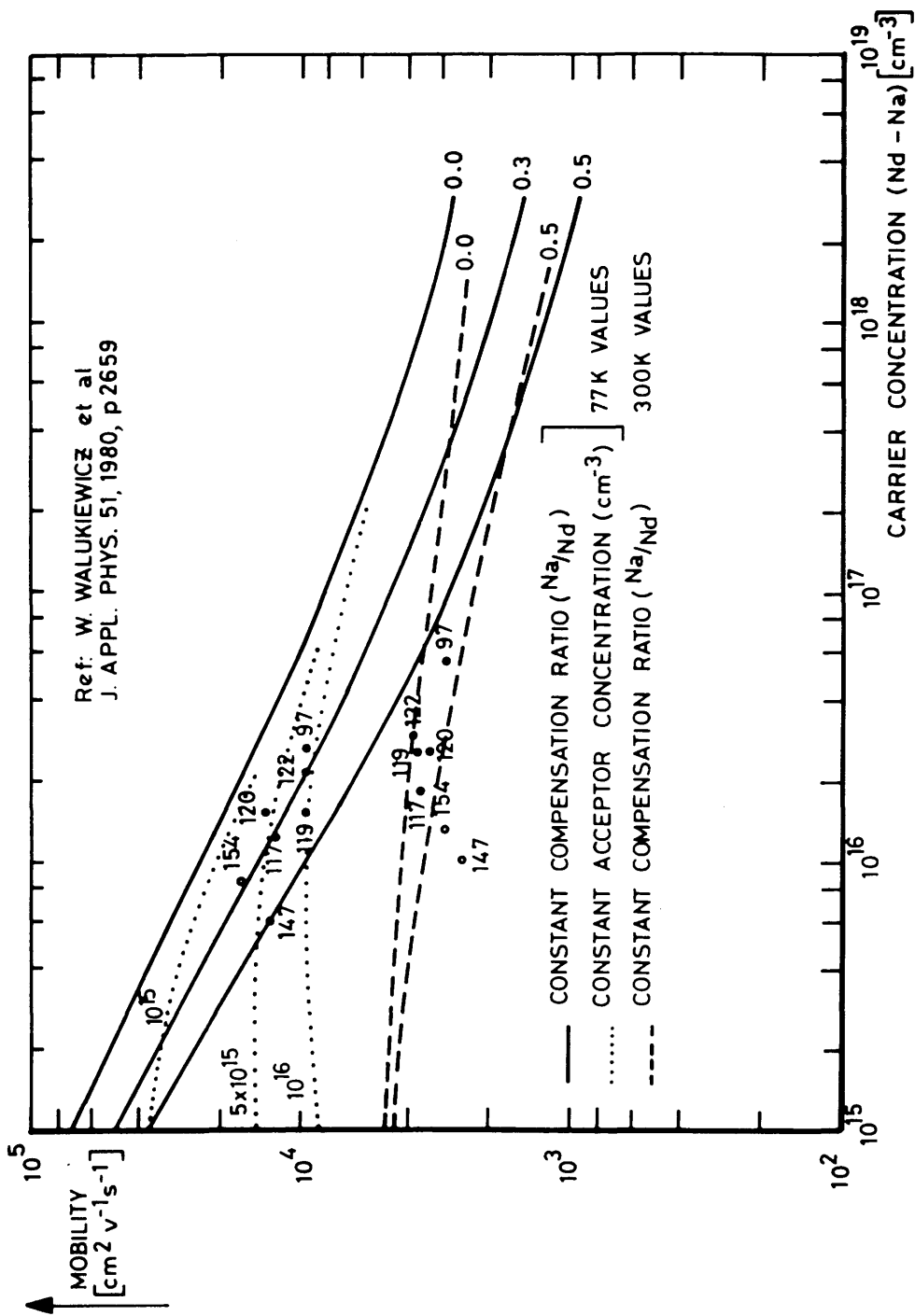


FIGURE 5.3 MOBILITY VERSUS CARRIER CONCENTRATION

- COMPARISON OF TM 147 AND 154 WITH DATA FROM EARLIER LAYERS GROWN IN CHAMBER 2

InP HALL DATA

| LAYER | Nd-Na 300K (cm^{-3}) | MOBILITY 300K ($\text{cm}^2 \text{V}^{-1} \text{s}^{-1}$) | Nd-Na 77K (cm^{-3}) | MOBILITY 77K ($\text{cm}^2 \text{V}^{-1} \text{s}^{-1}$) | COMPENSATION RATIO (77K DATA) | CARRIER FREEZEOUT | Nd (cm^{-3}) | Na (cm^{-3}) |
|-------|---------------------------------------|---|--------------------------------------|--|-------------------------------------|----------------------|----------------------------|----------------------------|
| 97 | 5.5×10^{16} | 2,900 | 2.6×10^{16} | 9,500 | 0.25 | 0.47 | 3.5×10^{16} | 8.6×10^{15} |
| 117 | 1.8×10^{16} | 3,615 | 1.2×10^{16} | 11,219 | 0.35 | 0.67 | 1.8×10^{16} | 6.5×10^{15} |
| 119 | 2.5×10^{16} | 3,675 | 1.5×10^{16} | 9,314 | 0.4 | 0.60 | 2.5×10^{16} | 1.0×10^{16} |
| 120 | 2.5×10^{16} | 3,350 | 1.5×10^{16} | 13,300 | 0.2 | 0.60 | 1.9×10^{16} | 3.8×10^{15} |
| 122 | 2.9×10^{16} | 3,840 | 2.1×10^{16} | 9,200 | 0.3 | 0.72 | 3×10^{16} | 9×10^{15} |
| 147 | 1×10^{16} | 2,500 | 6×10^{15} | 12,706 | 0.5 | 0.60 | 1.2×10^{16} | 6×10^{15} |
| 154 | 1.3×10^{16} | 2,890 | 8.4×10^{15} | 16,650 | 0.25 | 0.65 | 1.1×10^{16} | 2.8×10^{15} |

TABLE 5.1 COMPARISON OF HALL DATA RECORDED FOR TM 147 AND 154 WITH THAT INITIALLY
OBTAINED IN CHAMBER 2

Further studies of this type are required to fully characterise a , and any associated temperature dependence. However, given that at a sufficiently low growth temperature a will tend to 1, the available data indicates that, using this phosphorus batch [5.14], the minimum sulphur concentration which could be obtained would be $\sim 2 \times 10^{15} \text{cm}^{-3}$.

(ii) High temperature growth

At high temperatures ($>480^\circ\text{C}$), the desorption of sulphur is characterised by an activation energy of 4.5eV [5.15]. The incident sulphur flux is again given by equation 5.1 with the dependence of F_{dec} on growth temperature determined from figure 5.2. This increase in phosphorus (and hence sulphur) required to counteract decomposition can be characterised by an equation of the form:

$$F_{\text{dec}} \propto \exp \left[\frac{E_p}{K_B \times T} \right] \quad 5.2$$

which yields a value for E_p of 3.3eV. Therefore, at a sufficiently high temperature where $F_{\text{dec}} > F_{\text{gro}}$, a nett loss of sulphur can be predicted at a rate characterised by an activation energy $(E_a - E_p) = 1.2\text{eV}$.

However, as discussed in section 4.4, the temperature at which desorption becomes significant is dependent on the growth rate, for example, 490°C at a growth rate of $\sim 0.1 \mu\text{m hr}^{-1}$, and 550°C at a growth rate of $\sim 10 \mu\text{m hr}^{-1}$. At these temperatures, the phosphorus fluxes required to prevent thermal decomposition are already well in excess of F_{gro} being equivalent to ~ 8 and ~ 300 monolayers sec^{-1} respectively ($a = 1$). Therefore the concentration of incorporated sulphur will increase above its minimum value at low T_s , where $F_{\text{gro}} \gg F_{\text{dec}}$, before decreasing as desorption dominates with further increases in substrate temperature.

The kinetic model for incorporation of an impurity from a surface concentration (section 4.4) can be used to calculate the exact variation in sulphur concentration as a function of both growth rate and temperature. The temperatures at which the sulphur concentration is reduced below the minimum value for growth at low temperature can then be predicted. From the model, the bulk sulphur concentration (C_B) is related to the incident flux (F_s) as a function of growth conditions by:

$$C_B = \frac{F_s}{G_r \left[1 + \frac{D}{K \times G_r} \right]} \quad 5.3$$

where the terms are defined in section 4.4, $D/K[T]$ is a function of temperature given by equation 4.8 and $F_s = F_{dec} + F_{gro}$, with F_{dec} given by equation 5.2.

To use equation 5.3, it is necessary first to assign a value for D_1/K_1 (Equ 4.8). This can be obtained from the data presented in figure 4 of reference 5.15, in which F_s/C_B is plotted against G_r for different growth temperatures. The intercept at zero growth rate is the value of $D/K[T]$ at that growth temperature and together with the activation energy for sulphur desorption enables $D/K[T]$ to be calculated at all temperatures. The value for $D/K[T]$ of 1.1 at 520°C is used as the reference throughout all subsequent calculations. As a check on equation 5.3 the calculated values for the normalised carrier concentration versus reciprocal growth rate and the experimental results obtained at 480°C [5.15] and 540°C [5.16] are compared in figure 5.4. The value of F_s used in reference 5.16 has been taken as $1.5 \times 10^5 \text{ At } \mu\text{m}^{-2} \text{ hr}^{-1}$. Excellent agreement is seen, both across the temperature range and between the separate experiments.

By substituting for $D/K[T]$ and F_s in equation 5.3 and solving as a function of growth temperature for three growth rates (0.1, 1 and $10 \mu\text{m hr}^{-1}$) which extend over the maximum practical range, the results presented in figure 5.5 are obtained. In this figure, the carrier concentration is normalised to its minimum low temperature value. The effect of changing the accommodation coefficient (a) between 1 and 0.2 is illustrated for growth at $1 \mu\text{m hr}^{-1}$ only. The figure shows the separate mechanisms contributing to the incorporation of the sulphur from the phosphorus charge. For example, for the lower growth rates the increase in sulphur concentration becomes apparent at lower substrate temperatures, consistent with the requirement that $F_{dec} < F_{gro}$, and as the substrate temperature is increased the sulphur concentration increases at the rate required by the increase in the vapour pressure of P_2 over InP. The peak normalised carrier concentration is seen to be higher for lower growth rates, although reducing a from 1 to 0.2 reduces the difference between the carrier concentration at low temperature and the peak carrier concentration. For all growth rates an increase in carrier concentration prior to the onset of desorption is predicted.

At the high growth temperatures the sulphur concentration decreases at a rate characterised by $E_a - E_p$. The growth temperatures required to reduce the sulphur concentration to the low temperature minima are $\sim 610^\circ$ and $\sim 700^\circ\text{C}$ for values of a

equal to 0.2 and 1 respectively. An additional temperature increase of $\sim 110^\circ\text{C}$ would be required to further reduce the sulphur concentration by an order of magnitude. However, 650°C is probably an upper limit for the growth of InP since for $T_s > 650^\circ\text{C}$ the indium loss rate is greater than $1\mu\text{m hr}^{-1}$. The control of growth rate therefore becomes difficult, while in addition the phosphorus flux required to prevent thermal decomposition is $>10^{-3}\text{mbar}$, at the upper limit of molecular beam conditions.

SUMMARY

From the above detailed analysis it can be seen that there are potentially two sets of growth conditions under which the incorporation of sulphur from the phosphorus charge can be minimised.

The first is at growth temperatures below 480°C where sulphur desorption is insignificant. The optimum growth conditions are then obtained at growth rates where the phosphorus flux required to prevent thermal decomposition is small compared to that required for growth. Figures 5.2 and 5.5 indicate that if the growth rates are maintained at $1.5\mu\text{m hr}^{-1}$ (the typical value used for the results reported in section 3.3) but the growth temperature reduced from $\sim 500^\circ\text{C}$ to $\sim 450^\circ\text{C}$, the phosphorus flux may be reduced and an associated reduction in sulphur concentration obtained. The data from layers TM 147 and TM 154 (Fig 5.3, Table 5.1) grown at $T_s \approx 450^\circ\text{C}$ and with the incident phosphorus (sulphur) reduced by $\sim \times 3$ confirms this prediction. Further reductions by up to a factor of $\sim \times 5$ are predicted under conditions in which an accommodation coefficient of 1 can be realised.

The second set is at growth temperatures greater than 650°C . However, the phosphorus flux required to prevent thermal decomposition will be ~ 4 orders of magnitude larger than that required to desorb the oxide, taking growth outside the molecular flow regime. In addition, the indium loss rate will be greater than $1\mu\text{m hr}^{-1}$ making accurate thickness control impractical.

5.3 COMPARISON OF RED PHOSPHORUS SOURCE MATERIAL

The concentration of sulphur in the phosphorus source material used in the growth of layers TM 96–TM 126 was quoted by the vendor at $<0.1\text{p.p.m.a.}$ [5.14]. This impurity concentration was consistent with the sulphur concentration in the unintentionally doped layers, as can be seen from the following argument. The

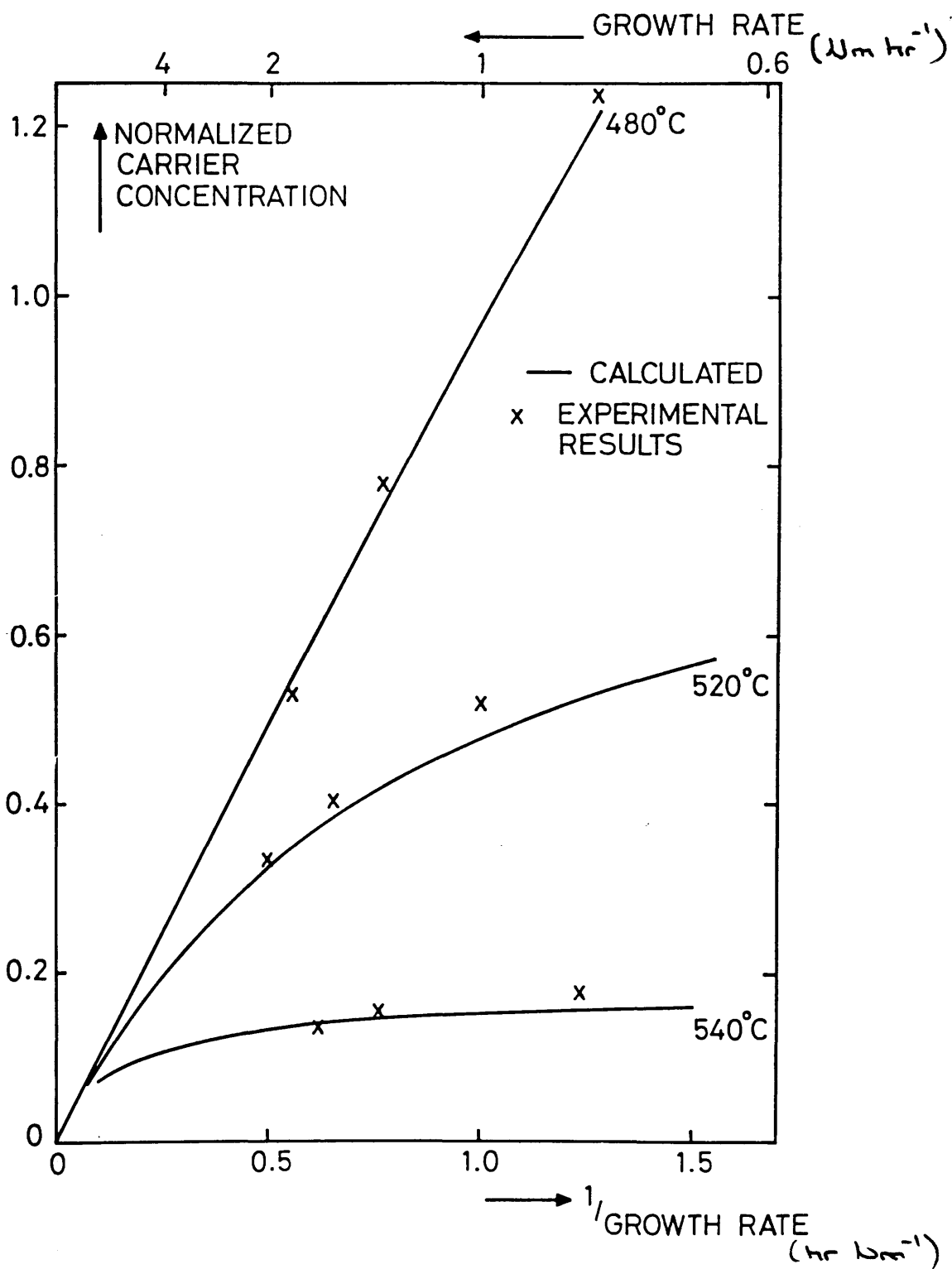


FIGURE 5.4 COMPARISON OF EXPERIMENTAL AND CALCULATED VARIATIONS IN CARRIER CONCENTRATION FOR SULPHUR DOPED InP.

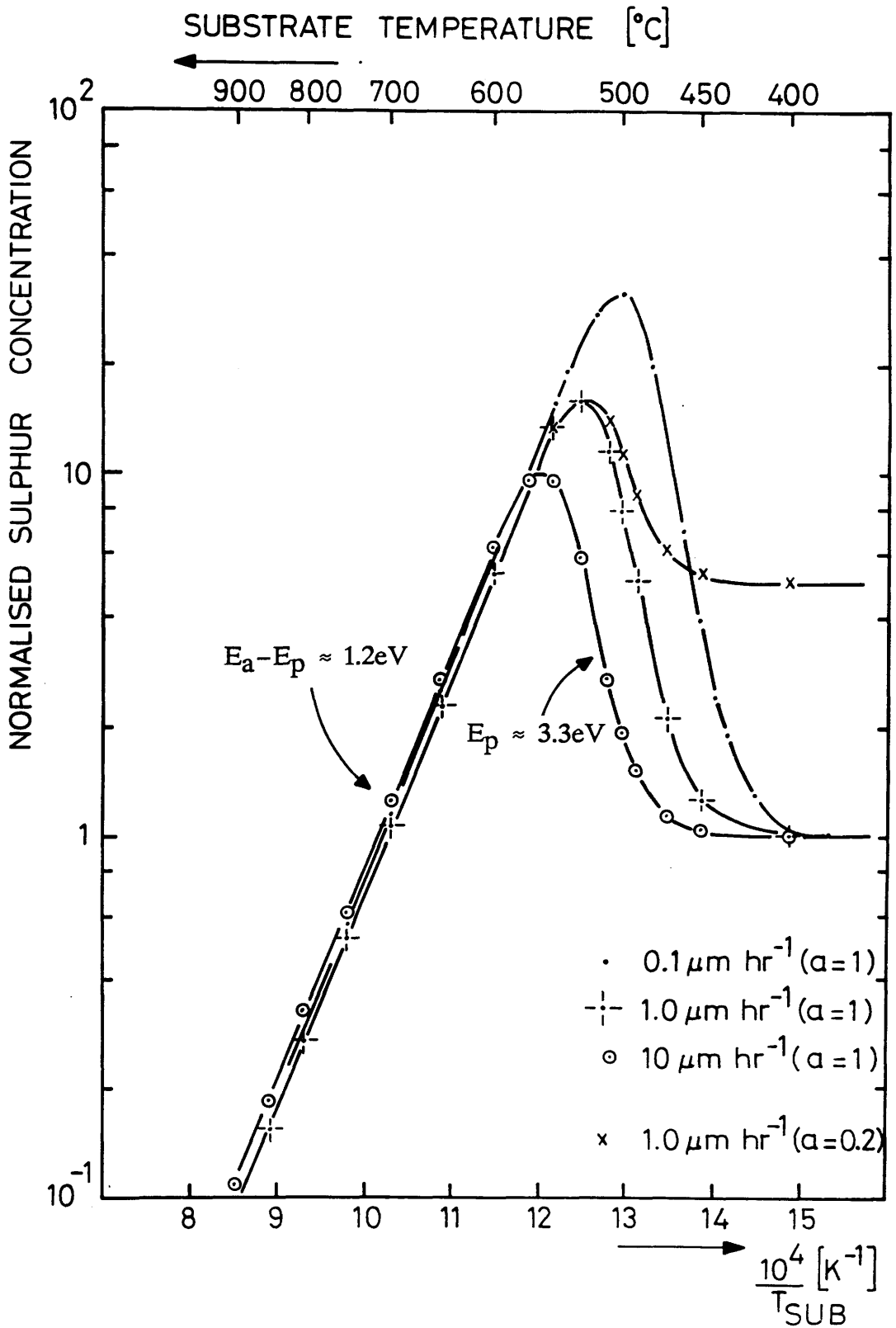


FIGURE 5.5 CALCULATED VARIATION IN MINIMUM SULPHUR CONCENTRATION VERSUS GROWTH TEMPERATURE AND GROWTH RATE

phosphorus flux required to stabilise the substrate against thermal erosion at $\sim 500^\circ\text{C}$ is determined experimentally as $\sim 9 \times 10^{15}$ atoms $\text{cm}^{-2}\text{s}^{-1}$ (~ 15 monolayers s^{-1}) (figure 5.2). Because the vapour pressures of sulphur and phosphorus are very similar (figure 4.3), the concentration of sulphur in the phosphorus flux will be the same as that in the source. The incident sulphur flux is therefore $< 9 \times 10^8$ atoms $\text{cm}^{-2}\text{s}^{-1}$ which translates to a bulk concentration of $< 3 \times 10^{16}$ cm^{-3} for a growth rate of $1 \mu\text{m hr}^{-1}$ (1 monolayer s^{-1}), in good agreement with measured concentrations (section 3.3). The concentration of sulphur in the red phosphorus which will give rise to a significant sulphur impurity concentration in the epitaxial InP is, therefore, below the detection limit of the chemical analysis used. In view of this, it was recognised that different vendors could unknowingly supply red phosphorus with different levels of residual sulphur.

Three batches of red phosphorus source material supplied by separate vendors were compared. One batch, lot L02910 supplied by MCP Electronic Materials (MCP) [5.01], was quoted as six 9s grade, Form 1. Form 1 red phosphorus is a specific allotrope obtained by condensing the vapour of white phosphorus heated to a temperature between 270°C and 480°C [5.01]. The second batch, lot A70095 from Johnson Matthey (JM) [5.17] was nominally six 9s grade polycrystalline lump, of unknown form. The third batch, 00259 supplied by Ventron [5.18] was six 9s electronic grade phosphorus lump, again of unknown form.

The sulphur concentration in each of these batches was assessed by the growth of unintentionally doped InP epitaxial layers. The same indium batch, group V cell and nominal growth conditions (growth rate $\sim 1.5 \mu\text{m hr}^{-1}$, growth temperature $\sim 480^\circ\text{C}$ and V:III nude ion gauge current ratio $\sim 10:1$) were used throughout. The sulphur concentration in the grown layers was calibrated from SIMS and residual carrier concentration profiles. A summary of the results is given in table 5.2.

TABLE 5.2

| Source | Run Number | Sulphur Conc (SIMS) (cm^{-3}) | Carrier Conc ($N_D - N_A$) (cm^{-3}) |
|---------|------------|--|---|
| MCP | 123 | 2×10^{16} | 2.5×10^{16} |
| JM | 137 | 1.8×10^{16} | — |
| Ventron | 132 | 1.2×10^{18} | 1.5×10^{18} |

It is evident that the concentration of sulphur in the red phosphorus supplied by

Ventron was two orders of magnitude larger than that present in the batches supplied by both MCP and JM. This high sulphur concentration was not identified in the purity specification [5.18]. The sulphur concentrations in the phosphorus source material supplied by MCP and JM were identical to within $\pm 30\%$, where the principal factor limiting the accuracy of the comparison was the control of the phosphorus flux. Significant variations in the sulphur concentration of nominally six 9s grade red phosphorus therefore exist.

Roberts et al [5.19] have reported subsequently a reduced sulphur concentration using a batch of vacuum-packed red phosphorus from MCP, growing InP with a residual donor concentration of $2 \times 10^{15} \text{cm}^{-3}$. The principal reason for packing the phosphorus under vacuum was to reduce oxide formation, as large quantities of oxide are observed to desorb from all phosphorus batches when they are heated under vacuum. The exact mechanism for the reduction in N_D obtained by Roberts et al has not been explained and may, indeed, be fortuitous. However, the concentration of sulphur in LPE InP has been reported to be increased by trace levels of acid absorbed from the atmosphere [5.20], and it is well documented that mechanisms exist whereby water and oxygen can cause either an increase or a decrease in the donor (Si) concentration in high purity vapour phase InP [5.21].

The available experimental data show significant batch to batch variations in the sulphur concentration of nominal six 9s purity red phosphorus. The growth of InP by MBE from solid sources consequently requires very careful monitoring of the phosphorus purity which is most readily achieved through controlled growth experiments. The highest purity InP grown from solid sources is still limited by a residual donor concentration of $\sim 2 \times 10^{15} \text{cm}^{-3}$ [5.19].

5.4 ALTERNATIVE SOURCES OF PHOSPHORUS

From the discussion in sections 5.2 and 5.3 it is apparent that the scope for limiting the concentration of sulphur both in the phosphorus charge and in the epitaxial layers is restricted. The question of other sources of phosphorus, therefore, has to be addressed if higher purity InP is to be grown.

A number of alternative sources of phosphorus have been used in the past, including InP itself [5.23], GaP [5.25], a tin melt saturated with phosphorus [5.25] and phosphine (PH_3) [5.06]. The captive sources all suffer from the similar problem of a co-evaporating group IIIb or group IVb flux. The discussion here will, therefore, be restricted to two alternatives: (a) a "gettered" source and (b) phosphine.

(a) Sulphur getter for Use with Red Phosphorus

The concept of using InP to getter the sulphur from the phosphorus flux has been considered, based on the relative stabilities of sulphur and phosphorus over InP. The proposal centres around the observation that sulphur as opposed to phosphorus preferentially accumulates on an InP surface (section 3.5.1). Thus an InP surface placed in the phosphorus beam between the red phosphorus source and the growing layer could potentially "getter" the sulphur from the phosphorus flux.

However, a number of practical difficulties arise in achieving such a "gettered" source, related principally to the surface area required and the need to hold the "getter" at a temperature intermediate between that of the source and the cracker. For these reasons it was not possible to demonstrate such a "gettered" source.

(b) Phosphine

In early experiments using phosphine, the purity of both the source and the cracker was a problem [5.26] [5.27]. However, recent results from both gas source MBE [5.28] and MOCVD growth [5.29] show that InP with total residual impurity concentrations less than $5 \times 10^{14} \text{cm}^{-3}$ and 77K mobilities greater than $100,000 \text{cm}^2 \text{V}^{-1} \text{s}^{-1}$ can be readily grown using commercially available phosphine. In addition, a significant increase in the number of publications describing InP based structures with state-of-the-art performance grown using the molecular beam technique, e.g. [5.30] [5.31] [5.32] [5.33] [5.34], has been associated with the introduction of phosphine into MBE.

In fact, in addition to purity a number of positive advantages result from the use of a gas, as opposed to a solid, phosphorus source. The most important of these, flux stability, allows the growth of lattice matched quaternary alloys containing two group V species much more readily than is possible with solid sources. Toxicity is a particular problem with phosphine which has a TLV of 0.3p.p.m. However, phosphine is used extensively within the semiconductor industry and, with the correct precautions, may be used safely. In addition, alternative and safer phosphorus alkyls, e.g. tertiary and isobutylphosphine [5.35] [5.36], triethylphosphine [5.37] and trimethylphosphine adducts [5.38], are actively being studied

Phosphine appears to be the best alternative source of phosphorus to replace the red phosphorus used in this study. Indeed, it offers a number of advantages over red phosphorus, including higher purity, better flux stability and extended run times.

5.5 SUMMARY

Reductions in the concentration of incorporated sulphur by optimising growth conditions are only viable at temperatures $<480^{\circ}\text{C}$ where sulphur desorption is negligible. Under these conditions, the concentration will be a minimum at growth rates where the proportion of the phosphorus flux required to stabilise the substrate against thermal decomposition is small compared to that contributing to growth.

Variations of over 2 orders of magnitude in the sulphur concentration of nominally six 9s purity red phosphorus source material have been detected. This emphasizes the need for very careful source selection procedures involving the growth of epitaxial layers under well controlled conditions.

The minimum residual donor concentration which has been achieved using a red phosphorus source is $2 \times 10^{15} \text{cm}^{-3}$ [5.19]. This contrasts with the MBE growth of InP using phosphine as the phosphorus source where total ionised impurity concentrations $\sim 5 \times 10^{14} \text{cm}^{-3}$ have been obtained [5.28]. Phosphine is thus the best source of phosphorus for the MBE growth of InP, with a demonstrated improvement in both purity and stability over red phosphorus, in addition to an effectively infinite source capacity.

CHAPTER 6

CONCLUSION AND SUGGESTIONS FOR FURTHER WORK

6.1 CONCLUSION

6.2 FURTHER WORK

6.1 CONCLUSION

A number of significant advances in the MBE growth of unintentionally and intentionally doped InP from solid sources have been described. The advances stem in large measure from the successful use of a specially devised series of experiments which involved making a deliberate step change to one of the growth parameters while maintaining the others constant. Variations in SIMS and C-V profiles were then correlated with the step change and have led to the identification of the principal residual impurities. The major residual donor is sulphur at a concentration of $\sim 10^{16} \text{cm}^{-3}$. The sulphur originates from the red phosphorus source material and significant variations in the concentration of sulphur in high purity red phosphorus supplied by different vendors have been recorded. The universal n-type behaviour of InP grown from solid sources is believed to be a direct consequence of persistent sulphur contamination in red phosphorus. Si is the only other donor impurity incorporated into MBE InP at detectable concentrations ($\sim 2 \times 10^{15} \text{cm}^{-3}$).

Ca is incorporated as the dominant acceptor-like impurity with a concentration estimated to be in the range $2 \times 10^{15} - 2 \times 10^{16} \text{cm}^{-3}$. From the more limited evidence available, Ca also appears to be a contaminant in the red phosphorus, although a more detailed study would be required to confirm this view. Moreover, the electrical role of Ca in InP remains unclear. In contrast to the results of Kubota et al [6.01], photoluminescence studies have provided no evidence for Ca acting as a shallow, electrically-active acceptor; indeed, the e-A recombination from the layers at $\sim 1.382 \text{eV}$ is assigned to magnesium at concentrations of only $\sim 10^{14} \text{cm}^{-3}$. It is concluded, therefore, that Ca is incorporated either as a deep acceptor or is electrically inactive. Further work, including low temperature PL and DLTS studies of Ca-doped or implanted InP, is required to establish the full behaviour of this element.

Intentional sulphur doping of MBE grown InP over the concentration range $5 \times 10^{16} - 10^{19} \text{cm}^{-3}$ has been reported for the first time. An electrochemical cell was used as the dopant source and variations in the sulphur concentration for nominally constant doping conditions have highlighted a previously unsuspected temperature sensitivity of the cell. The change in sulphur flux for a 1°C change in cell temperature is $\sim 7\%$, compared to $\sim 4\% ^\circ \text{C}^{-1}$ for a conventional thermal doping source such as Si.

The use of a constant current source as opposed to a constant voltage source to improve the flux control is proposed as a method of circumventing the temperature

dependence. The current in an electrochemical cell is a direct measure of the evaporating flux [6.02] and therefore provided leakage currents are not significant, current control should produce a very stable dopant source.

The electron mobility of sulphur-doped InP epitaxial layers has been characterised for free electron concentrations in the range $5 \times 10^{16} - 2 \times 10^{18} \text{cm}^{-3}$. The mobility was found to be ~40% of the maximum predicted by the theoretical calculations of Walukiewicz [6.03]. A reassessment of the calculations of Walukiewicz by Lancefield et al [6.04] has shown that at high carrier concentrations the assumption of a random impurity distribution is no longer valid, and the experimentally observed mobilities can be understood in terms of scattering from a correlated impurity distribution. Diffusion of sulphur under MBE growth conditions has not been observed.

A significant improvement in the morphology of sulphur-doped epitaxial layers, manifested by a decrease in the total concentration of surface defects from $\sim 10^4 \text{cm}^{-2}$ for undoped InP to $\sim 500 \text{cm}^{-2}$ for sulphur concentrations $\sim 10^{19} \text{cm}^{-3}$ was observed. This improvement is associated with a reduction in the dislocation density [6.05] and the possibility of using this effect to improve the morphology for certain device applications, e.g. lasers, requires evaluation. A heavily doped buffer layer ($\sim 10^{19} \text{cm}^{-3}$) could be deposited prior to the device structure to effect a sustained improvement in the morphology of the subsequent epitaxial layers.

A study of sulphur incorporation as a function of growth conditions has shown that for temperatures below 480°C desorption is not significant. Incorporation is suppressed by an increase in phosphorus flux, consistent with a reduction in the surface concentration of phosphorus vacancies. The change in sulphur concentration with group V flux is less than that reported for Si in GaAs [6.06] and underlines the potential of sulphur and the electrochemical cell as an n-type dopant source in the MBE growth of InP.

The more recent data of Airaksinen et al [6.07], who demonstrated that for substrate temperatures above 520°C sulphur desorbs from InP with a characteristic activation energy of 4.5eV, has been developed further. By calculating the ratio of the desorption and incorporation coefficients versus temperature ($D/K[T]$) the prospect of reducing sulphur incorporation into unintentionally doped InP by adjusting the growth parameters has been examined. The conclusion drawn is that no significant reduction in the concentration of sulphur can be obtained by increasing the growth temperature above 500°C . Indeed, for growth rates $\sim 1 \mu\text{m hr}^{-1}$, a minimum sulphur concentration

is predicted for growth temperatures $<450^{\circ}\text{C}$ where the phosphorus flux required to prevent thermal decomposition is small compared with that required for growth.

The use of red phosphorus as the phosphorus source in the MBE growth of InP has not resulted in residual donor concentrations $<2\times 10^{15}\text{cm}^{-3}$ [6.08], despite careful selection of phosphorus batch material. In contrast, the use of phosphine as the phosphorus source has resulted in residual impurity concentrations $<5\times 10^{14}\text{cm}^{-3}$ [6.09], indicating that the route to the growth of high purity InP by MBE is via the use of phosphine as a group V source. Significant additional advantages are to be gained from the use of a gas, as opposed to solid, source; firstly, the source capacity is effectively infinite; secondly, the flux stability is significantly improved. The accuracy which can be achieved using flow control is $\sim 0.5\%$ [6.10] and compares with solid phosphorus where drifts of $>10\%$ during growth are not uncommon. Thirdly, changes in flux are not limited by the thermal mass of the group V charge.

With phosphine as the group V source it is clear that the substrate temperature will become the critical parameter in the controlled growth of InP. Small ($\sim 20^{\circ}\text{C}$) changes in temperature not only affect the incorporation of impurities [6.07], but at the growth temperatures and rates typically used (500°C and $1\mu\text{m hr}^{-1}$) they can have a significant effect on the surface stoichiometry. For example, at 500°C where the phosphorus loss rate approaches 1 monolayer s^{-1} , a 35°C increase in substrate temperature will increase this loss by ~ 10 . Therefore, unless the phosphorus flux used for growth is $10\times$ larger than that required to balance the loss at 500°C , such a 35°C drift or overshoot in T_s will result in the formation of an indium rich surface.

To achieve this control over T_s and an understanding of the role of the surface stoichiometry on the material/device performance it will be necessary to give very careful attention to the calibration of substrate temperature, by the use of a range of techniques, and make self consistent *in situ* measurements of the phosphorus flux required to prevent thermal decomposition.

6.2 FURTHER WORK

Throughout this study it has been shown that although the growth of InP by MBE is less trivial than the growth of GaAs, molecular beam epitaxy is a viable route for the growth of InP. With the introduction of a gaseous group V source MBE will continue to provide a combination of purity, growth control and analysis unattainable by other epitaxial techniques. It is important that these advantages are used to their full to develop and understand the potential of hetero- and low dimensional-structures. To this end the use of InP in combination with ternary, e.g. GaInAs, and quaternary, e.g. GaInAsP, alloys requires continued development and close interaction with device expertise.

One essential for such devices which has not been characterised in this work is a suitable p-type dopant. Be is likely to be the optimum p-type dopant and although its incorporation has been reported to be ill behaved [6.11] it is clear that these problems are likely to have been associated with the poor unintentional purity of the layers. Confirmation of the results reported by Kawamura [6.12] for Be is therefore required.

Vital to heterostructure applications is the abruptness and purity of the interfaces. The high vapour pressures of the group V elements make abrupt changes in composition, with limited impurity accumulation, difficult to achieve in the mixed group V alloys commonly associated with InP. However, reactors using gaseous group V sources with the limitations imposed by the thermal response of the solid charge removed and their inherently high pumping speed, offer significant advantages. These advantages need to be quantified and assessed both directly e.g. RHEED, luminescence, TEM and SIMS and also in device configurations e.g. barrier structures and lasers.

The potential which a "total" gas source reactor (i.e. gaseous group III and dopant sources) has for large area uniformity and improved reliability, required in production applications, needs evaluation. For example, problems exist with the use of metal alkyl sources for the growth of mixed Ga-In alloys, because of a limited range of growth temperatures in which the group III incorporation is well behaved [6.13]. The mechanism(s) responsible for this temperature window needs to be established.

An additional field of growth where further research is required is that of selective area deposition. Although the ability to achieve selective area growth has been demonstrated the full device potential has not been exploited. The engineering

complexity and the repeatability problems associated with the use of shadow masks is clearly one reason for this, while self aligned growth is complicated by the production of the channel and, when solid sources are used, deposition of non crystalline material on the mask [6.14]. Again the advantages of gas sources need to be assessed. With a gas source growth is preceded by the breakdown of the precursor. This initial breakdown can be either surface specific [6.15] giving true selective area growth or photochemically induced with the potential for direct writing using lasers [6.16].

APPENDIX - ANALYSIS TECHNIQUES

A.1 INTRODUCTION

A.2 SECONDARY ION MASS SPECTROMETRY

**A.3 ELECTROCHEMICAL CAPACITANCE-VOLTAGE
PROFILING**

A.4 VAN-DER-PAUW HALL MEASUREMENT

A.5 PHOTOLUMINESCENCE

A.1 INTRODUCTION

To assess the quality of InP grown during this project, a range of complementary analysis techniques was used. The results obtained led to a detailed understanding of the factors which limited the quality of InP grown (e.g. chapters 2 and 3). In addition, they enabled the InP grown to be compared with that obtained both in other MBE reactors and by other growth techniques.

Analysis concentrated in three main areas:

- (i) quantitative characterisation of impurities
- (ii) majority carrier properties
- (iii) luminescence measurements

This appendix provides an overview of the principles of each assessment technique, together with brief details of the experimental equipment used. With each technique it is important to be aware of the limitations which exist, so that appropriate measures may be taken to minimise potential errors. Details of the limitations encountered and the methods used to minimise them are given with the review of each technique.

The appendix is divided into five sections covering (a) Secondary Ion Mass Spectroscopy (SIMS), (b) Electro-chemical Capacitance-Voltage profiling, (c) Van-der-Pauw Hall measurement and (d) Photoluminescence.

A.2 SECONDARY ION MASS SPECTROSCOPY

Secondary ion mass spectroscopy (SIMS) provides information on impurities present in a material by using a single isotope ion beam to sputter the material and then analysing the sputtered products with a mass spectrometer. Quantitative data is obtained by comparing each secondary ion signal with that from a sample of known impurity concentration. The technique can be either static, using low sputter rates and removing <1% of a monolayer, to look at surfaces, or dynamic where higher sputter rates ($\sim 0.1 \mu\text{m min}^{-1}$) are used to profile through the sample. In the latter case, accurate depth profiles with a resolution of $\sim 3\text{nm}$ can be obtained [A.01]. All of the SIMS studies reported in this thesis have involved dynamic profiling and were undertaken, courtesy of RSRE Malvern, at Loughborough Consultants [A.02].

The sensitivity of SIMS varies both from element to element and with the host matrix: it is particularly poor ($>1\text{ppma}$, $2 \times 10^{16} \text{cm}^{-3}$) for carbon and oxygen,

because these are the dominant residual gases present in the analyser vacuum, but is capable of detecting .0001ppma of chromium and manganese in GaAs, equivalent to an impurity concentration of $5 \times 10^{13} \text{cm}^{-3}$ [A.03]. These sensitivities are superior to either Auger Electron Spectroscopy (AES) or X-ray Photoelectron Spectroscopy (XPS) which are typically limited to $\sim 100 \text{p.p.m.a.}$, while other analysis techniques, such as photoluminescence and Hall, which are able to detect impurities at concentrations comparable to SIMS, only yield either the concentration or the identity of the impurity (sections A.4 and A.5).

A.2.1. EXPERIMENTAL DETAILS

All of the SIMS studies involved the use of a CAMECA IMS 3F instrument [A.04], equipped with both Cs^+ and O_2^+ ion sources. In this instrument, the primary ion source is magnetically filtered to ensure high purity ($M/\Delta M=30$) and the resultant beam, typically $10 \mu\text{m}$ in diameter, rastered to produce a square etch pit with side variable up to $500 \mu\text{m}$. Primary ion energy is variable between 1 and 20keV and the maximum beam current $\sim 0.5 \mu\text{A}$ for Cs^+ and $\sim 5 \mu\text{A}$ for O_2^+ .

The two ion sources enable high detection limits to be achieved for both electropositive (eg Ca, Mg, Mn, Fe) and electronegative (eg S, Se, O) elements. O_2^+ ions give a high yield of electropositive elements and Cs^+ ions a high yield of electronegative elements. Secondary ions extracted from the etch pit have their spatial relationship preserved and edge effects are eliminated by arranging for only those ions from the central area of the pit to be transferred by the ion-optics. This central area can be selected to be either 25, 150 or $400 \mu\text{m}$ diameter. The mass resolved image ($M/\Delta M=200-10,000$) can be viewed while maintaining spatial relationships, or alternatively focussed to give an integrated intensity at a particular mass. The spatial resolution obtained is typically $1 \mu\text{m}$ which enables particulate matter or defects on the scale $1-100 \mu\text{m}$ to be readily identified.

In addition to improving the sensitivity of the SIMS analyser by choice of the primary ion species, spurious ions present in the secondary ion beam due to gas reactions, fragmentation products and background impurities in the SIMS equipment can be rejected by the use of high voltage offset filtering, changes in mass resolution and studies of isotope ratios.

High Voltage Offset Filtering

High voltage offset filtering (HVO) permits discrimination between atomic and

polyatomic, or polyatomic derived ions [A.05]. The energy distribution of ions with the same mass number is broader for single atoms than it is for those related to polyatomic atoms. Thus by preventing low energy ions from entering the mass analyser, the SIMS output is biased in favour of the single atom species. There is, however, a penalty to be paid for this high mass resolution in that it reduces the total transmission and therefore quantitative comparison between profiles with different offsets is not possible.

High voltage offsets were used to confirm the step changes in Ca concentration recorded in layer TM 99 (figure 3.9). Interference can be obtained between the mass 40 isotope of Ca and MgO species. Mg was known to be present in the epitaxial layers and to confirm that the ion signal at mass 40 was Ca, the profile was repeated with a high voltage offset of $\sim 40V$. Comparable percentage changes in the mass 40 ion signal were obtained both with and without the high voltage offset, confirming the detected ion to be Ca.

Isotope Ratios and High Resolution

Most elements have more than one isotope with a relative abundance $>10\%$. Consequently, errors which arise when more than one ion species has the same mass number can be reduced by a careful choice of isotopes. The two principal isotopes of sulphur have masses of 32 and 34a.m.u. with relative abundances of 95% and 4% respectively. Analysis of sulphur using the more abundant 32 isotope is normally limited by interference from PH and O_2 and for most studies the 34 isotope is used.

However, in order to confirm the presence of sulphur in the unintentionally doped InP high resolution scans of the sulphur isotope at mass 32 were recorded. The precise atomic masses of S, PH and O_2 are 31.972, 31.981 and 31.989a.m.u. respectively, and to separate these species a mass scan at a resolution of $\sim 10,000$ was recorded. The scan revealed that the ion current for the PH species was ~ 3 higher than that of S while no signal associated with the O_2 species could be detected. Maintaining the high resolution mode, depth profiles of TM 123 were recorded for both the 31.972 and 31.981a.m.u. ions. The results, figure A.1, not only demonstrate the dominance of the PH_{32} species over S_{32} but also shows that the depth profile of the S_{32} isotope has exactly the same form as that of the S_{34} and residual carrier profiles shown in figure 3.10. Convincing evidence of the role of sulphur as the dominant residual impurity in the unintentionally doped InP.

The isotopes of an element are also used to confirm that the ion species detected

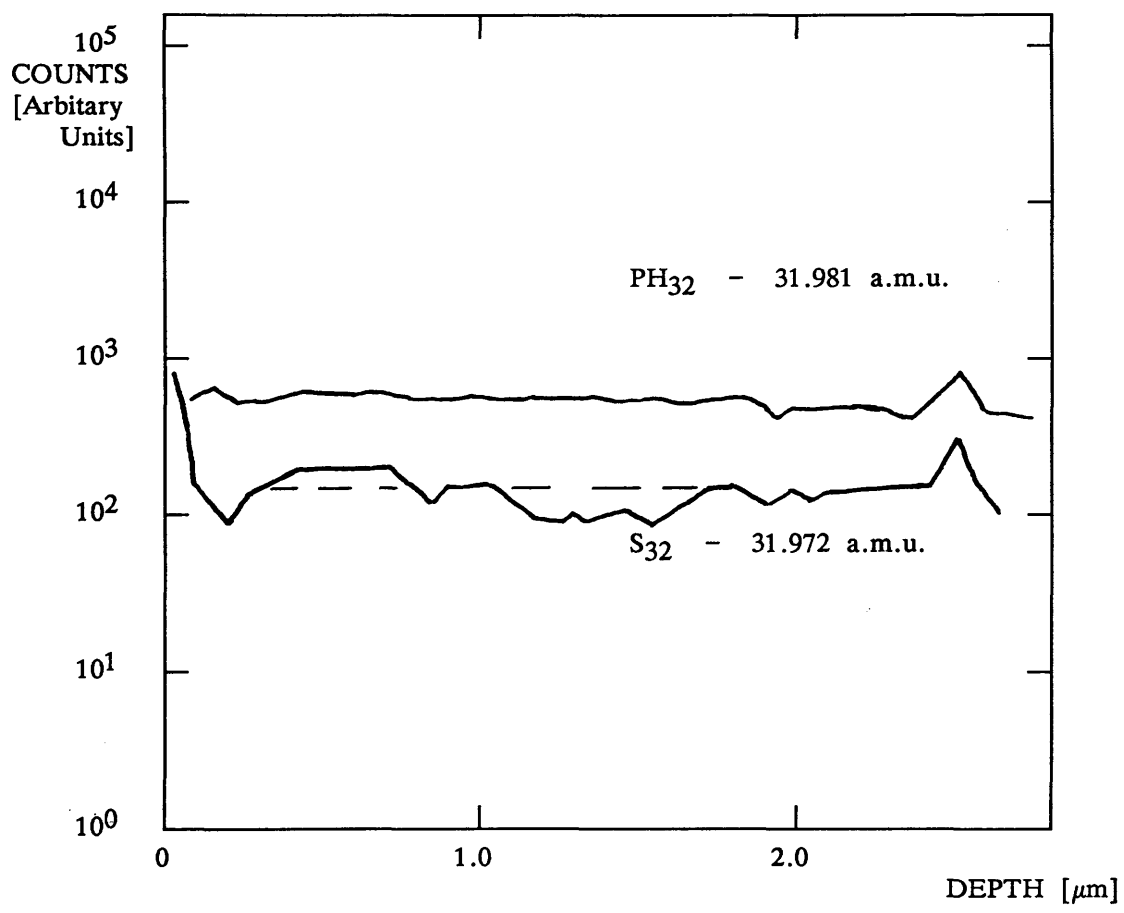
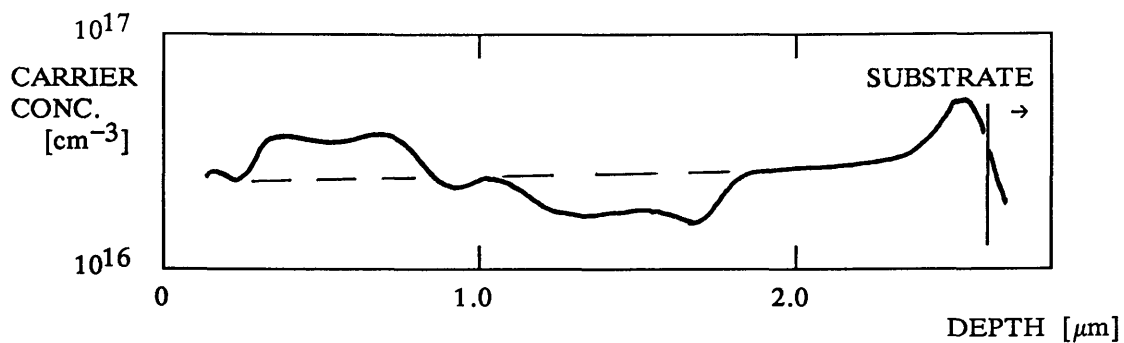


FIGURE A.1 HIGH MASS RESOLUTION SIMS PROFILE OF THE MASS 32 ISOTOPES IN TM 123

are those of that particular element. The relative abundances of all isotopes are well documented and a profile of the isotopes of an element should replicate these abundances. The study of tin in layer TM 86 is an example of the use of isotopes to separate real from spurious signals. Tin is particularly suited to this form of study as it has eight isotopes with relative abundance >1%. The mass 120 Sn isotope, relative abundance 33%, profiled in layer TM 86 was found to have a depth profile similar to that of the residual carrier profile, figure A.2. However, as also shown in figure A.2, subsequent profiles of the tin isotopes at 118 and 119amu, relative abundance 24 and 9% respectively, neither replicated the similarity with the carrier profile nor were present in the correct ratio, demonstrating that the detected ions were not tin.

Quantitative Calibration

Calibration of the concentration of elements identified in the SIMS profiles is most accurately achieved by profiling an implant of the impurity element in the matrix of interest. The profile of the implant and the integrated area under the profile can then be calibrated against the implant conditions and an absolute calibration with an accuracy of ~20% obtained [A.06]. In addition to providing calibration data, the implants readily identify the minimum detectable concentration for the profiling conditions. Figure A.3 shows the profile of the implant standard used to calibrate the silicon concentration. The minimum detectable concentration is seen to be $\sim 10^{15} \text{cm}^{-3}$.

When an implant standard is not available, the impurity concentration can be estimated from data on relative ion yields. The count rate for the ion signal of the uncalibrated impurity is scaled according to the ion yield of this element relative to that of an element for which an implant standard is available. Using this scaled count rate and the available implant standard, an approximate calibration can then be achieved. The calibration is only approximate because the actual ion yield of an element is a function of the matrix of which it is part and can be enhanced by the presence of certain neutral species [A.07]. Nevertheless, such a technique enables impurity concentrations to be estimated to within an order of magnitude.

The relative ion yield of Ca with respect to Mg was used to estimate the Ca concentration in the epitaxial InP grown in Chamber 2. Inspection of the SIMS depth profile for Ca and Mg in epitaxial layer TM 123 (Fig 3.10) shows that the Ca signal is $\times 100$ larger than that of Mg. The Mg concentration, calibrated using an implant standard, was $\sim 10^{14} \text{cm}^{-3}$ and the ion yield of Ca is $\sim \times 3$ larger than that

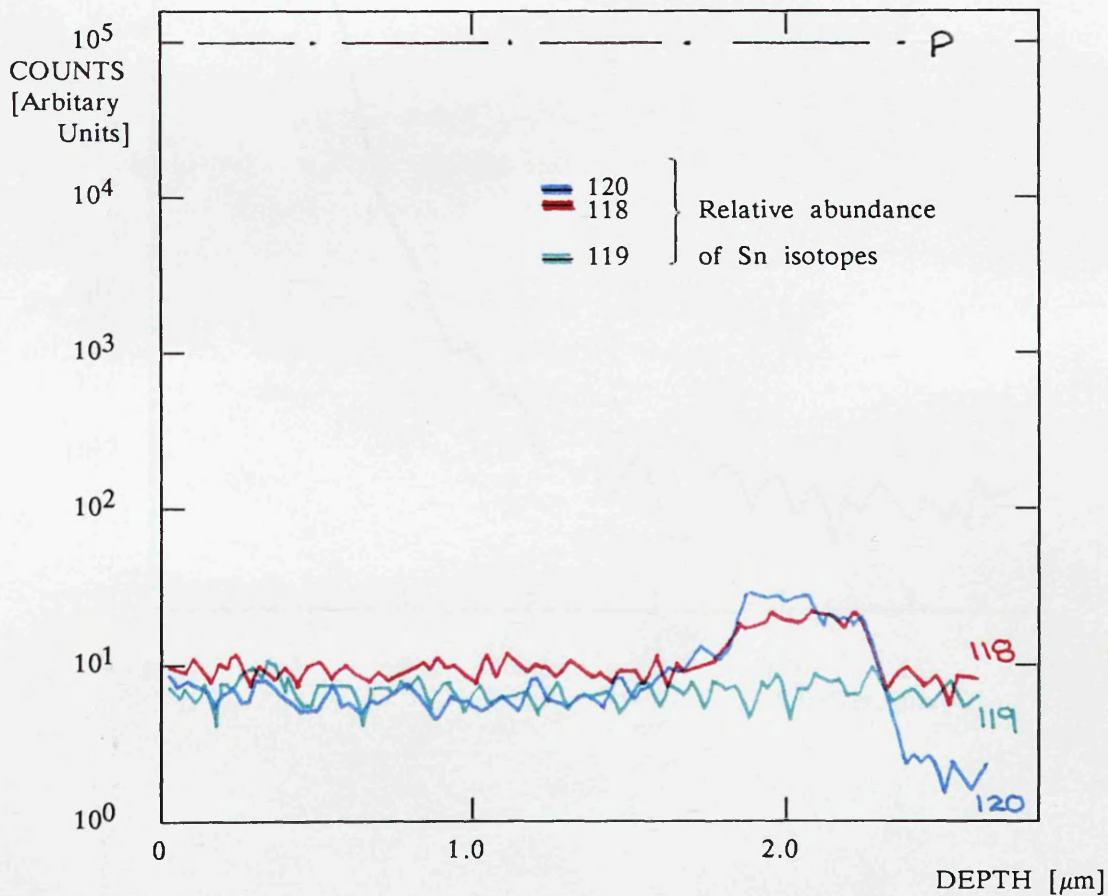
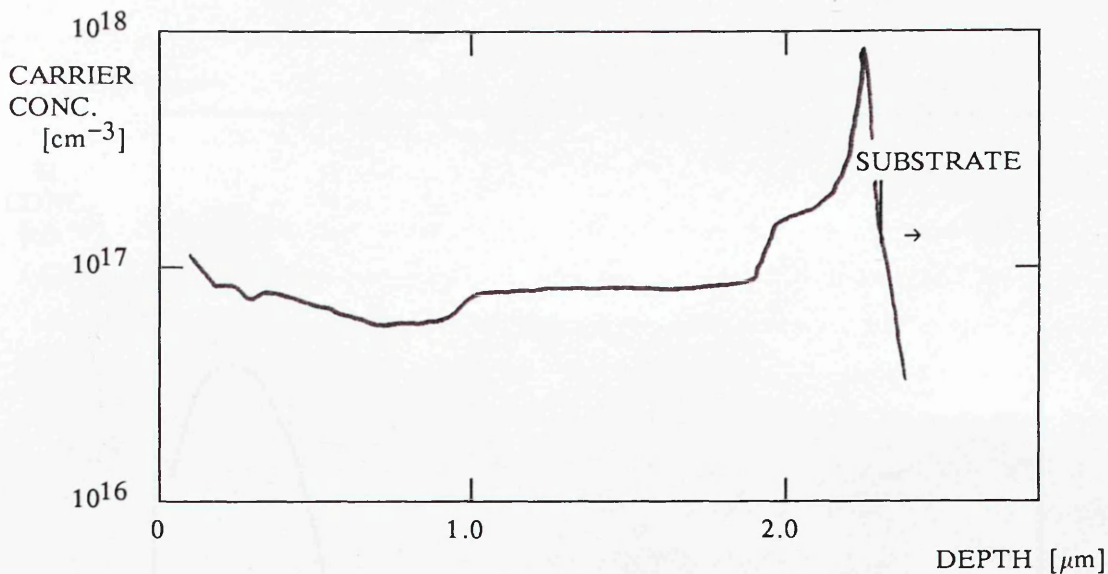


FIGURE A.2 C-V AND SIMS PROFILE ILLUSTRATING Sn ISOTOPE CHECK IN TM 86

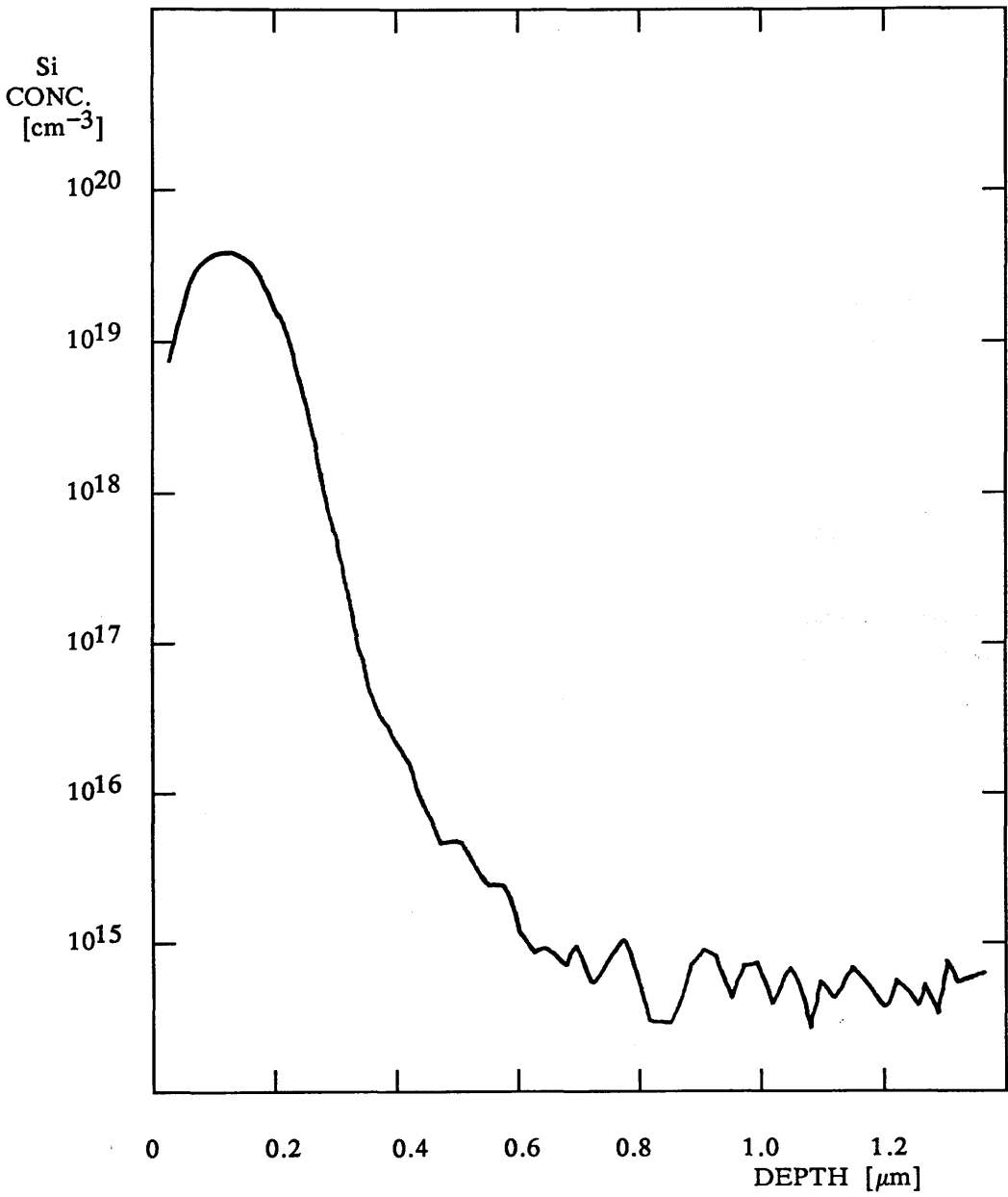


FIGURE A.3 SIMS PROFILE OF Si IMPLANT

of Mg [A.08]. Therefore when the relative abundances of the Mg_{24} and Ca_{40} isotopes, 79% and 97% respectively, are taken into account the Ca concentration in the epitaxial layer is $\sim 3 \times 10^{15} \text{cm}^{-3} \pm 3$.

To confirm that this was a reasonable estimate, the calcium concentration was also calibrated by reference to the concentration in the InP substrate. Table A.1 summarises the published data for the impurity concentration in InP substrate material from which it can be seen that the Ca concentration is typically in the range $5 \times 10^{14} - 5 \times 10^{15} \text{cm}^{-3}$. The profile of TM 123 identified the Ca concentration in the epitaxial layer to be ~ 5 higher than that in the substrate and therefore the epitaxial concentration in the range $2 \times 10^{15} - 2 \times 10^{16} \text{cm}^{-3}$, in agreement with the concentration estimated using the relative ion yield of Ca and Mg.

A.3 ELECTROCHEMICAL CAPACITANCE-VOLTAGE PROFILING

Electrochemical capacitance-voltage profiling quantifies the depth variation of the carrier concentration and the majority carrier type. A depletion region is formed by a reversed bias Schottky barrier or p-n junction, and the capacitance measured as a function of bias. It can be shown, by applying Gauss's theorem to the electric field and considering the change in capacitance produced by a small increase in reverse bias voltage, that the gradient of a plot of C^{-2} versus V yields a value for $N_D - N_A$:

$$N_D - N_A(x) = - \frac{2}{\epsilon e A^2} \left[\frac{\partial(1/C^2)}{\partial V} \right]^{-1} \quad \text{A.1}$$

or more conveniently for non-uniform profiles:

$$N_D - N_A(x) = - \frac{C^3}{\epsilon e A^2} \left[\frac{\partial C}{\partial V} \right]^{-1} \quad \text{A.2}$$

The thickness x of the depleted layer is derived from its capacitance:

$$C(x) = - \frac{\epsilon A}{x} \quad \text{A.3}$$

- x - depth
- A - diode area
- C - capacitance
- V - voltage
- ϵ - dielectric constant
- e - charge on an electron

| ELEMENT SUBSTRATE | Al | Ca | Cr | Cu | Fe | Na | Ni | Mg | S | Si | Zn |
|----------------------------------|--|---|--------------------|---------------------|--|--|---------------------|---|---|--|---|
| M.C.P. UNDOPED [A.09] | | | | | <2x10 ¹⁵ | | | <8x10 ¹⁵ | | 3x10 ¹⁶ ↓ <2x10 ¹⁶ | |
| CAMB. INST. UNDOPED [A.10] | 4x10 ¹⁴ ↓ <2x10 ¹⁴ | 6x10 ¹⁵ ↓ <3x10 ¹⁴ | | | 4x10 ¹⁵ ↓ <3x10 ¹⁴ | 1x10 ¹⁵ ↓ <3x10 ¹⁴ | | | <8x10 ¹⁵ ↓ 4x10 ¹⁴ | 8x10 ¹⁵ ↓ <4x10 ¹⁴ | <2x10 ¹⁵ ↓ 6x10 ¹⁴ |
| METALS RES UNDOPED [A.11] | 8x10 ¹⁴ ↓ <3x10 ¹⁴ | <8x10 ¹⁴ ↓ <3x10 ¹⁴ | | | 3x10 ¹⁵ ↓ <8x10 ¹⁴ | 1x10 ¹⁵ ↓ 3x10 ¹⁴ | | | <8x10 ¹⁵ ↓ <4x10 ¹⁵ | 3x10 ¹⁶ ↓ 8x10 ¹⁵ | <2x10 ¹⁵ ↓ <4x10 ¹⁴ |
| METALS RES Fe DOPED [A.11] | 4x10 ¹⁴ ↓ 3x10 ¹⁴ | 3x10 ¹⁵ ↓ 2x10 ¹⁵ | | | 4x10 ¹⁶ ↓ 2x10 ¹⁷ | 2x10 ¹⁵ ↓ 3x10 ¹⁴ | | 2x10 ¹⁵ ↓ 3x10 ¹⁴ | 2x10 ¹⁵ ↓ 4x10 ¹⁴ | 4x10 ¹⁵ ↓ 1x10 ¹⁵ | 2x10 ¹⁵ ↓ 1x10 ¹⁵ |
| R.S.R.E. UNDOPED [A.12] | <1x10 ¹⁵ | 1x10 ¹⁵ | 4x10 ¹⁴ | <8x10 ¹⁴ | 4x10 ¹⁴ | | <4x10 ¹⁴ | | | 3x10 ¹⁵ | 4x10 ¹⁵ |

units

cm⁻³

TABLE A.1 SUMMARY OF THE CONCENTRATION OF IMPURITIES IN InP SUBSTRATES

and therefore the carrier concentration can be determined as a function of depth.

However, because the accumulated surface charge increases as the width of the depletion layer increases, high electric fields are obtained which eventually breakdown the material and limit the depth which can be profiled. The maximum surface charge (doping concentration \times depleted thickness) is typically 2×10^{12} centres cm^{-2} [A.13].

To overcome this a combination of controlled etching and sequential C-V measurements is used, the most successful demonstration of which is the electrochemical profiling technique developed by Ambridge et al [A.14]. In this a Schottky barrier is obtained by placing an electrolyte in contact with a semiconductor, a reverse bias between the electrolyte and the semiconductor then enables a standard C-V measurement to be made. In addition, anodic dissolution of the semiconductor can be achieved by careful control of the conditions at the electrolyte-semiconductor interface. For n-type material this is achieved by illuminating the sample while maintaining a reverse bias, the anodic dissolution current being derived from the electron hole pairs created in the depleted region. For p-type material the junction is momentarily forward biased to obtain the dissolution current. The amount of material removed and, therefore, the etch depth can be calculated by applying Faraday's law to the integrated current through the cell. The depth at which the carrier concentration is being measured is then given by the sum of this etch depth, and the depletion width obtained from equation A.3.

A.3.1 EXPERIMENTAL DETAILS

All electrochemical C-V profiles reported in this work have been obtained using a "Polaron Profile Plotter" [A.15]. The application of both the technique and the equipment to InP was demonstrated by Ambridge et al [A.16] and the procedures adopted by Ambridge have been followed in this work. Both 0.5M HCl and KOH electrolytes were used and, in order to minimise parallel conduction, the potential maintained across the depletion region was $< 1.0\text{V}$. Carrier concentration was measured using a 30Hz 100mV modulation, while the depletion width was obtained from a 50mV 3kHz signal.

Care is required in the calibration and interpretation of the C-V profiles to prevent significant errors. The errors arise primarily from two sources; firstly, those associated with the parameters used to calculate depth and carrier concentration (i.e. contact area and series resistance) and, secondly, those arising from non-uniform

concentrations of shallow donors and acceptors.

The area of the Schottky barrier is a major source of error in all C-V measurements as it affects both the carrier concentration and depth calibration. The residual carrier concentration is inversely proportional to the square of the area, thus for the electrochemical profiler in which the contact is nominally 3.5mm diameter, an error of 0.2mm (6%) gives an error in the residual carrier concentration of 24%. The difficulty in obtaining an accurate measurement of this area is compounded by the use of an "O" ring and electrolyte to define the contact. Electrolyte can seep under the "O" ring and so increase the contact area. This effect is particularly noticeable with certain electrolytes, of which KOH is one. An additional effect of the "O" ring is that an unilluminated area is produced beneath it so that, when profiling n-type material, the contact area for the capacitance measurements is larger than that etched. However, account is taken of this area discrepancy by entering an excess area parameter into the calibration.

The equivalent circuit assumed in the calculation of the capacitance is a parallel combination of capacitor and resistor. A high resistance in the series contact made to the semiconductor will produce an erroneously low value of capacitance in this parallel model. Consequently a high value for the depth and low value for the carrier concentration are recorded. Such errors are most significant at two points in a profile. Firstly, at the start of a profile, where the capacitance is very low and so the depletion depth can appear to decrease with an increase in applied bias. Secondly, when profiling close to the epilayer substrate interface of semi-insulating substrates where the conducting channel becomes very narrow and high resistance.

The presence of both shallow and deep donor levels can also produce anomalies in the profiles of n-type material. These anomalies, which are discussed in detail by Kimerling et al [A.17] arise as a result of the inability of the carriers trapped in levels at the edge of the depletion region to follow the modulation and can, therefore, be monitored by changing the modulating frequency.

A.4 VAN-DER-PAUW HALL MEASUREMENT

The Van-der-Pauw technique enables Hall mobility and residual carrier concentration data to be evaluated using more general geometries than the conventional Hall bar. In the conventional Hall measurement the voltage (R_H) induced perpendicular to both the current and magnetic field is related to the sheet carrier concentration (n) by

$$R_H = \frac{1}{n e}$$

A.4

with the zero field resistivity (ρ) a function of both carrier concentration and mobility (μ):

$$\rho = \frac{1}{n e \mu} \quad \text{A.5}$$

Van-der-Pauw [A.18] analysed the more general case of currents between four contacts (A, B, C and D) at the edge of a plane and showed that the resistivity was given by:

$$\rho = \frac{\pi t (R_{AB,CD} + R_{BC,DA})}{2 \ln 2} f \left[\frac{R_{AB,CD}}{R_{BC,DA}} \right] \quad \text{A.6}$$

t - sample thickness

$R_{AB,CD}$ - voltage between CD per unit current through AB

$$f \left[\frac{R_{AB,CD}}{R_{BC,DA}} \right] \approx 1 \quad \text{for} \quad \left[\frac{R_{AB,CD}}{R_{BC,DA}} \right] = 1 \quad \text{[A.18]}$$

The change in resistance ($\Delta R_{BD,AC}$) induced by a magnetic field applied normal to the plane provides a value for the Hall mobility (μ_H) and hence sheet carrier concentration:

$$\mu_H = \frac{t \Delta R_{BD,AC}}{B \rho} \quad \text{A.7}$$

Errors associated with this more general geometry are minimised by ensuring that, in relation to the diameter of the sample, the contact area is small and close to the sample edge [A.18]. With these precautions and by using averages of the values obtained from both alternated current contacts and reversals of the magnetic field, total errors are less than 13% [A.19].

A.4.1 EXPERIMENTAL DETAILS

All the epitaxial InP studied was n-type and tin contacts were used throughout. The InP and the tin were first etched in 10% HCl and then the contacts annealed, using a 5% hydrogen-nitrogen ambient, at 325°C for approximately 3 minutes. Prior to the measurement a curve tracer was used to check that the contacts were ohmic.

Van-der-Pauw measurements were made at both room temperature and 77K using a magnetic field of 0.2 Tesla. Currents were typically 1mA and results were taken for both current and magnetic field in forward and reverse directions. The isotropy of the Van-der-Pauw specimens, as measured by the "f factor" (equation A.6), was in excess of 0.9 for all samples quoted.

Theoretical analysis of the scattering mechanisms which control the electron mobility reveals that at room temperature the mobility is dominated by optical phonon scattering, but that at 77K the effect of ionised impurities becomes significant [A.20] [A.21]. Comparison of the mobility carrier concentration data measured at 77K with a theoretical analysis can therefore be used to estimate the ionised donor and acceptor concentrations and throughout this study the theoretical analysis of Walukiewicz [A.20] has been used as the reference.

In making this comparison it is important to be aware of assumptions implicit in the model. The first is that the measured Hall mobility is equivalent to the theoretical drift mobility, ie the Hall scattering factor r_H defined by:

$$R_H = \left[\frac{1}{n e} \right] r_H$$

is unity. Such an assumption is valid in the high field limit, $\mu B > 1$ [A.13], but for the Hall measurements undertaken in this study the maximum value μB was 0.3 and therefore the assumption is not valid. However, all of the epitaxial InP characterised had residual impurity concentrations $> 10^{16} \text{cm}^{-3}$ and under such near degenerate conditions the errors introduced by assuming $r_H = 1$ are typically less than 20% [A.22].

A second assumption implicit in the theoretical analysis is that the impurity concentration is constant throughout the epitaxial layer. The residual carrier concentration profiles provided conclusive evidence that this was not the case and an assessment of the effect of such non-uniform carrier profiles was made.

To a first approximation the measured profiles can be considered as two layers, the high doped interfacial layer (thickness t_I) and low doped epitaxial layer (thickness t_E). Modelling the Hall measurement of two parallel conducting layers shows that the carrier concentration (n_{eff}) and mobility (μ_{eff}) are given by:

$$n_{\text{eff}} = \frac{(n_E t_E \mu_E + n_I t_I \mu_I)^2}{(t_E + t_I) \times (n_E t_E \mu_E^2 + n_I t_I \mu_I^2)} \quad \text{A.8}$$

$$\mu_{\text{eff}} = \frac{(n_{\text{E}}t_{\text{E}}\mu_{\text{E}}^2 + n_{\text{I}}t_{\text{I}}\mu_{\text{I}}^2)}{(n_{\text{E}}t_{\text{E}}\mu_{\text{E}} + n_{\text{I}}t_{\text{I}}\mu_{\text{I}})} \quad \text{A.9}$$

- n_{E} - carrier concentration of epitaxial layer
- μ_{E} - mobility of epitaxial layer
- n_{I} - carrier concentration interface layer
- μ_{I} - mobility of interface layer

These equations have been solved for a range of carrier concentrations and thicknesses typical of those observed experimentally in both the epitaxial and interface regions. All calculations have assumed that the material is uncompensated.

The results, which are more general than the specific result quoted by Ashen et al [A.23], highlight important artefacts which arise from Hall measurements made on epitaxial layers with non-uniform carrier concentrations.

The most notable feature is the large change in carrier concentration with measurement temperature, carrier freezeout, which can result. Figure A.5 shows the apparent carrier freezeout, defined as the Hall derived carrier concentration at 77K divided by that at 300K, as a function of interface thickness for a range of epitaxial and interface parameters which are typical of those observed experimentally. The data indicates that the apparent carrier freezeout associated with the epitaxial InP characterised in the present study (i.e. interface concentrations in the range $5 \times 10^{16} \text{cm}^{-3}$ – $5 \times 10^{17} \text{cm}^{-3}$) would be ~ 0.8 .

Significant carrier freezeout was also reported by Sullivan et al [A.24] for InP grown by MBE on ion cleaned substrates. Such a cleaning procedure is known to produce a highly doped interface region and although thickness or carrier profile data is not available to enable the results to be modelled in detail, a good comparison with the published data can be obtained.

Results quoted by Sullivan [A.25] were:

| $N_{\text{D}}-N_{\text{A}}$ (300K) cm^{-3} | $N_{\text{D}}-N_{\text{A}}$ (77K) $\text{cm}^2\text{V}^{-1}\text{s}^{-1}$ | $\mu_{300\text{K}}$ cm^{-3} | $\mu_{77\text{K}}$ $\text{cm}^2\text{V}^{-1}\text{s}^{-1}$ |
|---|---|---|---|
| 1.2×10^{16} | 3,400 | 6×10^{14} | 33,000 |
| 2×10^{16} | 2,600 | 7×10^{14} | 17,000 |
| 1.5×10^{16} | 3,000 | 8×10^{14} | 23,000 |

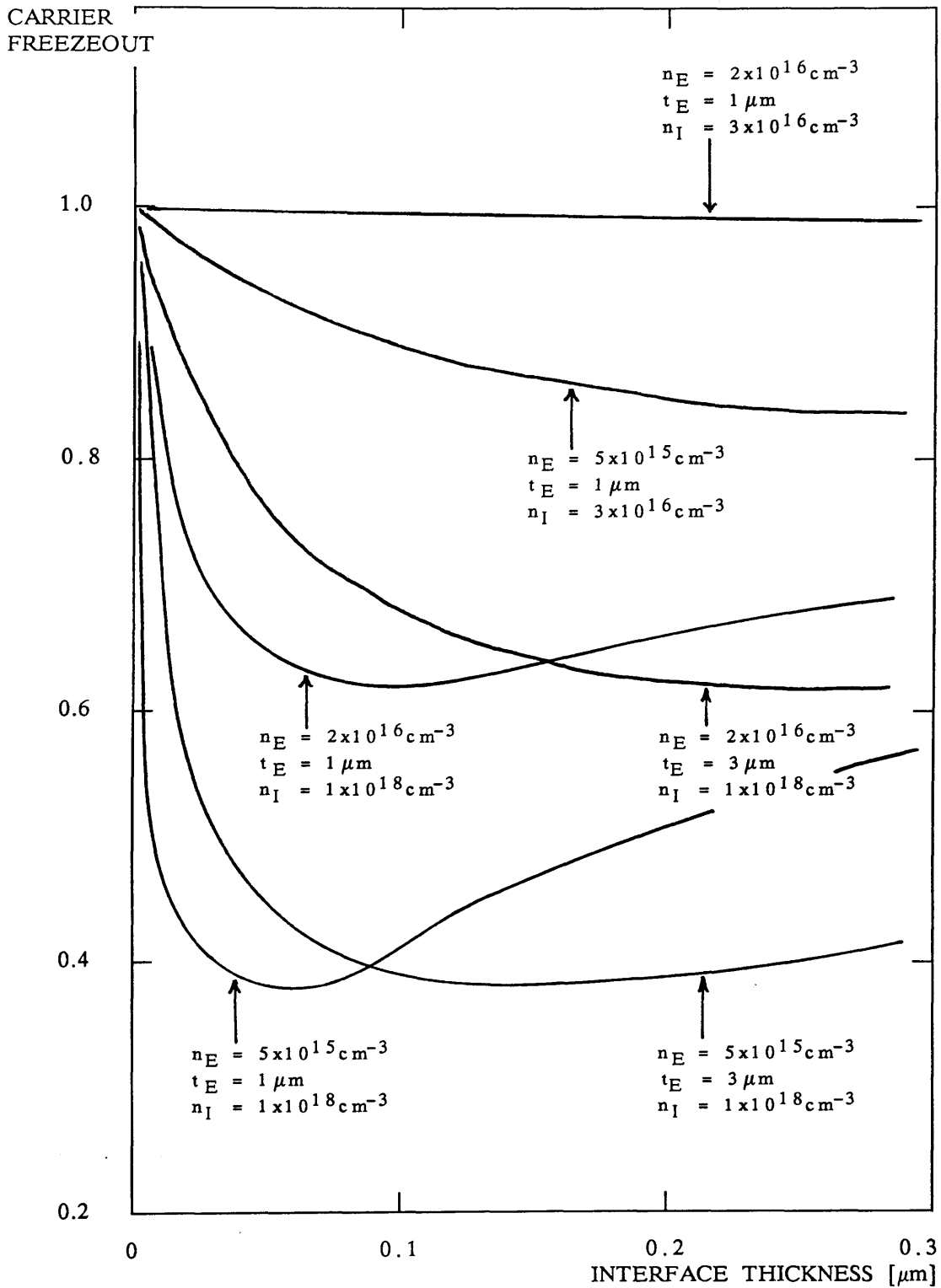


FIGURE A.4 CALCULATED VARIATION IN CARRIER FREEZEOUT AS A FUNCTION OF INTERFACE THICKNESS AND DOPING CONCENTRATION

If an epitaxial layer with residual carrier concentration $1 \times 10^{15} \text{cm}^{-3}$, $\mu_{300\text{K}} = 4700 \text{cm}^2 \text{V}^{-1} \text{s}^{-1}$, $\mu_{77\text{K}} = 50,000 \text{cm}^2 \text{V}^{-1} \text{s}^{-1}$ and active thickness $0.4 \mu\text{m}$ is considered in parallel with an interface, carrier concentration $2 \times 10^{17} \text{cm}^{-3}$, $\mu_{300\text{K}} = 2000 \text{cm}^2 \text{V}^{-1} \text{s}^{-1}$, $\mu_{77\text{K}} = 1000 \text{cm}^2 \text{V}^{-1} \text{s}^{-1}$ and thickness 40nm , the two-layer model would indicate the following results:

| $N_D - N_A$ (300K) cm^{-3} | $N_D - N_A$ (77K) $\text{cm}^2 \text{V}^{-1} \text{s}^{-1}$ | $\mu_{300\text{K}}$ cm^{-3} | $\mu_{77\text{K}}$ $\text{cm}^2 \text{V}^{-1} \text{s}^{-1}$ |
|---|---|---|---|
| 1.3×10^{16} | 2,400 | 1.8×10^{15} | 35,000 |

in reasonable agreement with the data of Sullivan.

The two-layer model also illustrates the magnitude of the error associated with estimating the compensation ratio using a combination of the 77K Hall mobility and epitaxial carrier concentration obtained from C-V measurements. This error arises because of the reduction in measured mobility produced by the interface layer and for InP grown in the present study would yield an apparent compensation ratio (N_A/N_D) of $\sim 0.2-0.3$. Interestingly the model also shows that if the two layers contributing to the measurement are uncompensated, the results from the 77K Hall measurement alone will also indicate zero compensation.

A.5 PHOTOLUMINESCENCE

Photoluminescence spectra record the radiative energy released when electrons excited to high energy states transfer to more stable low energy states. The electrons are excited to these high energy states using an optical source, photoluminescence, and in this study the excitation energy used was $\sim 1.96 \text{eV}$ (633nm). This energy is larger than the bandgap of InP, $E_{g0\text{K}} = 1.423 \text{eV}$ [A.26] and enables electrons to be excited to all states in the gap. In more specialised studies photon energies less than the bandgap are employed and only selected energy states excited (photoluminescence excitation spectroscopy) [A.27]. Alternative excitation sources may also be used, e.g. electrons - cathodoluminescence - and the energy released by the electrons may be non-radiative, e.g. Auger recombination.

Photoluminescence has been used in the work reported here primarily to monitor impurities in the epitaxial layers. The energy states of interest are principally those of the simple donor and acceptor impurities which lie $\sim 7 \text{meV}$ below the conduction band and $30-40 \text{meV}$ above the valence band respectively, and certain transition metal impurities, e.g. Fe and Mn, which form states in the centre of the bandgap [A.28].

The energy and width of the luminescence ^{are} related to parameters which include the measurement temperature and the impurity concentration. Temperature effects take two principal forms:

Firstly, the emission lines are broadened by the thermal distribution of the excited carriers to approximately $\frac{1}{2}kT$ and it is therefore usual to cool the specimens to temperatures below 50K ($\frac{1}{2}kT=2\text{meV}$). Secondly, most of the donor states are ionised at elevated temperatures and to ensure donor to acceptor transitions are observed it is necessary to cool samples to less than 5K. High impurity concentrations also broaden the width of the energy states, while the associated strain and interacting centres can shift the energy of individual transitions. In general, unique identification of impurities can only be achieved at concentrations $<10^{15}\text{cm}^{-3}$ [A.29].

The photon energy corresponding to transitions between donor and acceptor levels is, to a first approximation, given by:

$$E_{\text{photon}} \approx E_g - (E_D - E_A) + \frac{e^2}{\epsilon(r_{DA})} \quad \text{A.10}$$

- E_g - Energy gap
- E_D - Energy level of donor
- E_A - Energy level of acceptor
- r_{DA} - Donor-acceptor separation
- ϵ - dielectric constant
- e - electron charge

The final term $\{e^2/\epsilon(r_{DA})\}$ takes account of the Coulomb interaction of the centres involved and for concentrations in the range $10^{15}-10^{16}\text{cm}^{-3}$. This term is small, i.e. $<1\text{meV}$. The range of donor ionisation energies is also very small ($<1\text{meV}$) [A.30] and identification of individual donor impurities from donor-acceptor transitions is impossible, even at 2K. Techniques involving two electron donor satellites or far infrared excitation are, therefore, used to identify individual donor impurities and to be successful these techniques again require impurity concentrations $<10^{15}\text{cm}^{-3}$ [A.31]. Donor-acceptor transitions are thus used primarily to give qualitative data on acceptor impurities. With a reduction in the acceptor concentrations the observed transitions become dominated by band edge structure which, at low temperature, is excitonic in character.

A.5.1 EXPERIMENTAL DETAILS

Photoluminescence spectra were obtained using a helium-neon laser to provide above bandgap excitation at 633nm, a closed cycle liquid helium cold finger to cool the epitaxial layers to a minimum temperature of 16–20K, and a 1 metre monochromator with either a photomultiplier or germanium photodetector to analyse the luminescence. The unattenuated intensity of the excitation was 10Wcm^{-2} and this could be reduced to 10mWcm^{-2} using neutral density filters. The incident excitation was modulated using a mechanical chopper, 1kHz, and the luminescence signal at the output of the photodetector phase sensitively detected. Sample and hold circuits were incorporated in series with the signal to remove noise due to the sensitivity of the germanium photodetector to cosmic particles [A.32]. The spectral range of the photomultiplier was $\sim 1.2\text{--}2.0\text{eV}$ [A.33] and the Ge photodetector 0.7 to 1.5eV [A.34].

Qualitative identification of impurities is usually based on empirical evidence obtained under carefully controlled conditions. Ideally, these should involve deliberate doping of high purity material and comparison of the photoluminescence signature of the doped and undoped samples. Doping concentrations should be maintained at a minimum $\sim 10^{15}\text{cm}^{-3}$ and luminescence signatures obtained over a range of temperatures (2K–25K) and at low excitation intensities ($< 10\text{mW cm}^{-3}$). Such conditions ensure that both band-acceptor (e-A) and donor-acceptor (D-A), as well as impurity bound excitons, are observed.

Qualitative assignments to the photoluminescence signatures obtained in this study were made following an extensive survey of previous photoluminescence measurements on InP. The results of this survey, in which special attention was paid to the above points, are presented in table A.2. Both e-A and D-A recombinations are listed in the table. However, only e-A recombinations would have occurred under the experimental conditions used in this work.

SHALLOW ACCEPTOR EMISSIONS:

| ELEMENT | RECOMBINATION | | REF. | COMMENTS |
|---------|---------------|------------|------|---|
| | e - A [eV] | D - A [eV] | | |
| Be | 1.383 | 1.3785 | A.35 | $\approx 10^{15} \text{cm}^{-3}$ implant into high purity ($\mu_{77\text{K}} \approx 50,000 \text{cm}^2 \text{V}^{-1} \text{s}^{-1}$) InP |
| | 1.382 | | A.36 | implant into Fe substrate |
| Mg | 1.383 | 1.3785 | A.35 | $\approx 10^{15} \text{cm}^{-3}$ implant into high purity ($\mu_{77\text{K}} \approx 50,000 \text{cm}^2 \text{V}^{-1} \text{s}^{-1}$) InP |
| | 1.384 | 1.379 | A.37 | $\approx 10^{17} \text{cm}^{-3}$ implant |
| Ca | 1.382 | | A.38 | $\approx 10^{17} \text{cm}^{-3}$ doping, but large range of activation energies. |
| Zn | 1.3735 | 1.3785 | A.39 | high purity ($\mu_{77\text{K}} \approx 70,000 \text{cm}^2 \text{V}^{-1} \text{s}^{-1}$) InP but referenced to unidentified work |
| | 1.373* | | A.40 | $\approx 10^{16} \text{cm}^{-3}$ doping |
| | 1.377* | | A.41 | |
| Cd | 1.362* | | A.40 | $\approx 7 \times 10^{17} \text{cm}^{-3}$ doping |
| | 1.369* | | A.41 | |
| Hg | 1.324* | | A.40 | $\approx 3 \times 10^{16} \text{cm}^{-3}$ doping |
| C | 1.3795 | 1.3755 | A.35 | $\approx 10^{15} \text{cm}^{-3}$ implant into high purity ($\mu_{77\text{K}} \approx 50,000 \text{cm}^2 \text{V}^{-1} \text{s}^{-1}$) InP |
| Si | 1.386 | 1.3833 | A.46 | $\approx 10^{17} \text{cm}^{-3}$ implant |
| Ge | | | A.42 | |

* - 50K measurements

DEEP EMISSIONS:

| ELEMENT | EMISSION [eV] | REF. | COMMENTS |
|---------|---------------|-----------|--|
| V | | A.43 | † |
| Cr | 0.85 | A.43 | † |
| Mn | 1.15 | A.43,A.44 | $\approx 5 \times 10^{16} \text{cm}^{-3}$ - broad band 1.1-1.2eV |
| Fe | 1.10 | A.43,A.44 | broad band 0.9-1.15eV † |
| Co | 0.474 | A.43,A.45 | |
| Ni | | A.43 | † |
| Cu | 1.2889 | A.43,A.45 | strong phonon replica at 1.2eV |

† - not active in diffusion studies

TABLE A.2 PHOTOLUMINESCENCE EMISSIONS OBSERVED FOR InP

REFERENCES - CHAPTER 1

- 1.01 J D Crowley, D R Tringali, I V Zubeck, F B Frank, 1982, SPIE323, 50
- 1.02 J Czekaj, M P Shaw, J East, P A Blakey, H L Grubin, 1985, Physica. 134B 499
- 1.03 D Botez, G J Herskowitz, Proc IEEE, 1980, 68, 689
- 1.04 F Guterl, G Zorpette, IEEE Spectrum, Aug 1985, 30
- 1.05 C Hilsum, Proc., IRE, 1962, 50, 185
- 1.06 S M Sze, 1981, Physics of Semiconductor Devices, (J Wiley), 652.
- 1.07 J E Sitch, P N Robson, 1976, IEEE Trans Elec Dev, 1086
- 1.08 C Hilsum, H D Rees, 1970, Electronics Letts, 6, 277
- 1.09 H D Rees, 1969, Solid State Comm. 7, 267
- 1.10 J J Gallagher, 1980, Proc. InP NATO Workshop, 1
- 1.11 M Armand, D V Bui, J Chevrier, N T Linh, 1983, Proc. of IEEE/Cornell Conf. on High Speed Semiconductor Devices and Circuits, Ithica, 218
- 1.12 I Messick, D A Dollins, R Nguyen, A R Clawson, G E McWilliams, 1986, Proc. International Electron Devices Meeting, Los Angeles, 767
- 1.13 H H Wieder, 1981, J Vac Sci Technol, 18, 827
- 1.14 W E Spicer, P W Chye, P R Skeath, C Y Su, I Lindau, 1979, J Vac Sci Technol, 16, 1422
- 1.15 L G Meiners, D L Lille, D A Collins, J Vac Sci Technol, 1979, 16, 1458
- 1.16 Y Suematsu, 1983, Proc. IEEE, 71, 692
- 1.17 A W Nelson, R H Mos, P C Spurdens, S Cole, S Wong, 1986. Br. Telecom. Technol. J. 4, 85
- 1.18 G H Olsen, V S Ban, 1987, Solid State Technol, 99
- 1.19 J Stone, M S Whalen, 1982 Appl Phys Lett, 41, 1140
- 1.20 W Walukiewicz, J Lagowski, L Jastrzebrski, P Rava, M Lichtensteiger, C H Gatos, H C Gatos, 1980, J Appl Phys, 51, 2659
- 1.21 B Cockayne, 1987, in Advanced Crystal Growth; Eds P M Dryburgh, B Cockayne and K G Barraclough (Prentice-Hall UK Ltd) 555
- 1.22 L F Eastman, 1980, Proc. NATO InP Workshop, 117
- 1.23 S H Groves, M C Plonko, 1981, J Cryst Growth, 54, 81
- 1.24 R M Capella, J L Benchimol, J F Bresse, M Quillec, 1985, IOP Conf Ser 74, 163

- 1.25 H Seki, M Kinoshita, Jap J Appl Phys, 1968, 7, 1142
- 1.26 R C Clarke, L L Taylor, J Cryst Growth, 1978, 43, 473
- 1.27 K Fairhurst, D Lee, D S Robertson, H T Parfitt, W H E Wilgoss, 1981, J Mat Sci, 16, 1013
- 1.28 L L Taylor, D A Anderson, 1983, J Cryst Growth, 64, 55
- 1.29 R C Clarke, 1981, J Cryst Growth, 54, 88
- 1.30 C Pickering, P R Tapster, P J Dean, L L Taylor, P L Giles, P Davies, 1983, J Crystal Growth, 64, 142
- 1.31 P J Dean, M S Skolnick, L L Taylor, 1984, J Appl Phys 55, 957
- 1.32 B A Joyce, C T Foxon, 1977, Inst Phys Conf Ser 32, 17
- 1.33 L M Zinkiewicz, T J Roth, B J Skromme, G E Stillman, 1981, IOP Conf Ser 56, 19
- 1.34 T J Roth, B J Skromme, T S Low, G E Stillman, L M Zinkiewicz, 1982, Semiconductor Growth Technology, Proceedings SPIE 323, 36
- 1.35 R J M Griffiths, N G Chew, A G Cullis, G C Joyce, 1983, Electronics Letts 19, 988
- 1.36 N Watanabe, Y Mori, 1986, Surf Sci, 174, 10
- 1.37 M J Ludowise, 1985, J Appl Phys, 58, R31
- 1.38 J P Duchemin, M Bonnet, G Beuchet, F Koelsch, 1979, Inst Phys Conf Ser 45, 10
- 1.39 M Razeghi, J P Duchemin, 1983, J Crystal Growth, 64, 76
- 1.40 A C Jones, G Wales, P J Wright, P E Oliver, 1987, Chemtronics 2, 83
- 1.41 E J Thrush, C G Cureton, I M Trigg, J P Stagg, B R Butler, 1987, Chemtronics 2, 62
- 1.42 K Ploog, 1980, Crystal Growth Properties and Applications, Ed. H C Freyhardt (Springer, Berlin) 73
- 1.43 A C Gossard, 1981, Thin Films: Preparation and Properties, Ed K N Tu (Academic Press)
- 1.44 J C H Hwang, T M Brennan, A Y Cho, 1983, J Electrochem Soc 130, 493
- 1.45 P W Sullivan, R F C Farrow, G R Jones, 1981, Inst Phys Conf Ser 56, 45
- 1.46 J S Roberts, P A Claxton, J P R David, J H Marsh, 1986, Electronics Letts 22, 506
- 1.47 M A Di Forte-Poisson, C Brylinski, J P Duchemin, 1985, Appl Phys Lett 46, 476

- 1.48 Y Kawaguchi, H Asahi, H Nagai, 1986, Inst Phys Conf Ser 79, 79
- 1.49 A Y Cho, J R Arthur, 1975, Progress in Solid State Chemistry 10, 157
- 1.50 R F C Farrow, 1977, Crystal Growth and Mterials, Ed. E Kaldis (North Holland Publishing), 238
- 1.51 C T Foxon, B A Joyce, 1981, Current Topics in Material Science, Ed E Kaldis (North Holland Publishing)
- 1.52 Molecular Beam Epitaxy and Heterostructures, 1985, Ed. L L Chang, K Ploog (Martinus Nijhoff)
- 1.53 The Technology and Physics of Molecular Beam Epitaxy, 1985, Ed. E H C Parker E.H.C. (Plenum)
- 1.54 B A Joyce, C T Foxon, 1987, Philips Tech Rev 43, 143
- 1.55 G K Gunther, 1958, Z Naturforsch 13, 1081
- 1.56 J E Davey, T Pankey, 1968, J Appl Phys 39, 1941
- 1.57 J R Arthur, 1968, J Appl Phys 39, 4032
- 1.58 C T Foxon, J A Harvey, B A Joyce, 1973, J Phys Chem Solids 34, 1693
- 1.59 C T Foxon, B A Joyce, 1975, Surf Sci 50, 434
- 1.60 J H Neave, P Blood, B A Joyce, 1980, Appl Phys Lett 36, 311
- 1.61 H Kunzel, K Ploog, 1980, Appl Phys Lett 37, 416 .
- 1.62 Handbook of Toxic and Hazardous Chemicals, Pub. Marshall Sittig
- 1.63 C R Stanley, R F C Farrow, P W Sullivan, 1985, The Technology of Molecular Beam Epitaxy, Ed E H C Parker (Plenum)
- 1.64 R F C Farrow, 1974, J Phys D 7, 2436
- 1.65 R F C Farrow, 1974, J Phys D 7, L121
- 1.66 R F C Farrow, 1975, Extended Abs, Electrochem Soc Fall Meeting, 547
- 1.67 R F C Farrow, 1975, J Phys D, 8, L87
- 1.68 R F C Farrow, 1975, UK Patent Application No 9921/75
- 1.69 R F C Farrow, 1977, Crystal Growth and Materials, Ch.1.7 (North Holland)
- 1.70 B I Miller, J H McFee, K J Bachmann, 1976, 7th Int Conf on Electron and Ion Beam Sci, 427
- 1.71 Y Kawamura, M Ikeda, H Asahi, H Okamoto, 1979, Appl Phys Lett 35, 481
- 1.72 M T Norris, C R Stanley, 1979, Appl Phys Lett 35, 617

- 1.73 K J Bachmann, E Buehler, B I Miller, J H McFee, F A Thiel, 1977, J Crystal Growth 39, 137
- 1.74 P W Sullivan - Private Communication
- 1.75 M G Dowsett, R M King, E H C Parker, 1977, Appl Phys Lett 31, 529
- 1.76 A G Cullis, R F C Farrow, 1979, Thin Solid Films 58, 197
- 1.77 R F C Farrow, 1981, Thin Solid Films 80, 197
- 1.78 G J Davies, R Heckingbottom, H Ohno, C E C Wood, A R Calawa, 1980, Appl Phys Lett 37, 290
- 1.79 J S Roberts, P Dawson, G B Scott, 1981, Appl Phys Lett 38, 905
- 1.80 W T Tsang, R C Miller, F Capasso, W A Bonner, 1982, Appl Phys Lett 41, 467
- 1.81 Y Kawamura, H Asahi, H Nagai, 1983, J Appl Phys 54, 841
- 1.82 J H McFee, B I Miller, K J Bachmann, 1977, Electrochem Soc 124, 259
- 1.83 D E C Corbridge, 1974, The Structural Chemistry of Phosphorus, (Elsevier, Amsterdam)
- 1.84 J Drowart, P Goldfinger, 1967, Angew Chem 6, 581
- 1.85 J H Neave, P Blood, B A Joyce, 1980, Appl Phys Lett 36, 311
- 1.86 M B Panish, 1980, J Electrochem Soc 127, 2729
- 1.87 R Chow, Y G Chai, 1983, Appl Phys Lett 42, 383
- 1.88 Y Kawaguchi, H Asahi, H Nagai, 1985, Jpn J Appl Phys 24, 221
- 1.89 Y Kawaguchi, H Asahi, H Nagai, 1985, Inst of Phys Conf Ser 79, 79
- 1.90 M T Norris, C R Stanley, 1979, Appl Phys Lett 35, 617
- 1.91 B I Miller, J H McFee, 1978, J Electrochem Soc 125, 1310
- 1.92 H Asahi, Y Kawamura, M Ikeda, H Okamoto, 1981, J Appl Phys 52, 2852
- 1.93 M B Panish, H Temkin, 1985, J Vac Sci Technol B3, 657
- 1.94 T Martin, C R Stanley, A Iliadis, C R Whitehouse, D E Sykes, 1985, Appl Phys Lett 46, 994
- 1.95 V M Airaksinen, T S Cheng, C R Stanley, 1987, J Crystal Growth 81, 332
- 1.96 S Maruno, Y Morishita, T Isu, Y Nomura, H Ogata, 1987, J Crystal Growth 81, 338
- 1.97 P W Sullivan, 1980, Ph.D. Thesis, University of Glasgow
- 1.98 P W Sullivan - Private Communication

- 1.99 T Martin, C R Stanley, A Iliadis, C R Whitehouse, D Sykes, 1985, 3rd European MBE Workshop, Aussois, France
- 1.100 Y Kawamura, H Asahi, 1983, Appl Phys Lett 43, 780
- 1.101 R M Park, 1981, Ph.D Thesis, University of Glasgow
- 1.102 T M Kerr, 1984, Ph.D Thesis, University of Glasgow
- 1.103 H Asahi, Y Kawamura, M Ikeda, H Okamoto, 1981, Jap J Appl Phys 20, L187
- 1.104 B J Skromme, G E Stillman, J D Oberstar, S S Chan, 1984, Appl Phys Lett 44, 319
- 1.105 B I Miller, J H McFee, R J Martin, P K Tien, 1978, Appl Phys Lett 33, 44

REFERENCES - CHAPTER 2

- 2.01 A Chandra, C E C Wood, D W Woodard, L F Eastman, 1979, Solid State Electronics, 22 645
- 2.02 L Eaves, A W Smith, M S Skolnick, C R Whitehouse, B Cockayne, 1982, Semi-insulating III-V Materials, Evian, 199
- 2.03 P J Dean, A G Cullis, A M White. 1980, Characterisation and Properties of Semiconductors, Ed T S Moss (North Holland), 113
- 2.04 Loughborough Consultants Ltd, Loughborough University of Technology, Loughborough, Leics, UK
- 2.05 D W Williams, 1983, Private Communication
- 2.06 R E Honig, D A Kramer, 1969, RCA Review, 30, 285
- 2.07 M S Skolnick, E J Foulkes, B Tuck, 1984, J Appl Phys 55, 2951
- 2.08 THORN-EMI Electron Tubes Ltd, Bury Street, Ruislip, Middlesex HA4 7TA
- 2.09 FRIALT-DEGUSSIT AL23, Friedrichsfeld GmbH, Postfach 7, Steinzeugstr 50, D-6800 Mannheim 71, FRG
- 2.10 R C Clarke, L L Taylor, 1978, J Crystal Growth 43, 473
- 2.11 V L Wrick, K T Ip, L F Eastman, 1978, J Electr Mater 7, 253
- 2.12 G M Williams, C R Whitehouse, T Martin, N G Chew, A G Cullis, T Ashley, D E Sykes, K Mackey, 1986, 4th Int Conf on Molecular Beam Epitaxy, University of York, UK, 7-10 September 1986
- 2.13 G M Williams, C R Whitehouse, T Martin, N G Chew, A G Cullis, T Ashley, D E Sykes, K Mackey, R H Williams, 1988, J Appl Phys 63, 1526
- 2.14 C E C Wood, B A Joyce, 1978, J Appl Phys 49, 4854
- 2.15 D De Simone, C E C Wood, C A Evans, 1982, 53, 4938
- 2.16 A R Clawson, D A Collins, D I Elder, J J Monroe, 1978, Naval Ocean Systems Centre, San Diego - Tech Note 592
- 2.17 G J Davies, R Heckingbottom, H Ohno, C E C Wood, A R Calawa, 1980, Appl Phys Lett 37, 290
- 2.18 J S Roberts, P Dawson, G B Scott, 1981, Appl Phys Lett 38, 905
- 2.19 M Bafleur, A Munoz-Yague, A Rocher, 1982, J Cryst Growth 59, 531
- 2.20 K Ploog, 1980, Crystal Growth, Properties and Applications, Ed H C Freyhardt (Springer, Berlin) 73
- 2.21 Millipore (UK) Ltd, 11-15 Peterborough Road, Harrow, Middlesex HA1 2YH
- 2.22 J H Neave, P Blood, B A Joyce, 1980, Appl Phys Lett 36, 311

- 2.23 C R Stanley, 1988, Private Communication
- 2.24 R F C Farrow, P W Sullivan, G M Williams, C R Stanley, 1982, MBE-CST-2, Tokyo, Paper A-9-4
- 2.25 D L Miller, S W Zehr, J S Harris Jr, 1982, J Appl Phys 53, 744
- 2.26 C B Carter, D M DeSimone, T Griem, C E C Wood, 1982, 40th Ann Electron Microscopy Society of America, Washington D C, August 9-13
- 2.27 J H Neave, P K Larsen, J F Van der Veen, P J Dobson, B A Joyce, 1983, Surf Sci 131, 12
- 2.28 C R Whitehouse, M T Emeny, L Davis, G M Williams, T Martin, 1986, Fourth Int Conf on Molecular Beam Epitaxy, University of York, UK, 7-10 September 1986

REFERENCES - CHAPTER 3

- 3.01 O Kubaschewski, 1967, Metallurgical Thermochemistry, 4th Edition (Pergamon Press)
- 3.02 J H Neave, P Blood, B A Joyce, 1980, Appl Phys Lett 36, 311
- 3.03 C T Foxon, 1983, Private Communication
- 3.04 M Baker, L Laurenson, 1966, Vacuum 18, 633
- 3.05 P J Page, D L Trimm, P M Williams, 1974, J Chem Soc Far Trans 1, 20
- 3.06 J F O'Hanlon, A Users Guide to Vacuum Technology, 1980, (John Willey and sons, New York)
- 3.07 D E C Corbridge, 1974, The Structural Chemistry of Phosphorus (Elsevier, Holland)
- 3.08 R E Honig, D A Kramer, 1969,, RCA Review 30, 285
- 3.09 R F C Farrow, 1975, UK Patent Application No 9921/75
- 3.10 G J Davies, R Heckingbottom, H Ohno, C E C Wood, A R Calawa, 1980, Appl Phys Lett 37, 290,
- 3.11 B J Skromme, G E Stillman, J D Oberstar, S S Chan, 1984, Appl Phys Lett 44, 319
- 3.12 C R Stanley, 1988, Private Communication
- 3.13 J S Roberts, P A Claxton, J P R David, J H Marsh, 1986, Elec Letts 22, 506
- 3.14 V M Airaksinen, T S Cheng, C R Stanley, 1987, J Crystal Growth 81, 332
- 3.15 A Y Cho, F K Reinhart, 1974, J Appl Phys 45, 1812
- 3.16 D E Sykes, 1984, Private Communication
- 3.17 K A Prior, G J Davies, R Heckingbottom, 1984, J Crystal Growth 66, 55
- 3.18 A K Chin, I Camlibel, B V Dutt, V Swaminathan, W A Bonner, A A Ballman, 1983, Appl Phys Lett 42, 901
- 3.19 S M Sze, 1981, Physics of Semiconductor Devices, (J Wiley) 66
- 3.20 D A Andrews, R Heckingbottom, G J Davies, 1983, J Appl Phys 54, 4421
- 3.21 K Akimoto, M Dohsen, M Arai, N Watanabe, 1983, Appl Phys Lett 43, 1062
- 3.22 G Post, P Dimitriou, A Scavenec, N Duhamel, A Mircea, 1983, Elec Letts 19, 459

- 3.23 N Barbouth, Y Berthier, J Oudar, J-M Moison, M Bensoussan, 1986, *J Electrochem Soc* 133, 1663
- 3.24 INSPEC Literature Survey - September 1987
- 3.25 M Illegems, 1977, *J Appl Phys* 48, 1278
- 3.26 C E C Wood, D M DeSimone, K Singer, G W Wicks, 1982, *J Appl Phys* 53, 4230
- 3.27 D M DeSimone, C E C Wood, C A Evans Jr, 1982, *J Appl Phys* 53, 4938
- 3.28 MCP Electronic Materials Ltd, Alperton, Wembley, Middlesex HAD 4PE, UK
- 3.29 W Walukiewicz, J Lagowski, L Jastrzebski, PO Rava, M Lichtensteiger, C H Gatos, H C Gatos, 1980, *J Appl Phys* 51, 2659
- 3.30 E Kubota, Y Ohmori, K Sugii, 1984, *J Appl Phys* 55, 3779
- 3.31 C E C Wood, D Desimone, K Singer, G W Wicks, 1982, *J Appl Phys* 53, 4230
- 3.32 B J Skromme, T S Low, T J Roth, G E Stillman, J K Kennedy, J K Abrokwah, 1983, *J Electr Mater* 12, 433
- 3.32 M S Skolnick, 1987, Private Communication
- 3.34 W T Tsang, 1982, *Appl Phys Lett* 41, 467
- 3.35 T S Kim, S D Lester, B G Streetman, 1987, *J Appl Phys* 61, 4598
- 3.36 S D Lester, T S Kim, B G Streetman, 1987, *J Appl Phys* 62, 2950
- 3.37 K R Duncan, L Eaves, A Ramdane, W B Roys, M S Skolnick, P J Dean, 1984, *J Phys C* 17, 1233
- 3.38 E W Williams, H B Bebb, 1972, *Semiconductors and Semimetals* 8, 387, (Academic Press, New York 1972)
- 3.39 B Wakefield, L Eaves, K A Prior, A W Nelson, G J Davies, 1984, *J Phys D* 17, L133
- 3.40 C R Stanley, 1988, Private Communication
- 3.41 Batch A1A 86513 JK, Johnson Matthey Chemicals Ltd, Orchard Road, Royston, Herts SG8 5HE, UK

REFERENCES - CHAPTER 4

- 4.01 J Maguire, R Murray, R C Newman, R B Beall, J J Harris, 1987, Appl Phys Lett 50, 516
- 4.02 K Ploog, A Fischer, H Kunzel, 1979, Appl Phys 18, 353
- 4.03 K Ploog, 1980, Crystal Growth, Properties and Applications, Ed H C Freyhardt (Springer Verlag, Berlin), 73
- 4.04 R S Smith, P M Ganser, H Ennen, 1982, J Appl Phys 53, 9210
- 4.05 Y Kawamura, H Asahi, 1983, Appl Phys Lett 43, 780
- 4.06 D M Collins, J N Miller, Y G Chai, R Chow, 1982, J Appl Phys 53, 3010
- 4.07 C R Whitehouse, M T Emeny, T Martin, 1985, Unpublished Data.
- 4.08 J S Roberts, P Dawson, G B Scott, 1981, Appl Phys Lett 38, 905
- 4.09 P W Sullivan, 1981, PhD Thesis University of Glasgow
- 4.10 R C Clarke, 1979, Inst Phys Conf Ser No 45, 19
- 4.11 M Razeghi, M A Poisson, J P Larivain, J P Duchemin, 1983, J Electron Mater 12, 371
- 4.12 D Grundmann, H Jurgensen, M Heyen, J Korec, P Balk, 1985, J Electron Mater, 14, 749
- 4.13 C E C Wood, 1978, Appl Phys Lett 33, 770
- 4.14 G J Davies, D A Andrews, R Heckingbottom, 1981, J Appl Phys 52, 7214
- 4.15 D A Andrews, R Heckingbottom, G J Davies, 1983, J Appl Phys 54, 4421
- 4.16 R E Honig, D A Kramer, 1969, RCA Review 30, 285
- 4.17 C E C Wood, 1985, in Molecular Beam Epitaxy and Heterostructures, Ed L L Chang, K Ploog (Martinus Nijhoff), 149
- 4.18 D A Andrews, M Y Kong, R Heckingbottom, G J Davies, 1984, J Appl Phys 55, 841
- 4.19 R J Ratchford, H Rickert, 1962, Z Electrochem 66, 497
- 4.20 D Detry, J Drowart, P Goldfinger, H Keller, H Rickert, 1967, Z Phys Chem 55, 314
- 4.21 H Rickert, 1972, Physics of Electrolytes 2, (Academic, New York) 519
- 4.22 Kingshill Electronic Products Ltd, Torrens St, London EC1V 1NJ
- 4.23 W Walukiewicz, J Lagowski, L Jastrzebrski, P Rava, M Lichtensteiger, C H Gatos, H C Gatos, 1980, J Appl Phys 51, 2659

- 4.24 N Apsley, D A Anderson, J B Morrison, 1987, *Semicond Sci and Technol* 2, 44
- 4.25 C M Wolfe, G E Stillman, 1975, *Appl Phys Lett* 27, 564
- 4.26 F Sette, S J Pearton, J M Poate, J E Rowe, J Stohr, 1986, *Phys Rev Lett* 56, 2637
- 4.27 D A Anderson, N Apsley, P Davies, P L Giles, 1985, *J Appl Phys* 58, 3059
- 4.28 D Lancefield, A R Adams, M A Fischer, 1987, *J Appl Phys*, 62, 2342
- 4.29 D G Armour, M Wadsworth, R Badheka, J A Van den Berg, G Blackmore, S Courtney, C R Whitehouse, E A Clark, D E Sykes, R Collins, M T Emeny, R Smith, 1987, SIMS VI Conf, Versailles, Sept 1987.
- 4.30 D E Sykes, E A Clark, S J Courtney, G W Blackmore, C R Whitehouse, M T Emeny, 1986, *Vacuum* 36, 1011.
- 4.31 K Akimoto, M Dohsen, M Arai, N Watanabe, 1983, *Appl Phys Lett* 43, 1062
- 4.32 C B Carter, D M DeSimone, T Griem, C E C Wood, 1982, 40th Ann Electron Microscopy Society of America, Washington D C, August 9-13
- 4.33 L Suchow, 1982, *Mat Res Bull* 17, 1401
- 4.34 S Mahajan, A K Chin, 1980, NATO Workshop on InP, 495
- 4.35 S Mahajan, A K Chin, 1981, *J Crystal Growth* 54, 138
- 4.36 R Heckingbottom, C J Todd, G J Davies, 1980, *J Electrochem Soc* 127, 444
- 4.37 V M Airaksinen, T S Cheng, C R Stanley, 1987, *J Crystal Growth* 81, 332
- 4.38 V M Airaksinen, T S Cheng, C R Stanley, 1987, *J Crystal Growth* 84, 241
- 4.39 C E C Wood, B A Joyce, 1978, *J Appl Phys* 49, 4854

REFERENCES - CHAPTER 5

- 5.01 MCP Electronic Materials, Alperton, Wembley, Middlesex HAD 4PE, UK
- 5.02 C R Elliott, S O'Brien, 1982, *Analyst*, 107, 571
- 5.03 M B Panish, 1974, *J Crystal Growth* 27, 6
- 5.04 R F C Farrow, 1974, *J Phys D* 7, 2436
- 5.05 L L Chang, L Esaki, W E Howard, R Ludeke, G Schul, 1973, *J Vac Sci Technol* 10, 655
- 5.06 M B Panish, 1980, *J Electrochem Soc* 127, 2729
- 5.07 R F C Farrow, 1981, *Thin Solid Films* 80, 197
- 5.08 J W Otvos, D P Stevenson, 1956, *J Am Chem Soc* 78, 546
- 5.09 C E C Wood, D Desimone, K Singer, G W Wicks, 1982, *J Appl Phys* 53, 4230
- 5.10 W S Horton, 1986, *J Res N B S* 70A, 533
- 5.11 C R Whitehouse, M T Emeny, L Davis, G M Williams, T Martin, 4th Int Conf on Molecular Beam Epitaxy, University of York, UK, 7-10 September 1986
- 5.12 E S Hellman, J S Harris, 1987, *J Crystal Growth* 81, 38
- 5.13 B F Lewis, R Fernandez, A Madhukar, F J Grunthaner, 1986, *J Vac Sci Technol* B4, 560
- 5.14 Six 9s grade red phosphorus, Lot L02910, MCP Electronic Materials, Alperton, Wembley, Middlesex HAD 4PE, UK
- 5.15 V M Airaksinen, T S Cheng, C R Stanley, 1987, *J Crystal Growth* 81, 332
- 5.16 V M Airaksinen, T S Cheng, C R Stanley, 1987, *J Crystal Growth* 84, 241
- 5.17 Johnson Matthey Chemicals Ltd, Orchard Road, Royston, Herts SG8 5HE, UK
- 5.18 Ventron Alfa Products, Ventron GmbH, Zeppelinstrasse 7, Postfach 65 40, D-7500 Karlsruhe 1, FRG
- 5.19 J S Roberts, P A Claxton, J P R David, J H Marsh, 1986, *Electronics Letts* 22, 506
- 5.20 M R Aylett, J Haigh, 1982, *J Crystal Growth* 58, 127
- 5.21 L Palm, H Bruch, K H Bachem, P Balk, 1979, *J Electron Mater* 8, 555
- 5.22 S H Groves, M C Plonko, 1979, *Inst Phys Conf Ser* 45, 71
- 5.23 M T Norris, C R Stanley, 1979, *Appl Phys Lett* 35, 617

- 5.24 S L Wright, H Kroemer, 1982, J Vac Sci Technol 20, 143
- 5.25 Y G Chai, 1984, Appl Phys Lett 45, 985
- 5.26 M Razeghi, J P Duchemin, 1983, J Crystal Growth 64, 76
- 5.27 R Chow, Y G Chai, 1983, Appl Phys Lett 42, 383
- 5.28 Y Kawaguchi, H Asahi, H Nagai, 1985, Inst Phys Conf Ser 79, 79
- 5.29 E J Thrush, C G Cureton, J M Trigg, J P Stagg, B R Butler, 1987, Chemtronics 2, 62
- 5.30 W T Tsang, 1986, Appl Phys Lett 48, 511
- 5.31 A Antreasyn, W T Tsang, P A Garbinski, 1986, Appl Phys Lett 49, 874
- 5.32 R N Nottenburg, M B Panish, H Temkin, 1986, Inst Phys Conf Ser 83, 483
- 5.33 Y Kawaguchi, H Asahi, 1987, Appl Phys Lett 50, 1243
- 5.34 J C Campbell, W T Tsang, G J Qua, 1987, IEEE Electron Dev Lett 8, 171
- 5.35 C H Chen, C A Larsen, G B Stringfellow, D W Brown, A J Robertson, 1986, J Crystal Growth 77, 11
- 5.36 C H Chen, D S Cao, G B Stringfellow, 1988, Electron Mater 17, 67
- 5.37 W T Tsang, 1984, Appl Phys Lett 45, 1234
- 5.38 P Wolfram, F W Reier, D Franke, H Schumann, 1988, 2nd European Workshop on MOVPE, St Andrews, Scotland, June 1988.

REFERENCES - CHAPTER 6

- 6.01 E Kubota, Y Ohmori, K Suggi, 1984, J Appl Phys 51, 3779
- 6.02 H Rickert, 1972, Physics of Electrolytes, 2, 519 (Academic, New York)
- 6.03 W Walukiewicz, J Lagowski, L Jastrzebski, P Rava, M Lichtensteiger, C H Gatos, H C Gatos, 1980, J Appl Phys 51, 2659
- 6.04 D Lancefield, A R Adams, M A Fischer, 1987, J Appl Phys 62, 2342
- 6.05 L Suchow, 1982, Mat Res Bull 17, 1401
- 6.06 K Akimoto, M Dohsen, M Arai, N Watanabe, 1983, Appl Phys Lett 43, 1062
- 6.07 V M Airaksinen, T S Cheng, C R Stanley, 1987, J Cryst Growth 81, 332
- 6.08 J S Roberts, P A Claxton, J P R David, J H Marsh, 1986, Electron Lett 22, 506
- 6.09 Y Kawaguchi, H Asahi, H Nagai, 1985, Inst Phys Conf Ser 79, 79
- 6.10 M K S Instruments Inc, 34 Third Avenue Burlington MA 01803 USA
- 6.11 T M Kerr, 1984, Ph.D Thesis, University of Glasgow
- 6.12 Y Kawamura, H Asahi, H Nagai, 1983, J Appl Phys 54, 841
- 6.13 W T Tsang, 1986, J Electron Mat 15, 235
- 6.14 G Hasnain, D Mars, G H Dohler, M Ogura, J S Smith, 1987, Appl Phys Lett 51, 831
- 6.15 H Heinecke, A Brauers, F Grafahrend, C Plass, N Putz, K Werner, M Weyers, H Luth, P Balk, 1986, J Cryst Growth 77, 303
- 6.16 N HY Karam, H Liu, I Yoshida, S M Bedair, 1988, Appl Phys Lett 52, 1144

REFERENCES - APPENDIX

- A.01 D E Sykes, E A Clark, S J Courtney, G W Blackmore, C R Whitehouse, M T Emeny, 1986, *Vacuum*, 36, 1011
- A.02 Loughborough Consultants Ltd, University of Technology, Loughborough, Leicestershire
- A.03 J B Clegg, 1982, *Secondary Ion Mass Spectrometry III* (Eds A Benninghoven, J Giber, J Laszlo, M Riedel, H W Werner) in Springer Series in 'Chemical Physics' 19, 308
- A.04 Cameca, 103 Boulevard Saint-Dennis, BP 6, 92403 Courbevoie Cedex, France
- A.05 J M Walls, D E Sykes, 1982, "SIMS: A Diagnostic Technique for Semiconductor Processing", Proc. Tech. Prog. 'Semiconductor International 1982', Birmingham, Cahners Exposition Group, Guildford, UK; 214
- A.06 P Alnot, A M Huber, J Olivier, 1986, *Surface and Interface Analysis* 9, 283
- A.07 T Ambridge, 1983, *Scanning Electron Microscopy*, p31
- A.08 D Sykes, 1984, private communication
- A.09 J E Wardill, D J Dowling, R A Brunton, D A E Crouch, J R Stockbridge, A J Thompson, 1983, *J Crystal Growth* 64, 15
- A.10 I Grant, L Li, D Rumsby, J Ware, 1983, *J Crystal Growth* 64, 32
- A.11 D Rumsby, R M Ware, M Whitaker, 1981, *J Crystal Growth* 54, 32
- A.12 B Cockayne, G T Brown, W R MacEwan, 1981, *J Crystal Growth* 54, 9
- A.13 P Blood, J W Orton, 1978, *Rep. Prog. Phys.* 41, 1
- A.14 T Ambridge, C R Elliott, M M Faktor, 1973, *J Appl Electrochem* 3, 1
- A.15 Polaron Equipment Ltd, 21 Greenhill Crescenmt, Holywell Industrial Estate, Watford, Herts, UK.
- A.16 T Ambridge, D J Ashen, 1979, *Electron Lett* 15, 647
- A.17 L C Kimerling, 1974, *J Appl Phys* 45, 1839
- A.18 L J van der Pauw, 1985, *Philips Res Reports* 13, 1
- A.19 D M Boerger, J K Kramer, L D Partain, 1981, *J Appl Phys* 52, 269
- A.20 W Walukiewicz, J Lagowski, L Jastrzebrski, P Rava, M Lichtensteiger, C H Gatos, H C Gatos, 1980, *J Appl Phys* 51, 2659
- A.21 S J Bass, C Pickering, M L Young, 1983 64, 68
- A.22 N Apsley, D A Anderson, J B Morrison, 1987, *Semicond. Sci and Technol.* 2, 44

- A.23 D J Ashen, D A Anderson, N Apsley, M T Emeny, 1982, *J Crystal Growth* 60, 225
- A.24 P W Sullivan, R F C Farrow, G R Jones, 1981, *Inst Phys Conf Ser* 56, 45
- A.25 P W Sullivan, Ph.D Thesis, University of Glasgow, 1980
- A.26 A M White, P J Dean, L L Taylor, R C Clarke, D J Ashen, J B Mullin, 1972, *J Phys C* 5, 727
- A.27 P J Dean, D J Robbins, S G Bishop, 1979, *J Phys C* 12, 5567
- A.28 E W Williams, H B Bebb, 1972, in "Semiconductors and Semimetals" (Eds R K Willardson, A K Beer; Academic, New York)
- A.29 P J Dean, 1982, *Prog in Crystal Growth Charactersation* 5, 89
- A.30 K K Smith, 1981, *Thin Solid Films* 84, 171
- A.31 P J Dean, M S Skolnick, 1983, *J Appl Phys* 54, 346
- A.32 A T Collins, T Jeffries, 1982, *J Phys E* 15, 712
- A.33 THORN-EMI Electron Tubes Ltd, Bury Street, Ruislip, HA4 7TA
- A.34 Model EO-817L, North Coast Optical Systems and Sensors, PO Box 6812, Santa Rosa, CA 95406, USA
- A.35 B J Skromme, G E Stillman, J D Oberstar, S S Chan, 1984, *Appl Phys Lett* 44, 319
- A.36 J D Oberstar, B G Streetman, 1982, *J Appl Phys* 53, 5154
- A.37 G S Pomrenko, Y S Park, R L Hengehold, 1981, *J Appl Phys* 52, 969
- A.38 E Kubota, Y Ohmori, J Sugiik, 1984, *J Appl Phys* 55, 3779
- A.39 B J Skromme, T S Low, T J Roth, G E Stillman, J K Kennedy, J K Abrokwah, 1983, *J Elect Mater* 12, 433
- A.40 E W Williams, W Elder, M G Astles, M Webb, J B Mullin, B Straughan, P J Tufton, 1973, *J Electrochem Soc* 120, 1741
- A.41 A M White, P J Dean, K M Fairhurst, W Bardsley, E W Williams, B Day, 1972, *Solid State Commun* 11, 1099
- A.42 A M White, P J Dean, B Day, 1976, *Proc 13 Int Conf Physics Semiconductors, Rome*, 1057
- A.43 M S Skolnick, E J Foulkes, B Tuck, 1984, *J Appl Phys* 55, 2951
- A.44 L Eaves, A W Smith, M S Skolnick, C R Whitehouse, B Cockayne, 1982, *Semi-Insulating III-V Materials*, Evian, 199
- A.45 M S Skolnick, P J Dean, P R Tapster, B Cockayne, W R MacEwan, 1981, *J Luminescence*, 24/25, 241
- A.46 G S Pomrenke, 1983, *J Cryst Growth* 64, 158

LIST OF FIGURES

- 1.1 Band Structure of InP, GaAs and Si
- 1.2 Velocity-Field Characteristics
- 1.3 Energy Gap versus Lattice Constant for III-V Semiconductors

- 2.1 Photoluminescence Spectra of TM 39 and 49
- 2.2 Photoluminescence Spectra of TM 50 and 55
- 2.3 Schematic Illustrating the Improvements Made to the In Cell Fitted in Chamber 1
- 2.4 Photoluminescence Spectrum of TM 63
- 2.5 C-V Profiles of TM 65 and 66
- 2.6 C-V Profiles of TM 80 and 81
- 2.7 C-V and SIMS Profiles of TM 75
- 2.8 C-V and SIMS Profiles of TM 82
- 2.9 C-V and SIMS of the Effect of a Deliberate Step Change in Indium Cell Temperature (TM 86)
- 2.10 C-V and SIMS of the Effect of a Deliberate Step Change in the Phosphorus Source Temperature (TM 84)
- 2.11 C-V and SIMS Profiles of the Effect of a Deliberate Step Change in Substrate Temperature (TM 90)
- 2.12 Examples of Gross Morphological Problems Encountered at an Early Stage in the Project
- 2.13 Poor Epitaxial Morphology Attributed to *Ex Vacuo* Substrate Preparation Procedures
- 2.14 Nomarski Micrograph of Epitaxial InP, $\sim 3\mu\text{m}$ thick with defect density $\sim 2 \times 10^4 \text{ cm}^{-2}$
- 2.15 Schematic of the Substrate Thermocouple Configurations used in Chamber 1
- 2.16 Characteristic of the Phosphorus Cracking Source

- 3.1 Schematic of Chamber 2
- 3.2 Chamber 2
- 3.3 Illustration of the Group III and Group V Cells Designed and Constructed for use Chamber 2
- 3.4 Mobility versus Carrier Concentration - TM 97, 117, 119, 120 and 122

- 3.5 Photoluminescence Spectrum of TM 97
- 3.6 C-V Profile of TM 97
- 3.7 Photoluminescence Spectra of (a)TM 117, (b)TM 119 and (c)TM 122
- 3.8 Photoluminescence Spectra of TM 105 and 111
- 3.9 C-V and SIMS Profiles of TM 99
- 3.10 C-V and SIMS Profiles of TM 123
- 3.11 SIMS Sulphur Profile for Layer Grown on Sulphur Doped Substrate (TM 66)
- 3.12 C-V and SIMS Profiles of TM 83
- 3.13 Photoluminescence Spectrum of TM 114
- 3.14 The F.W.H.M. of the Band Edge Recombination versus Excitation Intensity (Layer TM 121)
- 3.15 Photoluminescence Spectrum of TM 123
- 3.16 Photoluminescence Spectrum of TM 120

- 4.1 Schematic of the Electrochemical Cell
- 4.2 Carrier Concentration versus Cell EMF for Sulphur Doped InP
- 4.3 Vapour Pressure of Sulphur and Red Phosphorus
- 4.4 Mobility versus Carrier Concentration - Sulphur Doped InP
- 4.5 Photoluminescence Spectra of Sulphur Doped Layers (TM 165 and 168)
- 4.6 SIMS Profile of a Sulphur Doping Spike (TM 157)
- 4.7 C-V and SIMS Profile of Sulphur Concentration as a Function of Substrate Temperature (TM 172)
- 4.8 C-V and SIMS Profiles of Sulphur Concentration as a Function of Phosphorus Flux (TM 153)
- 4.9 Sulphur Concentration versus V:III Flux Ratio.
- 4.10 Carrier Concentration versus Reciprocal Growth Temperature for Sulphur Doped InP.

- 5.1 Equilibrium Loss Rates for InP and GaAs
- 5.2 Minimum Phosphorus Flux Required to Prevent Thermal Decomposition of InP
- 5.3 Mobility versus Carrier Concentration - Comparison of TM 147 and 154 with Data from Earlier Layers Grown in Chamber 2

- 5.4 Comparison of Experimental and Calculated Variations in Carrier Concentration for Sulphur Doped InP
- 5.5 Calculated Variation in Minimum Sulphur Concentration versus Growth Temperature and Growth Rate
- A.1 High Mass Resolution SIMS Profile of Mass 32 Isotopes in TM 123
- A.2 SIMS Profile Illustrating Sn Isotope Check in TM 86
- A.3 SIMS Profile of Si Implant
- A.4 Calculated Variation in Carrier Freezeout as a Function of Interface Thickness and Doping Concentration.

LIST OF TABLES

- 1.1 Summary of the Major Epitaxial Growth Techniques used for InP
- 1.2 Summary of the Published Data on the MBE Growth of Unintentionally Doped InP
- 1.3 Dopant Species Used in the MBE Growth of InP
- 2.1 SIMS Impurity Analysis of Unintentionally Doped InP Epitaxial Layers Grown at the Start of the Programme (TM 16, 28, 31 and 44)
- 2.2 SIMS Impurity Analysis of Unintentionally Doped InP Epitaxial Layers Grown Using the Modified In Cell (TM 62, 63 and 64)
- 3.1 Growth Conditions and Properties of Layers Grown in Chamber 2 (TM 97, 117, 119, 120, 122)
- 3.2 Summary of Hall Data Recorded for Layers TM 97, 117, 119, 120, and 122
- 3.3 Summary of the Impurities in Unintentionally Doped InP Grown in Chamber 2 - As Identified by SIMS
- 3.4 Covalent Radii for Mg, Ca, Ga, In, P, As
- 5.1 Comparison of the Hall Data for TM 147 and 154 with that Initially Obtained in Chamber 2
- 5.2 Growth Comparison of the Sulphur Concentration in Different Batches of Red Phosphorus
- A.1 Impurities Present in Bulk InP
- A.2 Impurities Associated with Photoluminescence Emissions in InP